

1-1-1985

Polyacetylene polymerization, structure, and electrical transport properties/

Michael A. Schen
University of Massachusetts Amherst

Follow this and additional works at: https://scholarworks.umass.edu/dissertations_1

Recommended Citation

Schen, Michael A., "Polyacetylene polymerization, structure, and electrical transport properties/" (1985).
Doctoral Dissertations 1896 - February 2014. 696.
<https://doi.org/10.7275/4jgv-8467> https://scholarworks.umass.edu/dissertations_1/696

This Open Access Dissertation is brought to you for free and open access by ScholarWorks@UMass Amherst. It has been accepted for inclusion in Doctoral Dissertations 1896 - February 2014 by an authorized administrator of ScholarWorks@UMass Amherst. For more information, please contact scholarworks@library.umass.edu.



312066005717405

POLYACETYLENE POLYMERIZATION, STRUCTURE, AND
ELECTRICAL TRANSPORT PROPERTIES

A Dissertation Presented

by

MICHAEL A. SCHEN

Submitted to the Graduate School of the
University of Massachusetts in partial fulfillment
of the requirements for the degree of

DOCTOR OF PHILOSOPHY

February 1985

Polymer Science and Engineering

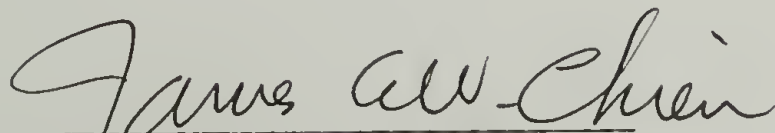
POLYACETYLENE POLYMERIZATION, STRUCTURE AND
ELECTRICAL TRANSPORT PROPERTIES

A Dissertation Presented

by

MICHAEL A. SCHEN

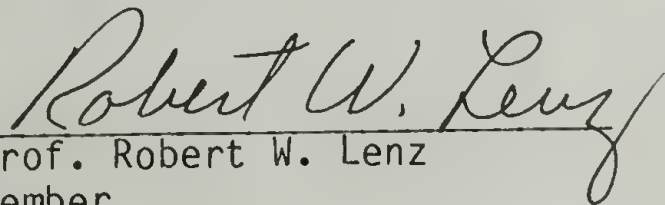
Approved as to style and content by



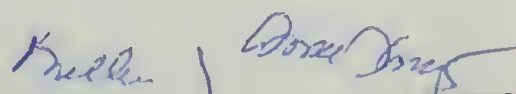
Prof. James C. W. Chien
Co-chairperson of Committee



Prof. Frank E. Karasz
Co-chairperson of Committee



Prof. Robert W. Lenz
Member



Prof. William J. MacKnight, Head
Department of Polymer Science
and Engineering

MICHAEL A. SCHEN 1985



All Rights Reserved

"He not busy being born is busy dying."

(B. Dylan)

To my mother and father, for their
love and wisdom.

ACKNOWLEDGEMENT

I wish to first thank and acknowledge my advisors Professor James Chien and Professor Frank Karasz for their scientific support and confidence throughout my stay in Amherst. I would also like to express my gratitude to Professor Robert Lenz for being a part of my committee, and for the professionalism to which he addressed his committee responsibilities.

I especially wish to extend my appreciation to Professor Chien for his help in bringing to fruition the post-doctoral appointment awaiting me in Montpellier, France. I eagerly anticipate the professional growth and personal enlightenment that are certain to ensue.

The presence and support of two wonderful colleagues and friends deserves to be noted. First, without the continuous availability of Dr. L. Charles Dickinson during the sabbatical leave of Professor Chien, I am certain that my personal goal to complete this Ph.D. before the 27th of December would not have been attained. Also I would like to acknowledge the many scientific and not so scientific discussions that we had. Without these, 6th floor life would not have been so alive and learning. Secondly, the experimental support provided by Jack Hirsch has been invaluable to say the least. His concerns for maintaining a safe and productive laboratory environment has earned him my highest respect. In addition, he and his wife Amy have become two very wonderful friends. I truly hope the friendship that has been kindled between us survives the years.

I would also like to acknowledge the support that was offered by two former colleagues: James Capistran and John Warakowski. Their help in the initial phase of this research was greatly appreciated. More recently, the scientific vitality and personal wit that are a part of Joseph Schlenoff has contributed greatly to the professional enjoyment of working in GRC-608.

I wish to mention a friend and former colleague, Dr. Tsang J. Chen of the Eastman Kodak Research Laboratories. Because he had confidence in my work and my potential, the decision to come to graduate school was not at all difficult. Many thanks indeed.

The timely completion of this dissertation would not have been possible without the help of Monique Br  s and Gina Harnois. They both worked very hard and their efforts are greatly appreciated.

Lastly, but perhaps most importantly, I wish to note two very special classmates: John Reynolds and Barbara Wood. The years we spent in Amherst learning and growing together will continue to be a part of me for many, many years. May our deep friendship and our scientific collaboration prosper throughout the years!

ABSTRACT

POLYACETYLENE POLYMERIZATION, STRUCTURE AND ELECTRICAL TRANSPORT PROPERTIES

(February 1985)

Michael A. Schen, A.A.S., SUNY @ Alfred, Alfred, N. Y., 1975

B.S., Rochester Institute of Technology, Rochester, N. Y., 1980

Ph.D., University of Massachusetts, Amherst, MA, 1985

Directed by: Professor James C. W. Chien and
Professor Frank E. Karasz

The field of highly conducting polymeric charge-transfer complexes has focused principally on conjugated polymers with polyacetylene, $[CH]_x$, receiving the greatest attention. From an electrical transport properties view, much is known about polyacetylene. However, due to its insolubility and intractability, some of the most fundamental polymeric aspects of polyacetylene have not been addressed. The aim of this dissertation has been to elucidate the interrelationships which exist between polyacetylene molecular weight and the observed structural and electrical transport properties.

Polyacetylene was polymerized using the Ziegler-Natta catalyst $Ti(OBu)_4/Al(Et)_3$. Using radioactive ^{14}C -labeled carbon monoxide and carbon dioxide as "specific labels" and 3H -labeled methanol as a "non-specific label", the polymerization kinetics were fully elucidated. Simultaneously, the number-average molecular weight, \overline{M}_n , of $[CH]_x$ obtained under a wide range of reaction conditions have been determined.

With polymer samples from 500 to 870,000 \overline{M}_n obtainable, the importance of molecular weight with regard to polymer structure and magnetic and electrical properties was addressed. It was found that the fibrillar morphology was retained for all \overline{M}_n 's using this catalyst. Proper specimen washing using 10% HCl/CH₃OH was absolutely necessary. Infrared, EPR, and conductivity studies showed cis-trans isomerization to occur to greater completion and in shorter times with low \overline{M}_n polymer.

Undoped conductivities and thermoelectric power measurements indicated a relationship between the catalyst concentrations used for polymerization and undoped characteristics. EPR analysis showed no dependence of soliton concentration on \overline{M}_n . These results imply that three dimensional carrier motion controls the macroscopic conductivity and neutral soliton concentration in undoped polyacetylene.

Upon doping with 125-labeled iodine, for all molecular weights prepared, a sharp semiconductor-to-metal transition was observed. Highly conducting materials resulted. No strong differences in doped polymer properties were detected. Therefore one dimensional defects in the form of chain ends have no impact on the three dimensional electrical conduction within the \overline{M}_n range investigated.

TABLE OF CONTENTS

DEDICATION - - - - -	iv
ACKNOWLEDGEMENT - - - - -	v
ABSTRACT - - - - -	vii
CHAPTER	
I. INTRODUCTION - - - - -	1
Ziegler-Natta Polymerization of Olefins - - - - -	1
Mechanism of Ziegler-Natta Polymerization - - - - -	1
Polymerization Kinetics - - - - -	6
Polymer Growth and Morphology - - - - -	13
Polymerization of Acetylene - - - - -	17
Overview of Catalytic Systems - - - - -	17
Titanium Tetra-n-butoxide/Triethyl Aluminum Catalyzed Polymerization - - - - -	19
Polyacetylene Structure - - - - -	21
Nascent Morphology and Crystal Packing - - - - -	21
Molecular Weight - - - - -	30
Optical and Vibrational Spectroscopy - - - - -	31
Nuclear Magnetic Resonance - - - - -	34
Cis-Trans Isomerization - - - - -	34
Polyacetylene Transport Properties - - - - -	38
Neutral Solitions and Electron Paramagnetic Resonance - - - - -	38
Chemical and Electrochemical Doping - - - - -	41
Proposed Conduction Mechanisms - - - - -	45
Importance of This Research - - - - -	48
II. EXPERIMENTAL TECHNIQUES - - - - -	52
Handling Air Sensitive Materials - - - - -	52
Vacuum Lines - - - - -	52
Inert Gas Lines - - - - -	53
Schlenk Glassware - - - - -	53
Syringe Techniques - - - - -	54
Dry Box and Glove Bags - - - - -	54
Solvent Purification - - - - -	55
Acetylene Purification - - - - -	56
Handling Radioactive Compounds - - - - -	56
Safety Precautions - - - - -	56
Dilution, Transfer and Storage of $\text{CH}_3\text{O}^3\text{H}$ - - - - -	57
Dilution, Transfer and Storage of ^{14}CO and $^{14}\text{CO}_2$ - - - - -	58
Dilution, Transfer and Storage of $^{125}\text{I}_2$ - - - - -	62

II. EXPERIMENTAL TECHNIQUES (continued)

Polyacetylene Synthesis	- - - - -	64
Schlenk Tube Pop Bottle and Flat Bottomed Reactors	-	65
Catalyst Preparation	- - - - -	67
Monomer Solubility	- - - - -	68
Polymerizations for Kinetics Elucidation	- - - - -	69
Polymerization on Electron Microscopic Grids	- - -	71
Polymerizations to Obtain Ribbons and Oriented Films	- - - - -	72
Polymerizations to Obtain Films	- - - - -	72
Washing, Handling and Storage	- - - - -	74
Specific Activity and Elemental Analysis	- - - - -	75
Structural Characterization	- - - - -	76
Infra-Red Spectroscopy	- - - - -	76
Electron Microscopy	- - - - -	76
Electron Paramagnetic Resonance	- - - - -	76
Quantitative Determination of Unpaired Spins	- - -	77
Relaxation Measurements	- - - - -	78
Variable Temperature Experiments	- - - - -	79
Iodine Doping	- - - - -	79
Sample Preparation and Equipment	- - - - -	79
Slow Doping Procedure	- - - - -	80
Isotopic $^{125}\text{I}_2$ Doping and Assay	- - - - -	83
Transport Measurements	- - - - -	84
Conductivity Measuring Devices and Instruments	- -	84
Thermoelectric Power Apparatus and Measurements	- -	88

III. ACETYLENE POLYMERIZATION KINETICS AND MOLECULAR WEIGHT - - 90

Rate of Polymerization	- - - - -	90
Temperature Effects	- - - - -	93
Catalyst Cocatalyst Composition	- - - - -	93
Catalyst Concentration	- - - - -	102
Catalyst Aging	- - - - -	102
Monomer Pressure	- - - - -	102
Non-Specific Labeling Using $\text{CH}_3\text{O}^3\text{H}$	- - - - -	106
Insertion Kinetics	- - - - -	106
Polymerization Conditions and Number Average Molecular Weights	- - - - -	114
Metal-Polymer Bond Concentration	- - - - -	121
Specific Labeling of Polyacetylene Using ^{14}CO	- - - - -	123
Insertion Kinetics	- - - - -	123
Active Center Concentration	- - - - -	129
Specific Labeling of Polyacetylene Using $^{14}\text{CO}_2$	- - - - -	133
Insertion Kinetics	- - - - -	133
Active Center Concentration	- - - - -	135
High and Low Molecular Weight Polyacetylenes	- - - - -	135
Discussion	- - - - -	143

IV. STRUCTURAL CHARACTERIZATION	- - - - -	159
Elemental Analysis	- - - - -	159
C, H, O, Ti, and Al Results	- - - - -	159
Morphology	- - - - -	162
Nascent Morphology and Effect of Contaminants	- - - - -	162
Catalytic Activity and Micromorphology	- - - - -	167
Polymerization Conditions	- - - - -	167
Crystal Structure	- - - - -	174
Infrared Spectroscopy	- - - - -	175
Spectra of Pristine Polymer	- - - - -	175
Thermal Isomerization Kinetics and Trans Spectra	- - - - -	179
Perdeuterated Polyacetylene	- - - - -	190
Oxidized Polyacetylene	- - - - -	194
I ₂ Doped Spectra	- - - - -	195
Discussion	- - - - -	195
V. ELECTRON PARAMAGNETIC RESONANCE	- - - - -	200
Undoped Cis-Rich Polyacetylene	- - - - -	200
Quantitative EPR	- - - - -	200
Saturation and Relaxation Times	- - - - -	200
Cis-Trans Isomerization	- - - - -	204
Relative Spin Intensities	- - - - -	204
Peak-to-Peak Linewidths	- - - - -	207
Undoped Trans Polyacetylene	- - - - -	209
Effect of HCl/CH ₃ OH Washing	- - - - -	209
Quantitative EPR	- - - - -	209
Saturation and Relaxation Times	- - - - -	212
I ₂ Doped Cis-Low Molecular Weight Polyacetylene	- - - - -	219
Quantitative EPR	- - - - -	219
Saturation and Relaxation Times	- - - - -	223
Variable Temperature EPR	- - - - -	227
I ₂ Doped Trans-Low Molecular Weight Polyacetylene	- - - - -	231
Quantitative EPR	- - - - -	231
Saturation and Relaxation Times	- - - - -	234
Variable Temperature EPR	- - - - -	246
I ₂ Doped High Molecular Weight Polyacetylene	- - - - -	252
Quantitative EPR	- - - - -	252
Saturation and Relaxation Times	- - - - -	256
Discussion	- - - - -	260
VI. TRANSPORT PROPERTIES	- - - - -	263
Undoped Cis-Rich Polyacetylene	- - - - -	263
Room Temperature Conductivities	- - - - -	263
Cis-Trans Isomerization Kinetics	- - - - -	264

V. TRANSPORT PROPERTIES (continued)

Undoped Trans Polyacetylene - - - - -	274
Room Temperature Conductivity and Thermoelectric	
Power - - - - -	274
Variable Temperature Conductivity - - - - -	277
¹²⁵ I ₂ Doped Cis Low Molecular Weight Polyacetylene - - -	287
Room Temperature Conductivity and Thermoelectric	
Power Measurements - - - - -	287
¹²⁵ I ₂ Doped Trans Low Molecular Weight Polyacetylene - -	289
Room Temperature Conductivity and Thermoelectric	
Power Measurements - - - - -	289
¹²⁵ I ₂ Doped Trans High Molecular Weight Polyacetylene - -	293
Room Temperature Conductivity and Thermoelectric	
Power Measurements - - - - -	293
Discussion - - - - -	295

VII. FINAL CONCLUSIONS AND FUTURE WORK - - - - - 301

REFERENCES - - - - - 308

LIST OF TABLES

Table

1.1	Components of Ziegler-Natta Initiators	-	-	-	-	-	-	-	-	2
1.2	Unit-Cell Parameters for Cis-[CH] _x	-	-	-	-	-	-	-	-	26
1.3	Unit-Cell Parameters for Trans-[CH] _x	-	-	-	-	-	-	-	-	27
2.1	Specific Activity of CH ₃ O ³ H Reagents	-	-	-	-	-	-	-	-	59
3.1	Effect of Temperature on Acetylene Polymerization	-	-	-	-	-	-	-	-	100
3.2	Effect of Al/Ti Ratio on Acetylene Polymerization	-	-	-	-	-	-	-	-	103
3.3	Effect of Catalyst Concentration on Acetylene Polymerization	-	-	-	-	-	-	-	-	104
3.4	Effect of Catalyst Aging on Acetylene Polymerization	-	-	-	-	-	-	-	-	105
3.5	Effect of Monomer Pressure on Acetylene Polymerization	-	-	-	-	-	-	-	-	107
3.6	Comparison of ¹⁴ CO and ¹⁴ CO ₂ Labeling	-	-	-	-	-	-	-	-	138
3.7	Ideal Polymerization Conditions for LMnP and HMnP	-	-	-	-	-	-	-	-	139
3.8	Molecular Weight and Yield of Low Molecular Weight Powders and Films	-	-	-	-	-	-	-	-	141
3.9	Molecular Weight and Yield of High Molecular Weight Gels and Films	-	-	-	-	-	-	-	-	144
4.1	Direct Elemental Analysis Results	-	-	-	-	-	-	-	-	160
4.2	Mean Fibril Diameter versus Catalyst Aging	-	-	-	-	-	-	-	-	168
4.3	d-Spacings and Reflection Indices for Cis-Polyacetylene	-	-	-	-	-	-	-	-	176
4.4	d-Spacings and Reflection Indices for Trans- Polyacetylene	-	-	-	-	-	-	-	-	177
4.5	Unit-Cell Parameters	-	-	-	-	-	-	-	-	178
4.6	1010 cm ⁻¹ Peak Position and PWHH	-	-	-	-	-	-	-	-	192
5.1	Cis-[CH] _x EPR Spin Concentrations	-	-	-	-	-	-	-	-	202
5.2	Trans-[CH] _x EPR Spin Concentrations	-	-	-	-	-	-	-	-	211

5.3	Trans-[CH] _x EPR Relaxation Times - - - - -	213
5.4	Iodine Doped 500 \overline{M}_n Trans-[CH] _x EPR Relaxation Times - -	243
5.5	Iodine Doped 500 \overline{M}_n Trans-[CD] _x EPR Relaxation Times - -	244
5.6	Fractional Broadening of ΔH_{pp} from 298 to 133 K for Low Molecular Weight Polymers - - - - -	254
5.7	Iodine Doped 210,000 \overline{M}_n [CH] _x EPR Relaxation Times - - -	259
6.1	Undoped Cis-[CH] _x Conductivities - - - - -	265
6.2	Undoped Trans-[CH] _x Conductivities - - - - -	275
6.3	Predicted Temperature Dependence on Conductivity for Various Conduction Mechanisms - - - - -	278
6.4	Summary of Variable Temperature Conductivity Measurements - - - - -	286
6.5	Maximum Iodine Doped Trans 500 \overline{M}_n Polyacetylene Conductivities - - - - -	292

LIST OF FIGURES

Figure		
1.1(a)	Four Centered Olefin Insertion - - - - -	5
1.1(b)	Metallacyclic Mechanism - - - - -	5
1.2	Monometallic Polymerization of Acetylene - - - - -	7
1.3	Model of Nucleation of Polymer Chains From Catalytic Sites - - - - -	16
1.4	Polyacetylene Isomeric Configurations - - - - -	24
1.5	Cis-[CH] _x Crystalline Reflections - - - - -	28
1.6	Trans-[CH] _x Crystalline Reflections - - - - -	29
1.7	Polyacetylene (a) Neutral, (b) Negative, and (c) Positive Charged Solitons - - - - -	39
1.8	Soliton and Polaron (a) p-Type, (b) n-Type, and (c) Electrochemical Doping - - - - -	43
1.9	Polaron-Polaron Annihilation in Polyacetylene - - - - -	44
1.10	Bipolaron Hopping in Trans Polyacetylene - - - - -	49
2.1	¹⁴ CO Storage Bulb - - - - -	60
2.2	¹⁴ CO ₂ Storage Bulb - - - - -	61
2.3	¹²⁵ I ₂ Storage Bulb - - - - -	63
2.4	Flat Bottomed Reactor for Preparing High and Low Molecular Weight [CH] _x Films - - - - -	66
2.5	Acetylene Solubility in Toluene at 1 atm. Total Pressure - - - - -	70
2.6	Standard Reactor for Obtaining Polyacetylene Films - - - - -	73
2.7	Iodine Doping Apparatus - - - - -	81
2.8	¹²⁵ I ₂ Doping Apparatus - - - - -	82

2.9	Pressure Contact Four-Probe Isomerization Chamber - - - - -	87
3.1	Labeling Mechanistic Scheme for ^{14}CO , $^{14}\text{CO}_2$, and $\text{CH}_3\text{O}^3\text{H}$ - - - - -	91
3.2	Variation of (a) Polymer Yield and (b) [MPB] with Time of Polymerization at 298 K, Al/Ti = 4 - - - - -	94
3.3	Variation of (a) Polymer Yield and (b) [MPB] with Time of Polymerization at 195 K, Al/Ti = 4 - - - - -	95
3.4	Variation of (a) Polymer Yield and (b) [MPB] with Time of Polymerization at 298 K, Al/Ti = 10 - - - - -	97
3.5	Variation of (a) R_p and (b) k_p with Time of Polymerization from Fig. 3.2 - - - - -	98
3.6	Variation of (a) R_p and (b) k_p with Time of Polymerization from Fig. 3.3 - - - - -	99
3.7	Arrhenius Plot of the Relative Rate of Polymerization - - - - -	101
3.8	Rate of Incorporation of Tritium by the Reaction of CH_3OT^* with Metal Polymer Bonds - - - - -	108
3.9	Variation of Specific Activity of ^3H in Polyacetylene with the Amount of CH_3OT^* Added - - - - -	111
3.10	Variation of \bar{M}_n of $[\text{CH}]_x$ with Catalyst Concentration for Polymerization at 195 K and 460 torr of Acetylene - - - - -	115
3.11	Molecular Weight of Specimens Cut at Various Heights of the Polyacetylene Film and of the Polymer Gel - - - - -	117
3.12	Variation of \bar{M}_n with Temperature of Polymerization - - - - -	118
3.13	Variation of \bar{M}_n with Time of Polymerization at 195 K and 298 K - - - - -	120

3.14	Arrhenius Plot of [MPB]	- - - - -	122
3.15	Rate of Transfer versus Polymerization Time for Al/Ti = 4, 10	- - - - -	124
3.16	Rate of Incorporation of C*O in the Absence of Acetylene	- - - - -	126
3.17	Variation of ^{14}C Specific Activity in Polyacetylene with Quantity of C*O Added	- - - - -	128
3.18	Variation of (a) [C] and (b) \bar{M}_n with Time of Polymerization at 298 K, Al/Ti = 4	- - - - -	130
3.19	Variation of (a) [C] and (b) \bar{M}_n with Time of Polymerization at 195 K, Al/Ti = 4	- - - - -	131
3.20	Variation of (a) [C] and (b) \bar{M}_n with Time of Polymerization at 298 K, Al/Ti = 10	- - - - -	132
3.21	Rate of Incorporation of C*O ₂ in the Absence of Acetylene	- - - - -	134
3.22	Variation of ^{14}C Specific Activity Versus Quantity of C*O ₂ Added	- - - - -	137
3.23	Second-Order Kinetics Plot for the Termination of Low Activity C ₂ Sites at 298 K	- - - - -	147
3.24	Second-Order Kinetics Plot for the Termination of Low Activity C ₂ Sites at 195 K	- - - - -	148
3.25	Initial Variation of R_p with Time from Fig. 3.5	- - - - -	151
3.26	Initial Variation of R_p with Time from Fig. 3.6	- - - - -	152
3.27	Plot of R_p^{-1} versus Time During the Initial Period for Fig. 3.5	- - - - -	154
3.28	Plot of R_p^{-1} versus Time During the Initial Period for Fig. 3.6	- - - - -	155

4.1	TEM of Toluene Washed $[\text{CH}]_x$ Polymerized Using $[\text{Ti}]_0 = 1 \text{ mM}$	- - - - -	164
4.2	TEM of 10% $\text{HCl}/\text{CH}_3\text{OH}$ Washed $[\text{CH}]_x$ Polymerized Using $[\text{Ti}]_0 = 1 \text{ mM}$	- - - - -	165
4.3	Polymerization of Acetylene Under a Hydrodynamic Flow Field	- - - - -	170
4.4	SEM of Interwoven $[\text{CH}]_x$ Ribbons	- - - - -	171
4.5	TEM of Tightly Woven Two Dimensional Ribbons	- - - - -	172
4.6	TEM of Loosely Woven Ribbons	- - - - -	173
4.7	IR Spectra of Pristine $[\text{CH}]_x$ Films of Varying \overline{M}_n	- - - - -	181
4.8	Thermal Isomerization of 500 \overline{M}_n $[\text{CH}]_x$ at 423 K	- - - - -	184
4.9	Thermal Isomerization of 10,500 \overline{M}_n $[\text{CH}]_x$ at 423 K	- - - - -	186
4.10	Cis-Trans Isomerization Kinetics at 423 K for $[\text{CH}]_x$ of Varying \overline{M}_n	- - - - -	187
4.11	Thermal Isomerization of 500 \overline{M}_n $[\text{CH}]_x$ at 383 K	- - - - -	189
4.12	Trans Peak Position for 423 K Isomerized $[\text{CH}]_x$ of Varying \overline{M}_n	- - - - -	191
4.13	IR Spectra of Low \overline{M}_n Perdeuterated Polyacetylene	- - - - -	193
4.14	Unoxidized and Air Oxidized $[\text{CH}]_x$	- - - - -	196
5.1	Characteristic EPR Spectra of Cis-Rich and Thermally Isomerized Trans- $[\text{CH}]_x$	- - - - -	201
5.2	Cis- $[\text{CH}]_x$ Signal Amplitude Saturation Plots for LMnP Film and Powder	- - - - -	203
5.3	Increase in Spin Concentration With Isomerization Time for 500 \overline{M}_n $[\text{CH}]_x$	- - - - -	205
5.4	First-Order Kinetics Plot for the Formation of Unpaired Spins in 500 \overline{M}_n $[\text{CH}]_x$	- - - - -	206

5.5	Variation of EPR Linewidth with Isomerization Time - - - - -	208
5.6	EPR Signal Amplitude Saturation Curves at 298 K for Trans-[CH] _x - - - - -	215
5.7	Variation of EPR Linewidth at 298 K for Trans-[CH] _x of Varying \overline{M}_n - - - - -	217
5.8	Variation of Neutral Soliton Concentration in Cis-500 \overline{M}_n [CH] _x with (I ₃) ⁻ Doping - - - - -	221
5.9	Polaron Doping in Cis-[CH] _x and Subsequent Cis-Trans Isomerization - - - - -	222
5.10	Variation of EPR Linewidth of Cis LMnP with Iodine Level Concentration - - - - -	224
5.11	EPR Signal Saturation Plots of Iodine Doped Cis LMnP - - - - -	226
5.12	Temperature Dependence of Normalized Integrated EPR Signal Amplitude for Iodine Doped Cis LMnP - - - - -	228
5.13	Temperature Dependence of EPR Linewidth for Iodine Doped Cis LMnP - - - - -	230
5.14	Variation of Neutral Soliton Concentration with (I ₃) ⁻ Doping for Trans 500 \overline{M}_n [CH] _x - - - - -	233
5.15	EPR Signal Saturation Plots of Iodine Doped Trans LMnP - - - - -	236
5.16	EPR Signal Saturation Plots of Iodine Doped ca. 500 \overline{M}_n Trans [CD] _x - - - - -	238
5.17	Variation of EPR Linewidth with Microwave Power for Iodine Doped 500 \overline{M}_n Trans-[CH] _x - - - - -	240
5.18	Variation of EPR Linewidth with Microwave Power for Iodine Doped ca. 500 \overline{M}_n Trans-[CD] _x - - - - -	241
5.19	Variation of Zero-Power EPR Linewidth with Iodine Concentration for 500 \overline{M}_n Trans-[CH] _x - - - - -	242
5.20	Variation of Spin-Spin Relaxation Times, T ₂ , with Iodine Concentration for 500 \overline{M}_n Trans-[CH] _x - - - - -	245

5.21	Temperature Dependence of Normalized Integrated EPR Signal Amplitude for Iodine Doped 500 \overline{M}_n Trans-[CH] _x - - - - -	247
5.22	Continuation of Fig. 5.21 - - - - -	249
5.23	Temperature Dependence of Normalized Integrated EPR Signal Amplitude for Iodine Doped ca. 500 \overline{M}_n Trans-[CD] _x - - - - -	250
5.24	Variation of Curie Slope of Iodine Doped 500 \overline{M}_n Trans-[CH] _x - - - - -	251
5.25	Variation of EPR Linewidth with Temperature for Iodine Doped 500 \overline{M}_n Trans-[CH] _x - - - - -	253
5.26	Variation of (a) Absolute Spin Concentration in Iodine Doped 210,000 \overline{M}_n Trans-[CH] _x , and (b) Relative EPR Intensity in Iodine Doped 10,500 \overline{M}_n [CH] _x - - - - -	255
5.27	EPR Signal Saturation Plots of Iodine Doped 210,000 \overline{M}_n Trans-[CH] _x - - - - -	258
6.1	Conductivity Isomerization of 500 \overline{M}_n [CH] _x - - - - -	266
6.2	Conductivity Isomerization of 10,500 \overline{M}_n [CH] _x - - - - -	268
6.3	Conductivity Isomerization of 870,000 \overline{M}_n [CH] _x - - - - -	269
6.4	Arrhenius Plot of t_c for 500 \overline{M}_n , 10,500 \overline{M}_n , and 870,000 \overline{M}_n [CH] _x - - - - -	272
6.5	Log σ versus T^{-1} for 500 \overline{M}_n and 25,000 \overline{M}_n Trans-[CH] _x - - - - -	280
6.6	Log σ versus Log Temperature for 500 \overline{M}_n and 25,000 \overline{M}_n Trans-[CH] _x - - - - -	281
6.7	Log σ versus $T^{-1/4}$ for 500 \overline{M}_n and 25,000 \overline{M}_n Trans-[CH] _x - - - - -	283
6.8	Log σ versus $T^{-1/2}$ for 500 \overline{M}_n and 25,000 \overline{M}_n Trans-[CH] _x - - - - -	285
6.9	Log σ versus Log Fractional I_3^- Concentration for Cis 500 \overline{M}_n [CH] _x - - - - -	288
6.10	Log σ versus Log Fractional I_3^- Concentration for Trans 500 \overline{M}_n [CH] _x - - - - -	291

6.11	S versus $Y(I_3)^-$ for 500 \overline{M}_n Trans-[CH] $_x$ and [CD] $_x$	- - - - -	294
6.12	Log σ versus Log $Y(I_3)^-$ for Trans-[CH] $_x$ of 210,000 \overline{M}_n and 10,500 \overline{M}_n	- - - - -	296

CHAPTER I

INTRODUCTION

The field of organic charge-transfer (CT) conductors and specifically that of conducting polymers has rapidly exploded within the last ten years. Certainly the premier and most widely studied conducting polymer has been polyacetylene, $[\text{CH}]_x$. Recently, Chien¹ has published an extensive review of polyacetylene chemistry and physics. What follows though is an introduction into the preparation of $[\text{CH}]_x$, the physical and chemical structure of the undoped and doped polymer, and the observed transport properties of $[\text{CH}]_x$. A review of proposed conduction mechanisms for various dopant regimes is presented. Lastly, a brief insight will be presented outlining the significance of this dissertation research.

Ziegler-Natta Olefin Polymerization

Mechanism of Ziegler-Natta Polymerization

Ever since the initial discoveries of K. Ziegler and G. Natta, an ever increasing number of initiators of this type have been identified and studied. The common thread that runs throughout all of these compositions is the reaction of a Group I-III organometallic compound or hydride with different Group IV-VIII transition metals. Table 1.1 shows some of the different components which have been reported.² All of these materials are moisture sensitive.

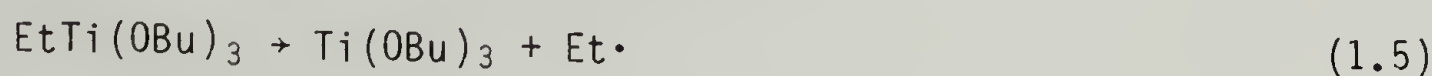
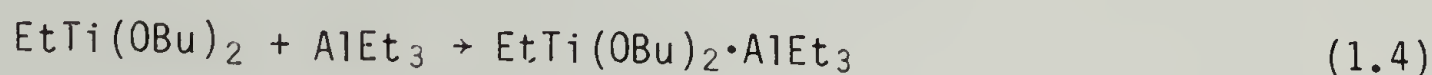
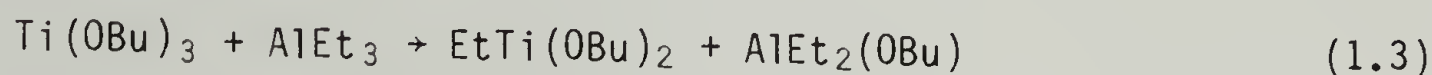
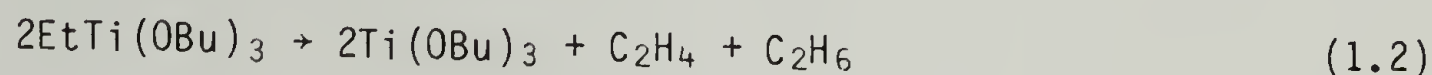
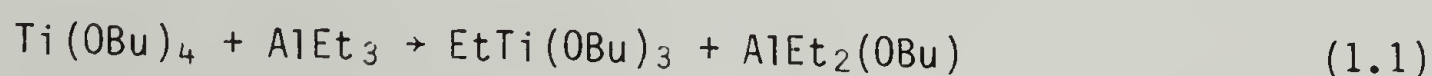
Upon mixing the transition metal "catalyst" with a Group I-III

Table 1.1

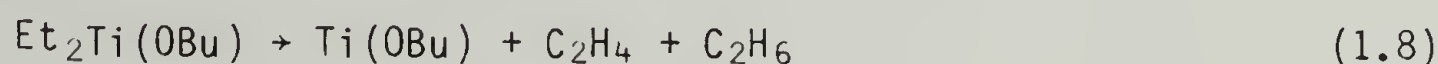
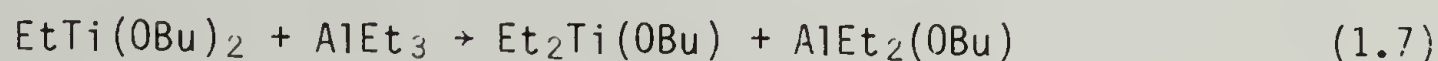
Components of Ziegler-Natta Initiators.

Group I-III Metal	Transition Metal
$(C_2H_5)_3Al$	$TiCl_4$
$(C_2H_5)_2AlCl$	$TiCl_3$
$(C_2H_5)_2AlBr$	VCl_4
$(C_2H_5)AlCl_2$	VCl_3
$(i-C_4H_9)_3Al$	$(C_2H_5)_2TiCl_2$
$(C_2H_5)_2Mg$	$Ti(OC_4H_9)_4$
C_4H_9Li	$MoCl_5$
$(C_2H_5)_2Zn$	$CrCl_3$
$\phi MgBr$	$ZrCl_4$
$(C_2H_5)_2Cd$	WCl_6
$(C_2H_5)_3Ga$	$MnCl_2$

"co-catalyst", a complex set of reactions take place, the extent of which depends upon the stochiometry. Generally, reduction of the transition metal is involved. In the case of the $\text{Ti}(\text{n-OC}_4\text{H}_9)_4/\text{Al}(\text{C}_2\text{H}_5)_3$ catalyst, the below set of reactions can be proposed



At surfeit ratios of Al/Ti, over reduction of titanium is possible giving catalytically inactive species.



Partly due to the complexity of the above reactions, the variety of catalyst-cocatalyst compositions, and also the types of monomers involved, not all mechanistic aspects of Ziegler-Natta polymerizations are known.³ Some points though have been established and are considered universal. The generally accepted mechanism for stereospecific Ziegler-Natta polymerization of non-polar and polar monomers involves two steps: π complexation of the monomer to the transition metal, followed by a coordinated insertion of the incoming monomer into the metal-carbon bond. The anionic nature of the polymer chain end seems

to have been established too. For example, it has been observed that the polymerization rate for α -olefins increases in the order ethylene > propylene > 1-butene. A reverse order would be expected if the incoming monomer was converted to the corresponding carbenium ion after insertion. Feldman and Perry⁴ have shown that when ethylene polymerization is terminated with $\text{CH}_3\text{O}^3\text{H}$, the polymer contained bound tritium. Also, hydrogen, as well as deuterium, act as transfer agents that lower molecular weight. When D_2 is used, bound deuterium is found in the polymer.⁵

Many mechanisms of primary carbon-carbon bond formation have been proposed. Figure 1.1(a) and 1.1(b) outline the traditional four-centered olefin insertion mechanism of Cossee and Arlman^{6,7} and the more recent metallacyclic proposal of Green et al.,⁸ respectively, as applied to acetylene polymerization.

Using NMR, recently Clarke and co-workers⁹ investigated this point for acetylene polymerization using $\text{Ti}(\text{OC}_4\text{H}_9)_4/\text{Al}(\text{C}_2\text{H}_5)_3$ catalyst. Their results show that the metallacycle mechanism is not operative but instead insertion by the four-centered insertion process occurs.

Within the framework of a four-centered insertion process, a number of structures have been proposed for the active Ziegler-Natta initiator species. The proposed active centers fall into one of two categories: a bimetallic or monometallic polymerization center. In the bimetallic mechanism, the active center occupies a site bridged between the titanium and aluminum atoms. The monomer is coordinated

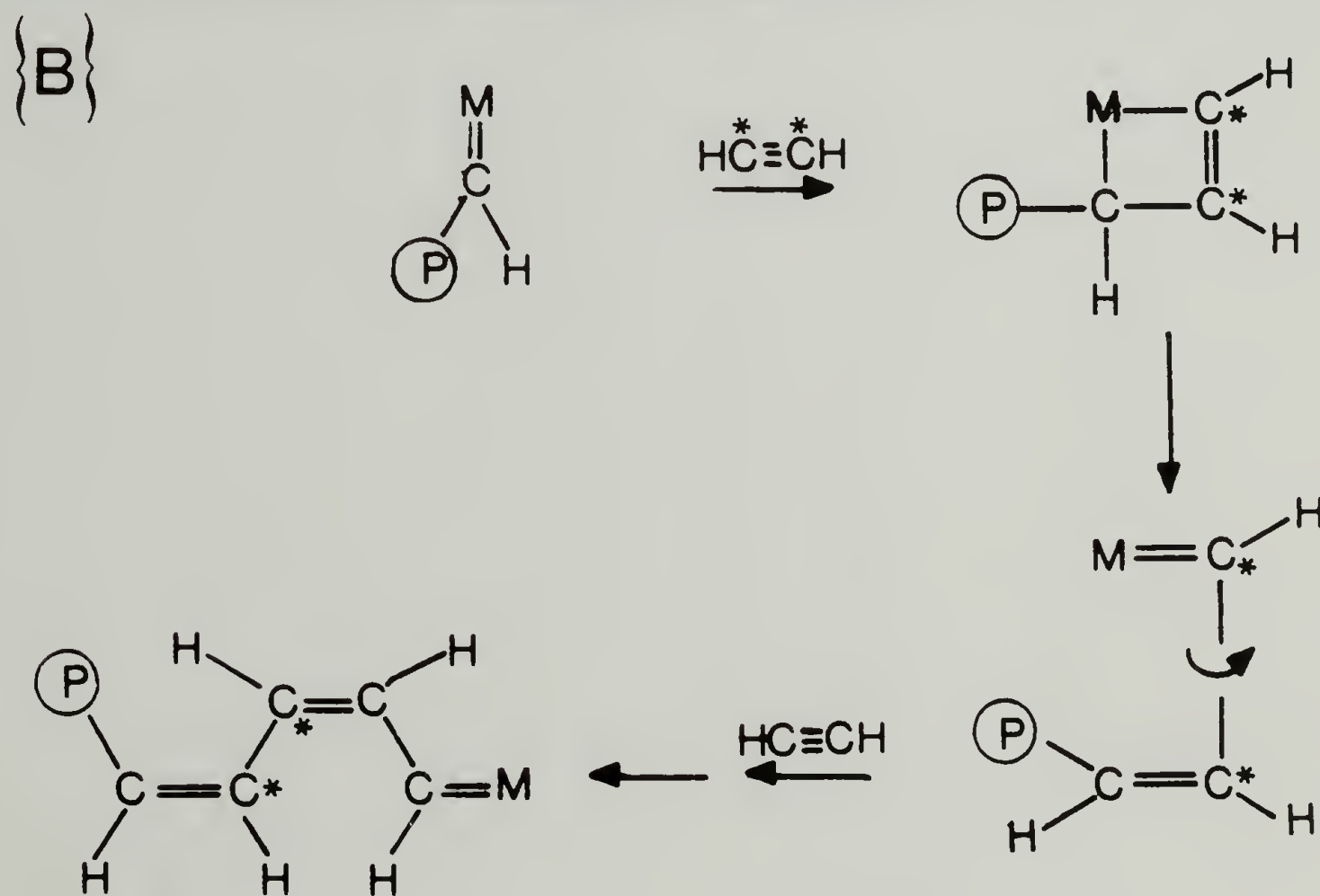
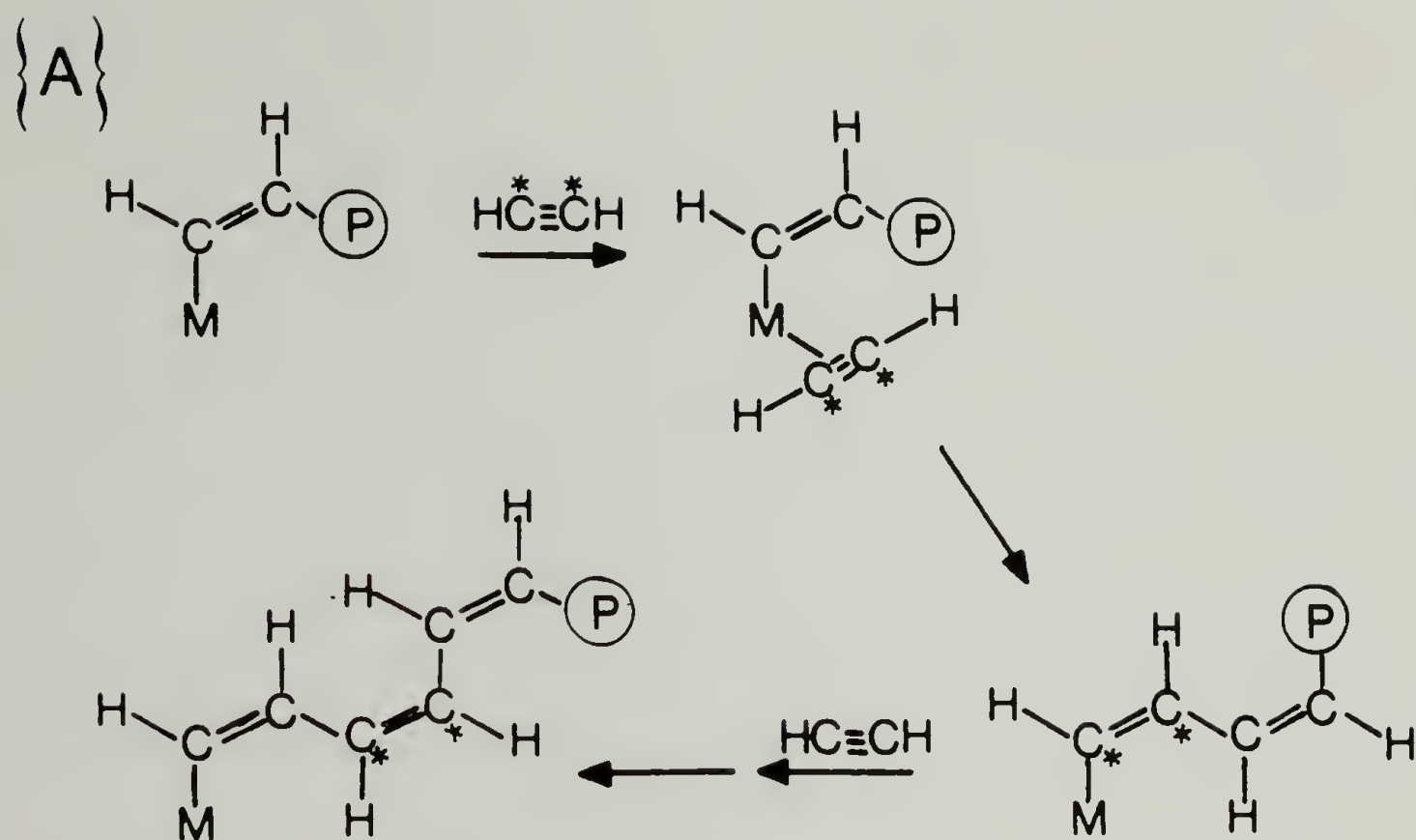


Figure 1.1 (a) Four Centered Olefin Insertion, (b) Metallacyclic Mechanism.

with the transition metal and the propagating chain end and then inserted into the polarized aluminum-carbon bond. The monometallic mechanism involves propagation at a single Ti atom as seen in Figure 1.2 for acetylene. The monomer is coordinated to the vacant orbital of the octahedral transition metal complex and then inserted into the polymer chain at the transition metal-carbon bond. Independent of the mechanism invoked, cis opening of the double or triple bond has been observed in the copolymerization of 1-d-propylene with perdeutero-propylene¹⁰ and in acetylene polymerization^{11,12} respectively.

Polymerization Kinetics

To say that the kinetics of Ziegler-Natta polymerizations are well understood and uncomplicated is at best a gross understatement. This is especially true with heterogeneous polymerizations which constitute the bulk of the more useful systems. The fundamental problem has been in the evaluation of such basic parameters as active-center stability and concentration, monomer concentration, and polymerization temperature at the growth center, to name a few. These points have been the focus of many reports.^{13,14,15}

As in all other addition polymerization mechanisms, a set of kinetically controlled sequences can be defined as seen in Equations 1.9 through 1.16. A number of kinetic models have been proposed based on these various steps, by Keii,¹⁶ Eirich and Mark,¹⁷ Reich and Schindler,¹⁸ and Burfield, McKenzie and Tait.¹⁹⁻²²

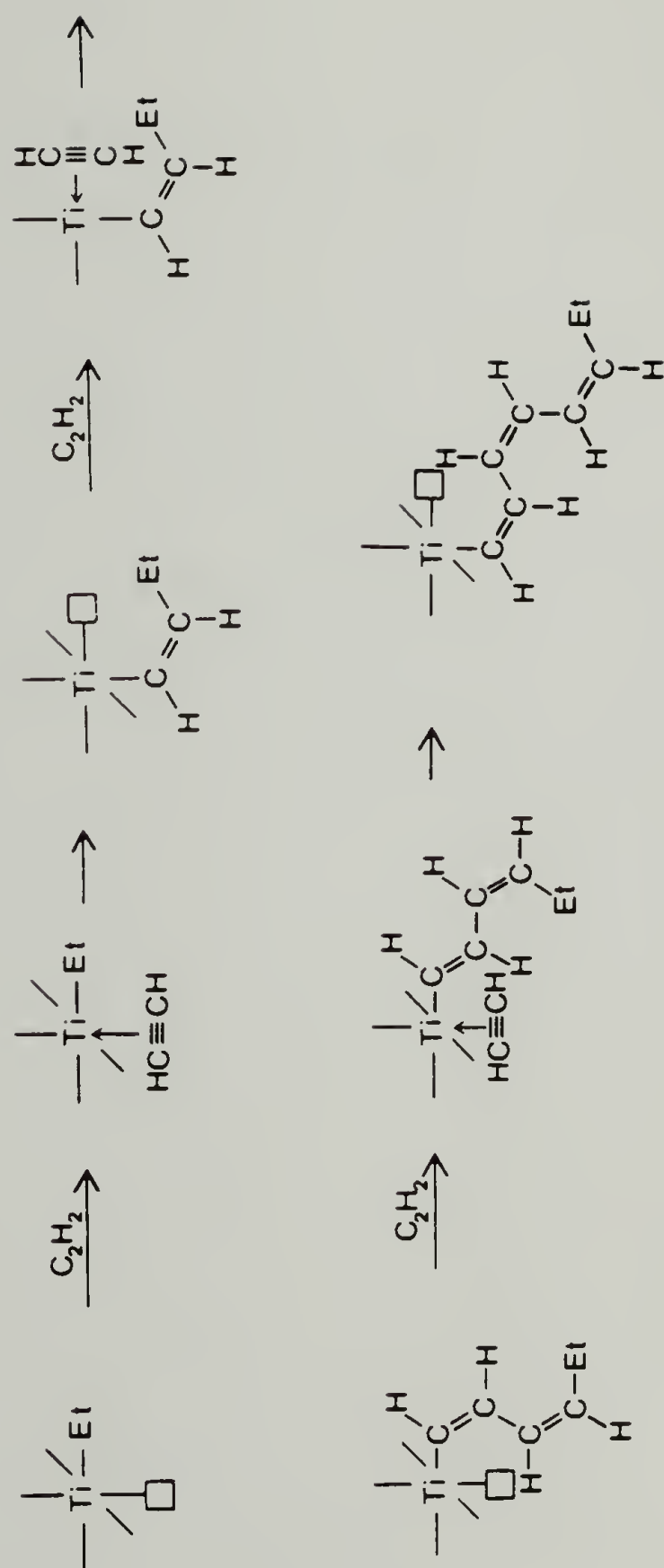
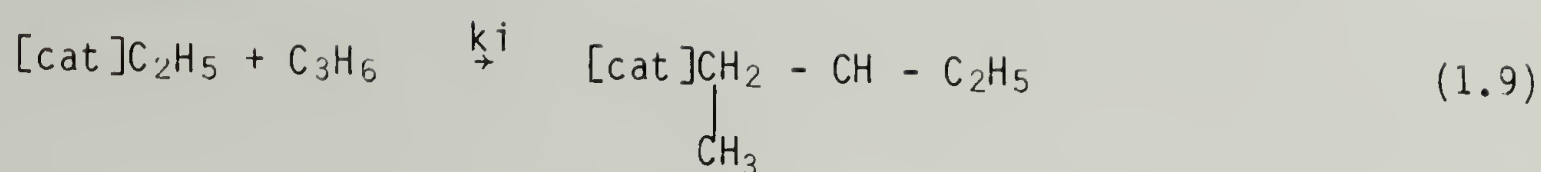
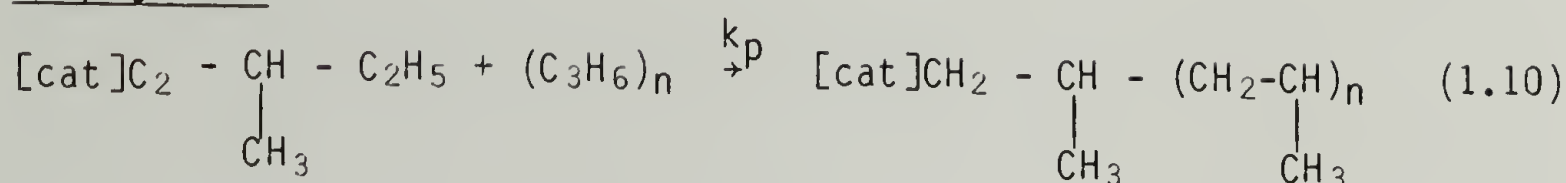
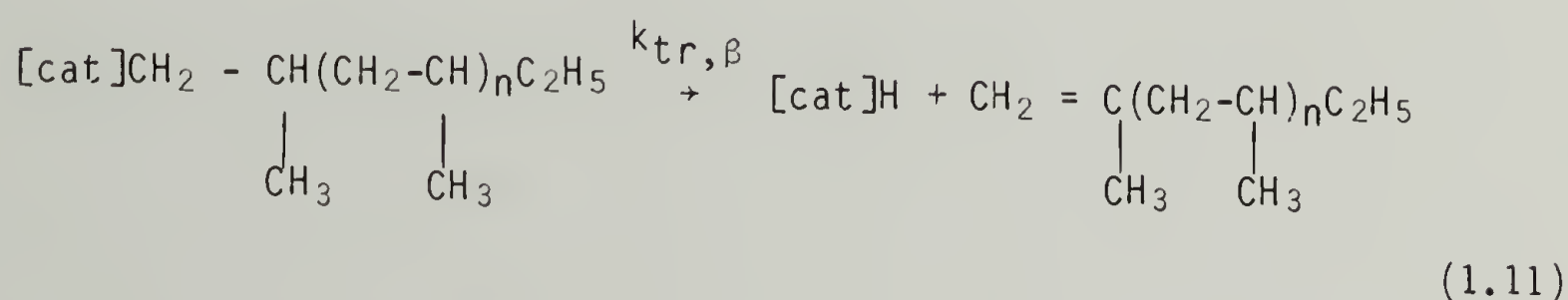
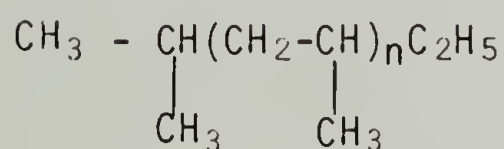
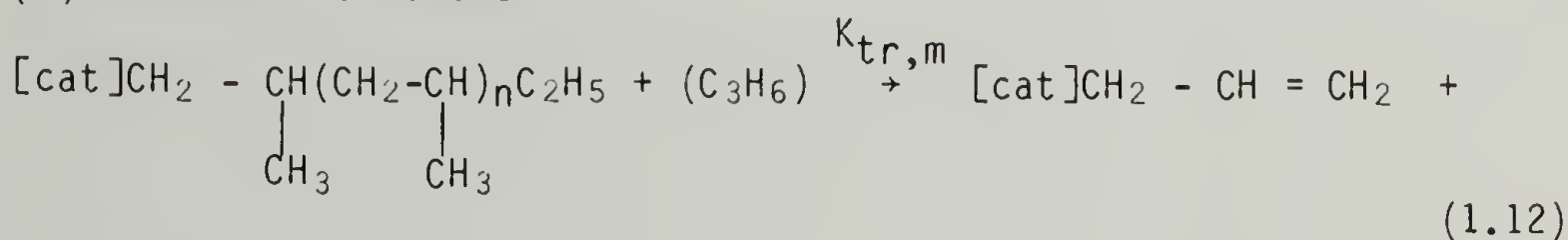


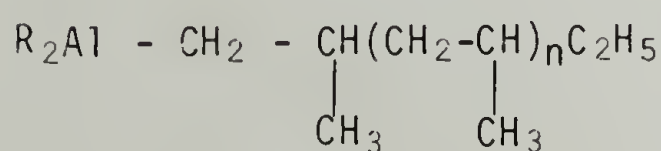
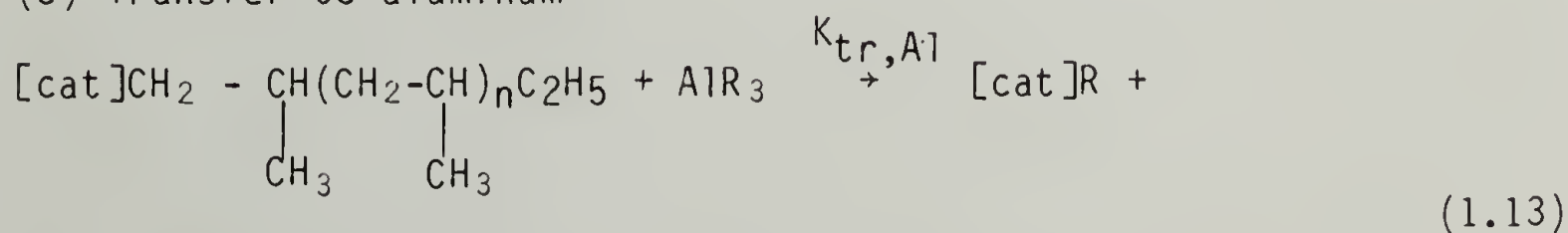
Figure 1.2 Monometallic Polymerization of Acetylene.

InitiationPropagationChain Transfer(a) Intramolecular β -hydride transfer

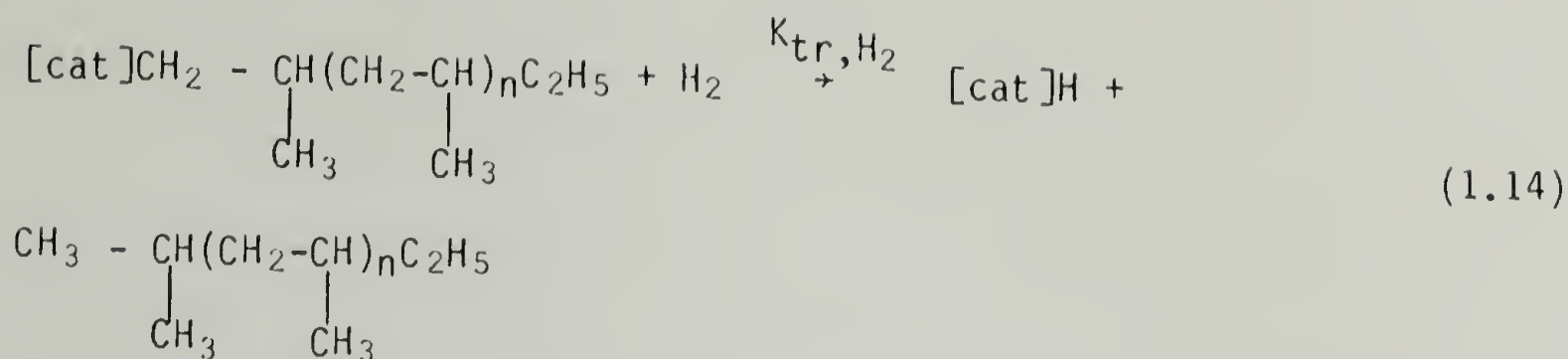
(b) Transfer to monomer



(c) Transfer to aluminum

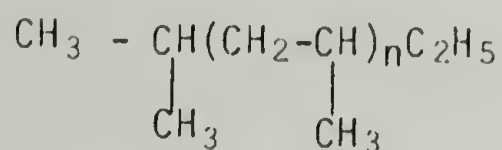
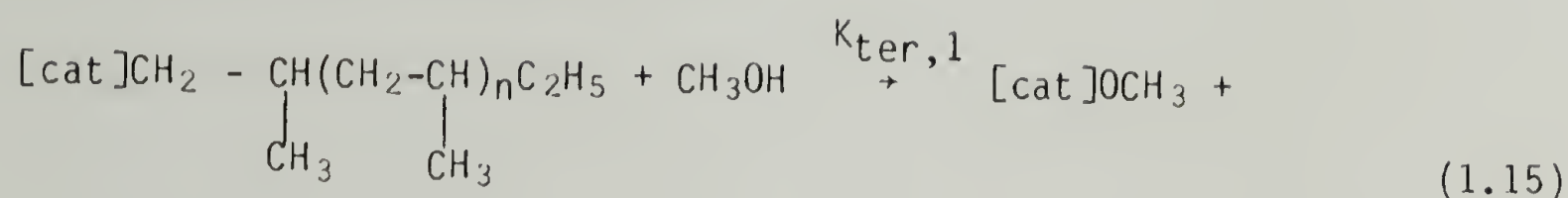


(d) Transfer by H_2

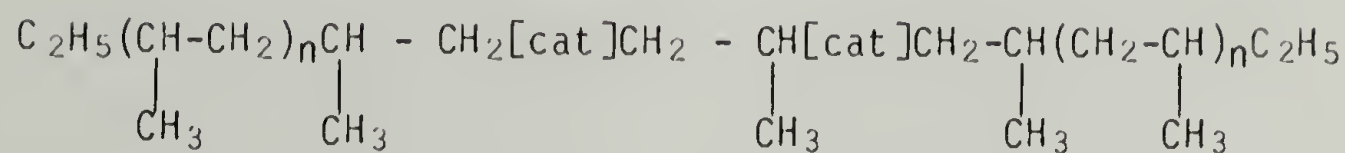
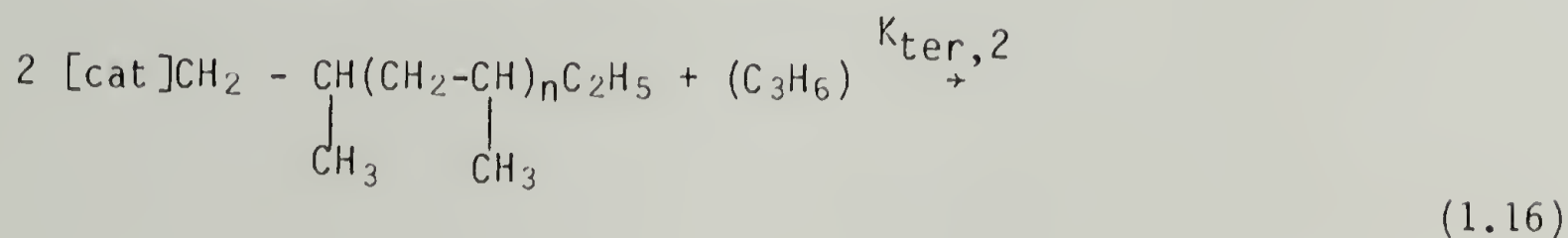


Chain Termination

(a) Termination with Lewis Acid



(b) Bimolecular termination with monomer

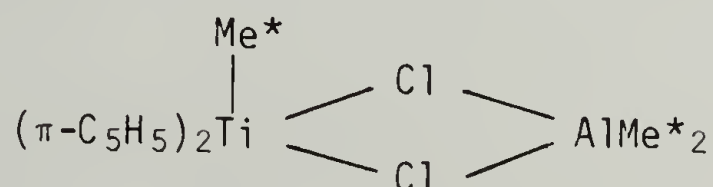


To obtain the rate constants for these various processes it is necessary to determine the rate of polymerization R_p , the concentration of active centers $[C]$, the total concentration of metal polymer bonds

(MPB) which are the polymer chains bound to Ti or Al, and the dependence of these quantities on various polymerization parameters.

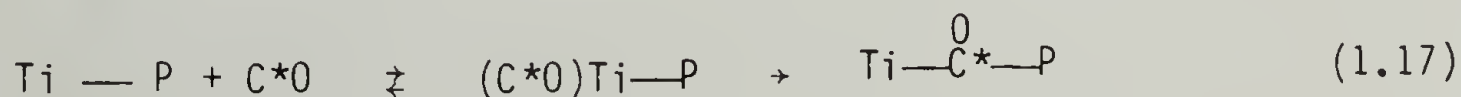
Principally, two different types of polymerization rate curves are seen: (a) a constant-rate type and, (b) decaying-rate type. With both, induction periods until maximum polymerization rate can vary from a few seconds to many minutes. In the heterogeneous $\text{AlEt}_3/\alpha\text{TiCl}_3$ propylene polymerization, Natta and Pasquon,¹⁵ attributed this build-up time to a number of possible sources: formation of active centers by the surface reaction of the metal alkyl and transition metal, monomer diffusion, or cleavage of catalyst particles thereby exposing new surfaces and allowing new centers to form. The decay in polymerization rate was attributed to a decrease in activity of the growth centers, irreversible termination of active centers, or monomer starvation within heterogeneous systems.

Kinetic investigations of olefin polymerization have in recent years relied heavily on the use of "non-specific" radiolabels such as $\text{CH}_3\text{O}^*\text{H}$ and "specific" radiolabels like $^*\text{CO}$ or $^*\text{CO}_2$. Molecular weight, \overline{M}_n and (MPB) concentration determinations by radioisotopic techniques have been established for Ziegler-Natta catalyst initiated olefin polymerizations. For instance, in ethylene polymerization by $(\pi\text{-C}_5\text{H}_5)_2\text{TiCl}_2/\text{AlMe}^*_2\text{Cl}$, a ^{14}C -labeled methyltitanium species



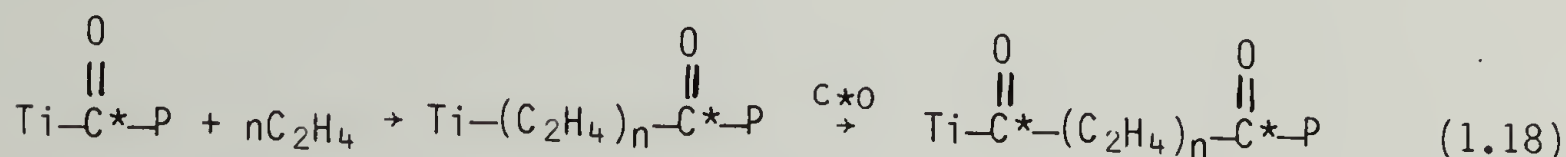
was formed, and polymerization proceeds via insertion of ethylene into the Ti-Me* bond. Quenching the polymerization with $^{131}\text{I}_2^*$ labeled the polyethylene chain with $^{131}\text{I}^*$ and/or $^{14}\text{C}^*$.²³ This elaborate double radiolabeling was employed to differentiate and quantify various chain-transfer and termination processes. The values of \overline{M}_n thus obtained were in agreement with values obtained by fractionation. Similarly, ^{14}C -labeled $\text{Al}(\text{C}^*_2\text{H}_5)_2\text{Cl}$ was synthesized and used to produce the active site $\text{TiCl}_2\text{C}^*_2\text{H}_5(\text{s})$, where (s) represents the surface of TiCl_3 crystallites. The values of \overline{M}_n for polypropylene obtained by radioassay and by fractionation were in excellent agreement.²⁴ Later Feldman and Perry⁴ used tritiated alcohol to quench ethylene polymerization using $\text{TiCl}_4\text{-AlR}_3$. A kinetic isotope effect, K_H/K_T was measured to be from 3.0-4.5. Molecular weights in agreement with GPC results and active-center concentrations were obtained.

^{14}C -labeled carbon monoxide was introduced by Zakharov and co-workers²⁵⁻²⁷ as a specific quenching agent for the active centers in Ziegler-Natta catalyzed polymerization of ethylene and propylene. These authors found that rapid incorporation of C^*O in the polyolefin after the first few minutes of contact time was followed by a steady increase in specific activity. The initial radiolabeling was attributed to the reaction

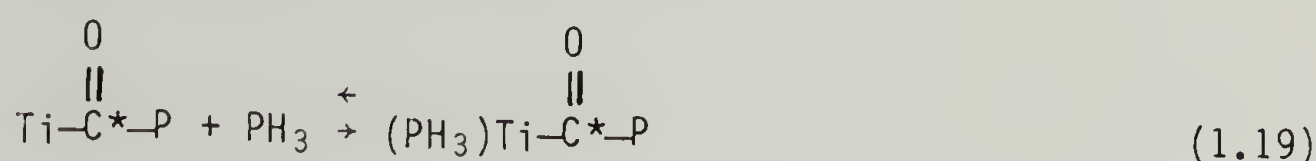


where P is a polymer chain. The subsequent increase in specific

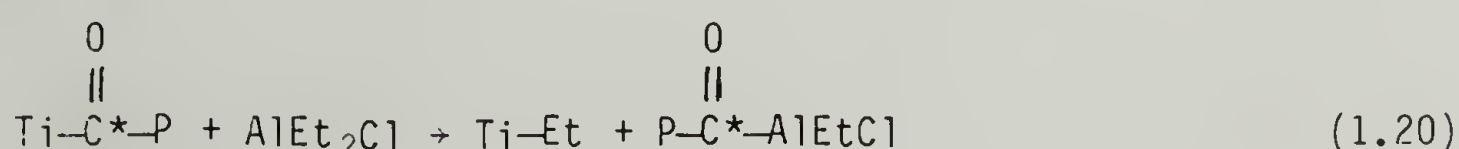
activity was first attributed to the reinsertion of monomer and copolymerization followed by insertion of additional C*O as illustrated for ethylene:



To inhibit copolymerization, phosphine was introduced to block the vacant coordination site of Ti. The phosphine was added a few minutes after the addition of C*O to prevent reaction (1.18).



Mejzlik and Lesna²⁸ showed that this method had severe drawbacks because reaction (1.17) is slow and almost completely reversible. Evacuation of CO-inhibited olefin polymerization recovered at least 80% of the initial polymerization rate when the monomer was reintroduced. The reversibility occurred even after 17 hr. of contact time for reaction (1.17). A further complication was encountered when the incorporation of C*O for ethylene polymerization initiated by TiCl₂ with and without AlEt₂Cl was compared.²⁹ The increase in ¹⁴C specific activity with time of reaction (1.17) is large in the presence of AlEt₂Cl, whereas the small increase in its absence suggested the following exchange reaction:



Reactions analogous to 1.17, 1.19, and 1.20 are involved when

*CO₂ is used. The advantage of course is that reaction (1.18) does not occur. Also, because *CO₂ is a weaker inhibitor than *CO, larger excesses are generally needed.

More recently Warzelhan and coworkers³⁰ have taken a closer look at the importance of reactions (1.18) and (1.20) in the ¹⁴CO and ¹⁴CO₂ labeling of polypropylene prepared from TiCl₃/0.3AlCl₃ and TiCl₃/0.3AlCl₃ + tributylphosphine. It was found that if monomer was evacuated and excess catalyst residues washed free, a constant ¹⁴CO or ¹⁴CO₂ was incorporated within five or eight hour reaction times respectively. Therefore, the validity of this technique seems to have been established if reactions 1.18 and 1.20 are prevented.

Polymer Growth and Morphology

The course of polymer growth during Ziegler-Natta polymerizations has been the focus of considerable effort. The focal point for any discussion must first start with the physical structure of the activated catalyst itself, i.e., is it a heterogeneous or homogeneous reaction. Typically, homogeneous catalysts are prepared with alkoxy substituted or cyclopentadienyl substituted transition metals and alkyl aluminums. Heterogeneous first generation and high mileage supported catalysts involve a transition metal chloride component.

The influence catalyst physical state, polymerization temperature and solvent have on the crystallization and interchain aggregation processes has been addressed by Wunderlich,³¹ St. John Manley and coworkers,^{32,33} Keller and Willmouth³⁴ and Chanzy and coworkers.³⁵

Wunderlich points out that crystallization before the polymerization is complete may be separated into two categories: simultaneous and successive polymerization-co-crystallization. Simultaneous polymerization-co-crystallization occurs when the primary covalent bonds and the secondary bonding (i.e., hydrogenbonding, dipole-dipole interactions, or Van der Waals forces) are set at the same time. Successive polymerization and crystallization processes occur when crystallization occurs somewhat later than polymerization, but before the polymer molecule is completely formed. In this case, one needs to consider the case in which the polymer molecule is polymerized in the dissolved or molten state before crystallization commences.

The question of intramacromolecular or intermacromolecular nucleation and crystal growth within a non-solvent was addressed for the polymerization of polyethylene by Georgiadis and St. John Manley.³³ Their results indicate that the nascent morphology was controlled principally by the physical state of the Ziegler-Natta catalyst. If a soluble catalyst was used, folded chain lamellae were always obtained. Whereas, if a heterogeneous catalyst was used, extended chain crystals and fiber formation resulted. The two crystal forms grow by different nucleation and crystallization mechanisms. In a homogeneous polymerization the active sites are molecularly dispersed. If each site generates one chain at a time, each polymer chain will intramolecularly nucleate and crystallize by a chain-folding mechanism. In heterogeneous systems, the active catalyst sites are within clusters. Thus polymer chains which grow from adjacent sites

have a common orientation and are in a favorable position to nucleate intermolecularly and form extended chain crystals (Fig. 1.3).

Keller, et al.³⁴ has pointed out that polyethylene particles which polymerize in solution can contain both types of crystals. The presence of clusters with sites of differing activities was proposed, in which case, unequal growth rates could result in shish-kabob, fibrillar or lamellae morphologies simultaneously.

The formation of polymer on heterogeneous catalyst surfaces and the influence of catalyst morphology on polymer macro-morphology was addressed by Rodriguez and Gabant,³⁶ Guttman and Guillet,³⁷ Hock³⁸ and Mackie et al.³⁹ Using electron microscopy, Rodriguez observed the formation of polypropylene on the spiral dislocations and surface defects of the αTiCl_3 crystal face. It is generally believed that the active centers are located on the lateral rather than the basal planes, or on natural defects of the TiCl_3 crystal. Guttman extended the polymerization of propylene and observed the evolution of the small mounds of polypropylene into hairlike protuberances. On a larger scale, Hock and Mackie found that regardless of the parent catalyst particle shape, the polymer particles were always replicas of them. For example, irregular, stringy, blocklike or nearly spherical particles yielded the corresponding macro polymer morphology. This discovery was very important since it allows commercial polyolefin producers to control the size, shape, density and texture of polymer particles.

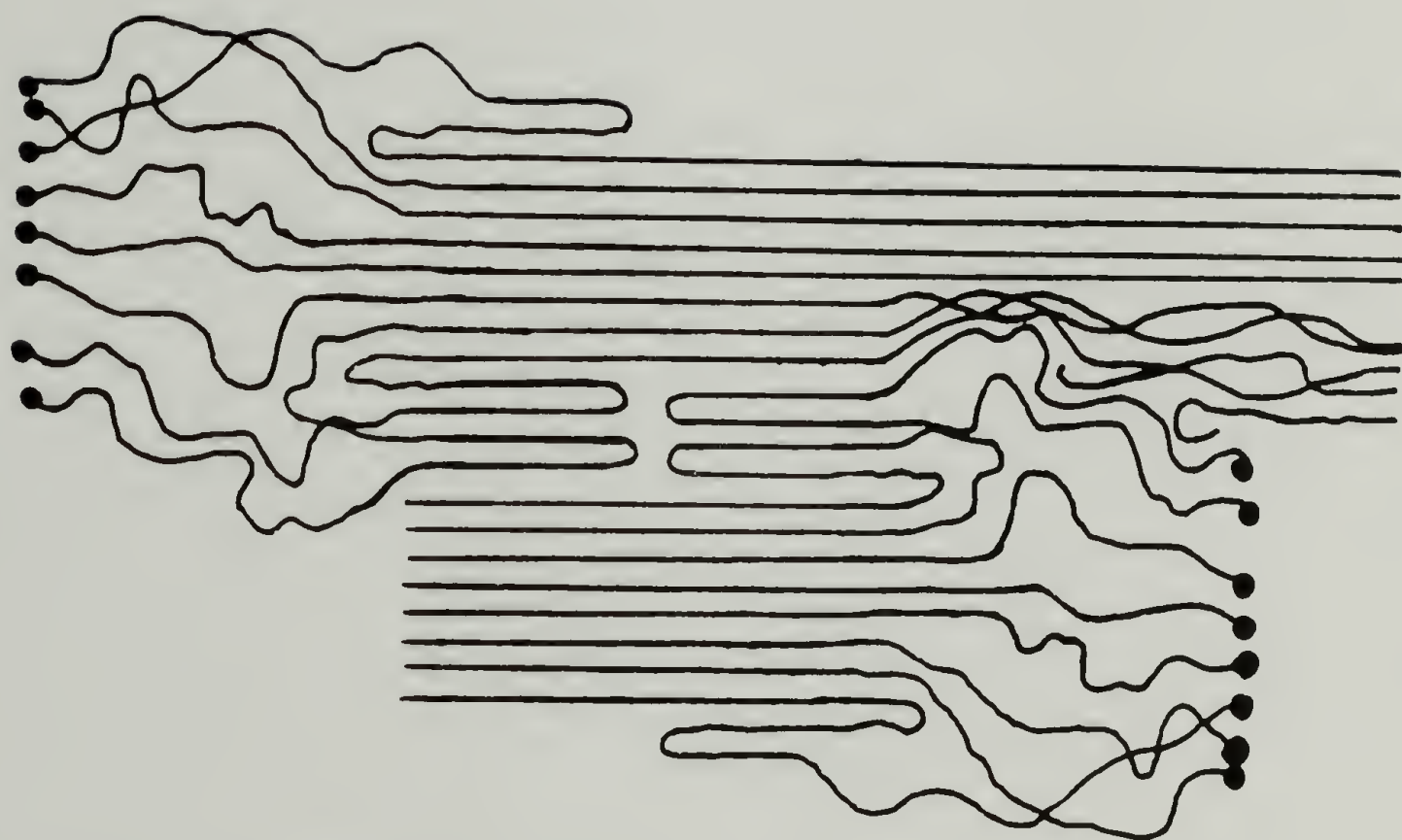


Figure 1.3 Model of Nucleation of Polymer Chains from Catalytic Centers.

Polymerization of Acetylene

Overview of Catalytic Systems

Acetylene was first polymerized using a $\text{Ti}(\text{OBu})_4/4\text{AlEt}_3$ catalyst system in 1958 by Natta and coworkers.⁴⁰ Since that time, a number of synthetic routes have been described. Using the $\text{Ti}(\text{OBu})_4/4\text{AlEt}_3$ catalyst, Shirakawa, et al.^{41,42} discovered that under quiescent conditions and using concentrated catalyst solutions, a film of polyacetylene formed on the catalyst surface during polymerization. Later Ito et al.^{43,44} found that thin films could be made by depositing a layer of viscous catalyst solution at 195 K on the reactor wall. Free-standing $[\text{CH}]_x$ films of controlled thickness could then be made. It is with this procedure that most research has been accomplished on polyacetylene.

Radiation induced polymerization in the solid and liquid state were reported by Tabata et al.⁴⁵ The polymer obtained in the solid state was mainly the trans isomer and that obtained in the liquid state was mainly cis. In both cases, polymer with very high sp^3 hybridized stretching were seen by IR and the films and solutions varied from yellow-orange to deep brown.

In 1964, Tsuchida and coworkers⁴⁶ reported complete dehydrohalogenation of polyvinyl chloride to form amorphous polyacetylene. Deits et al.⁴⁷ later reproduced this work and found that acid catalyzed autooxidation was a severe problem and that samples below 11-16% oxygen could not be obtained.

By using a $\text{TiCl}_4/\text{AlEt}_3$ based catalyst, and using various solvents

and polymerization temperatures, Hatano⁴⁸ in 1961 was able to prepare polyacetylene with varying degrees of crystallinity. Work by Harberkorn et al.⁴⁹ showed this polymer to also contain significant levels of sp^3 carbon atoms as evidenced by FTIR and ^{13}C MAS-NMR. The WAXS also show a strong diffuse scattering with but one rather weak and broad crystalline reflection.

In 1962, Luttinger⁵⁰ reported the use of sodium borohydride ($NaBH_4$) as a reducing agent along with hexahydro-cobaltous nitrate ($Co[NO_3]_2 \cdot 6H_2O$) to give linear, high molecular weight $[CH]_x$. These are generally prepared as powders. Films can be made by suspension deposition of powders. FTIR show this polymer to contain very little sp^3 carbons. Very little diffusive background and strong crystalline reflections in WAXS indicate this polymer to be highly crystalline.

More recently, metathesis type catalysts have been used. Voronkov⁵¹ reported the polymerization of acetylene in the presence of halides and oxohalides of molybdenum (Mo) and Tungsten (W). Aldissi et al.⁵² has extended that work to also include tetrabenzyl titanium $[Ti(Bz)_4]$.

A very interesting and exciting approach to preparing $[CH]_x$ has been taken by Edwards and Feast.⁵³ This route is based on the ring opening polymerization of 7,8-bis-(trifluoromethyl)-tricyclo-[4,2,2,0]-deka-3,7,9-triene (BTfM-TCDT), followed by elimination of o-hexafluorozylene. This synthetic route offers the advantages of obtaining a soluble, processable polymer intermediate, and later procuring a highly conducting film that shows minimal sp^3 hybridized carbon content.

Titanium Tetra-n-butoxide[Ti(Obu)₄]/Triethyl Aluminum [Al(Et)₃] Catalyzed Polymerization

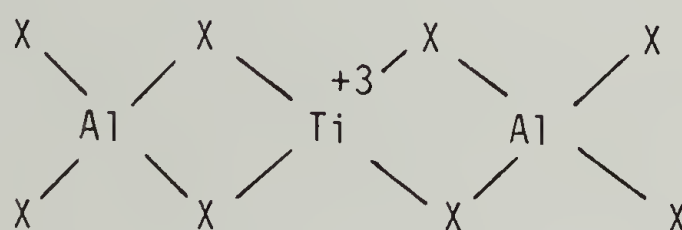
The preferred catalyst for acetylene polymerization is still the one first used by Natta et al.⁴⁰ which is Ti(n-Obu)₄/4AlEt₃ aged for 30 min. at 298 K. This catalyst system is still preferred by most workers because the film is mechanically strong, the cis-trans content can be controlled by varying the polymerization temperature, and virtually no benzene is produced.

The Ti(Obu)₄/AlEt₃ is a versatile catalyst and has been used to polymerize a number of monomers. Its ability to polymerize acetylene rapidly from 195 to 423 K is unusual among Ziegler-Natta catalysts which usually have a more limited polymerization temperature range for olefin monomers. The reaction between Ti(Obu)₄ and AlEt₃ results in the reduction of titanium to its lower oxidation states (Eqs. 1.1 thru 1.8). In the styrene polymerization Takeda et al.⁵⁴ found a fairly good correlation between the polymerization yield and the intensity of the Ti⁺³ EPR signal.

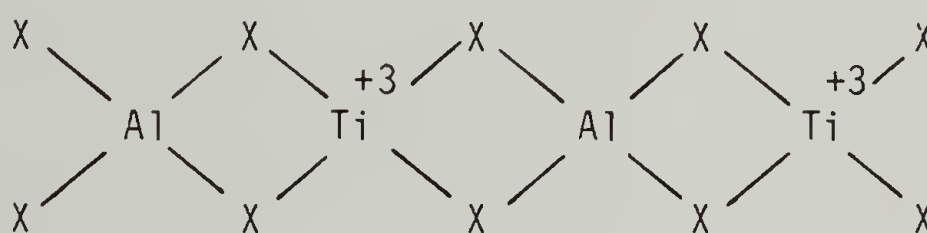
Hirai et al.⁵⁵ investigated the EPR spectra at Al/Ti ratios from 0.5-10.0 at room temperature and 195 K. Their results showed that the catalyst system yielded many kinds of titanium (III) compounds, depending on the Al/Ti ratio, reaction time, and temperature. They claim that two series of titanium (III) compounds exist at Al/Ti ratios smaller and larger than 2.9. Below a ratio of 2.9, three signals with g values of 1.960±0.002, 1.976, and 1.980 were seen. Above a ratio of 2.9, four signals with g of 1.934, 1.952, 1.966 and 1.979 were seen.

The signals of $g = 1.960 \pm 0.002$ and 1.952 showed 11 hyperfine lines. All catalysts showed a single signal with g of 1.951 at 195 K.

Chien and coworkers⁵⁶ more recently also have evaluated this catalyst. At 195 K the catalyst solution had four EPR signals with g values of 1.981, 1.978, 1.966 and 1.945. The last paramagnetic species was believed to be catalytically inactive. In the presence of monomer and at room temperature the $g = 1.966$ signal showed 11 hyperfine lines and it may have the structure



where X is either Et or OBu group. The $g = 1.981$ species exhibited 21 hyperfine lines and for various other considerations was attributed to have the structure



Because OBu is a better bridging ligand, it is likely to occupy those positions.

As mentioned previously, recent Nutation NMR results have shed light on the mechanism of acetylene polymerization using this catalyst.⁹ A four-center olefin insertion as proposed by Cossee and Arlman^{6,7} was shown to be operative.

Little had been reported regarding the kinetics of acetylene polymerization. Aldissi and coworkers⁵⁷ studied the polymerization by following the consumption of C_2H_2 over time. Two very major deficiencies exist in this work. First, acetylene gas was introduced into a quiescent 0.02 M $[Ti]_0$ solution. Consequently, when the polymerization starts, the short-time polymerization rate is limited by the speed at which acetylene is able to dissolve into the toluene. Secondly, because such large catalyst concentrations were used, films formed on the surface of the catalyst. Therefore, long-time polymerization rates were suppressed by macroscopic monomer diffusion.

As mentioned earlier, acetylene is usually polymerized to obtain films. Skirakawa⁵⁸ has shown that the macromorphology can be modulated from films to gels to powders by reducing the $[Ti]_0$ concentration. The micromorphology was observed to be a random fibrillar matrix independent of catalyst concentration. Highly oriented thin films of $[CH]_x$ were obtained by Meyer^{59,60} using a Couette-type polymerization vessel by imposing a shear flow during the polymerization. Films consisted of well aligned fibers which, when closely examined by TEM, closely resembled flat ribbons. Ribbons were very long but only 0.1-0.2 μm wide.

Polyacetylene Structure

Nascent Morphology and Crystal Packing

Because $[CH]_x$ is formed by a polymerization-simultaneous-crystallization process, the morphology of the polymer should depend on the physical nature of the catalyst system. For instance, different

catalysts or solvents may produce polymers with different morphologies. Intensive morphological studies using scanning electron microscopy and transmission electron microscopy have focused on two catalyst systems for acetylene polymerization: (1) Luttinger's catalyst by G. Wegner and coworkers, and (2) the Ziegler-Natta catalyst by J. C. W. Chien and coworkers.

When Ito et al.⁴³ first prepared free standing $[\text{CH}]_x$ films, they showed the material is composed of fibrils of ca. 20 nm in diameter. The highly reflecting side of the film facing the reactor wall has flattened fibrils, whereas the dull side of the film facing away from the wall is composed of a loose web of $[\text{CH}]_x$ fibrils. The fibrillar micro-morphology was observed to be independent of whether films, gels or powders were formed.

Polymerization directly on EM grids using the Ziegler-Natta catalyst was developed by Chien and coworkers⁶¹⁻⁶³ to investigate the nascent micromorphology of $[\text{CH}]_x$. Well defined and sometimes partly oriented microfibrils were observed. The fibrils have diameters of ca. 200 Å, though variations as a function of polymerization time have been seen.⁶⁴ The fibrillar morphology is not unique to $[\text{CH}]_x$ prepared with the Ziegler-Natta catalyst. Polymerization of α -olefins using Ziegler-Natta catalysts have been known to lead directly to crystalline polymers that precipitate from the solvent. Fibrillar morphologies were observed for polyethylene obtained with $\text{TiCl}_4\text{-AlEt}_3$ ⁶⁵ and also for polypropylene with the same catalyst.³⁷ Up until this dissertation research, little was known of the importance of washing techniques to

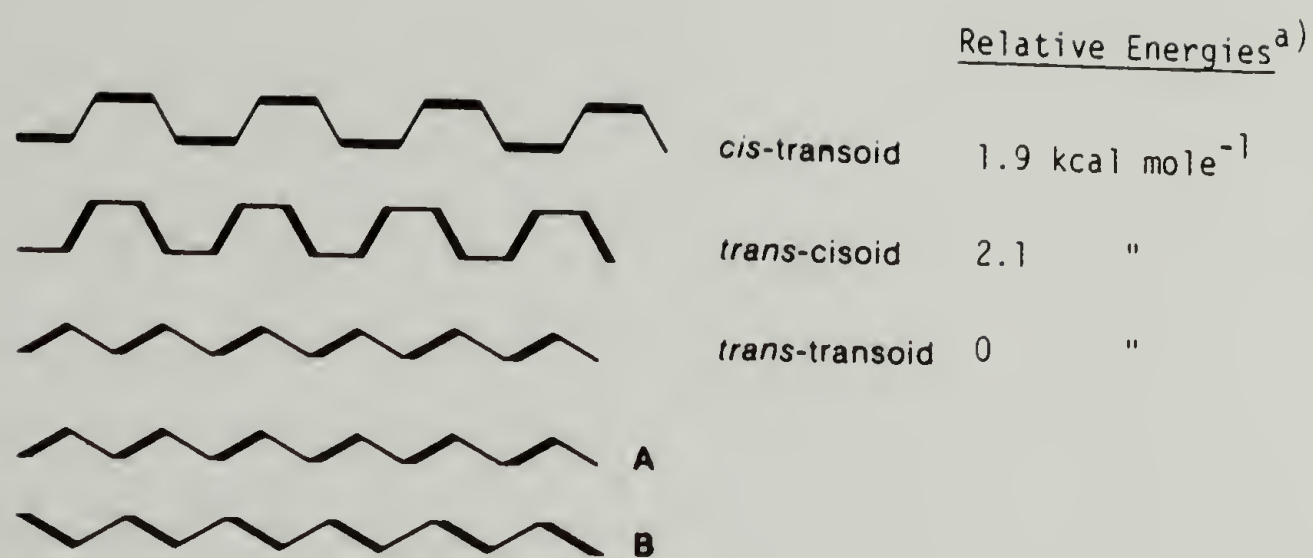
obtaining micrographs free of catalytic artifacts.

These results were disputed by Wegner and co-workers.⁶⁶⁻⁶⁹ In this work, $[\text{CH}]_x$ powders were prepared using both the Ziegler-Natta and Luttinger catalysts and scooped up onto EM grids from a suspension. Independent of the polymerization method, catalyst concentration, or catalyst type, they reported the same overall morphology was obtained. Samples "consist of irregularly shaped lamellar-like particles of typically of few hundred Å diameter and a thickness of 50-100 Å as the smallest discernible morphological subunit." The particles were said to aggregate to form loose networks or sponges in a pseudo-fibrillar arrangement.

The controversy over the two conflicting crystal types, ie. lamellae versus chain extended, was resolved by White, Bott and Weatherhead.⁷⁰ Using $[\text{CH}]_x$ from Luttinger and Ziegler-Natta catalyst, they observed a mat of randomly oriented fibrils. Combining electron diffraction, bright-field and dark-field observations, they concluded that the structural arrangement within the fibrils has the molecular chain axis aligned parallel to the fibril axis.

Four energetically nonequivalent backbone configurations have been envisioned for $[\text{CH}]_x$, three of which are shown in Fig. 1.4. The fourth, cis-cisoid, would take on a helical conformation and be of much higher energy. Only the cis-transoid and trans-transoid isomers have been observed.

The crystal structures of cis and trans $[\text{CH}]_x$ were evaluated within various laboratories using x-ray scattering of as-grown and



^{a)} Karpfen et al., Solid State Commun., 37, 179(1981).

Figure 1.4 Polyacetylene Isomeric Configurations.

stretch-aligned films⁷¹ and electron diffraction of scooped powders^{67,68} and thin films grown on grids.⁶¹⁻⁶³ Results have been summarized in Tables 1.2 and 1.3. A schematic representation of the observed diffraction pattern and reflection assignments for both cis and trans- $[\text{CH}]_x$ taken from Shimamura, et al.^{61,63} are shown in Figures 1.5 and 1.6.

It is seen that there are discrepancies in the crystal structures for $[\text{CH}]_x$. It has been suggested that $[\text{CH}]_x$ may exist in polymorphic forms.¹ Polyacetylene polymerization and crystallization takes place simultaneously. Therefore, the cis crystal structure may be influenced by the polymerization kinetics. In the case of trans $[\text{CH}]_x$, proper isomerization conditions are of the utmost importance.

X-ray and electron diffraction of alkali-metal and iodine doped $[\text{CH}]_x$ have also been reported by Baughman⁷² and Chien and coworkers⁶³ respectively. Baughman determined that alkali complexes were tetragonal, with the $[\text{CH}]_x$ chains forming a host lattice with the alkali metal ions present within channels. Lithium doped $[\text{CH}]_x$ was amorphous and postulated to be too small to stabilize the channel structure. Chien found that in iodine complexed polymer, at moderate levels of doping, reflections from both undoped and doped regions were observed. In the metallic regime, new reflections characteristic of the doped structure are only seen. From this, a model of linear I_3^- molecules arranged in a stage 1 intercalated structure was proposed.

Table 1.2
Unit Cell Parameters for *cis*-Polyacetylene

	E.D. ^a aligned fibrils	X-ray ^b randomly oriented film	E.D. ^c polymer suspension
Lattice type	Orthorhombic	Orthorhombic	Orthorhombic
<i>a</i> (Å)	7.68	7.61	7.74
<i>b</i> (Å)	4.46	4.47	4.32
<i>c</i> (Å)	4.38 ^d	4.39	4.47
ρ (g cm ⁻³)	1.15	1.16	1.16
C—C—C	125°	127°	
setting angle ϕ	32° ^e	59°	

^a Chien *et al.* (1982a,e).

^b Baughman *et al.* (1978) took the *b* to be along the molecular axis.

^c Lieser *et al.* (1980a).

^d Molecular chain axis and fiber axis.

^e Value for the *cis*-transoid structure.

Table 1.3
Unit Cell Parameters for *trans*-Polyacetylene

	E.D. ^a aligned fibrils	E.D. ^b Model I unoriented	E.D. ^b Model II	X-ray ^c
Lattice type	"Orthorhombic" ^d	Orthorhombic	Monoclinic $\gamma = 98^\circ$	Monoclinic $\beta = 91-93^\circ$
$a(\text{\AA})$	7.32	5.62	3.73	4.24
$b(\text{\AA})$	4.24	4.92	3.73	7.32
$c(\text{\AA})$	2.46	2.59	2.44	2.46
$\rho(\text{g cm}^{-3})$	1.13	1.20	1.27	
C—C—C angle	122°	135°	120°	
Setting angle ϕ	24–28°			55°

^a Shimamura *et al.* (1981).

^b Lieser *et al.* (1980b).

^c Fincher *et al.* (1982).

^d Approximate lattice type.

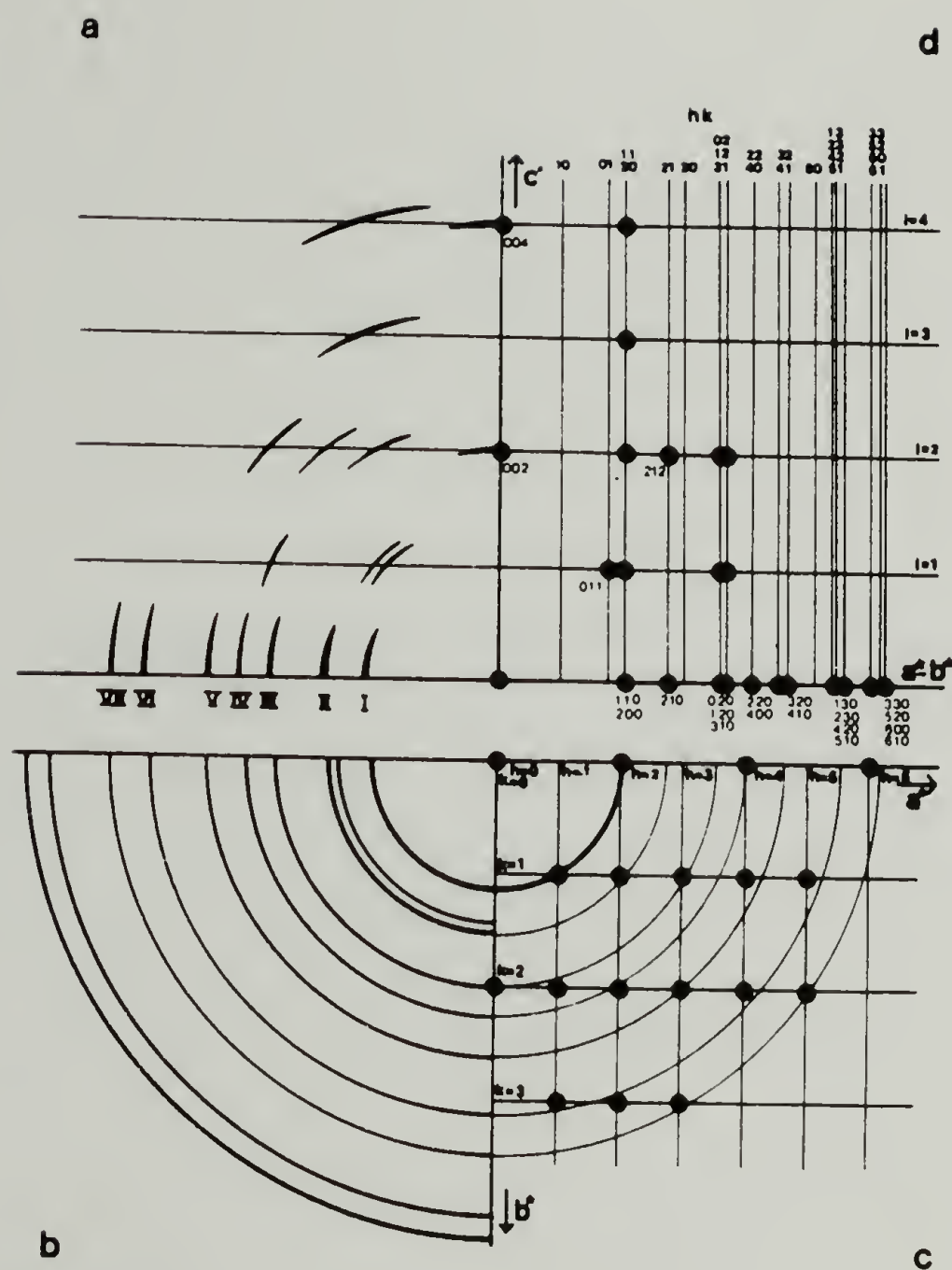


Figure 1.5
 Cis- polyacetylene: (a) electron diffraction of oriented fibrils; (b) Debye rings of randomly packed fibrils; (c) lattice for the a^*b^* plane; (d) reciprocal lattice projection of the first five a^*b^* planes.

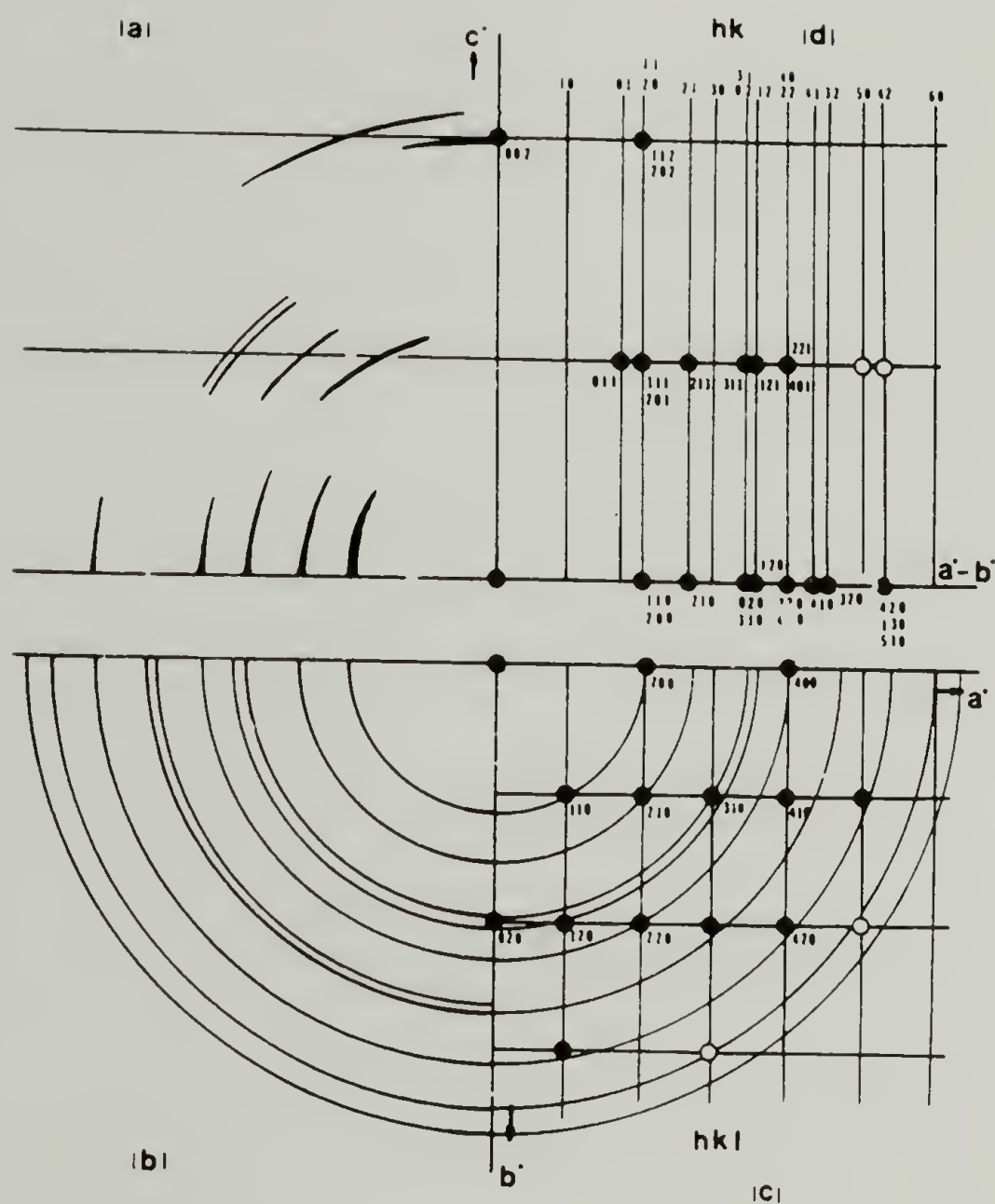


Figure 1.6
 Trans- polyacetylene: (a) electron diffraction of oriented fibrils; (b) Debye rings of randomly packed fibrils; (c) lattice for the a^*b^* plane; (d) reciprocal lattice projection for the first five a^*b^* planes.

Molecular Weight

Prior to this dissertation research, two existing estimations of polyacetylene molecular weights were reported, both based on indirect determination by polymer derivatization. Because polyacetylene is insoluble and intractable other more conventional techniques can not be applied.

In 1980, Shirakawa and co-workers⁷³ demonstrated that Na-doped $[\text{CH}]_x$ can be hydrogenated at elevated temperatures and pressures. About 60% of the product was soluble in refluxing tetralin. Infrared examination showed the polymer to be polyethylene-like but contained a detectable amount of isolated trans C=C bond vibrations at 965 cm^{-1} . Also, when hydrogenated at 470K, the $[\text{CH}]_x$ film retained the initial shape which may indicate partial crosslinking of the polyacetylene and/or hydrogenated polymer. The GPC determined \overline{M}_n was ca. 6200 with $\overline{M}_w/\overline{M}_n=2.44$.

In 1981, Enkelmann et al.⁷⁴ reported the chlorination of Luttinger and Ziegler-Natta polymerized $[\text{CH}]_x$. They reported that when $[\text{CH}]_x$ was prepared with the Luttinger catalyst at $\leq 243\text{K}$ and chlorinated immediately thereafter, a completely soluble, chlorinated polymer with a GPC \overline{M}_n value of 5900 was obtained. After storage at 243K for two hours, an insoluble fraction was obtained and the GPC \overline{M}_n of the soluble fraction rose to 9100. Ziegler-Natta prepared films had a \overline{M}_n of ca. 12,000 after sixteen hour storage.

Both of these reports suffer from a common deficiency. That is: (1) they are based on post polymerization handling, and (2) they do not lend themselves to routine determinations.

Optical and Vibrational Spectroscopy

Fincher et al.⁷⁵ reported the near infrared-visible absorption spectra for undoped cis and trans-[CH]_x. In the cis isomer, the absorption begins gradually, rising sharply between 1.8 and 1.9 eV. The first absorption maximum occurs at 2.1 eV followed by two others at 2.3 and 2.4 eV. The intrinsic optical π - π^* transition is taken as 1.8 eV. The intrinsic absorption edge for trans-[CH]_x is shifted to lower energies, with the absorption beginning slowly at 1.0 eV, rising sharply at 1.4 eV, and peaking at 1.9 eV. Therefore, for trans-[CH]_x, valance band to conduction band transitions occur at 1.4 eV.

Upon exposure to iodine, Fincher et al.⁷⁶ also noticed a small decrease in the interband transition maximum and the appearance of a new absorption at ca. 0.7 eV. Suzuki et al.⁷⁷ recorded the spectra for AsF₅ doped polymer and observed a steady increase of the 0.7 eV band. This has been taken as the midgap state in which electrons are excited upon doping and lies halfway within the bandgap. The population of these states can therefore be followed by the measured intensity of the midgap transition.

Recently Baker⁷⁸ reported photothermal reflection spectroscopy (PRS) absorption spectra from 0.6 to 2.1 eV for cis and trans-[CH]_x. He concluded that the number of charged defects does not change with isomerization based on the absorption intensity at 0.7 eV and that the population of charged impurities diminishes by a factor of 50 after compensation with NH₃. Lastly, he speculates that the source of adven-

titious doping to be some organo metallic species derived from the catalyst solution.

There have been several studies of the Resonance Raman spectra of $[\text{CH}]_x$.^{42,79-83} There are two strong resonance bands for the trans polymer and three for the cis. In the cis isomer, sharp, intense resonances appear at 915 cm^{-1} , 1252 cm^{-1} , and 1544 cm^{-1} . Once isomerized, intense but rather disperse peaks appear at $1090\text{--}1120\text{ cm}^{-1}$ and $1470\text{--}1520\text{ cm}^{-1}$. A weak, broad peak appears at 1008 cm^{-1} . The intense Raman bands are due to the resonance enhancement effect when the exciting frequency approaches or enters the $\pi\text{--}\pi^*$ electronic transition absorption band. A controversial aspect of the Raman work has been the long wavelength dispersion effect in trans polyacetylene with increasing excitation frequency. There are concomitant increases in bandwidths and the bands show two or even three maxima. This dispersion anomaly is sample dependent.⁸⁰ Samples subjected to longer air exposure or prepared under non-ideal isomerization conditions show Raman profiles that are shifted increasingly to higher frequencies.

One interpretation given to the dispersion anomalies for trans- $[\text{CH}]_x$ is that shorter conjugation lengths have higher vibrational frequencies and are excited at higher photon energies.^{82,83} Estimates were made of conjugation lengths based on a distribution of the sum of two log normal distributions with maxima at $n=5$ and 40 . A similar approach has been recently used by Furukawa et al.⁸⁴ on partially hydrogenated trans- $[\text{CH}]_x$.

An alternative interpretation has been taken by Mele,⁸⁵ and Mele and

Rice.⁸⁶ They propose that the frequency-dependent Raman line shapes are due to hot luminescence in very long trans polymer chains.

"Satellite" lines in the Raman spectra result as a consequence of relaxation processes.

Infrared spectra of undoped poly(C₂H₂), (C₂D₂), poly(C₂H₂)-co-(C₂D₂) and poly(C₂H₂)-co-(C₂HD)-co-(C₂D₂) were taken by Shirakawa et al.⁴¹ along with vibrational mode peak assignments. From this work cis/trans ratios were extracted based on the cis and trans B_{2u} out of plane deformation peaks at 740 cm⁻¹ and 1015 cm⁻¹ respectively.

Similar frequency results were later published by Haberkorn et al.⁴⁹

Upon chemical doping, two newly infrared-active vibrational modes appear centered at ca. 900 cm⁻¹ and 1370 cm⁻¹.⁷⁵ The appearance and position of these peaks are insensitive to dopant species. Cis and trans [CH]_x doped with AsF₅,⁷⁵ I₂,⁷⁵ HF,⁸⁷ and Na⁷⁵ spectra have been recorded. In highly doped polymer, the population of charged carriers within the midgap state results in a featureless highly absorbing spectra. There have been many theories proposed to account for these observations. Mele and Rice⁸⁸ and Etemad et al.⁸⁹ believe the bands arise from the presence of charged solutions. Rabolt et al.⁹⁰ explained the spectra according to a vibronic intensity enhancement of Raman active bands by the dopant. In [CH]_x, the Raman band at 1385 cm⁻¹ was said to be weakened by the electron transfer of the dopant molecule, and coupling of the charge oscillation along the [CH]_x chain with the skeletal stretching of the backbone makes it IR active.

Nuclear Magnetic Resonance (NMR)

Natural abundance ^{13}C -MAS NMR spectra of cis and trans $[\text{CH}]_x$ with and without cross polarization have been recorded by several groups.⁹¹⁻⁹⁴ The trans chemical shift is 136-139 ppm upfield from TMS and the shift for cis is 126-129 ppm. Mehring et al.⁹³ and Teras et al.⁹⁴ both present the principle chemical shift tensor elements, T_{11} , T_{22} , T_{33} as well as the isotropic average, T_{iso} . Considerable disagreement exists. Terao et al.⁹⁴ also report for 30%- ^{13}C enriched $[\text{CH}]_x$ a resonance at ca. 47 ppm upfield of TMS. This they account to methylene sp^3 hybridized carbon centers and represent ca. 3.4 mol. percent.

Using ^{13}C -enriched C_2H_2 , ^{13}C -Nutation NMR of cis and trans $[\text{CH}]_x$ was reported by Yannoni and Clarke⁹⁵ to obtain directly the carbon-carbon bond lengths. Their results indicate: (1) the double bond length in cis polymer is $1.37 \pm 0.01 \text{ \AA}$, (2) spectra for trans polymer exhibit two bond lengths, 1.36 ± 0.01 and $1.44 \pm 0.01 \text{ \AA}$ for the double and single bonds respectively, and (3) over the temperature range of 4.2-300K, the trans spectra show no direct evidence of the dynamical interchange of double and single bonds predicted to occur as a result of rapid motion of neutral soliton defects.

Cis-Trans Isomerization

When acetylene is polymerized, the cis-transoid configuration is favored due to a cis opening of the triple bond^{6,9}. This is thermodynamically unstable and converts to the trans-transoid structure

given sufficient energy. Calculations by Karpfen et al.⁹⁶ predict a minimum configurational energy state for the trans-transoid structure.

When polymerized at 195 K, a nearly defect free cis configuration is formed as evidenced by a signal free EPR spectrum at $g=2.0026$. Neutral defects in the form of soliton-antisoliton pairs can form, however, by the interchange of adjacent single and double bonds.⁹⁷ The neutral defects, or solitons, \dot{S} , do not diffuse apart because as the defect moves, it converts cis-transoid units to the trans-cisoid structure; a thermodynamically unstable state. Recombination can be either radiative or nonradiative at room temperature. Luminescence is always observed at low temperatures.⁹⁸

Upon heating, cis polyacetylene isomerizes from the cis-transoid to the trans-transoid form (Fig. 1.4). Yamabe et al.^{99,100} has performed MINDO/3 calculations on this process and found the energy barrier for bond rotation of one cis-transoid monomer unit by 180° to be ca. 1 eV. This model has been criticized since it does not include the effect of steric constraints imposed by the crystal lattice for solid state isomerization. Yamabe et al.⁹⁹ has also considered the mechanism of chemically induced isomerization by a polaron mechanism.

Several direct and indirect methods have been used to follow the progress and extent of cis-trans isomerization. The most direct probe and most commonly used method has been to compare the relative intensities of the infrared bands at 740 cm^{-1} and 1015 cm^{-1} for the cis and trans out of plane deformations, respectively. Based on work by Ito et al.⁴³ the cis content is given by:

$$\% \text{ cis} = \frac{1.30 A_{\text{cis}}}{1.30 A_{\text{cis}} + A_{\text{trans}}} \cdot 100 \quad (1.21)$$

Where A is the band absorbance. A more recent work by Jing et al.¹⁰¹ has ascribed a constant of 1.50 in lieu of 1.30. The results of Ito et al.⁴³ showed that the cis-trans process is quite complicated. The cis CH out of plane deformation 740 cm⁻¹ band decreases initially very rapidly, but comes nearly to a stop at longer times. Continued heating still results in an increase of the 1010 cm⁻¹ peak. The rate curve did not follow simple first order kinetics. An Arrhenius plot of the initial isomerization rate gave an initial activation energy of 17 Kcal·mole⁻¹. As the cis content of the polymer decreases, the activation energy for isomerization increases rapidly, to ca. 38 Kcal·mole⁻¹ at 80% trans content. This has been interpreted in terms of a decreasing ease of bond rotation for residual cis segments at high trans contents. Complete isomerization has been difficult to achieve thermally. A weak 747 cm⁻¹ band persists even after prolonged heating at 473 K. A shift of the 747 cm⁻¹ for the cis out of plane deformation has been assigned to single or double cis linkages flanked on either sides by trans segments. Gibson and coworkers¹⁰² have estimated ca. 5% residual cis linkages after 74 hours at 373 K.

Isomerization of [CH]_x results in the formation of neutral defects, \dot{S} , characterized by a g=2.0026 EPR signal. However, the intensity of the resonance is not directly proportional to the isomeric content of the polymer.⁹⁷

In ¹³C-NMR, the cis and trans structures have resonances at

126-129 ppm and 136-139 ppm upfield of TMS, respectively. Therefore, this can be used to monitor the degree of isomerization.⁹² Earlier discrepancies between NMR and IR cis/trans contents¹⁰³ have evidently been resolved¹⁰⁴ by using ^{13}C linewidths to extract relative cis/trans contents instead of integrated resonance intensities.⁹²

A very sensitive indirect measure of isomerization is by electrical conductivity. The two isomers differ by as much as $10^{5-6} (\Omega \cdot \text{cm})^{-1}$. However, the transport property is really governed by the concentration of neutral and charged carriers and their mobility: both of which may or may not be a function of isomer content. Rolland et al.¹⁰⁵ showed that at a given isomerization temperature the variation of resistivity with heating times gives a concave curve. At low temperatures it takes a long time, t , for a sample to reach the minimum resistivity before it increases. At high temperatures, t was reached quickly. An Arrhenius plot of t gave an activation energy of $18 \text{ Kcal} \cdot \text{mole}^{-1}$.¹⁰⁶

Wide angle x-ray synchrotron scattering studies of cis-trans $[\text{CH}]_x$ isomerization have been reported by Robin et al.¹⁰⁷ and Riekel.¹⁰⁸ In both studies a continuous monotonic decrease of the cis 110/200 reflection d-spacing into the trans 110/200 reflection was observed. Both authors attribute this to a homogeneous isomerization process throughout the $[\text{CH}]_x$ crystal. Results by Chien and Dickinson¹⁰⁹ see both cis and trans meridional 004 and 002 reflections using electron diffraction during 373K isomerizations. Therefore, isomerization appears to be heterogeneous. Robin¹⁰⁷ also estimates the degree of crystallinity to be ca. 90%, independent of configuration.

Polyacetylene Transport Properties

The electrical transport within polyacetylene can be attributed to the presence of charged carriers and uncharged, unpaired spins. The nature of these species, their creation, and their demise is the subject of this section. Again, several excellent reviews exist which should be consulted for greater detail.^{1,110-112}

Neutral Solitons, \dot{S} , and Electron Paramagnetic Resonance, EPR

As mentioned earlier when $[CH]_x$ is prepared at 195 K, no detectable EPR signal at $g=2.0026$ is observed. Upon warming to room temperature, a weak signal of ca. 5×10^{-5} mole percent spins based on CH units appears with a peak-to-peak linewidth, ΔH_{pp} , of 5-10 Gauss. Isomerization leads to a ca. 8x increase in spin concentration, $[\dot{S}]$ and a narrowing of linewidth to ca. 1.0 Gauss.⁶⁴ Soliton theory has been invoked to explain these results.

Trans polyacetylene, in the perfectly dimerized trans-transoid state, may have either structure A or B as seen in Figure 1.4. If a chain contains both A and B phases, then there exists a topological defect as seen in Figure 1.7(a). The π -wave functions change phases and their amplitudes vanish at the defect. Such domainwall or topological defects have been referred to as a π kink or neutral soliton, \dot{S} .¹¹³⁻¹¹⁵ This one-particle state is without charge, has spin 1/2, and can be seen with EPR. The energy to create a soliton-antisoliton pair was calculated to be ca. 0.4 eV, has a mass of 6x free electron mass,

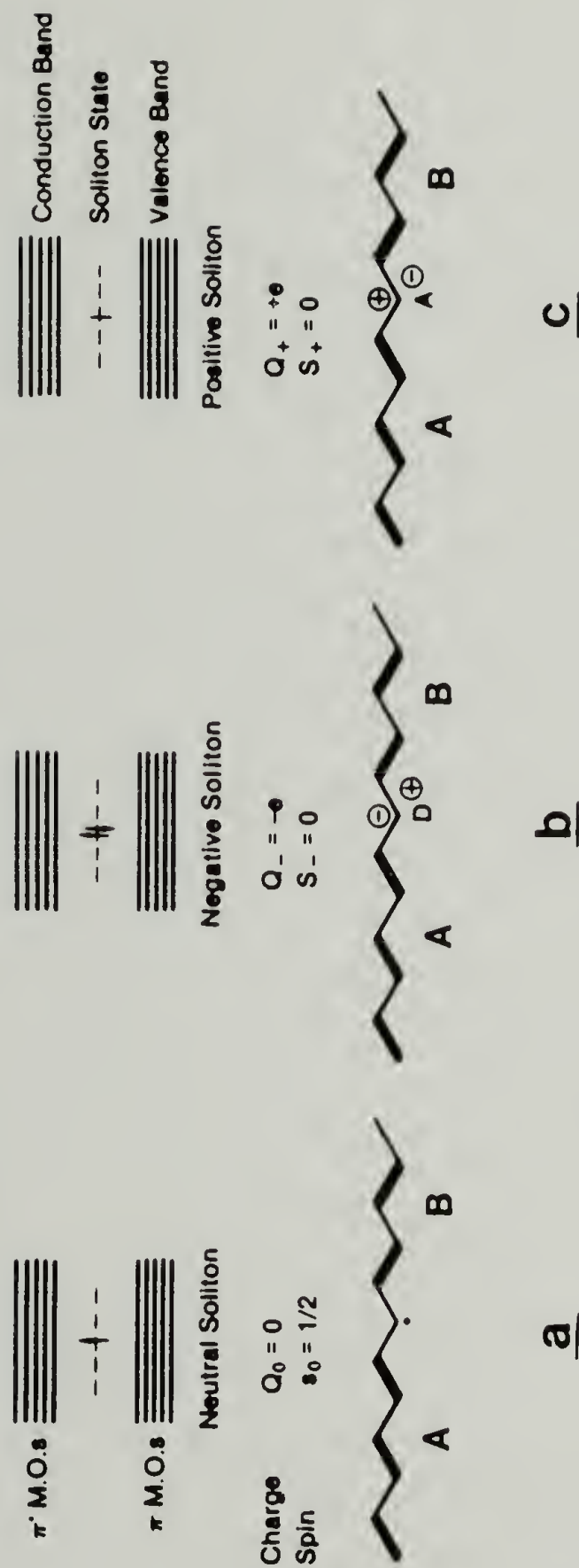


Figure 1.7 Polyacetylene (a) Neutral, (b) Negative, and (c) Positive Charged Solitons.

is delocalized over 15 carbon atoms, and occupies a state midway within the bandgap. The ground state of a perfectly dimerized polyene chain with an odd number of CH groups has a kink located between the two ends, whereas for a long, even CH chain, the ground state has double bonds at the ends but no soliton. Upon chemical doping with a Lewis base or acid, reduction or oxidation of \dot{S} will leave negative or positive solitons respectively (Figure 1.7(b) and 1.7(c)).

The g value observed in the EPR of undoped trans-[CH]_x identifies the spins origin to the π electron system. Analysis of the lineshape and its temperature dependence for [CH]_x and [CD]_x indicate motionally narrowed resonances which broaden with decreasing temperature consistent with mobile defects.¹¹⁶ The trans-[CH]_x spectrum deviates from a pure Lorentzian function having substantial intensity in the low field and high-field wings characteristics of a motionally narrowed resonance.¹¹⁷ The unpaired spins in cis-[CH]_x are relatively immobile and show a nearly Gaussian lineshape with broader linewidths.¹¹⁸

The EPR saturation curve for undoped trans-[CH]_x approaches the case of homogeneous broadening. Taking extreme care to prevent oxygen contamination, spin-lattice, T_1 , and spin-spin, T_2 relaxation times of $(2.7 \pm 1.7) \times 10^{-5}$ sec and $(7.8 \pm 1.0) \times 10^8$ sec have been reported by Chien et al.¹¹⁸ for a number of samples. Deviations from this appear in the literature presumably due to poor sample handling or sample preparation.

A number of techniques have been used to determine the parallel and perpendicular spin diffusion coefficients and anisotropy: EPR line

shape analysis,¹¹⁷ proton spin-lattice, T_1 , relaxation times^{119,120}, and spin echo measurements.¹²¹ Results vary considerably but show \tilde{D} ca. 10^{11} - 10^{13} rad·sec⁻¹ and D ca. 10^8 rad·sec⁻¹. \tilde{D}/D is on the order of 10^3 - 10^4 . Nevertheless, taking into account all of the results, it is clear that neutral defects in cis-[CH]_x are immobile and in trans-[CH]_x the neutral solitons have very high inchain diffusion rates and the diffusion is highly anisotropic.

A number of EPR studies have been made on p-doping of polyacetylene using AsF₅^{116,118} and I₂.¹¹⁸ Because AsF₅ is such a strong oxidizing agent, inhomogeneously doped polymer many times results as evidenced by Dysonian EPR lineshapes and multiple EPR linewidths.^{118,122,123} Based on an extensive study of I₂ doped [CH]_x below and above the semiconductor-to-metal transition, SMT, Chien and coworkers^{1,122} have come up with a list of consequences of "homogeneous" doping: (1) a sharp SMT, (2) a disappearance of unpaired spins at high levels of doping, and (3) a single, symmetric EPR signal.

Chemical and Electrochemical Doping

Polyacetylene, when doped with electron donors or acceptors, undergoes a 10^{13} and 10^8 increase in conductivity, σ_{RT} , for cis and trans polymer respectively. At room temperature pristine cis and trans-[CH]_x have σ_{RT} 's of ca. 10^{-10} and $10^{-5.5}$ ($\Omega\cdot\text{cm}$)⁻¹ respectively. Chemical and electrochemical doping techniques show the greatest versatility and control, though photochemical and ion implantation tech

niques have been described.

A number of reagents have been shown to dope polyacetylene by solution or vapor techniques: I_2 , Br_2 , AsF_5 , SbF_5 , WCl_6 , $MoCl_5$, $FeCl_3$, $FeCl_4$, BF_3 , H_2SO_4 , $ClSO_3H$, Li , Na , K , Cs , to name a few. Electrochemically, ClO_4^- , $SO_3CF_3^-$ anions have been used. Figure 1.8 outlines the two commonly held soliton and polaron doping mechanisms.

In either mechanism, the effect of doping is to introduce charged carriers which at low doping levels, experience a pinning potential from the counter ion. Mele and Rice⁸⁶ calculated the energy of a bare S^+ created by soliton doping to be about 0.4 eV higher than for \dot{S} and with a much larger domain width. In the polaron doping mechanism the radical-cation occupies a state 0.65 eV above the valence band. Brédas et al.^{124,125} calculated this energy is minimized when the two defects forming the polaron are in close proximity. With respect to the midgap energy at 0.7 eV, the polaron binding energy is 0.05 eV. Presumably, at high levels of doping, polaron-polaron annihilation occurs via bipolaron formation¹²⁴ (Figure 1.9). In electrochemical doping, the electrode removes an electron from the polyacetylene backbone and a counterion from the electrolyte becomes associated with the charged soliton or polaron. In electrochemical doping, the results suggest the main mechanism to be via polaron injection.¹²⁶

In most doping systems, little is known of the actual counterion composition. Often simple elemental analysis will only give an average composition. In many cases the extent of doping is based only on weight uptake with no knowledge of the extent of charge-transfer interaction.

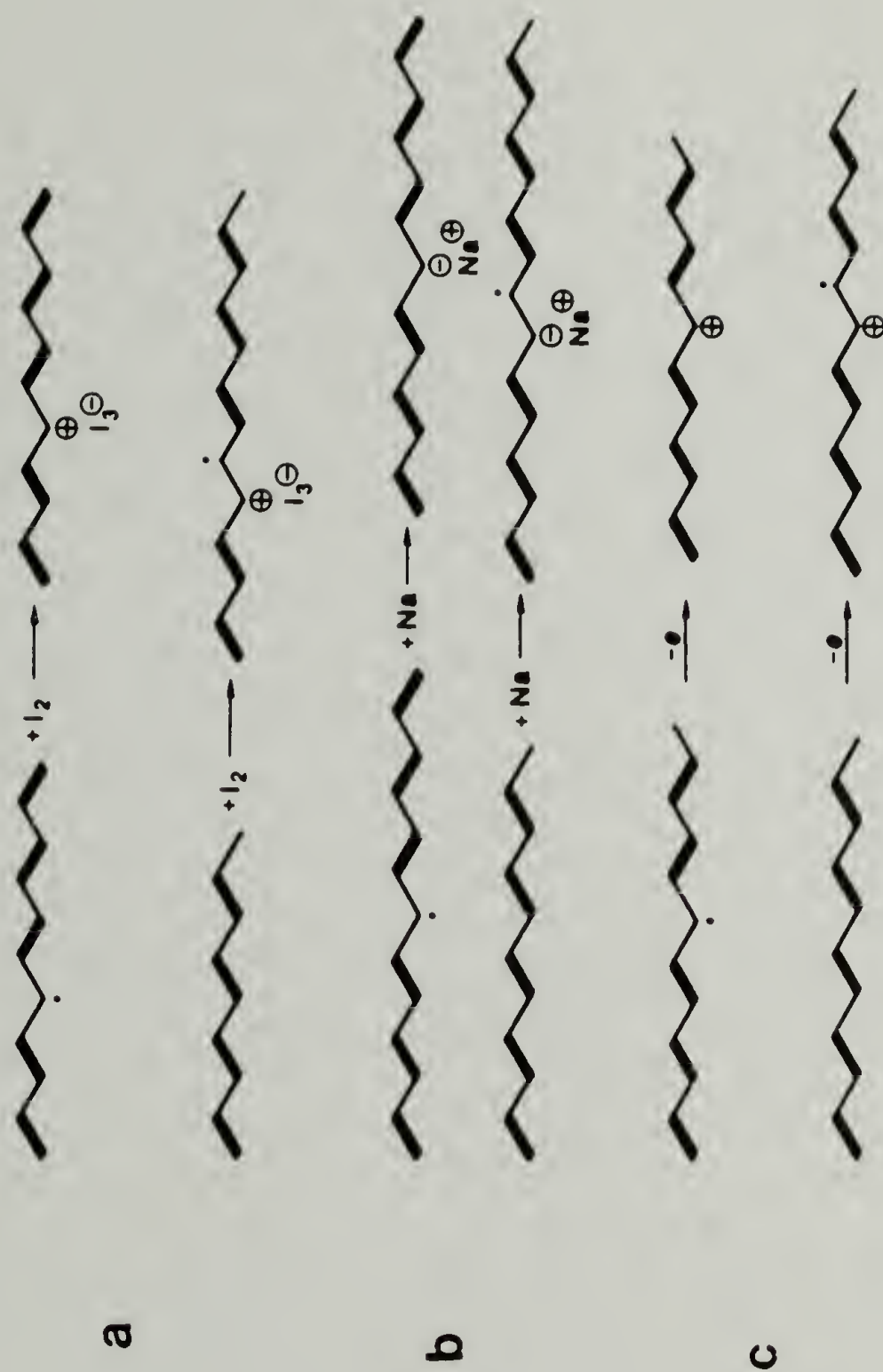


Figure 1.8 Soliton and Polaron (a) p-Type, (b) n-Type, and (c) Electrochemical Doping of Polyacetylene.

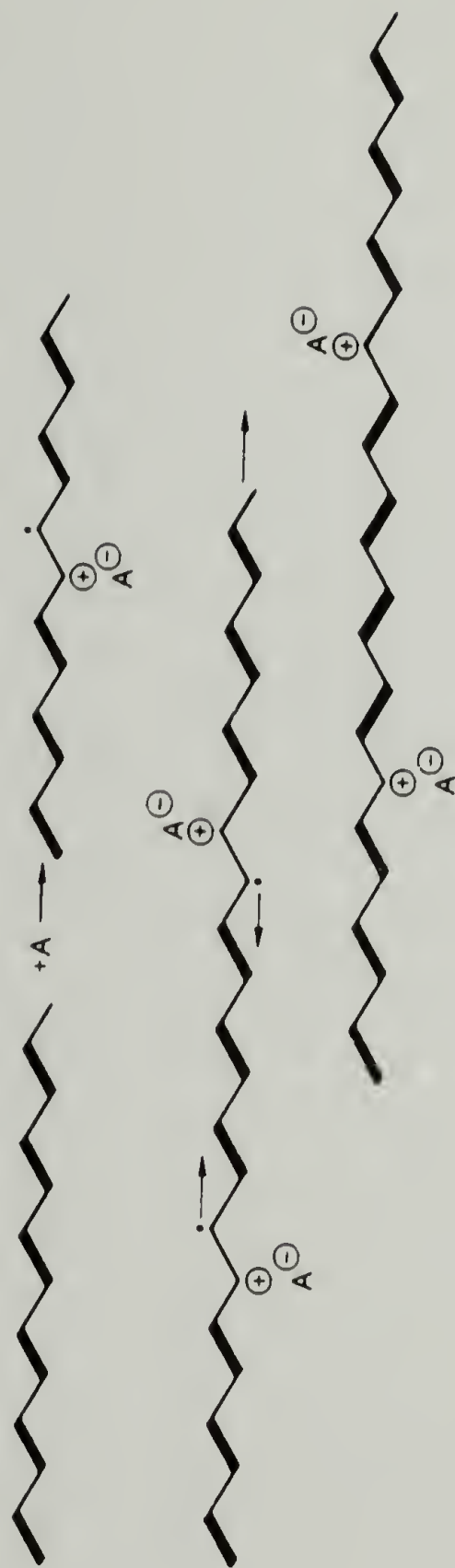


Figure 1.9 Polaron-Polaron Annihilation in Polyacetylene.

Among the dopants for $[\text{CH}]_x$, only the nature of iodine in the polymer is known with any degree certainty. It exists largely as I^- , I_3^- and I_5^- in lightly, moderately, and heavily doped samples. Hsu et al.¹²⁷ observed intense Raman bands in the low-frequency region of I_2 doped $[\text{CH}]_x$ and ascribed them to I_3^- based on model compounds. Resonance maxima due to I_5^- were also detected. Matsuyama, et al.¹²⁸ was able to make quantitative estimates of the amounts of these two species using ^{129}I - Mössbauer spectroscopy. Heavily doped samples contained no I^- species but a distribution of linear I_3^- and I_5^- molecules exists.

Early studies by Chaing et al.¹²⁹ and Park et al.¹³⁰ using I_2 and AsF_5 showed a steep increase in conductivity at 1-3% dopant levels. This was taken at the semiconductor-to-metal transition, SMT. Chien et al.¹²² found this transition to occur at ca. $\gamma(\text{I}_3^-)=10^{-3}$. A similar precipitous change in thermoelectric power coefficient, \dot{S} , was also observed at 10^{-3} mole percent I_3^- . Doping of cis-polyacetylene has been found to induce chemical isomerization. Yet workers consistently find that final maximum doped conductivities of cis- $[\text{CH}]_x$ are greater than for thermally isomerized trans- $[\text{CH}]_x$: $300\text{-}800 (\Omega\cdot\text{cm})^{-1}$ versus $1\text{-}200 (\Omega\cdot\text{cm})^{-1}$ respectively. No sound explanation has been given for this observation.

Proposed Conduction Mechanisms

Undoped polyacetylene is at best a weak semiconductor, but upon oxidation or reduction, becomes highly conductive and even metal-like.

To explain the conduction and transport properties across this thirteen orders-of-magnitude rise in conductivity, a number of physical models have been proposed: all based on the contributions of neutral solitons, charged solitons, polarons and bipolaron pairs. What follows is a description of conduction mechanisms which are believed to describe polyacetylene from the semi-conductive to nearly metallic regime.

Kivelson's intersoliton hopping mechanism (ISH) of conduction in adventitiously and lightly doped polymer proposes a mechanism for three dimensional conductivity based on phonon assisted hopping of charge between neutral and charged solitons like states.¹³¹⁻¹³³ DC transport is predicted to follow a power law dependence with temperature, $\sigma \sim T^n$ with $n \approx 13$. Equation 1.22 and 1.23 are the derived equations for ISH transport.

$$\sigma_{dc} = A \frac{e^2 \gamma(T)}{k_B T N} \left(\frac{\xi}{R_0^2} \right) \frac{Y_n Y_{ch}}{(Y_n + Y_{ch})^2} \exp\left(\frac{-2B R_0}{\xi} \right) \quad (1.22)$$

where $A = 0.45$

$B = 1.39$

$N =$ number of carbon atoms per chain

$Y_n =$ concentration of \dot{S}

$Y_{ch} =$ concentration of S^+

$R_0 =$ separation between impurities

$$= [(4\pi/3)C_{im}]^{-1/3}$$

$\xi =$ three dimensional wave function decay length

$$= (\xi_{\parallel}^2 \cdot \xi_{\perp}^2)^{1/3}$$

$\gamma(T) =$ hopping frequency

$$S = \pm \left| \frac{k_B}{e} \right| \left[\bar{\epsilon}/k_B T + \ln\left(\frac{Y_n}{Y_{ch}}\right) + \ln Z(T) \right] \quad (1.23)$$

Where $\bar{\epsilon}$ =average energy transported per hop. Observed power-law dependence of σ_{dc} on temperature,¹¹⁰ the strong temperature dependence of σ_{ac} ,¹³³ the effect of pressure on σ_{dc} ,¹³⁴ and the temperature independent thermoelectric power coefficient, S ,^{130,134} have been cited as evidence in support of the ISH model. At high temperatures and low doping levels, Kivelson also proposed a secondary mechanism based on thermally liberated charged solitons.

$$\sigma = \sigma_f \exp(-E_b/k_B T) \quad (1.24)$$

$$S = \pm \left| \frac{k_B}{e} \right| \left(\frac{E_b}{k_B T} + \text{const} \right) \quad (1.25)$$

Where σ_f : conductivity contribution of free solitons

E_b = binding energy

$\cong 0.3$ eV

The ISH model fits experimentally observed results for $Y(I_3^-) \leq 0.001$.

When $Y(I_3^-)$ exceeds 10^{-3} , Warakomski¹²² found a disappearing EPR signal when $[CH]_x$ is doped uniformly. Epstein and coworkers have proposed from $Y(I_3^-)$ of 0.017 to 0.048 a variable range hopping (VRH) among soliton-like states transport mechanism.¹³⁵⁻¹³⁷ This mechanism is based on a dense array of solitons near the Fermi energy. The model predicts

$$\sigma(T) = (0.39[N(E_f)/\alpha k_B T]^{1/2} v_0 e^2) \exp[-(T_0/T)^{1/4}] \quad (1.26)$$

Where $N(E_F)$ = density of states at the Fermi level

α^{-1} = decay length of localized state

ν_0 = hopping frequency

$T_0 = 16x^3/k_B N(E_F)$

Spin susceptibility, χ_{spin} , is equated as the sum of χ_{Curie} and χ_{Pauli} , i.e.

$$\chi_{\text{spin}} = (N_C g \mu_B^2 / 3k_B T) + (2\mu_B^2 N(E_F)) \quad (1.27)$$

Where: μ_B = Bohr magneton.

N_C = density of Curie spins

$N(E_F)$ = density of states at the Fermi level

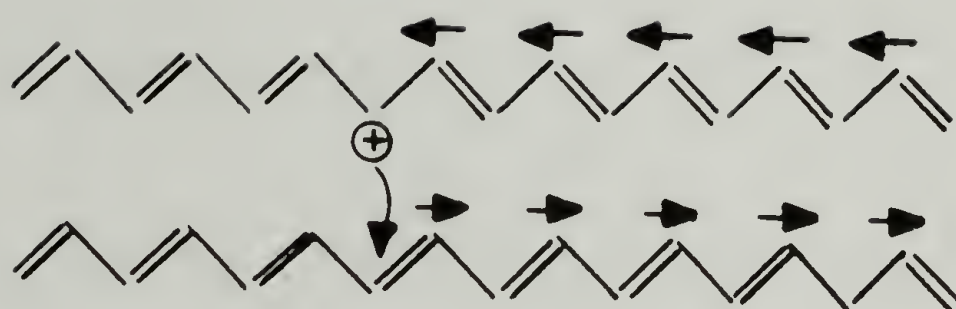
Quantitative analysis of $\sigma(T)$, $S(T)$, $\chi(T)$, optical reflectivity and x-ray structure are in agreement with this model.^{134,135}

Recently, Brédas and coworkers^{138,139} have considered, on a mechanistic scale, hopping mechanisms involving charged solitons in the nearly metallic regime. They point out that a single soliton cannot hop easily to the next chain since an infinitely large activation barrier is required in the reorganization of bond lengths that would supervene from such a jump. To circumvent this, a bipolaron hopping mechanism is proposed (Figure 1.10).

Importance of This Research

Prior to this dissertation research a number of extremely fundamental questions, from a "polymeric" viewpoint, remained unanswered regarding polyacetylene. No question, these points had not been fully

{A}



{B}

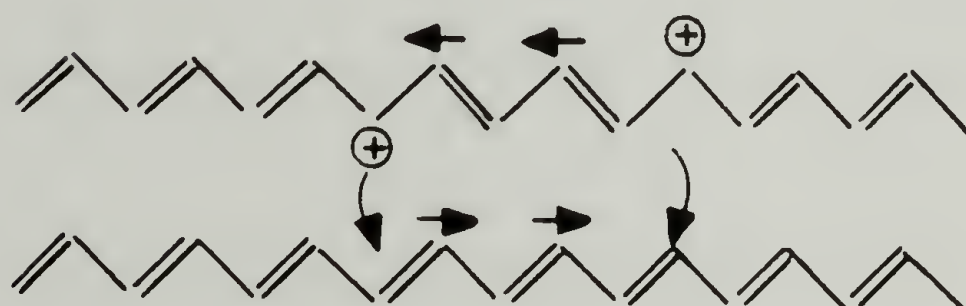


Figure 1.10 Bipolaron Hopping in Trans Polyacetylene.

addressed due to the difficulty in handling the polymer.

From a traditional materials science vantage, the molecular weight of a polymer composition greatly influences its final properties. High molecular chain lengths are necessary to obtain limiting performance. Sufficiently low molecular weights are needed for improved handling. Does such a relationship hold true with polyacetylene as a model conducting polymer? This is the principal question.

To this end, a number of points had to be first addressed regarding the polymerization of acetylene. The Ziegler-Natta polymerization of olefins is an addition reaction. As a consequence, polymer molecular weight is kinetically controlled and can be expressed as the sum of a series of initiation, propagation, transfer, and termination rates. Assuming steady state conditions:

$$\frac{1}{\bar{X}_n} = \frac{k_t R_p}{k_p^2 [M]^2} + \frac{k_{tr,M}}{k_p} + \frac{k_{tr,cat}[cat]^x}{k_p [M]} + \frac{k_{tr,cocat}[cocat]^y}{k_p [M]} + \dots \quad (1.28)$$

Using radio-labeling techniques developed to study ethylene and propylene polymerization, the kinetics of acetylene polymerization using the $Ti(OBu)_4/4Al(Et)_3$ catalyst were examined. Number average molecular weights, \bar{M}_n , could then be easily and routinely extracted by end group analysis.

Knowing the important parameters which control polyacetylene molecular weights, the goal was now to examine in detail the significance of molecular chain lengths. The point which must be kept in mind is

that this is a dissertation on "conducting polymers". It therefore dictates that an examination of the more traditional aspects of polymer science be addressed in addition to the affect \overline{M}_n has on the physics which make polyacetylene a potentially useful electronic material.

Contemporary theories by Su, Schrieffer, and Heeger¹¹³⁻¹¹⁵ predict the presence of neutral kinks within the perfectly dimerized chain. These are thought to exhibit high mobility up and down the chain as evidenced by the rapid in-chain diffusion constant. A test of this model would then be to examine the soliton concentration as a function of molecular chain length. Along a similar vein, the impact of deliberately introduced defects in the form of chain ends on the conductive properties both in the undoped and doped state are to be examined. This question of three dimensional conduction has not been specifically addressed prior to this dissertation research.

CHAPTER II

EXPERIMENTAL TECHNIQUES

Research in the field of conducting polymers requires handling of all materials in inert environments. This is especially true with polyacetylene $[CH]_x$. These procedures also lend themselves to the controlled and safe handling of radioactive compounds. This chapter will describe the techniques, materials and equipment necessary for the research described here within.

Handling Air Sensitive Materials

Vacuum Lines

All monomer purification, catalyst preparation, synthesis, polymer radio-labeling, isomerization, EPR, doping and conductivity measurements require the use of high vacuum lines. All of these steps require the exclusion of oxygen and water vapor. Pyrex glass vacuum lines were constructed at the University of Massachusetts Glass Shop. Welch Duo-Seal forepumps in line with a mercury diffusion pump were used. As a safety precaution and to trap volatiles, liquid N_2 traps were in place on either side of the diffusion pump. High vacuum grease (Apiezon N or M) or teflon stopcocks were installed. Glassware was attached using glass ball joints in conjunction with a metal clamp. Flexible, vacuum tight metal tubing from Cajon, Inc. was sometimes used between the vacuum line and the glassware being evacuated. Vacuums on the order of 10^{-4} torr were routinely achieved. A Tesla Coil was used to qualitatively determine good vacuum.

Inert Gas Lines

When materials were not stored or handled under vacuum, they were instead kept under a blanket of purified Argon. Argon was the noble gas of choice since its density is greater than air. High grade Argon (Linde) was purified by passing over a 373 K BASF catalyst R3-11 reduced copper catalyst to remove oxygen, followed by a column of activated 13X molecular sieves to remove gross amounts of moisture. Thereafter, the gas was bubbled through a deoxygenated oil bubbler containing 20-50 volume percent trioctyl aluminum, TOA (Ethyl Corp.) to remove final traces of O_2 and H_2O . The gas line was constructed of glass and butyl rubber tubing with greased stopcocks.

Schlenk Glassware

All materials were handled and stored in Schlenk tubes of various sizes and styles. The common feature was that all had a glass side-arm with stopcock through which purified Argon could be passed. The top of the Schlenk tube had either a 24/40 male joint or o-ring joint (#7, #15, or #25). Tops for the Schlenk tubes had the complementary joint for attaching to the bottom half, and a 2 mm greased or 0-3 or 0-5 mm teflon stopcock with an 18/7 balljoint for evacuation through the vacuum line. Generally, after the assembled Schlenk glassware was evacuated, they were flame-dried under dynamic vacuum to help remove traces of moisture physisorbed on glass surfaces.

Syringe Techniques

Air sensitive liquids, purified solvents and radioactive liquids and gases were transferred using gas tight or matched barrel syringes. Gas tight syringes were manufactured by Hamilton Syringe and matched barrel syringes by either Hamilton or B&D. Custom made 10" 23 to 16 gauge needles were most often used. On the other hand, for injecting liquids or gasses through rubber gas tight septa, 23 gauge needles were always used since it was found that good vacuum could still be maintained in glassware after the septa was punctured. Before use, syringes and needles were oven dried and flushed multiply using purified argon.

Dry Box and Glove Bags

A Vacuum Atmospheres stainless steel drybox with safety glass front (Model DLX-001-SG) equipped with Pedatrol pressure controller (Model HE-63-P) and drying train (AE-493) was used for handling undoped and doped polymer samples. Prepurified nitrogen or purified argon was used and the atmosphere continuously circulated through the drying train to remove moisture and oxygen. On a weekly basis, the dry box was regenerated using a 10% mixture of hydrogen in nitrogen. Within the box, a Mettler A30 digital balance accurate to ± 0.1 mg was used. To bring samples/glassware into the dry box, they were first evacuated within the anti-chamber for 30 minutes. A high vacuum Marathon Electric Co. (Model HUL56C17D885A-P) pump with a liquid N₂ trap was used. When the dry box was not used because solvents were needed or when polyacetylene samples only needed to be handled for short times,

polyethylene glove bags from Instruments for Industry and Research, Inc. were used. Purified nitrogen passed through a drierite column provided the atmosphere. Before use, all equipment was placed in the glove bag and the volume purged a minimum of five times.

Solvent Purification

Toluene and pentane were purified to remove thiophenes, water and oxygen.¹⁴⁰ To two liters of solvent, 300 ml concentrated sulfuric acid was added and stirred for 24 hrs. After separating off the spent acid, a new aliquot of sulfuric acid was added and stirred for another 24 hrs. The solvent was washed three times with distilled water, then two times with 500 ml portions of 10% NaOH, then with enough distilled water such that the wash water was neutral. Gross amounts of moisture were removed using MgSO_4 . Then the solvent was filtered and added to a distillation still, containing boiling chips and calcium hydride.⁶⁴ A blanket of argon was passed over the refluxing solvent for 24 hrs. before use.

Technical grade methanol was purified by first drying over MgSO_4 , then distillation under a blanket of argon. To 1.5 l methanol, a small amount of I_2 crystals were added followed by 5 g Mg filings. The solvent was warmed gently while H_2 was being evolved. When a steady reflux rate was achieved, 10 g additional Mg was added. Solvent was collected and stored in a 2 l round bottomed Schlenk flask containing activated 3 Å molecular sieves.

Acetylene Purification

A tank of purified acetylene (Linde) was equipped with a Matheson Model 6103 flash arrestor and regulator. The gas was purified by passing through two concentrated sulfuric acid bubblers to remove acetone and a U-tube containing activated 13X molecular sieves kept at 195 K to remove water. When not in use, nitrogen was flushed through the line to eliminate any explosion hazard. Consequently, when acetylene was to be collected, the line was flushed with acetylene for a minimum of 30 minutes. Acetylene was purged through to the hood. To collect C_2H_2 , a 2 l round bottomed flask with cold finger was evacuated on the vacuum line and flame dried. Acetylene was passed through a vacuum sub-manifold into the storage bulb while the C_2H_2 pressure was monitored by Hg monometer. Bulbs were never filled to over 1.1 atmospheres since in the purified form, C_2H_2 becomes extremely shock sensitive when above 1.3 atmospheres. To further purify the collected acetylene, a minimum of three freeze-pump-thaw cycles using liquid N_2 was performed to remove any non-condensables. Sometimes, the gas was also cryogenically passed back and forth between two bulbs with a 195 K cold trap in between. This removes vapors which may freeze/condense above 195 K.

Handling Radioactive Compounds

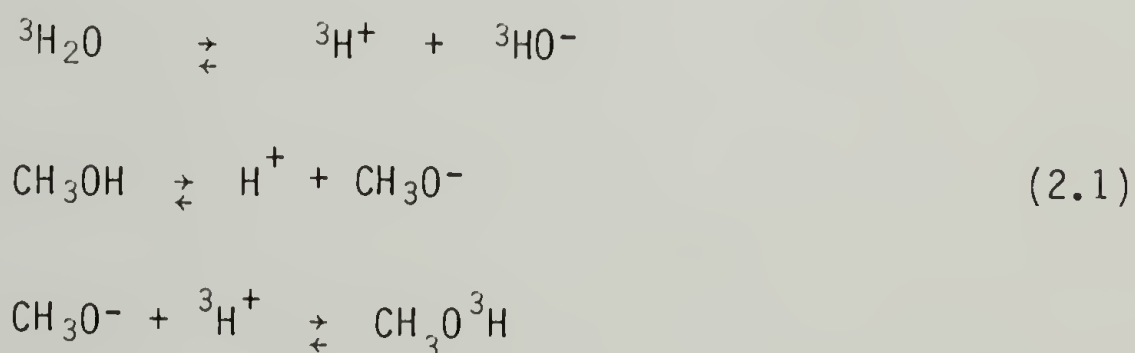
Safety Precautions

Before working with any radioactive materials (RAD), it is first necessary to consult the available literature^{141,142} concerning the

safe practice of handling radioactive isotopes. Protective laboratory gear such as a labcoat, disposable gloves, and safety glasses were always used. Radioactive reagents were always handled in a well ventilated, preferably hooded environment. A plastic coated bench towel was laid out on the bench top to prevent contamination of the work space. Solid RAD waste was stored in a double plastic bagged trash container. Liquid ^3H , ^{14}C RAD waste of low activity and which were miscible in water were flushed down the drain with copious amounts of water. Organic RAD waste was routinely delivered to Environmental Health and Safety (EH&S) for disposal. ^3H and ^{14}C are weak beta emitters of 0.0186 and 0.156 MeV energies respectively, so no shielding was necessary. The glass containment is an effective absorber. $^{125}\text{I}_2$, however, is a relatively high energy gamma emitter of 28 KeV so 1 mm lead shielding is needed.

Dilution, Transfer and Storage of $\text{CH}_3\text{O}^3\text{H}$

Stock supplies of tritiated methanol were prepared by an exchange reaction between tritiated water and anhydrous, oxygen free distilled methanol



Under the guidance of EH&S, 0.25 ml of extremely "hot" $^3\text{H}_2\text{O}$ (ca. 5 Ci·ml⁻¹) was added via syringe to a 200 ml Schlenk-tube pop-bottle (STPB)

containing 100 ml freshly distilled methanol and activated 3Å molecular sieves. This solution was assayed using a Biofluor Scintillation Cocktail from New England Nuclear and Beckman LS-100C liquid scintillation counter and found to be 522 ± 2 mCi·mole⁻¹ or 12.90 ± 0.06 mCi·ml⁻¹. Counting efficiency was found to be ca. 45% based on a ³H-toluene standard. Equation 2.2 shows how the specific activity was calculated.

$$\text{cpm} \times \frac{\text{dpm}}{0.45\text{cpm}} \times \frac{1 \text{ mCi}}{2.22 \times 10^9 \text{ dpm}} \times \frac{1}{\text{ml}} = \text{mCi} \cdot \text{ml}^{-1}$$

(2.2)

$$\frac{\text{mCi}}{\text{ml}} \times \frac{\text{ml}}{0.7914\text{g}} \times \frac{32.04\text{g}}{\text{mole}} = \text{mCi} \cdot \text{mole}^{-1}$$

From this very hot stock solution, several other working solutions of various activities were prepared by syringing aliquots of the stock solution into 200 ml STPB containing methanol and molecular sieves. Table 2.1 reports those activities. Once prepared, solutions were stored within the hood. Tritium has a 12.26 year half life so no decay corrections of these reagents was necessary.

Dilution, Transfer and Storage of ¹⁴CO and ¹⁴CO₂

Two 1 mCi ampoules of ¹⁴C labeled carbon monoxide and carbon dioxide were purchased from New England Nuclear, Inc. These were diluted with one liter volumes of cold CO and CO₂ by attaching the break seal ampoule to modified 1 l bulbs as seen in Figures 2.1 and 2.2. A toepler pump on the ¹⁴CO bulb was able to maintain the pressure

Table 2.1Specific Activity of $\text{CH}_3\text{O}^3\text{H}$ Reagents.

	mCi/mole	mCi/ml
Solution #1	32.2	0.795
Solution #2	47.33 ± 1.06	1.17 ± 0.03
Solution #3	4.28 ± 0.17	0.106 ± 0.004
Solution #4	0.471 ± 0.016	0.0116 ± 0.0004

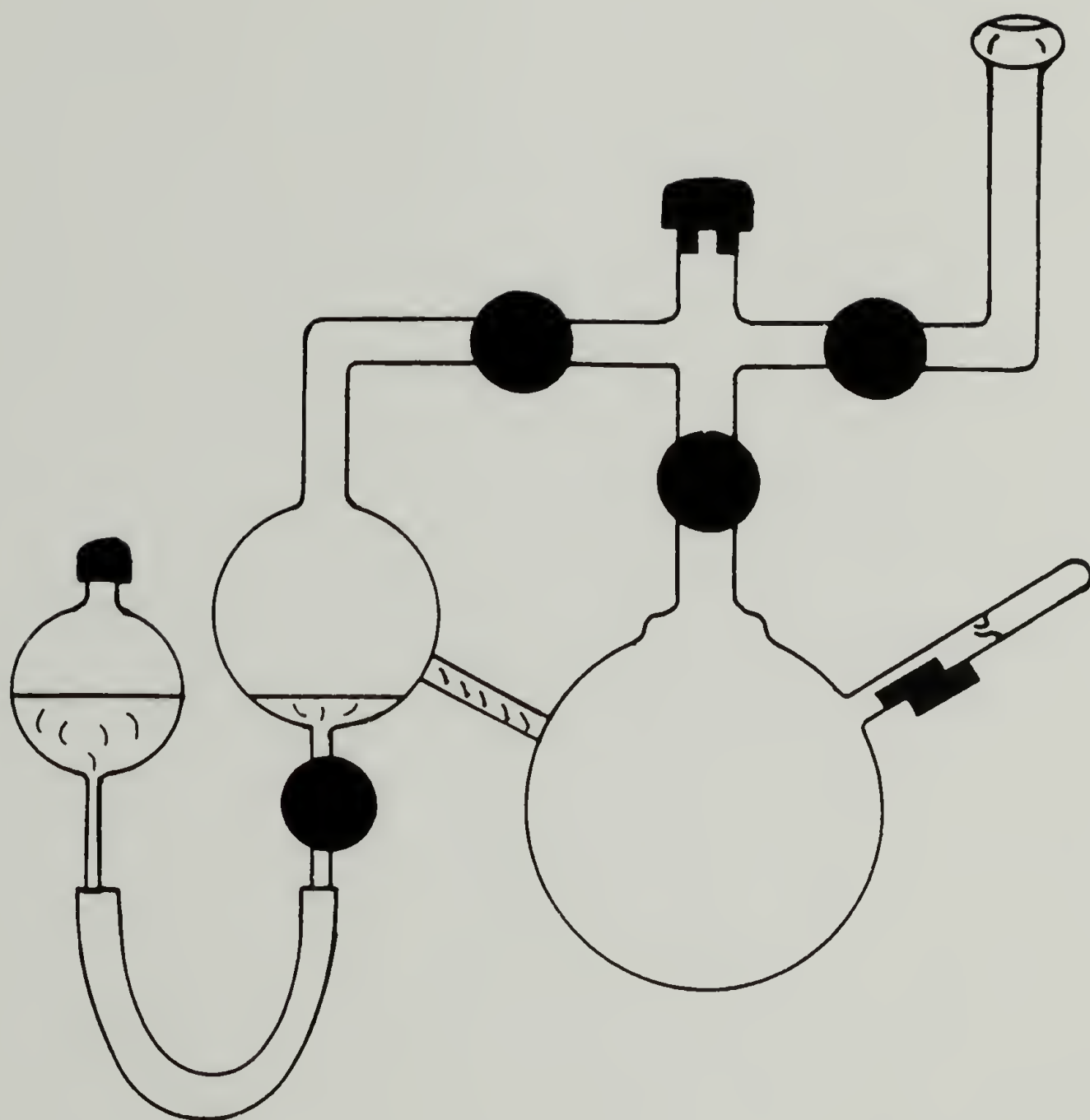


Figure 2.1 $^{14}\text{C}0$ Storage Bulb.

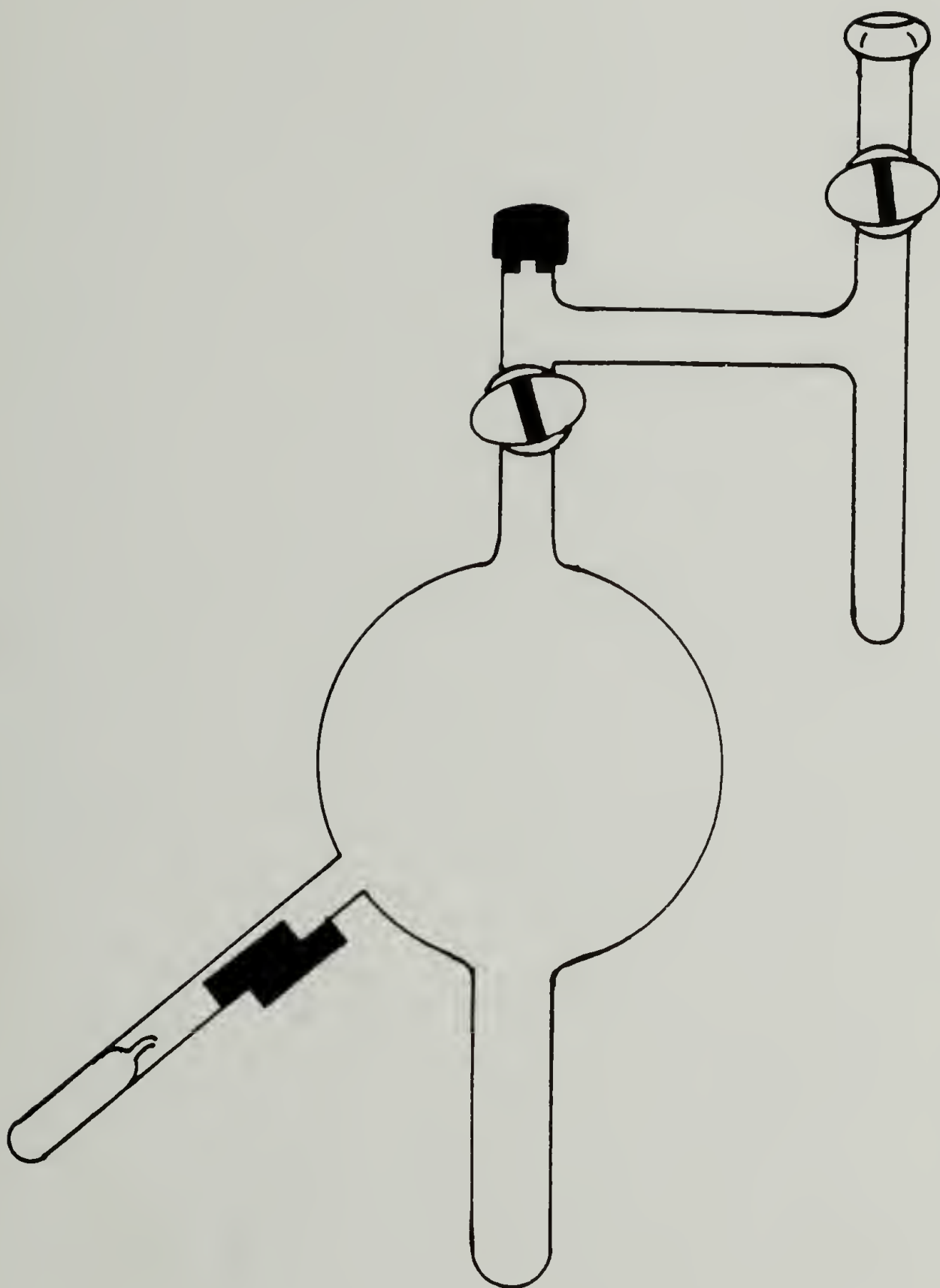


Figure 2.2 ^{14}C Storage Bulb.

at 1 atmosphere for withdrawal using a gas tight syringe. Since CO_2 can be condensed with liquid nitrogen, gas could be condensed in the smaller cold finger and the pressure maintained at 1 atmosphere.

To assay the specific activity of the $^{14}\text{CO}_2$ supply, aliquots of $^{14}\text{CO}_2$ were injected into degassed 1 N NaOH solutions such that there was a 10X excess of base. Assay by liquid scintillation counting showed:

$$A_{^{14}\text{CO}_2}: (3.90 \pm 0.08) \times 10^{-3} \text{ mCi} \cdot \text{ml}^{-1}$$

$$86.7 \pm 1.8 \text{ mCi} \cdot \text{mole}^{-1}$$

Oxidation of ^{14}CO over a heated CuO BASF R3-11 catalyst and adsorption in 1 N NaOH solution showed the CO specific activity to be:

$$A_{^{14}\text{CO}}: (5.94 \pm 0.80) \times 10^{-4} \text{ mCi} \cdot \text{ml}^{-1}$$

$$13.3 \pm 1.8 \text{ mCi} \cdot \text{mole}^{-1}$$

^{14}C has a 5730 year half life so no adjustment in the activity over the course of this dissertation research was necessary.

Dilution, Transfer and Storage of $^{125}\text{I}_2$

An ampoule containing 100 mg $^{125}\text{I}_2$ crystals was received from ICN Chemical and Radioisotope Division with a reported activity of $85 \mu\text{Ci} \cdot \text{mg}^{-1}$. This was transferred to a 50 ml round bottomed flask with teflon 0-3 stopcock and #7 o-ring joint (Figure 2.3) by cryogenic sublimation from the ampoule to the receiver flask. Since $^{125}\text{I}_2$ is a gamma emitter, the apparatus was surrounded by Pb foil. The specific acti-

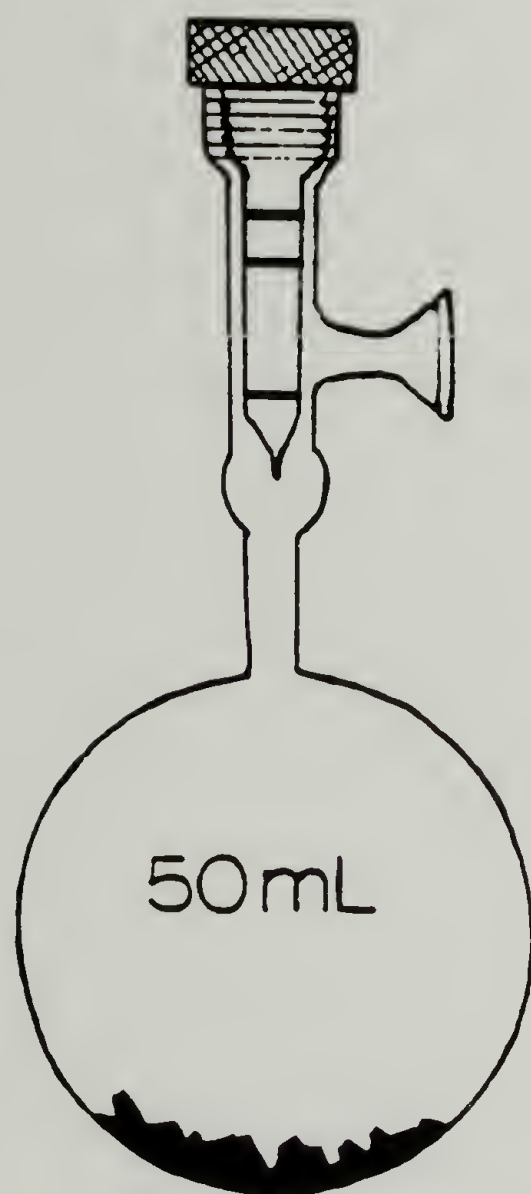


Figure 2.3 $^{125}\text{I}_2$ Storage Bulb.

vity was calculated by doping strips of $[\text{CH}]_x$ to maximum doping, removing the excess I_2 , measuring the weight uptake and then assaying the samples using a Packard Auto-Gamma, Model AP-GD gamma counter. The activity was found to be:

$$A_0^{125}\text{I}_2: \quad (3.05 \pm 0.49) \times 10^{-2} \text{ mCi} \cdot \text{mg}^{-1}$$

$$(3.88 \pm 0.62) \times 10^3 \text{ mCi} \cdot \text{mole}(\text{I}^-)^{-1}$$

$$t_0: \quad 29 \text{ April } 1983$$

$^{125}\text{I}_2$ has a half life of 60.2 days. At any time, the specific activity may be calculated using Equation 2.3.

$$A_t = A_0 \exp(-0.693 \, t/T) \quad (2.3)$$

where

T = half-life

t = elapsed time

A_0 = initial activity

A_t = activity at time t

Polyacetylene Synthesis

The effecient polymerization of acetylene using the soluble Ziegler-Natta catalyst $\text{Ti}(\text{OBu})_4$ and $\text{Al}(\text{Et})_3$ requires the use of scrupulously purified reagents, transfer techniques which exclude oxygen and moisture, and reactor designs such that easy manipulation of the product regardless of its macro-morphology is possible without oxygen contamination. To these ends what follows are the procedures for pre-

paring $[\text{CH}]_x$ of various macro-morphologies.

Schlenk Tube Pop Bottle (STPB), and Flat Bottomed Reactors

For the kinetics phase of this dissertation, 40 ml and 200 ml crown capped high pressure/high vacuum pop-tubes (Lab Glass, Inc.) were outfitted with Schlenk-like side arms. Either 2mm high vacuum grease stopcocks or 0-3 teflon stopcocks with 18/7 balljoints were used. These reactors were capped with butyl rubber septa and crown caps which had two holes on the top cutout. This made it possible to inject, using syringes, various reagents during the course of the polymerization without disrupting the experiment. Some 200 ml STPB's were also modified by cutting the reactor in half and adding a #50 o-ring joint for joining the top and bottom sections.

For preparing low molecular weight polyacetylene (LMnP) and high molecular weight polyacetylene (HMnP) films, a flat bottomed reactor was designed (Figure 2.4) so that films could be grown under quiescent conditions. A #50 o-ring joint joined the Schlenk-type top to the modified vacuum erlenmeyer bottom. A solvent wash bottle is attached to the side so that gross amounts of catalyst can be washed free of the film before washing with deoxygenated 10% HCl/CH₃OH. Two tops were designed. One had a #7 o-ring joint through which the reactor was attached to the vacuum line. The other had a crown cap such that reagents could be injected during the experiment.

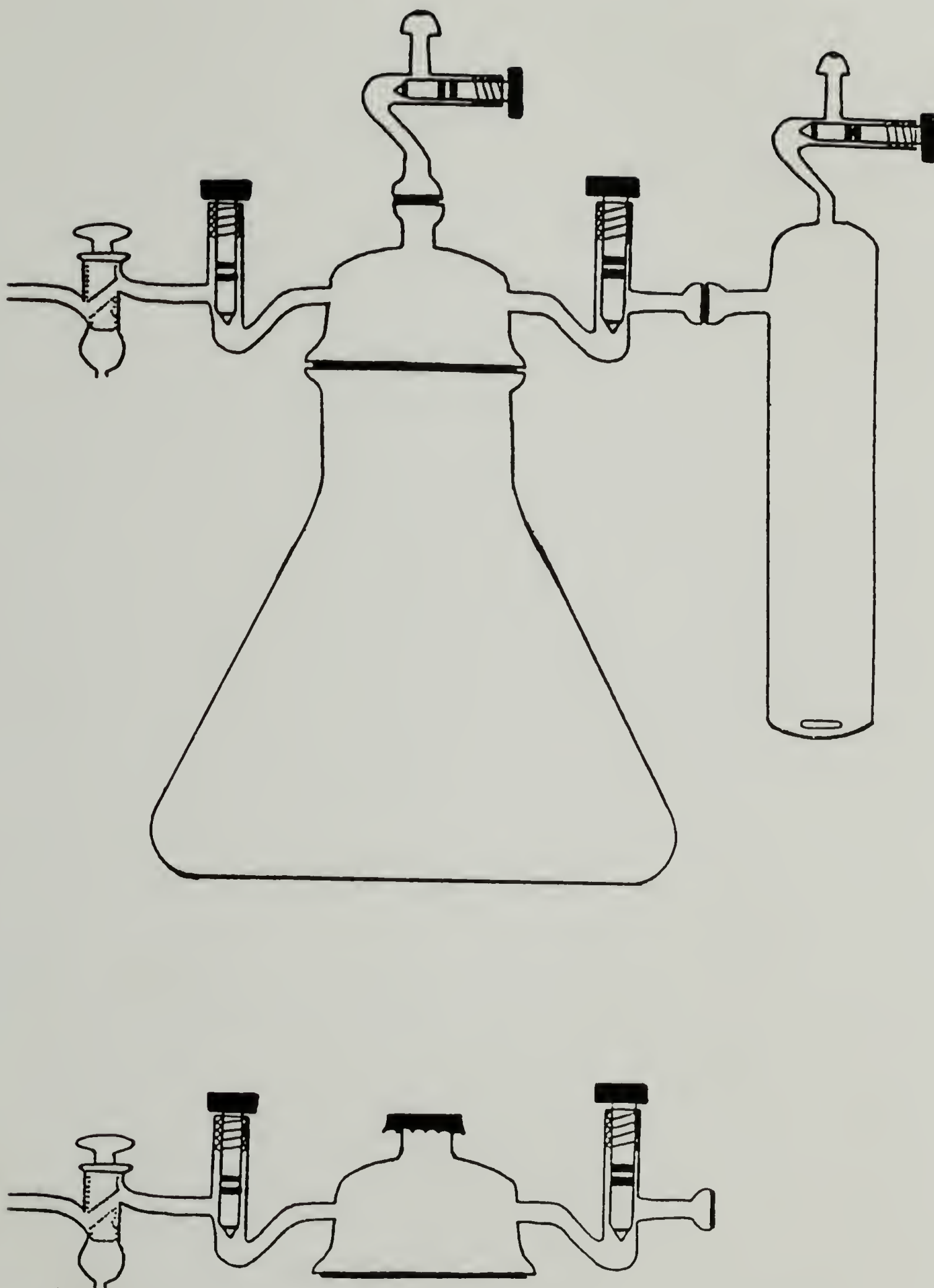


Figure 2.4 Flat Bottomed Reactor for Preparing High and Low Molecular Weight $[\text{CH}]_x$ Films.

Catalyst Preparation

Titanium tetra-n-butoxide $[\text{Ti}(\text{OBu})_4]$ (Alfa Products) was first distilled under high vacuum to remove reactive contaminants such as n-butanol. Product recovered at 413-443 K at ca. 0.1 mm Hg, was shown by ^1H -NMR to contain only the tetra substituted organo-titanium adduct. Product was stored in a light tight Schlenk tube under argon. Triethyl aluminum $[\text{Al}(\text{Et})_3]$ (Ethyl Corp.) was used as received. Important reagent constants after purification are:

$$\text{Ti}(\text{OBu})_4 = 2.93 \text{ M}$$

$$\text{Al}(\text{Et})_3 = 0.807 \text{ M}$$

The activated catalyst at 204 mM $[\text{Ti}]_0$ was prepared as follows. To an evacuated Schlenk tube was added the appropriate amount of distilled toluene. $\text{Ti}(\text{OBu})_4$ was syringed in. After cooling to 195 K by using a dry ice/ethanol bath, $\text{Al}(\text{Et})_3$ was carefully and slowly added by syringe. Initially, two layers should form. While at 195 K, the mixture was gently swirled to mix the two layers and a dark reddish brown color developed. Before further dilution and use, the activated catalyst was aged at room temperature for one hour. Generally, three different catalyst concentrations based on titanium were used,

Reference	$[\text{Ti}]_0 \text{ mol}\cdot\text{l}^{-1}$
Neat	7.40×10^{-1}
Film	2.04×10^{-1}
Gel	5.10×10^{-3}
Hot	1.02×10^{-3}

Activated catalyst was always prepared at "Film" strength and dilutions followed.

For the kinetics experiments, Al/Ti ratios varied from 2/1 to 10/1, though generally a 4/1 ratio was used. This is the composition described by Shirakawa and coworkers^{41-43, 143} and generally used in the field. Most frequently, "Hot" strength was used because the polymerization mixture could be continuously stirred with a magnetic stir-bar, Macroscopic monomer diffusion was therefore minimized. In addition, by using small amounts of catalyst, minimal radioactive labeling reagents were needed.

Monomer Solubility

The solubility of acetylene in toluene was experimentally determined as follows. The volume of a storage bulb was determined and then filled to 1 atm. C_2H_2 . Using the well known pressure/volume equation (Eq. 2.4), the moles of C_2H_2 can be obtained. This was then used to calculate the

$$PV = nRT \quad (2.4)$$

$$R = 0.08206 \text{ l} \cdot \text{atm} \cdot \text{K}^{-1} \text{mol}^{-1}$$

volume of the vacuum submanifold with Hg monometer and 40 ml STPB. After injecting 25 ml toluene, the equilibrium solubility of C_2H_2 at various temperatures was calculated by observing the uptake of C_2H_2 using the monometer. Solubilities were normalized to 1 atm. total pressure taking into account contributions from C_2H_2 and toluene. An

Arrhenius plot (Figure 2.5) gave a straight line and a molar heat of solution of $-0.0824 \text{ Kcal mol}^{-1}$.

Polymerizations for Kinetics Elucidation

Polymerizations for kinetic experiments were carried out using a submanifold such that four reactions could be carried out side-by-side. Since dilute catalyst concentrations were generally used, it was critical that contaminants be excluded. Reactors were evacuated overnight, flame dried, and equipped with a rubber stoppered argon flowing antichamber stretched atop the crown cap. A Hg monometer was used to monitor C_2H_2 pressure.

Most experiments were carried out at a constant monomer pressure. To do this, two or three acetylene bulbs were first filled and purified. Just prior to the experiment, all of the acetylene was transferred to a single bulb and the pressure regulated by keeping the cold finger immersed in a slush bath or keeping it within the cooled airspace above a liquid N_2 dewer. Catalysts were prepared as described earlier and any subsequent dilutions done in Schlenk tubes.

Two polymerization procedures were used in this work. Each had their own advantages as will be outlined later. In the first, the activated catalyst solution was first injected into the STPB, stirred and equilibrated to the desired temperature. Acetylene was then added whereupon an immediate formation of polymer was observed. In the second approach, a given amount of toluene was first injected into the reactor and acetylene allowed to saturate at the given reaction pressure and temperature. Once equilibrated, a concentrated aliquot of

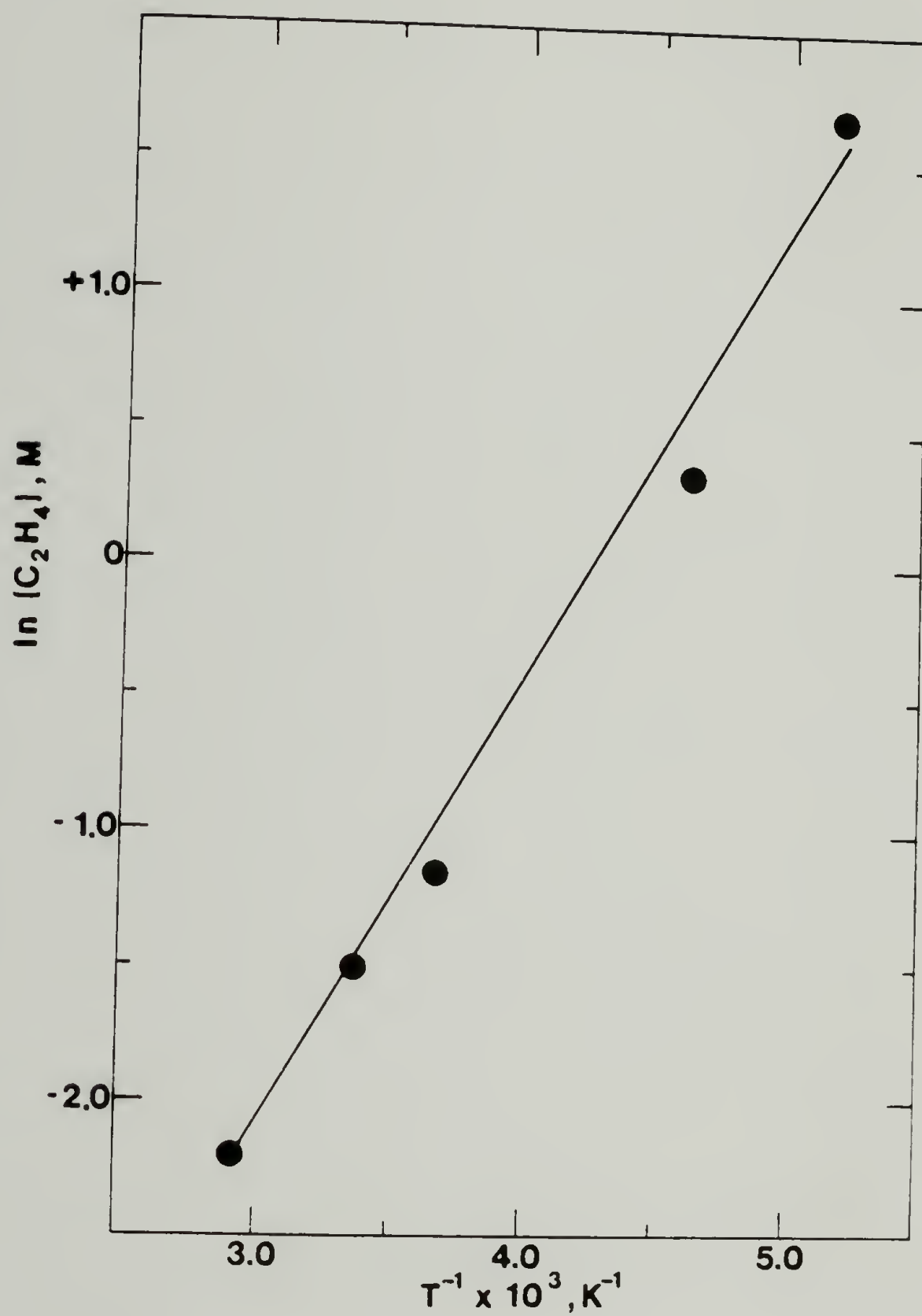


Figure 2.5 Acetylene Solubility in Toluene at 1 atm. Total Pressure.

activated catalyst was injected and the final $[Ti]_0$ calculated based on the total reaction volume. Polymerization would commence immediately. The later procedure was used during most of the kinetic experiments since higher yields were generally seen.

In these experiments, immediately after polymerization, the product would be labeled using either $^{14}CO_2$, ^{14}CO or CH_3O^3H . When carbon monoxide or carbon dioxide was used, monomer was first cryogenically removed since carbon monoxide is known to copolymerize with olefins.²⁷ The required volume of gas was then injected using a gas tight syringe and allowed to quench at room temperature for the required time. Afterwards, an excess of cold methanol was added. Labeling with CH_3O^3H did not require monomer removal since alcohols are known to deactivate Zeigler-Natta catalysts very rapidly. Before labeling, enough additional toluene was added so that all of the polymer was immersed in the solvent. Hot methanol was then injected and the mixture allowed to react at room temperature.

Polymerization on Electron Microscopic Grids

To study the nascent morphology of polyacetylene, two approaches were taken. One was to scoop-up small specimens from a dilute polymer dispersion onto carbon coated grids. Acetylene was polymerized under stirred conditions at three catalyst concentrations: low $[Ti]_0=1$ mM; medium $[Ti]_0=5$ mM, and high $[Ti]_0=40$ mM. Only at the highest concentration did free standing films form. The others gave suspended particles of polymer. The second approach was to polymerize polymer directly on gold grids, as has been outlined previously.⁶¹ In the case

of direct polymerization of 500 \overline{M}_n polymer on grids, catalyst was prepared at 200 mM[Ti]₀ and Al/Ti ratio of 7/1. Grids were coated with catalyst and acetylene metered in at 12 mm Hg for 90 sec. Samples were washed with pentane.

The effect of solvent washing was also investigated. In this case, prepared grids or polymer powders were washed in deoxygenated toluene, methanol, or 10% HCl/CH₃OH. Samples were kept free of oxygen, except for a short exposure time for mounting the grids in the microscope.

Polymerization to Obtain Ribbons and Oriented Films

Under sheared conditions, oriented [CH]_x could be obtained in the form of ribbons and films. To a 200 ml STPB, 1 mM Ti(OBu)₄ at 4/1 Al/Ti ratio was injected. A 1 inch teflon coated magnetic stirrer was used for agitation and its initial rotation speed was ca. 800 rpm as found by a stroboscope. Acetylene was introduced at ca. 0.7 atm. and was polymerized for 1 hour. Samples were washed as outlined elsewhere. The number average molecular weight of the polymer was determined by radiolabeling to be about 42,000.

Polymerizations to Obtain Films

To obtain films of standard [CH]_x as prepared by workers in the field and described by Shirakawa et al.,⁴¹ a reactor as shown in Figure 2.6 was used and films grown on the vertical walls. A detailed description of the procedure can be found elsewhere.¹¹⁰ When preparing both low and high molecular weight [CH]_x, the polymerization rates are considerably slower than when preparing standard polymer

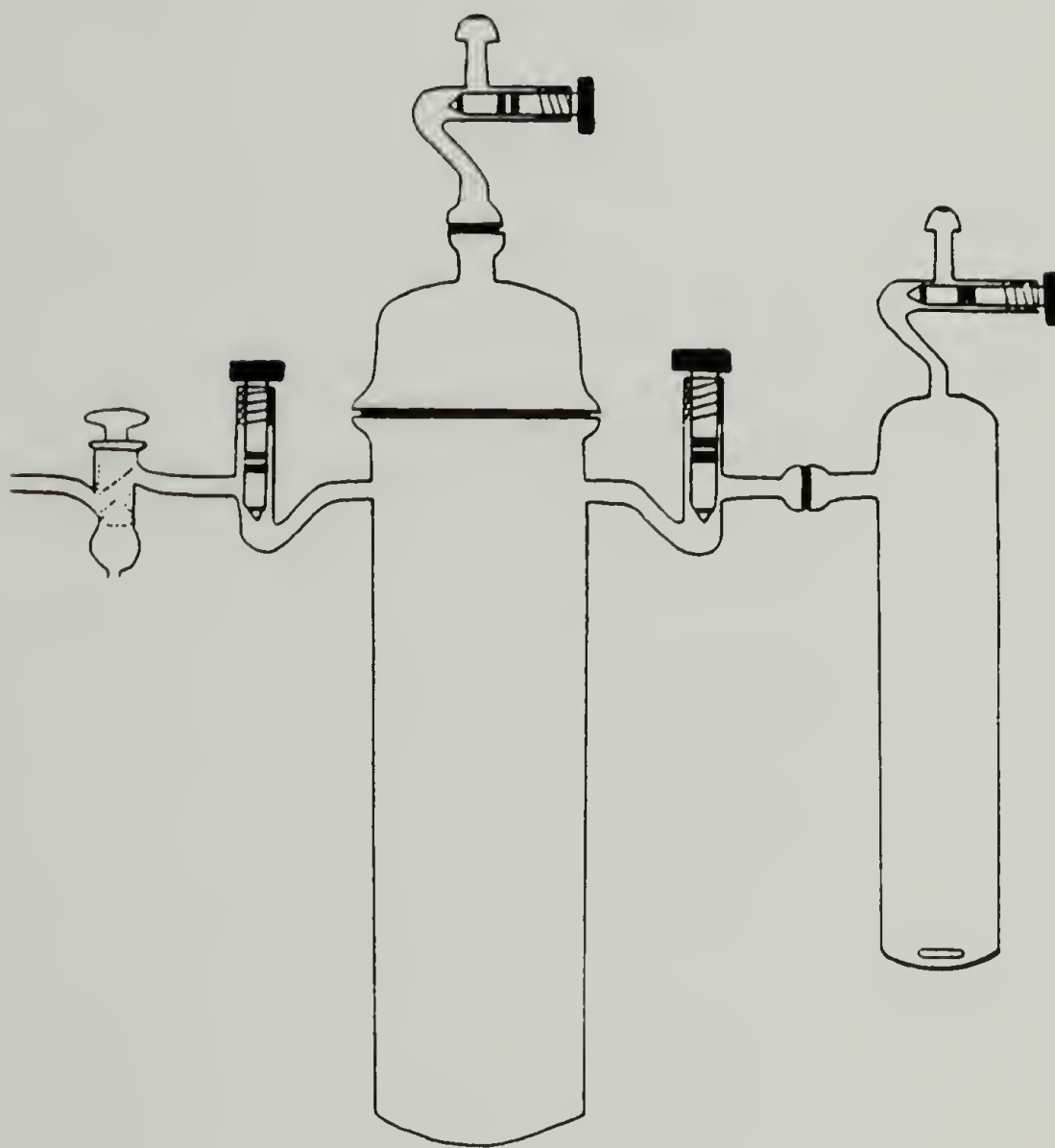


Figure 2.6 Standard Reactor for Obtaining Polyacetylene Films.

films. Therefore, these films can not be polymerized on the vertical reactor walls since the films are not self-supporting. The reactor shown in Figure 2.4 was consequently used.

To obtain low molecular weight polymer, LMnP, the below set of reaction conditions were used:

$[Ti]_0$: 0.740 M ("Neat")

Al/Ti : 7/1

Catalyst aging : 1 hour

$P_{C_2H_2}$: 15-30 mm Hg

Temperature : 195 K

Order of addition : monomer to catalyst

Polymerization time : 2 hours

To obtain HMnP, the below set of reaction conditions were used:

$[Ti]_0$: 0.001 M ("Hot")

Al/Ti : 4/1

Catalyst aging : 1 hour

Temperature : 195 K

Order of addition : Catalyst to monomer

Polymerization time : 2 hours

Washing, Handling and Storage

Samples prepared for kinetics experiments did not need to be excluded from oxygen since only combustion analysis for their radioactivity was performed. It was found that this short exposure to the atmosphere had no effect on the polymer specific activity. Solvents were not deoxygenated and samples were handled out in the open and in

the hood. First samples were scrupulously washed with 10% HCl/CH₃OH which solublized the catalytic debris and afterwards rinsed with methanol and dried at room temperature under vacuum.

Films which were prepared for physical studies were continuously excluded from oxygen and moisture. These were first multiply washed with pentane or toluene to remove the excess catalyst, then deoxygenated 10% HCl/CH₃OH. This also had the effect of loosening the fragile films from the glass walls. They were lastly rinsed in toluene. Wet films were taken into the dry box and floated onto teflon discs. Toluene was removed, and the samples dried in a vacuum desiccator at room temperature.

After drying, these extremely fragile films were taken back into the dry box and placed between aluminum foil sheets and folded into storage tubes with #25 o-ring tops. Samples were stored under vacuum or under argon at 195 K.

Specific Activity and Elemental Analysis

Samples labeled with ³H or ¹⁴C were sent to New England Nuclear, Boston, Massachusetts for combustion analysis. One to five milligram samples were burnt in an oxygen rich atmosphere and the effluent gases trapped for scintillation counting. Activities were reported as disintegrations per milligram (dpm).

For elemental analysis 5-10 mg films were sent in sealed glass ampoules to Galbraith Labs, Knoxville, Tennessee. Direct C, H, O, Ti, and Al were obtained.

Structural Characterization

Infra-Red Spectroscopy

Absorption infra-red (IR) spectra were taken on $[\text{CH}]_x$ films using a Perkin-Elmer Model 283 Spectrophotometer. It was found that film thicknesses on the order of 40-90 μm gave spectra in which all the absorption peaks could fit on the chart paper. All spectra were taken in air since it was found that within the 20 minute time over which spectra were taken, no detectable changes in the IR spectra could be seen. Samples were mounted on cut-out cardboard holders within the dry box or glove-bag and transferred to the spectrophotometer in a ziplock polyethylene bag.

Electron Microscopy

Micro-morphologies were examined by scanning electron microscopy (SEM) using a ETEC Autoscan microscope. Samples were sputtered with ca. 400 Å thickness gold as a conductive support. For transmission electron microscopy (TEM), a JEOL 100 kV scope was used. Samples were prepared as described earlier on gold, carbon coated grids. Micrographs and electron diffraction images were obtained.

Electron Paramagnetic Resonance (EPR)

Electron paramagnetic resonance experiments were performed using a Varian E-9 x-band spectrophotometer equipped with dual cavities and a Varian variable temperature controller. The temperature controller was calibrated over a temperature range of 123 K to 473 K using a copper-constantan thermocouple with the EPR cavity. Microwave power, modula-

tion amplitude, scan width, scan speed and recorder time constant were set to give an undistorted spectra.¹⁴⁴ EPR tubes were made of clear fused quartz of 3.0 mm inside diameter, 0.5 mm wall thickness. A #7 o-ring joint atop the tube allowed the tube and its contents to be sealed under vacuum. Samples of 1.0 to 2.0 mg were loaded within the dry box and weighed to ± 0.1 mg.

Quantitative Determination of Unpaired Spins

Within the EPR cavity, there is a ca. 1 cm region of maximum microwave flux. Therefore, all samples including the standard were packed within 1 cm of the bottom of the tube. When inserted into the cavity, the horizontal position was adjusted to give a maximized signal. Spectra were recorded and integrated using a Fabri-Tek Model 1072 computer. The integral was recorded and the area under the absorption curve determined by weighing using a Mettler Model H70 Microbalance. Two 2,2,6,6 tetra methyl-piperidinoxy radical (Aldrich) standards containing 10^{-7} and 10^{-6} mole spins were also recorded.

Spin concentrations were calculated using Equations 2.5, and 2.6 and usually reported as the molar ratio of spins to CH units in the specimen.¹⁴⁵

$$N_x = \frac{S_x^2 \gamma_x V_x H_s P_s^{1/2} G_s N_s I_s}{S_s^2 \gamma_s V_s H_x P_x^{1/2} G_x I_x} \quad (2.5)$$

where H = modulation amplitude (G)

P = microwave power (mW)

G = spectrometer gain

S = scan width (G)

V = vertical display

I = integration constant

Y = integral mass (g)

N = moles of spins

x denotes sample

s denotes standard

$$[S]^{-1} = \frac{13 \cdot N_x}{m} \quad (2.6)$$

where m = mass of sample (g).

Relaxation Measurements

Spin-lattice relaxation time, T_1 , and spin-spin relaxation time, T_2 were determined by the saturation method. EPR spectra were taken at microwave powers from 1-121 mW. Peak-to-peak amplitude, A, and peak-to-peak linewidth, ΔH_{pp} , of the derivative signal were plotted against the square root of the microwave power, $P^{1/2}$, in mW. The power where A reaches a maximum is P_{sat} and the peak-to-peak linewidth below P_{sat} is taken as ΔH_{pp}^o .

T_1 and T_2 relaxation times were calculated using Equations 2.7 and 2.8, as derived by Warakowski,¹¹⁰

$$T_1 = \frac{1.97 \times 10^{-7} \cdot \Delta H_{pp}^o}{g \cdot 0.49 \cdot P_{sat}^{1/2}} \text{ sec.} \quad (2.7)$$

$$T_2 = \frac{1.313 \times 10^{-7}}{g \cdot \Delta H_{pp}^o} \text{ sec.} \quad (2.8)$$

where g = signal g-value.

Variable Temperature Experiments

Curie spin susceptibility was evaluated by measuring the variation in signal intensity over temperatures from 133 K to 293 K. Spectra integrals at each temperature were weighed and the mass relative to 273 K or 293 K reference temperature were plotted against T^{-1} . The Curie slope is taken as the slope of the relative signal intensity versus T^{-1} .

EPR isomerizations of cis-rich samples were also done at temperatures from 373-483 K. First at room temperature the signal would be maximized. With the sample out of the cavity, the temperature was set and allowed to equilibrate. Once the sample was inserted, spectra were taken at regular intervals and the signal linewidth ΔH_{pp} plotted versus isomerization time. Since both the linewidth and signal amplitude were changing over time, adjusted signal amplitudes were plotted over time by assuming Lorentzian line shape. Equation 2.9 was used to obtain the corrected amplitudes.

$$A_o = A[1+0.75\Delta H_{pp}^2] \quad (2.9)$$

where A_o = corrected amplitude

A = measured amplitude

ΔH_{pp} = peak-to-peak linewidth

Iodine Doping

Sample Preparation and Equipment

Chemical doping with iodine, i.e., oxidation of the polyacetylene

chain, was accomplished by treating a $[\text{CH}]_x$ film with iodine vapor at a given vapor pressure. Figure 2.7 shows the apparatus which was used for "cold" iodine doping which allows simultaneous conductivity measurements. Within the side arm would be several milligrams of iodine crystals.

Because of the limited amount of polymer for $^{125}\text{I}_2$ doping, this apparatus was modified such that a 100 ml cow with six removable EPR tubes extending was attached to the doping chamber (Figure 2.8). In this way, polymer samples of known mass could be doped and sealed off with a torch at various points. These then would be used for gamma counting, EPR and thermoelectric coefficient measurements. $^{125}\text{I}_2$ crystals were contained within the side arm tube.

$[\text{CH}]_x$ samples for conductivity measurements were mounted within the dry box. A rectangular strip of polymer was cut and the width, w , and thickness, t , measured using a metric measuring calliper and micrometer respectively. Samples were then mounted between the platinum wires extending from the 4 fingers of the apparatus and the fingers themselves. Electrodag 502 (Acheson Colloids Co.) was used to make contact between the wires and the film. The distance measured between the inner two electrodes was taken as the sample length, l .

Slow Doping Procedure

Before assembling the apparatus, the iodine within the side chamber of Figure 2.7 was condensed with liquid N_2 and evacuated for a minimum of one hour. Once attached to the vessel containing the polymer sample, the entire vessel was thoroughly evacuated and checked

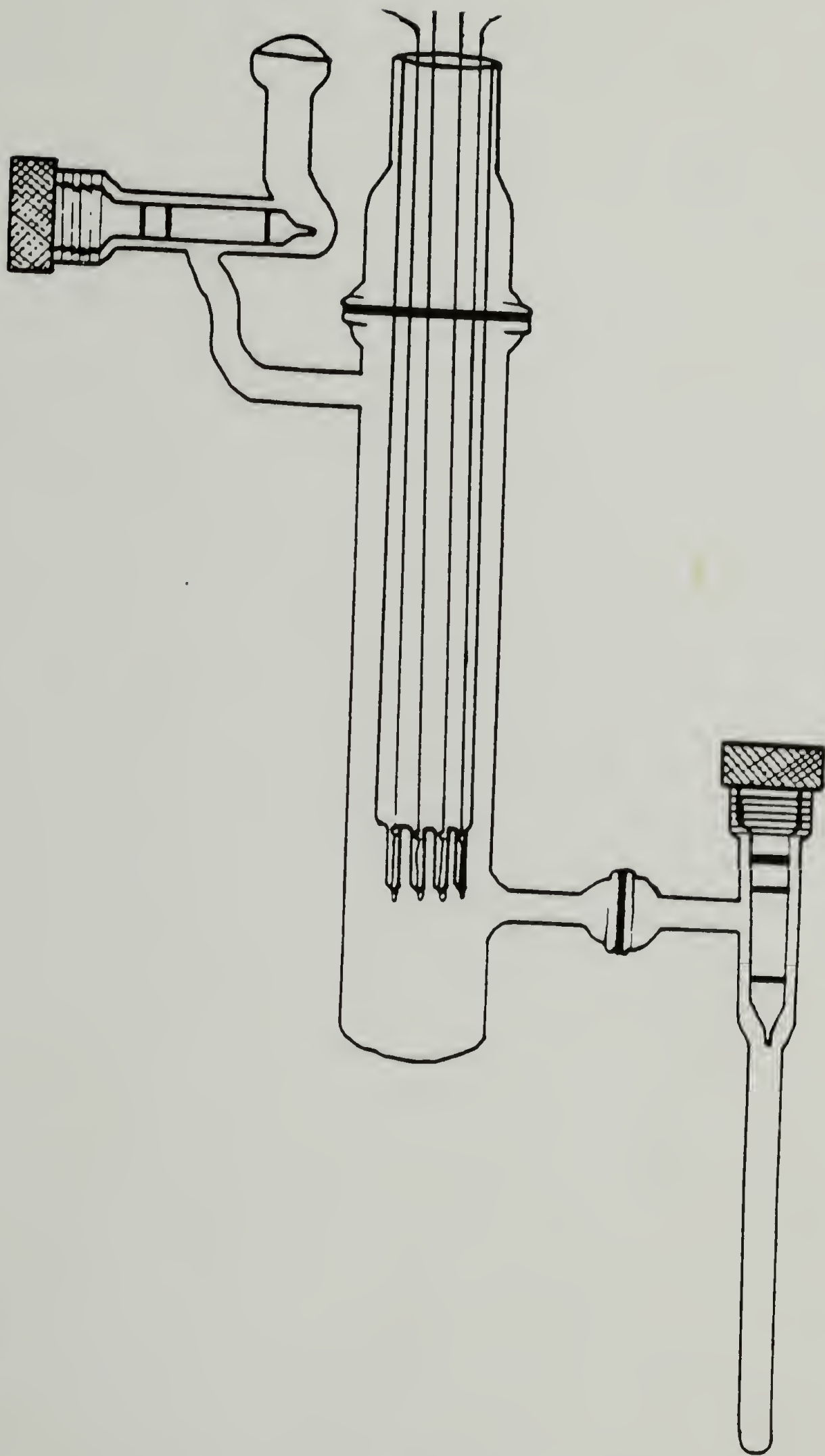


Figure 2.7 Iodine Doping Apparatus.

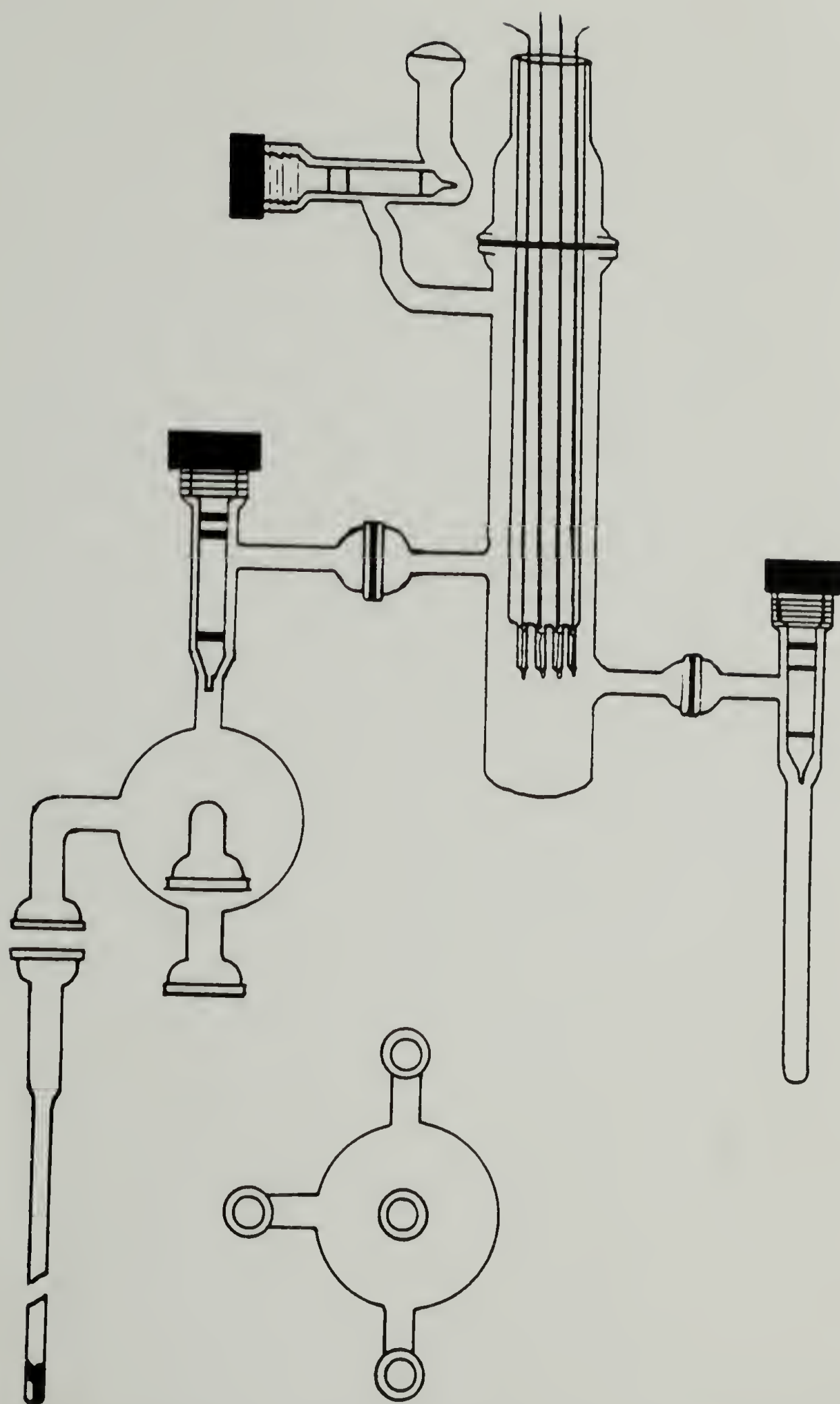


Figure 2.8 $^{125}\text{I}_2$ Doping Apparatus.

to be leak-proof. The extent of doping was controlled in two ways: (1) by regulating the time of doping and (2) by the temperature and therefore the vapor pressure of iodine. The iodine temperature was regulated using dry ice or slush baths. Low level doping was accomplished by keeping the I_2 at 195 K by using dry ice/ethanol. Higher levels of doping were obtained at temperatures from 243 K to 273 K using either a carbontetrachloride/liquid N_2 slush (250 K) or adding small amounts of dry ice to ethanol (243 K to 273 K). For maximum doping, I_2 was at room temperature.

In some cases, when samples were to be maximum doped, after exposure to I_2 for a given time, excess I_2 was cryogenically removed from the doping vessel, and then reintroduced under a new set of doping conditions. This cycling back and forth would be continued until the sample was doped overnight at room temperature to give maximum doping. Most often, however, to get a maximum doped film, I_2 was introduced and the temperature of the I_2 reservoir gradually increased over time. In both procedures, after exposure to iodine overnight at room temperature, excess iodine would be cryogenically removed using liquid N_2 .

The composition of heavily doped films was determined by weight uptake using the digital balance within the dry box and expressed as mole fraction of $I_3^-(Y)$ with respect to CH repeat unit.

$$Y = \frac{\text{mass Iodine(g)}}{\text{mass } [CH]_x(g)} \cdot 3.41 \times 10^{-2} \quad (2.10)$$

Isotopic $^{125}I_2$ Doping and Assay

Doping from $-8.0 \leq \log Y \leq -1.0$ was possible using $^{125}I_2$. After

loading six EPR tubes with 1.0-2.0 mg polymer and mounting a sample for conductivity measurements, the doping vessel was evacuated as described earlier. Doping was always performed in the hood and the iodine reservoir shielded with lead foil. Doping level was controlled in a similar way as earlier described. However, before sealing off any sample, excess $^{125}\text{I}_2$ was condensed back into the reservoir using liquid N_2 until a stable resistance was measured.

Iodine content was quantified by gamma counting the samples sealed within the EPR tubes using a Packard Auto-Gamma, Model AP-GD gamma counter. Instrumental efficiency was found to be routinely 49.3% based on a $^{129}\text{I}_2$ standard. Using Equation 2.3 to calculate A_t , the level of doping, Y , can be found using Equation 2.11.

$$Y = \frac{\text{cpm}}{A_t \cdot g(\text{CH})_x} \cdot 1.19 \times 10^{-8} \quad (2.11)$$

Y = mole fraction of I_3^-

cpm = instrument counts per minute

$g(\text{CH})_x$ = mass of polymer (g)

Transport Measurements

Transport properties, which include electrical conductivity σ_{RT} and thermoelectric power coefficient (S), were measured for LMnP, standard films, and HMnP.

Conductivity Measuring Devices and Instruments

Basically, $[\text{CH}]_x$ conductivities were measured either as a function

of cis-trans content, temperature, or dopant concentration.

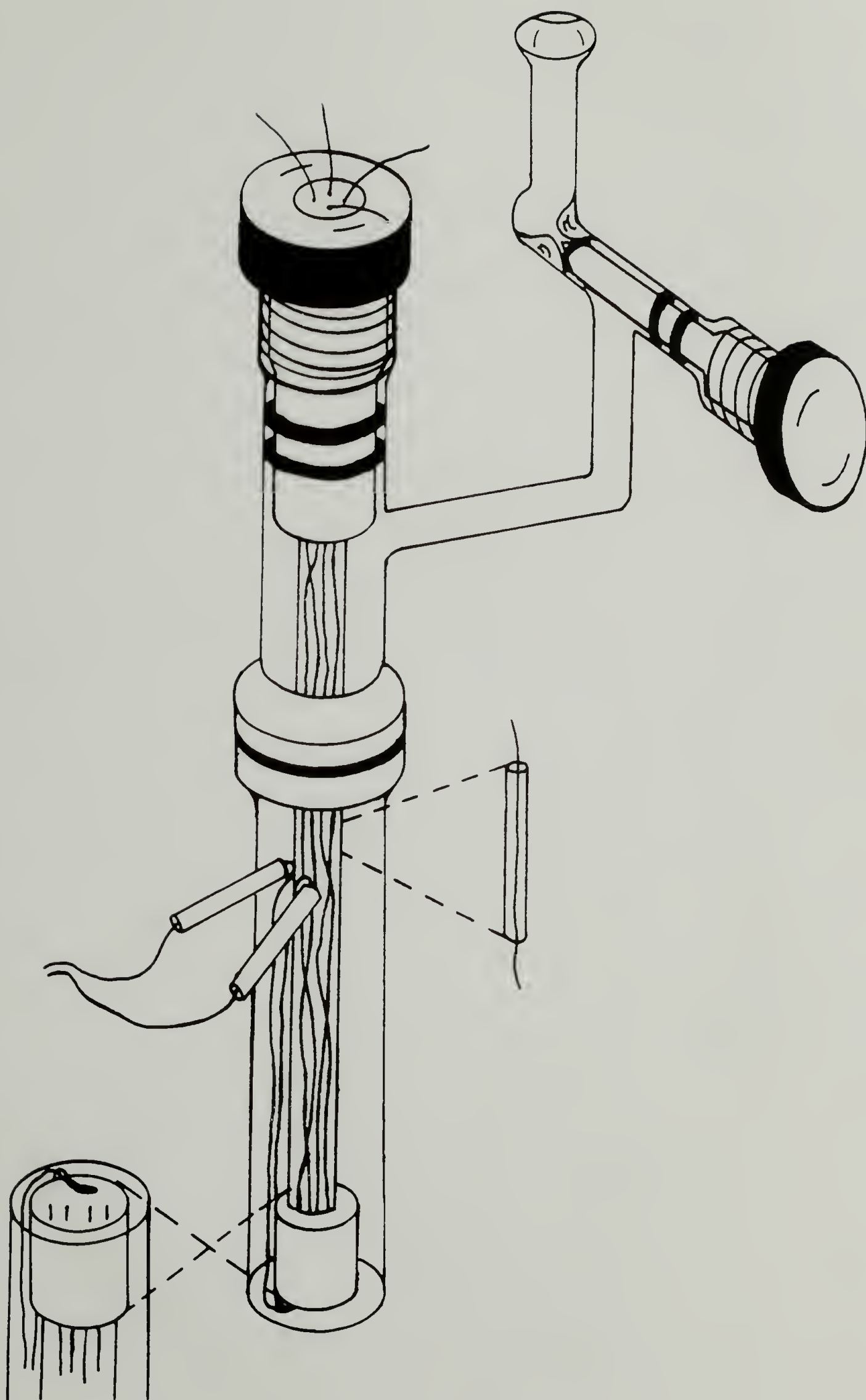
To follow the isomerization kinetics of cis films, conductivities were measured using two different apparatuses. The first was very similar to the doping chamber shown in Figure 2.7 except the outer glass housing did not have an o-ring joint to attach a side bulb. Also, running down the center, a copper-constantan thermocouple feed-through made it possible to measure the sample temperature directly. Two deficiencies become apparent. First, more than 15 minutes was needed to reach thermal equilibrium after immersing the chamber in a molten salt bath. Secondly, there was often a 10°C temperature differential after equilibrium was established.

These two points lead to the design of the conductivity isomerization vessel shown in Figure 2.9. In this design, the $[\text{CH}]_x$ film was pressed against the glass bottom using a teflon disc. Platinum wires coming through the teflon make pressure contact with the sample. A copper-constantan thermocouple is also pressed between the teflon disc and the glass bottom. In this way, thermal equilibrium was achieved after 6 minutes. All measurements were two point conductivities.

For measurements during chemical doping, the apparatus in Figure 2.7 was used without modification.

For low temperature conductivity measurements an Air Products LT-3-110 Liquid Transfer Heli-Tran system with liquid N_2 and APD-E Model 3700 Digital Temperature Indicator/Controller was used. Temperatures were read by an Au(7% Fe) versus chromel thermocouple. One end of the Heli-Tran transfer line extended into a 40 liter liquid N_2 dewar and

Figure 2.9 Pressure Contact Four-Probe Isomerization Chamber.



pressurized. The other end fitted within a vacuum shroud which holds the sample. Samples were mounted in the dry box using Electrodag to make good electrical contact. Measurements were made under dynamic vacuum. It was found that because the sapphire sample support had a resistance of ca. $10^{10.8} \Omega$, measurements down to $10^9 \Omega$ sample resistance could only be made.

Sample resistances were determined using either two probe or four probe measurements. For sample resistances greater than $10^5 \Omega$, two probe determinations using a Keithley 616 electrometer were made. For $10^5 \leq \Omega \leq 500$, a Fluke 1020B multimeter was used. Below 500 ohms, 4 point measurements were made to eliminate the effect of contact resistances.^{64,110} Equation 2.12 is used to calculate sample conductivity.

$$\sigma_{RT} = [R \cdot \frac{w \cdot t}{l}]^{-1} (\Omega \text{cm})^{-1} \quad (2.12)$$

where R = sample resistance

w = sample width

l = sample length

t = sample thickness

Thermoelectric Power Apparatus and Measurements

Thermopower measurements were made on an instrument designed and built within the University. A piece of $[\text{CH}]_x$ of ca. 4x8 mm was clamped between two copper plates, of which one was slightly heated by a nichrome wire and a DC power supply. A 2-5 K temperature difference

was measured with copper-constantan thermocouples and the output voltage, after on Omega ice point compensation, measured on a Keithley 147 Nanovolt Null Detector. The potential difference was measured with a Keithley 610C electrometer. The sample chamber was kept within an N_2 filled environment. The overall device resistance was ca. $10^{10}\Omega$ so samples with $R \leq 10^8\Omega$ could only be measured. The thermopower or Seebeck coefficient, S , is then given as microvolts per degree, $\mu V \cdot K^{-1}$.

C H A P T E R I I I

ACETYLENE POLYMERIZATION KINETICS AND MOLECULAR WEIGHT

The kinetics of acetylene polymerization initiated by $\text{Ti}(\text{OBu})_4/4\text{AlEt}_3$ catalyst was studied by radioquenching with C^*O to count the number of active sites, $[\text{C}]$, and by CH_3OT^* to determine the total metal polymer bonds, $[\text{MPB}]$, and \bar{M}_n of the polymer.¹⁴⁶⁻¹⁴⁹ The amount of quenching agent and time of reaction required and the kinetic isotope effect for CH_3OT^* were determined. The overall mechanistic scheme for these experiments is given in Figure 3.1. The effects of Al/Ti ratio, catalyst aging, catalyst concentration, temperature, and monomer pressure on the polymerization were investigated. Detailed kinetic data on the variation of rate of polymerization, R_p , $[\text{C}]$, $[\text{MPB}]$, and \bar{M}_n with time were obtained at 298 and 195°K. The results required the assumption that the catalytic species C, is initially active and within less than 30 min. all are converted by bimolecular kinetics to a far less active species. Analysis of the data yielded rate constants of propagation and termination and their energies of activation. Estimates of chain transfer efficiency and rate constants were obtained.

Rate of Polymerization

Free-standing polyacetylene formed on the reactor wall is the most desirable form for spectroscopic, physical, chemical, mechanical, and electrical measurements. It is mechanically strong and ohmic contacts can be attached to it. For its formation a catalyst solution of suf-

ficient viscosity is vigorously shaken so that a layer of it is coated and physisorbed on the wall of a large glass reactor. Monomer is admitted immediately thereafter before the catalyst solution has a chance to run down the wall. Needless to say, if one is to study the kinetics as a function of temperature or catalyst concentration, the catalyst solvent would have to be changed to attain the proper viscosity. As might be expected, because the polymer is physically attached to the reactor wall and exposed to catalyst components of undeterminate quantity and ratio, the kinetics of its polymerization are complicated.

If a dilute catalyst solution is used and stirred during polymerization, a mostly fibrous powdery polymer can be obtained. Though the products are inferior for electrical and other measurements, polymerization conditions are as uniform as possible for kinetic studies.

At moderate and high catalyst concentrations, under quiescent conditions or even agitation with a magnetic stir bar, polymerization occurs so rapidly at the surface of the reaction mixture that a polymer gel layer is formed. The density and thickness of this surface gel depends strongly on the catalyst concentration and monomer pressure which act as a barrier against diffusion of monomer to other parts of the growing polyacetylene gel and even more so into the reaction medium beneath it. The indeterminate monomer concentration and catalyst composition thus would, under these conditions, render any kinetic measurements both uncertain and ill defined.

More than 60 polymerizations were carried out at 298 K and 195 K under otherwise identical conditions of $[\text{Ti}(\text{OBu})_4]_0 = 1 \text{ mM}$, $\text{Al/Ti} = 4$

or 10, catalyst aging time = 30 min., and $P_{C_2H_2} = 760$ torr. The polymerizations were stopped after a predetermined time and radioquenched with CH_3OT^* or C^*O . The yields of polymer as a function of polymerization time are shown in Figures 3.2a, 3.3a and 3.4a.

Most of the polyacetylene was produced in the initial period. At 298 K 60% of the polymer was obtained during the first 20 min., compared with the total yield after 240 min. The yield at 25 min. of polymerization at 195 K was about 75% of that at 240 min. In other words, the rate of polymerization was initially rapid but then decreased (Figures 3.5 and 3.6). At both temperatures R_p decreased about 30-fold during the first 30 min. of polymerization.

Temperature Effects

The effect of temperature on the polymerization is shown in Table 3.1 for reactions carried out with $[Ti]_0 = 1$ mM, Al/Ti = 4, for 2 hr. The yield of polyacetylene increased as the temperature increased, then decreased at the highest level. However, a significant temperature dependence occurred for the solubility of acetylene in toluene (Figure 2.5 and footnote in Table 3.1). The relative rate of polymerization was then obtained as polymer yield/ $[C_2H_2]$; Figure 3.7 is an Arrhenius plot of the relative rate. The overall activation energy of polymerization of acetylene was $4.2 \text{ kcal}\cdot\text{mol}^{-1}$.

Catalyst-Catalyst Composition

The Al/Ti ratio affects the rates of polymerization as shown in

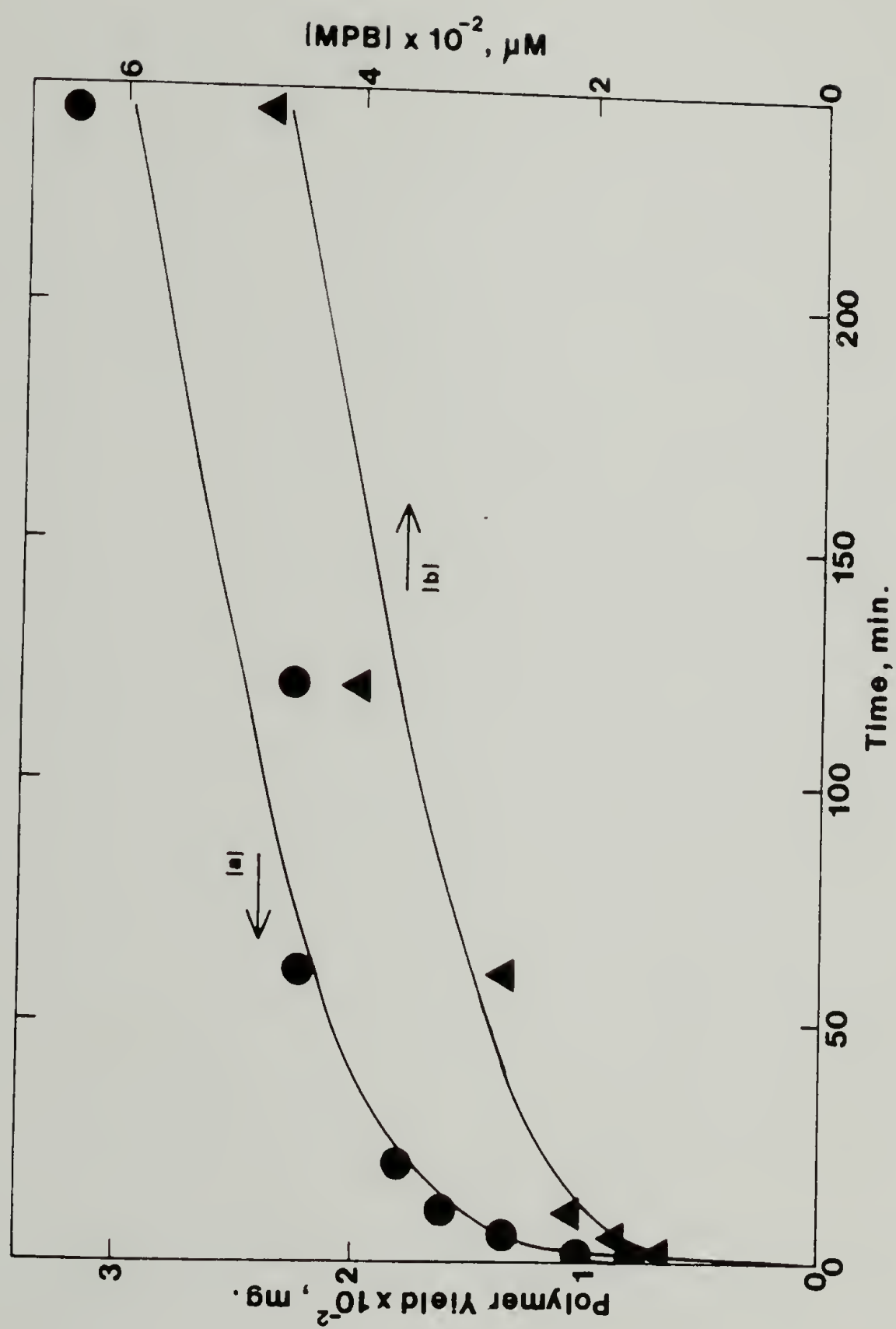


Figure 3.2 Variation of (a)(●) polymer yield; and (b)(▲) $[MPB]$ with time of Polymerization: $[Ti]_0 = 1$ mM, $Al/Ti = 4$, catalyst aging time = 30 min., temperature = 298 K, $P_{C_2H_2} = 760$ torr.

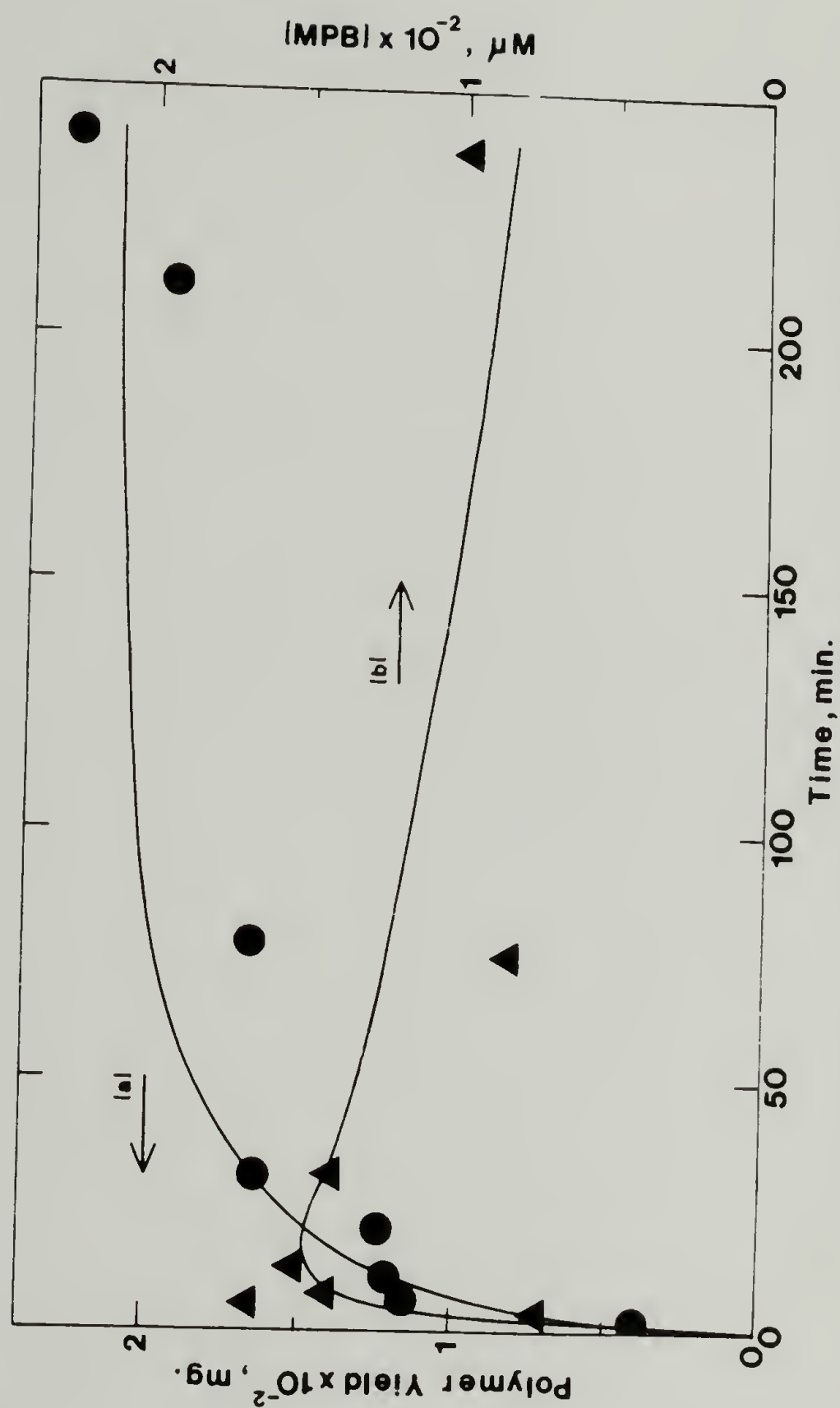
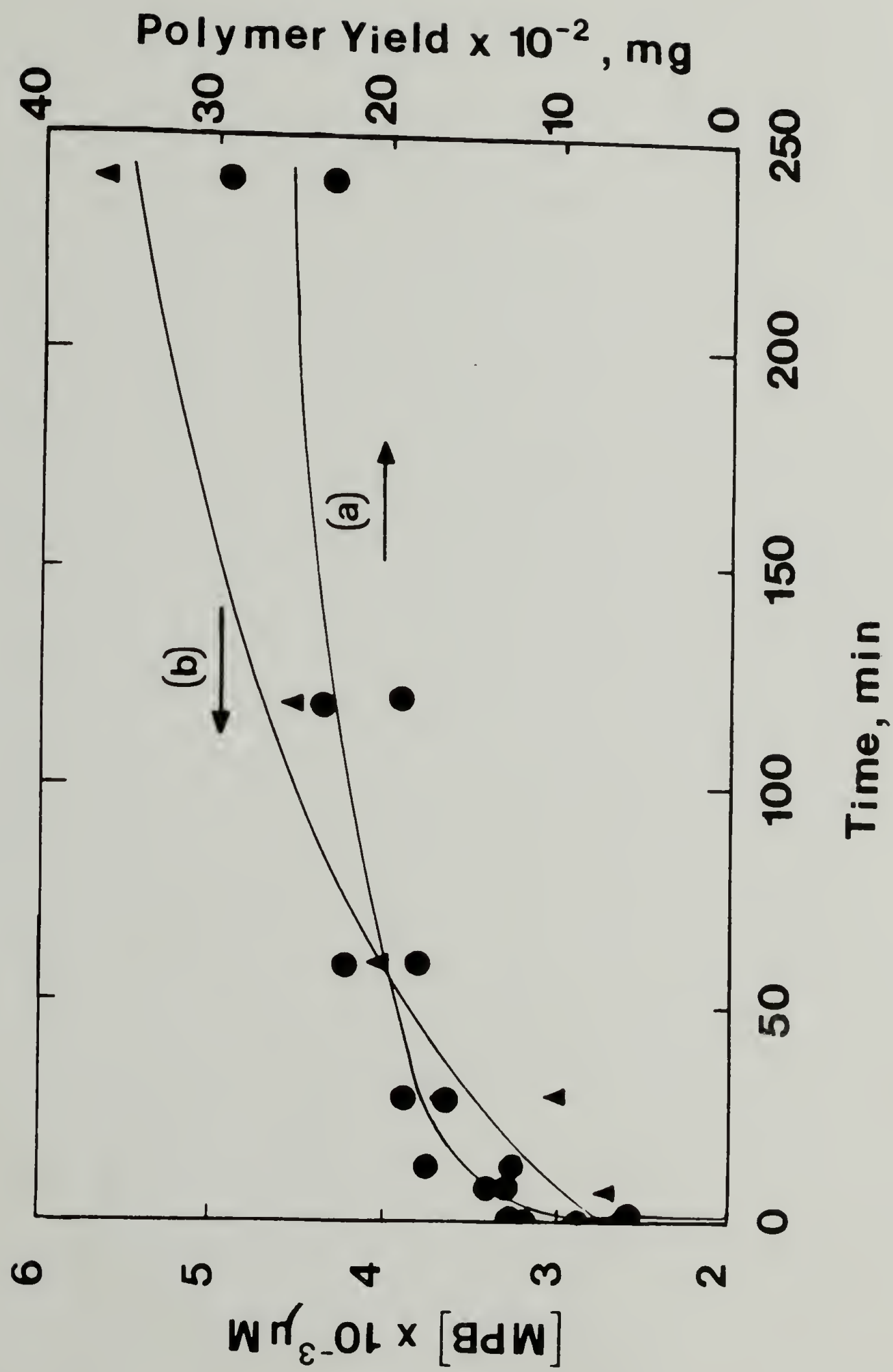


Figure 3.3 Variation of (a)(●) polymer yield; and (b)(▲) [MPB] with time of Polymerization: $[\text{Ti}]_0 = 1 \text{ mM}$, $\text{Al/Ti} = 4$, catalyst aging time = 30 min., temperature = 195 K, $P_{\text{C}_2\text{H}_2} = 760 \text{ torr}$.

Figure 3.4 Variation of (a) polymer yield (●) and (b) [MPB](▲) with Polymerization Time: $[Ti]_0 = 1 \text{ mM}$, $Al/Ti = 10$, catalyst aging = 30 min., temperature = 298 K, $P_{C_2H_2} = 760 \text{ torr}$.



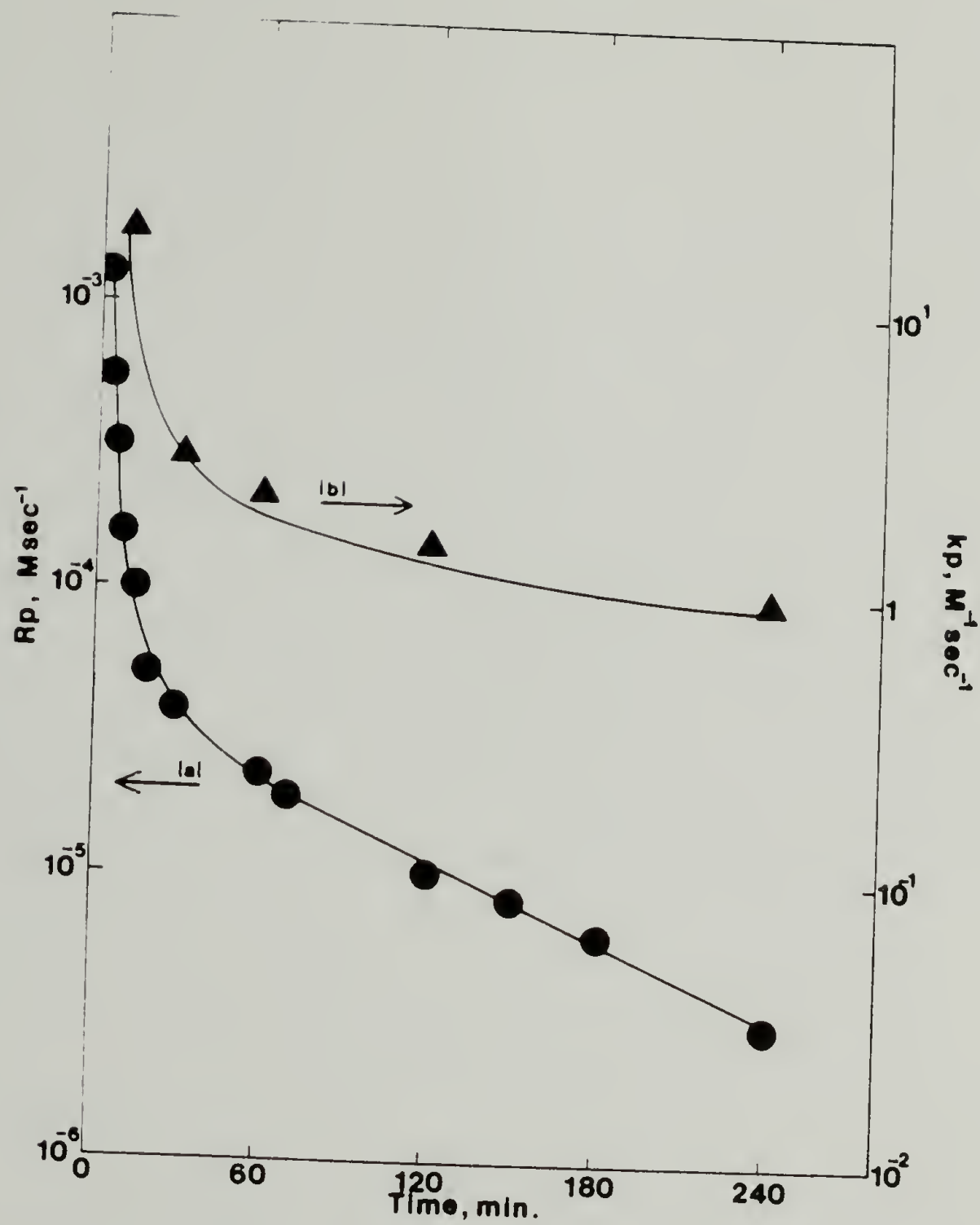


Figure 3.5 Variation of (a)(●) R_p ; and (b)(▲) k_p with Time of Polymerization: Conditions are the same as in Figure 3.2.

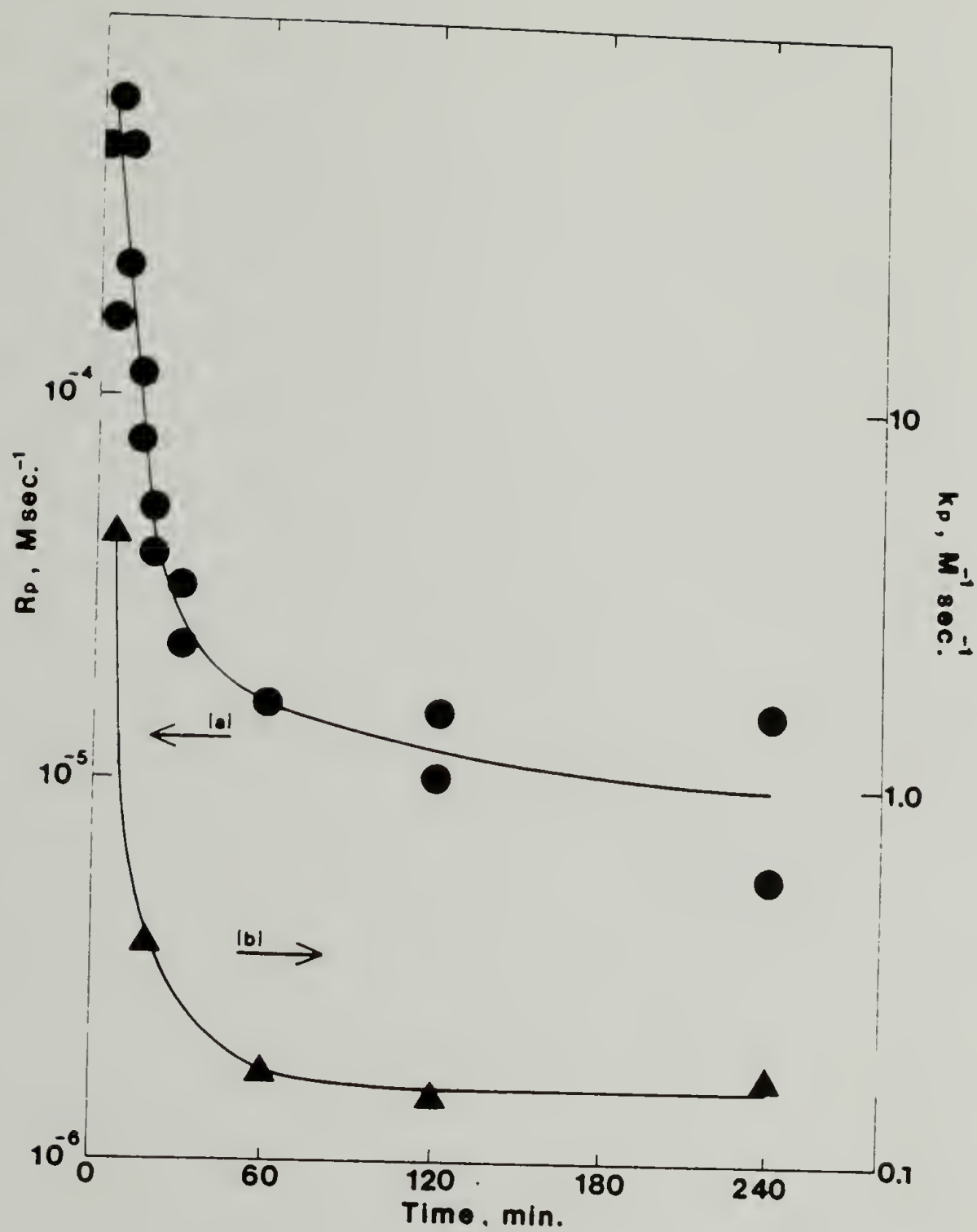


Figure 3.6 Variation of (a)(●) R_p ; and (b)(▲) k_p with Time of Polymerization: Conditions are the same as in Figure 3.3.

Table 3.1
Effect of Temperature on Acetylene Polymerization^a

Temperature (°C)	Polyacetylene yield (mg)	[MPB], (mM)	\overline{M}_n
70	115.2	0.35	16,300
70	78.0	0.30	13,100
70	112.4	0.40	14,000
20	228.1	0.36	31,700
20	242.6	0.38	31,600
-10	203.5	0.24	43,100
-10	198.0	0.24	42,000
-78	81.5	0.23	17,500
-78	56.9	0.12	23,000
-78	52.9	0.14	19,100

^a [Ti]₀ = 1 mM, Al/Ti = 4, time = 2 h, P_{C₂H₂} = 456 ± 40 torr, [C₂H₂] = 0.06M (70°C), 0.13M (20°C), 0.28M (-10°C), 2.1M (-78°C)

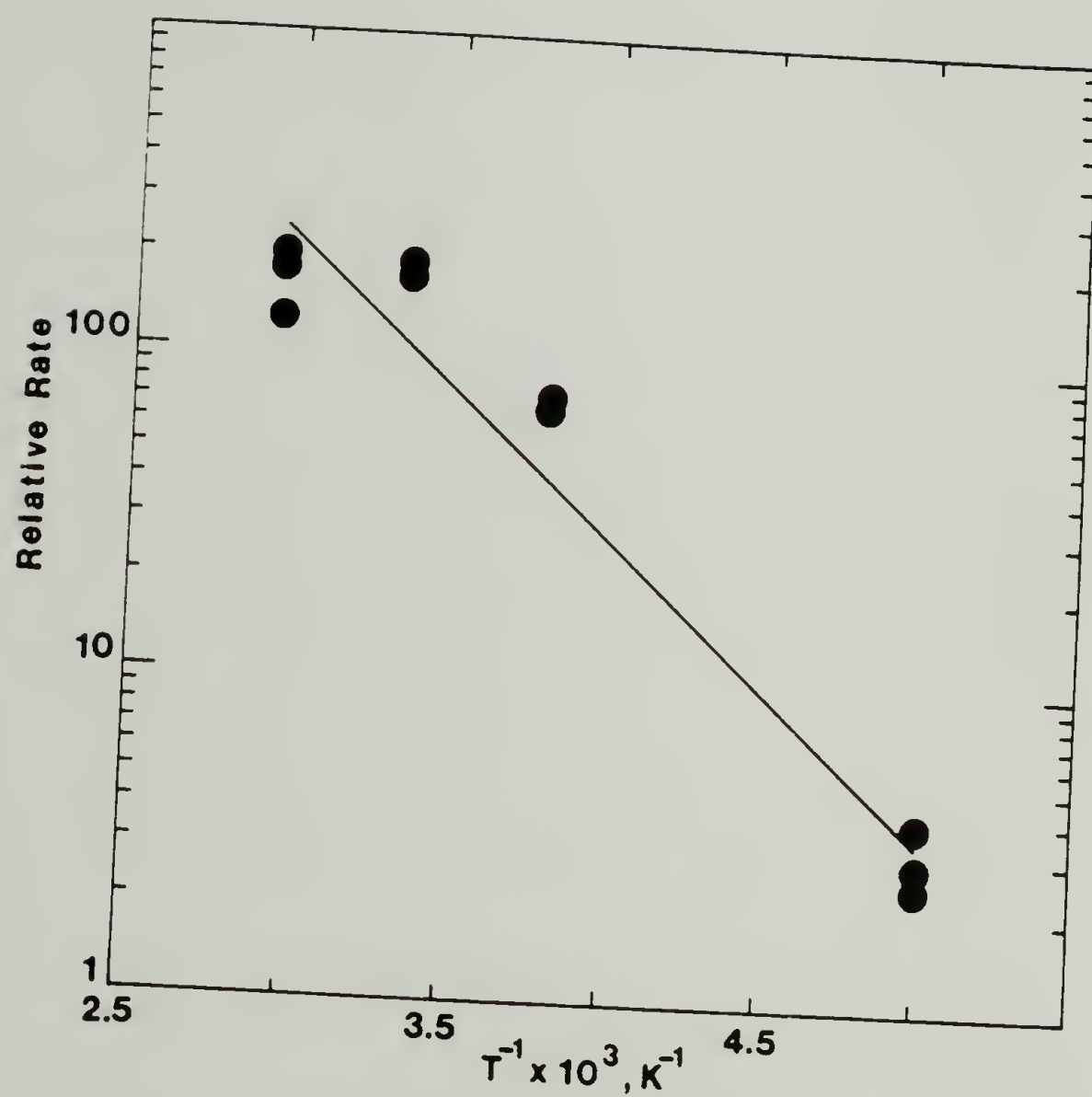


Figure 3.7 Arrhenius Plot of the Relative Rate of Polymerization: $[Ti(OBu)_4]_0 = 1 \text{ mM}$, $Al/Ti = 4$, $P_{C_2H_2} = 456 \text{ torr}$, $time = 2 \text{ hr.}$

Table 3.2. There was no appreciable polymerization for $Al/Ti \leq 2$. The maximum R_p was obtained at $4 \leq Al/Ti < 7$. At $Al/Ti = 10$ the yield of polyacetylene was reduced. The results suggest that it takes 4 mole of $AlEt_3$ to produce the most active catalytic species.

Catalyst Concentration

Table 3.3 lists the results of polymerization at various catalyst concentrations. The complexity of the system is seen in these experiments. At $[Ti]_0 = 1 \text{ mM}$ only fibrous powder polyacetylene was formed. At $[Ti]_0 = 5.1 \text{ mM}$, the polymer yields were 8-16 times greater than at $[Ti]_0 = 1 \text{ mM}$. In some experiments at this catalyst concentration only polyacetylene gel was produced whereas in other experiments both gel and powder forms of polyacetylene were obtained. The same was true at $[Ti]_0 = 41 \text{ mM}$. The polymer yields decreased with an increase in catalyst concentration at high concentrations.

Catalyst Aging

Table 3.4 shows the results of acetylene polymerization affected by the aging process of the catalyst. The rate of polymerization reflected in the yield of polyacetylene decreased monotonically with the increase of catalyst aging. The same relationship holds for $[MPB]$. The best compromise of polymer yield and molecular weight was obtained with catalyst aged for 30-60 min.

Monomer Pressure

The effect of monomer pressure on polymerization was also studied;

Table 3.2
Effect of Al/Ti Ratio on Acetylene Polymerization^a

Al/Ti	Polyacetylene yield (mg)	[MPB](mM)	\bar{M}_n
1	0	—	—
2	0	—	—
4	300	0.4	40,000
7	314	2.5	6,200
10	171	2.8	3,050

^a [Ti]₀ = $10^{-3}M$, $P_{C_2H_2}$ = 1 atm, temperature = 25°C, time = 2 h, catalyst aging time = 1 h.

Table 3.3
Effect of Catalyst Concentration on Acetylene Polymerization^a

[Ti] (mM)	Powder		Gel		Film \bar{M}_n
	Yield (mg)	[MPB] (mM)	Yield (mg)	[MPB] (mM)	
1	60.6 ± 14	0.15			20,100
5.1			462 ± 15	3.0	7600
5.1	978 ^b ± 71				8400
41.0	129 ± 10	24	340 ± 59	6.0	5700
204			298 ^c ± 16		5800
					11,800

^a Al/Ti = 4, temperature = -78°C, P_{C₂H₂} = 456 ± 40 torr, time = 2 h., and values for yields were an average of four runs.

^b Total yield of gel and powder.

^c Total yield of gel and film.

Table 3.4
Effect of Catalyst Aging on Acetylene Polymerization^a

Aging time (h)	Polyacetylene yield (mg)	[MPB], mM	\overline{M}_n
0	380	1.0	18,900
1	300	0.4	90,000
192	180	0.33	27,200
1200	74	0.69	53,100
6216	71	0.1	34,300

^a [Ti]₀ = $10^{-3}M$, $P_{C_2H_2}$ = 760 torr, temperature = 25°C, time = 2 h.

the results are summarized in Table 3.5. In the first seven runs the polymer yield increased as the pressure increased, but much more than expected for a linear relationship. The variation in [MPB] was large, but no definite trend toward a dependence on monomer pressure was revealed. The polyacetylene molecular weight also increased with acetylene pressure, but like the polymer yield the increase in \bar{M}_n was greater than expected. In these experiments the catalyst was mixed first with toluene and then with acetylene in the typical procedure for the preparation of free-standing polyacetylene film. Under these conditions the solvent was not saturated with monomer in equilibrium concentration. Because the approach to equilibrium may be expected to be more rapid at a higher acetylene pressure, the observed variations in yield and \bar{M}_n with $P_{C_2H_2}$ can be understood. In runs 8-10 of Table 3.5, the toluene was saturated with acetylene before the catalyst was injected. Compared with the results of runs 5-7, the yield was about twice as large and \bar{M}_n was higher when the solvent was saturated with monomer. Consequently, subsequent kinetic experiments were similarly performed.

Non-Specific Labeling Using CH_3O^3H

Insertion Kinetics

Methanol reacts with all metal alkyl bonds and also exchanges with metal-alkoxyl groups. Acidic alcohol is used traditionally to remove metal ions from polyolefins initiated by Ziegler-Natta catalysts. Figure 3.8 shows the results of 3H specific activity in polyacetylene

Table 3.5
Effect of Acetylene Pressure on Its Polymerization^a

No.	P _{C₂H₂} (torr)	Time (min)	Polyacetylene yield (mg)	[MPB] (M)	\overline{M}_n
1	190	120	26	0.15	8500
2	190	120	31	0.13	11,600
3	380	120	48	0.13	18,700
4	380	120	39	0.10	19,200
5	760	120	118	0.06	100,000
6	760	120	128	0.16	40,000
7	760	120	101	0.09	85,000
8	760 ^b	20	144	0.07	105,000
9	760 ^b	75	201	0.08	121,600
10	760 ^b	240	235	0.10	120,400

^a [Ti]₀ = 1 mM, Al/Ti = 4, temperature = -78°C; the acetylene was added after the catalyst was injected.

^b Same as above except that acetylene was equilibrated with toluene and the catalyst was then injected.

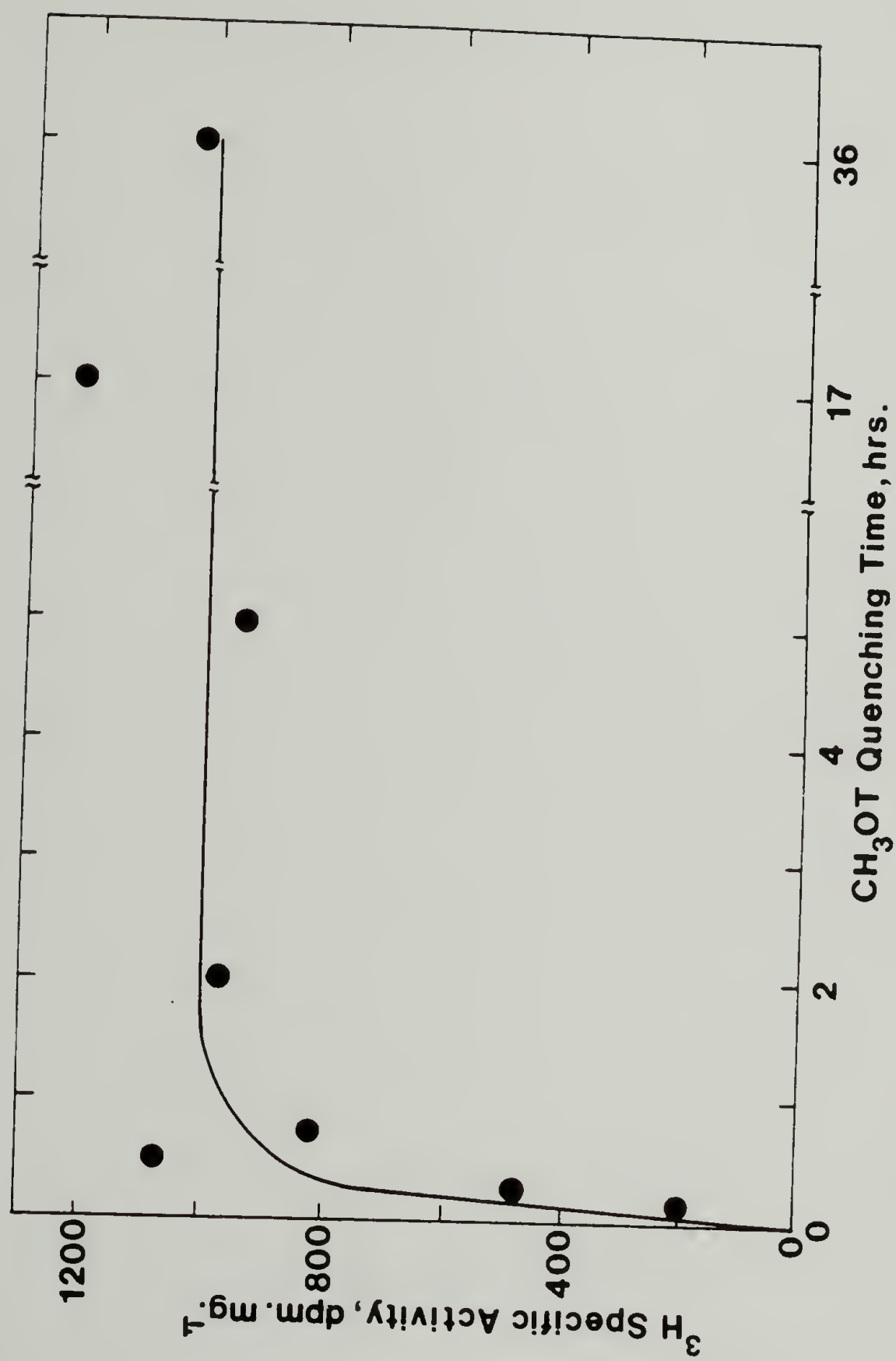
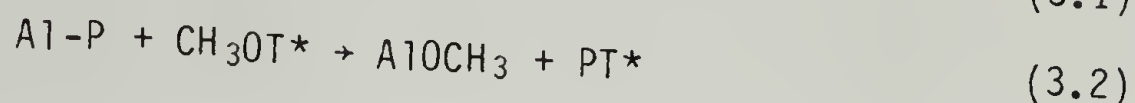
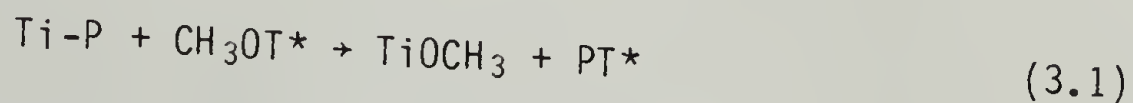


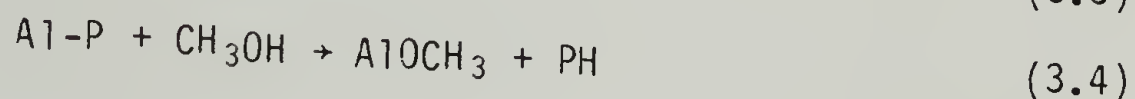
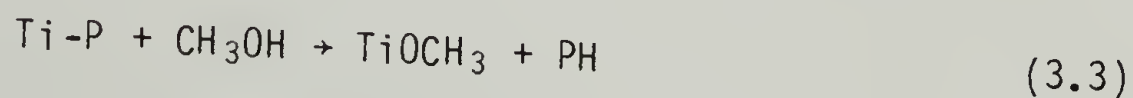
Figure 3.8 Rate of Incorporation of Tritium by the Reaction of CH_3OT^* with Metal Polymer Bonds. Polymerization Conditions: $25 \mu\text{mol}$ $[\text{Ti}]_0$, $100 \mu\text{mol}$ AlEt_3 , 20 ml Toluene, $P_{\text{C}_2\text{H}_2} = 530$ torr, 298 K, Time = 2 hr.

quenched with CH_3OT^* and worked up after various periods of contact time. A constant specific activity was attained for contact times of one-half hour or longer.

The reactions that lead to radiotagging of the polymer are



In addition, the parallel reactions for nonradioactive methanol are



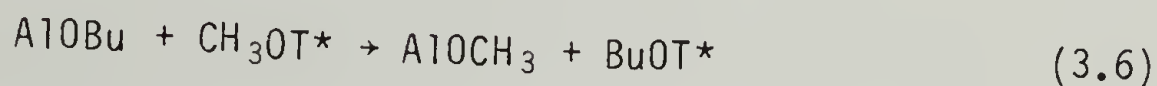
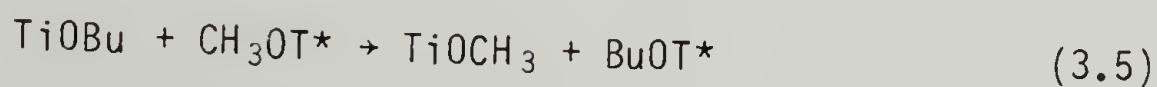
The rates for reactions (3.3) and (3.4) are expected to be faster than for those of (3.1) and (3.2). The ratio of the rate constants is the kinetic isotope effect. Ideally, $k_{\text{H}}/k_{\text{T}}$ should be determined separately for reactions (3.1) and (3.3) and for reactions (3.2) and (3.4).

However, no ingenuous method has been designed for this determination. Instead, only an average kinetic isotope effect was obtained by two separate experiments.

In the first method, polymerization was stopped by removing the monomer and then titrated with 17.5 μmol aliquots of CH_3OT^* . Each aliquot was allowed to react for 1 hr. before the addition of the next. A total of 1.4 mmol of CH_3OT^* was added; this is a 3.5-fold excess of the equivalent total number of potential metal carbon bonds. The ^3H specific activity in polyacetylene obtained was about 1.7 times greater than the ^3H incorporated in an identical polymerization but quenched by a

single addition of an excess of CH_3OT^* . Thus, the average value of $k_{\text{H}}/k_{\text{T}} \approx 1.7$. This method is based on the limited availability of methanol, therefore both isotopic methanol species in each aliquot reacted completely, even though the reaction is slower for CH_3OT^* than for CH_3OH .

The second method is illustrated in Figure 3.9. Parallel polymerizations were carried out with $[\text{Ti}(\text{OBu})_4]_0 = 2 \times 10^{-5} \text{ mol}$, $\text{Al/Ti} = 4$, $P_{\text{C}_2\text{H}_2} = 456 \pm 40 \text{ torr}$ at 263 K for 2 hr. Unreacted acetylene was removed by evacuation and different amounts of CH_3OT^* were added. With large excesses of CH_3OT^* , that is, more than 10^{-2} mol , the ^3H specific activity is low and constant. As the amount of CH_3OT^* decreased, the specific activity increased until a maximum value was reached. This point corresponds approximately to the stoichiometric amounts of methanol and reactive organometallic groups. The arrow corresponds to $4 \cdot [\text{Ti}(\text{OBu})_4]_0 + 3X \cdot [\text{AlEt}_3]_0 = 3 \times 10^{-4} \text{ mol}$. The results suggest that



also compete with reactions (3.1-3.4). The $k_{\text{H}}/k_{\text{T}}$ for this experiment is 3.4. Several similar experiments were carried out at other catalyst concentrations and polymerization temperatures. Isotope effects ranged from 2.8-3.6. When polyacetylene film and gel were produced in the same reaction, the $k_{\text{H}}/k_{\text{T}}$ values obtained separately for each agreed within an experimental accuracy of $\pm 20\%$. In some experiments, the amount of CH_3OT^* for maximum ^3H specific activity corresponded to one-

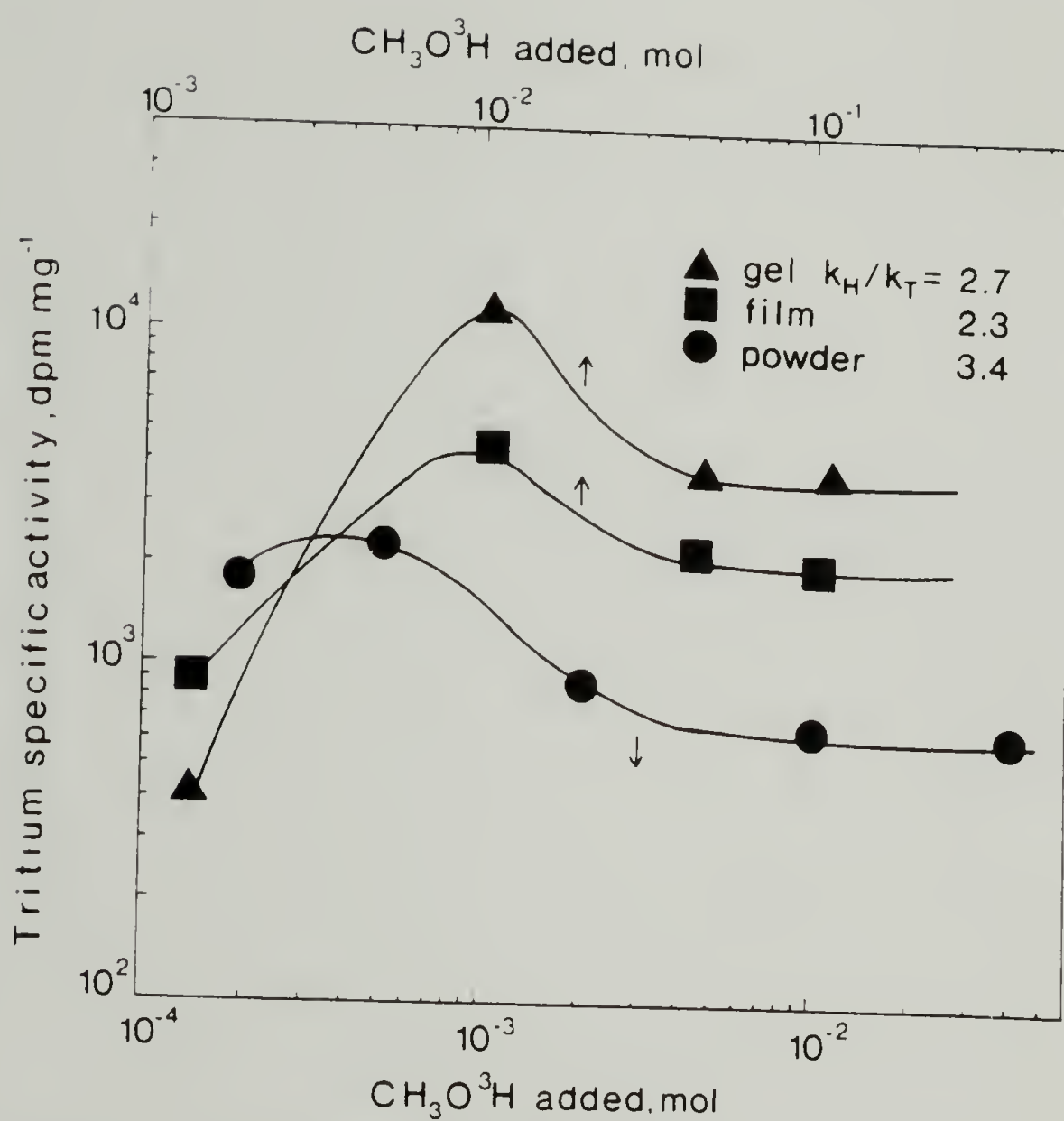


Figure 3.9 Variation of Specific Activity of ³H in Polyacetylene with the Amount of CH₃OT* Added. Polymerization Conditions: [Ti]₀ = 2 × 10⁻⁵ mol., Al/Ti = 4, P_{C₂H₂} = 760 torr, temperature = 263 K, time = 2 hr. Contact Time of CH₃OT* with Reaction Mixture was 2 hr.

half to one-third of the theoretical amount of organometallic groups. The average value of kinetic isotope effect for subsequent determination of [MPB] and \bar{M}_n is 2.8 ± 0.4 . Isotope effect values that lie between 1 and 10 have been reported for various Ziegler-Natta catalyst systems.

Burfield and Savarian¹⁵⁰ reported the exchange of tritium between CH_3OT^* and vinyl polymers in the presence of a Ziegler-Natta catalyst. The mechanism of the process is unclear. The catalyst activity for tritiation of vinyl polymers for the transition metal compounds decreases in the order of $\text{VCl}_4 \sim \text{TiCl}_4 > \text{TiCl}_3 \cdot 0.3\text{AlCl}_3 > \text{TiCl}_3 \sim \text{VCl}_3$; the order of the cocatalyst is $\text{AlCl}_3 > \text{AlRCl}_2 > \text{AlR}_2\text{Cl} > \text{AlR}_3$. Tritium exchange occurred most readily with polystyrene, and decreases in the order of polyethylene, poly(4-methylpentene-1), and polypropylene. There was a solvent effect as well. Tritiation was greater in petroleum ether than in toluene. It seemed that high Lewis acidic compounds promote this tritium exchange.

In the present catalyst system the metal compounds are free of chlorine ligands. Also, most of the CH_3OT^* added was consumed in reactions 3.1-3.6. When the CH_3OT^* was in excess, the ^3H specific activity in polyacetylene did not increase with the amount of CH_3OT^* added (Figure 3.9). Therefore, there was no indication of tritium exchange. Nevertheless, were experiments carried out to ascertain that the above mentioned exchange would not occur under conditions other than those used in radioquenching. Polyacetylene was worked up in the usual manner and redispersed in toluene. Fresh $\text{Ti}(\text{OBu})_4$ and AlEt_3 , alone and together in the 1:4 ratio, were added to different reactors and a ten-

fold excess of CH_3OT^* was introduced. After 1 hr. of standing the polymer was worked up again with nonradioactive methanol. In none of these cases was radioactivity above the background count detected. Therefore, with the weakly Lewis acidic $\text{Ti}(\text{OBu})_4$ and AlEt_3 the tritium exchange reactions reported by Burfield and Savarian¹⁵⁰ do not occur with polyacetylene.

On the basis of these experiments, the following method was used to determine metal polymer bond concentrations, $[\text{MPB}]$, and number average molecular weights, \bar{M}_n . The polymerization was quenched by the addition of a fivefold excess of CH_3OT^* above the stoichiometric number of available organometallic groups, that is, $5(4[\text{Ti}]_0 + 3[\text{Al}]_0)$. The labeling reactions were allowed to proceed for ≥ 2 hr. at room temperature. An excess of methanol was added and the polymer was worked up as already described. After vacuum drying the polymer was weighed to obtain the yield and sent to New England Nuclear for radioassay of ^3H specific activity. The $[\text{MPB}]$ in $\text{mole}\cdot\text{l}^{-1}$ and \bar{M}_n is obtained from the tritium specific activity of polyacetylene in $\text{dpm}\cdot\text{mg}^{-1}$, A_{CH_x} , the yield of polyacetylene, g_{CH_x} , the specific activity of methanol, $A_{\text{CH}_3\text{O}^*\text{H}}$, and the volume of the polymerization, V , in liters.

$$[\text{MPB}] = \frac{A_{\text{CH}_x} \cdot g_{\text{CH}_x} (k_{\text{H}}/k_{\text{T}})}{V \cdot A_{\text{CH}_3\text{OH}} (2.22 \times 10^9)} \quad (3.7)$$

$$\bar{M}_n = \frac{A_{\text{CH}_3\text{OH}^*} (2.2 \times 10^6)}{A_{\text{CH}_x} (k_{\text{H}}/k_{\text{T}})} \quad (3.8)$$

Polymerization Conditions and
Number Average Molecular Weights, \bar{M}_n

Variation of catalyst concentration was found to strongly influence the molecular weight of polyacetylene. Figure 3.10 shows the \bar{M}_n values obtained over a 200-fold change in the catalyst concentration. At 10^{-3} M $[\text{Ti}]_0$, only $[\text{CH}]_x$ powder was obtained with $\bar{M}_n \sim 20,000$. At 0.2 M $[\text{Ti}]_0$, both gel and film forms of $[\text{CH}]_x$ were obtained with \bar{M}_n values of 5400 and 11000, respectively. At intermediate $[\text{Ti}]_0$, both powder and gel forms of $[\text{CH}]_x$ resulted; \bar{M}_n of the powder polymer reached as low as 500, whereas the \bar{M}_n values of the gel polymers were much larger. In general the polyacetylene molecular weights in a given polymerization decrease in the order film > gel > powder. This is due to two factors. The accessibility of monomer to the catalyst follows the same order. The polymer gel at the surface of the catalyst solution acts as a barrier for the replenishment of depleted acetylene in the reaction medium beneath. The second factor is chain transfer and termination. This occurs much more frequently in the reaction medium because of the abundance of catalyst components. Consequently, the powder polymer formed in the catalyst solution has a very low \bar{M}_n . In contrast, on the reactor wall, only a small amount of catalyst is deposited and most is adsorbed on the glass surface and is more or less immobilized. Thus, chain transfer reactions which were found to strongly limit chain length are greatly reduced.

Since most investigations have been made on polyacetylene films, we carried out a study of the uniformity of such materials. Acetylene was polymerized using the conditions $[\text{Ti}]_0 = 0.20$ M, $\text{Al/Ti} = 4$,

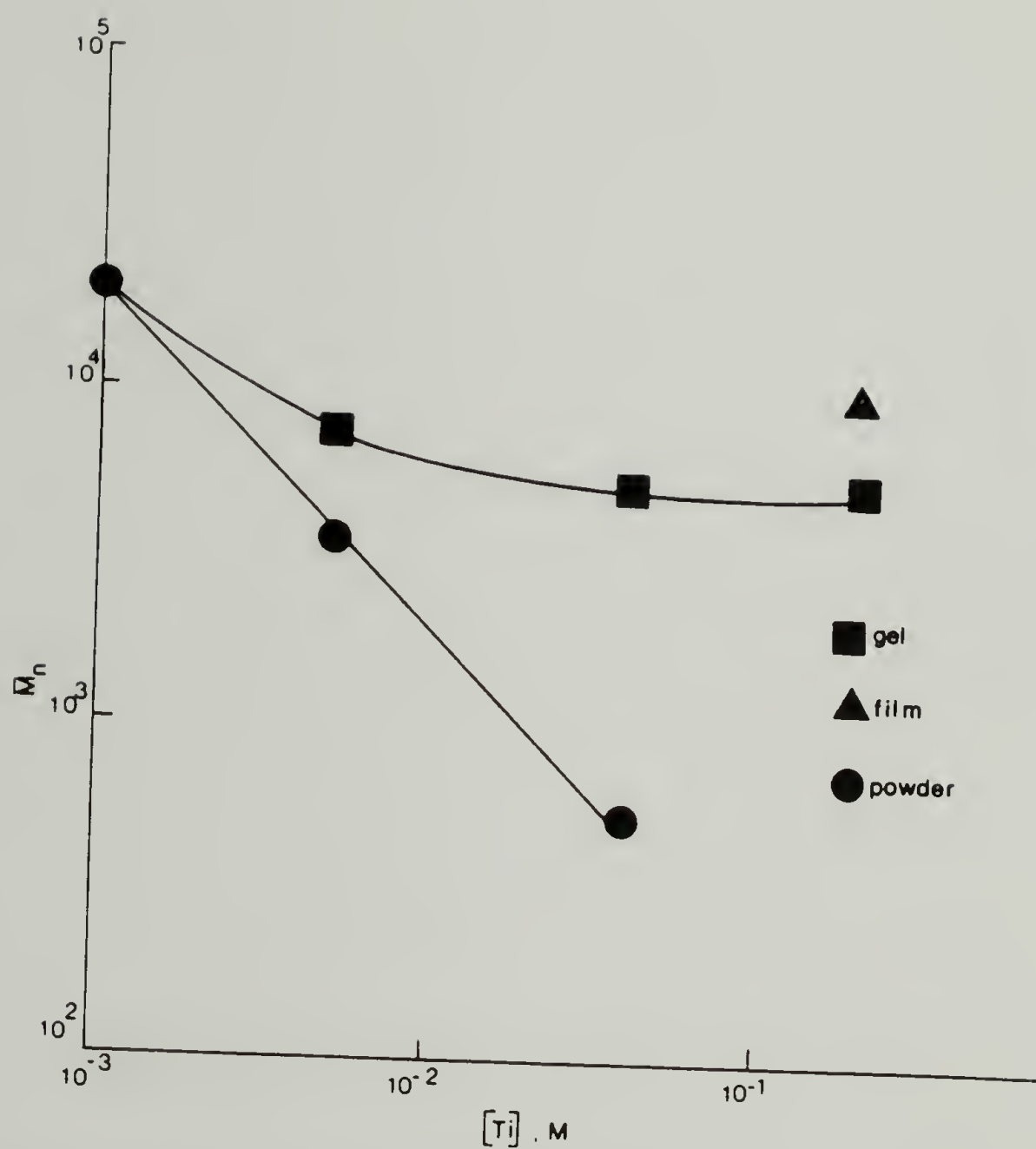


Figure 3.10 Variation of \bar{M}_n of $[\text{CH}]_x$ with Catalyst Concentration for Polymerization at 195 K and 460 torr of Acetylene.

$P_{C_2H_2} = 630-560$ torr, and temperature = 195 K for 30 min. and quenched by CH_3OH^* . These are the conditions employed commonly by researchers in the field to obtain high-quality cis-polyacetylene films. A 1 cm wide specimen was cut from the free-standing film immediately above the surface of the catalyst solution. Then 0.5 to 1 cm wide sections of the film were cut at heights of 3, 5.5, and 8 cm, respectively, from the surface of the catalyst solution as shown in Figure 3.11. Each sample was radioassayed in quadruplicates. Virtually identical \bar{M}_n values were found for the three lower specimens; the average value was $10,500 \pm 1500$ with a very small standard deviation. The top-most specimen had nearly the same molecular weight also, but a greater variation in the specific activity of the quadruplicates: $\bar{M}_n = 11700 \pm 3200$. The polyacetylene formed on the surface of the catalyst, i.e., the gel material, has a much lower \bar{M}_n value of 5300 ± 1200 . Consequently, the polyacetylene film is quite uniform in molecular weight.

The effect of temperature is shown in Figure 3.12. Above 263 K the \bar{M}_n decreased with increasing temperature. This is due to different temperature dependences for the individual processes in Ziegler-Natta polymerizations. For instance, above 273 K polyethylenes obtained with the $(\pi-C_5H_5)_2TiCl_2/2AlMe_2Cl$ catalyst showed a 2.6-fold decrease of \bar{M}_n for a 30 K increase in temperature, and a similar effect was observed in the $\alpha-TiCl_3/AlEt_2Cl$ catalyzed polymerization of propylene. In the present case there is a threefold decrease of \bar{M}_n for about a 70 K increase in temperature. Molecular weight decreases with decreasing

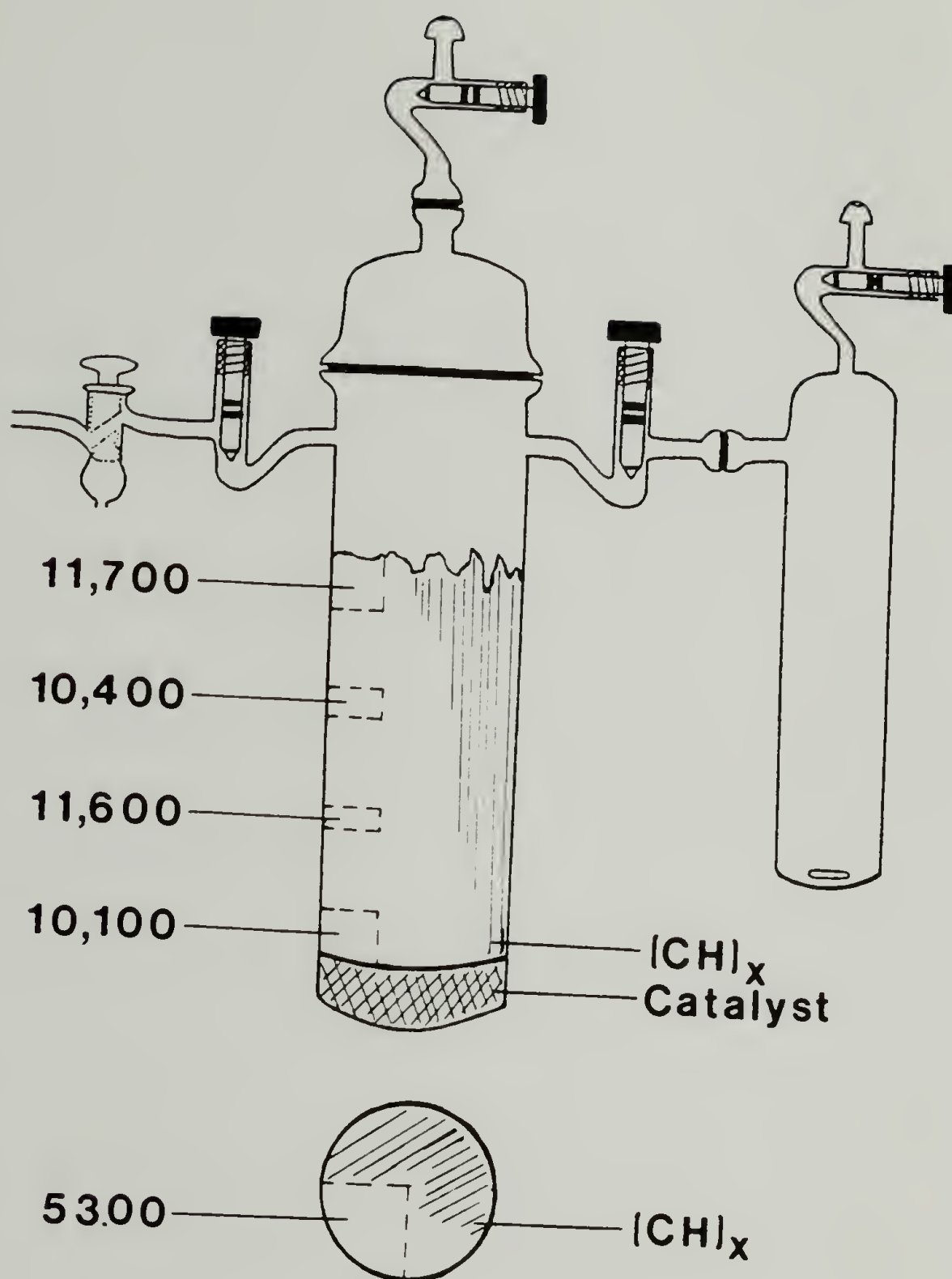


Figure 3.11 Molecular Weight of Specimens Cut at Various Heights of the Polyacetylene Film and of the Polymer Gel.

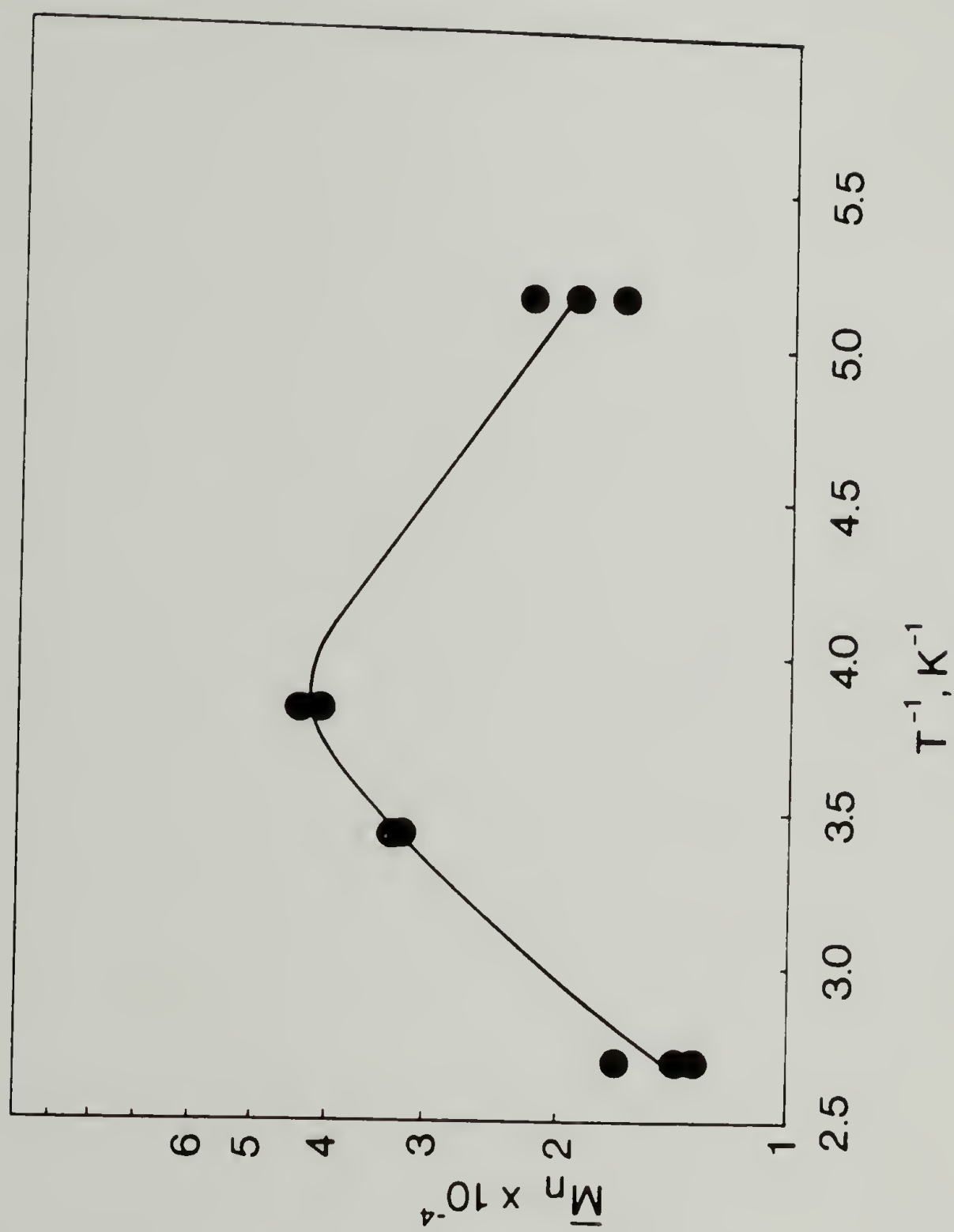


Figure 3.12 Variation of \bar{M}_n with Temperature of Polymerization: $[Ti]_0 = 2.0 \times 10^{-5}$ mol., time = 2 hr, $P_{C_2H_2} = 460$ torr.

temperature below 263 K. Our kinetic study showed this to be due entirely to slow rate of propagation at low temperatures.

Polymerizations of olefins by Ziegler-Natta catalysts were seldomly carried out at such low temperature..

The influence of pressure on polymerization at 195 K is shown by the results summarized in Table 3.5. As expected the increase of monomer concentration increases \bar{M}_n . The two sets of \bar{M}_n values in the table are for duplicate polymerizations.

The Al/Ti ratio can affect acetylene polymerization in two ways. The first is the activation of $\text{Ti}(\text{OBu})_4$ by reducing it to a trivalent complex. Thus, no acetylene polymerization occurred for $\text{Al/Ti} < 2$. At higher Al/Ti ratios the frequency of chain transfer increases, resulting in lowering of the polymer molecular weight. For polymerizations using $[\text{Ti}]_0 = 10^{-3} \text{ M}$, $P_{\text{C}_2\text{H}_2} = 760 \text{ torr}$, temperature = 298 K, and time = 2 hr., the polyacetylenes obtained with Al/Ti ratios of 4, 7 and 10 \bar{M}_n values of 40000, 6200, and 3050, respectively.

Finally, the variations of \bar{M}_n with time of polymerization are shown in Figure 3.13 at both 195 and 298 K at Al/Ti ratio of 4/1. The polymer chain grows rapidly at first, reaching maximum \bar{M}_n values in about 30 min. There is no further increase in \bar{M}_n with time at 195 or 298 K even though more polymer is formed. Thus, chain-transfer processes limit the chain growth. At 195 K there was no additional polymerization after 50 min.

Similar results were observed at Al/Ti ratio of 10/1 polymerized at 298 K, $[\text{Ti}]_0 = 1 \times 10^{-3} \text{ mol} \cdot \text{l}^{-1}$, $P_{\text{C}_2\text{H}_2} = 760 \text{ torr}$ (Figure 3.20b). A

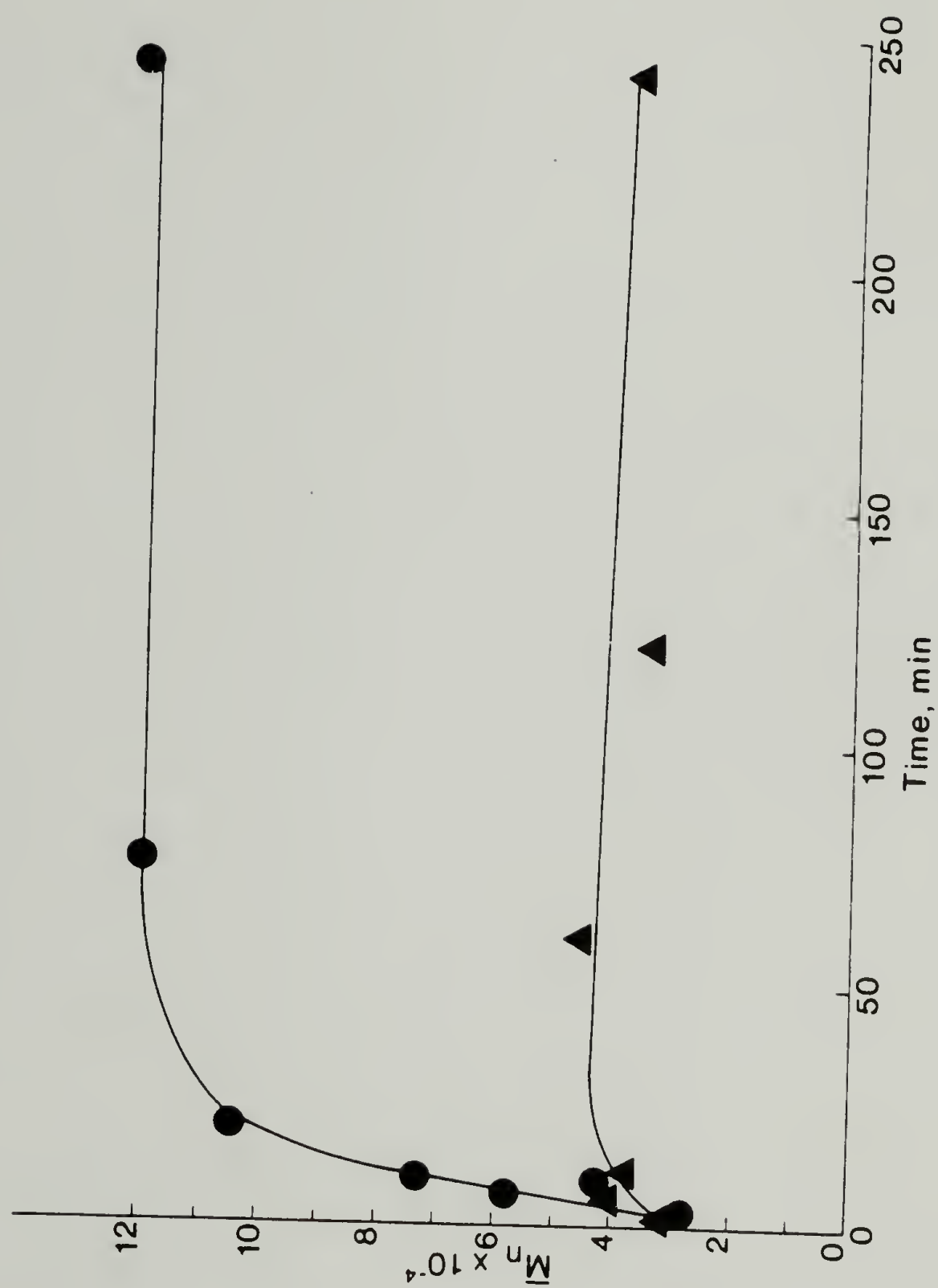


Figure 3.13 Variation of \bar{M}_n with Time of Polymerization: (●) 195 K; (▲) 298 K, $[Ti]_0 = 1 \text{ mM}$, $P_{C_2H_2} = 760 \text{ torr}$.

steady-state polyacetylene \bar{M}_n of 2600 was obtained by 40 min.

Metal Polymer Bond Concentration, [MPB]

The effect of catalyst-cocatalyst composition on the total number of polymer chains polymerized is seen in Table 3.2. For polymerization at an Al/Ti ratio of 4, the [MPB] was 0.4 mM at the end of 2 hr. which corresponds to 40% of the $[\text{Ti}(\text{OBu})_4]_0$. Chain transfer occurs under this condition. As Al/Ti ratio increases, the [MPB] increases and \bar{M}_n decreases. This is strongly indicative of chain transfer with aluminum alkyls:



Table 3.3 shows the effect of catalyst concentration on [MPB]. At $[\text{Ti}]_0 = 1 \text{ mM}$, the [MPB] after 2 hrs. of polymerization corresponds to only 15% of the $\text{Ti}(\text{OBu})_4$ present. At $[\text{Ti}]_0 = 5.1 \text{ mM}$, the [MPB] are 20 times greater than at $[\text{Ti}]_0 = 1 \text{ mM}$. Overall, the [MPB] increased with an increase in catalyst concentration, being much larger in the powder than in the gel.

Over the range of polymerization temperatures, from 195 to 343 K, a small increase in [MPB] with an increase in temperature was seen (Table 3.1). Figure 3.14 gives an apparent activation energy of only $0.95 \text{ Kcal}\cdot\text{mol}^{-1}$.

The evolution of [MPB] over polymerization time can be seen in Figures 3.2b, 3.3b and 3.4b. The steady increase in total chains over the polymerization time while \bar{M}_n stays constant implies transfer reactions, most likely involving aluminum alkyls. A regeneration of

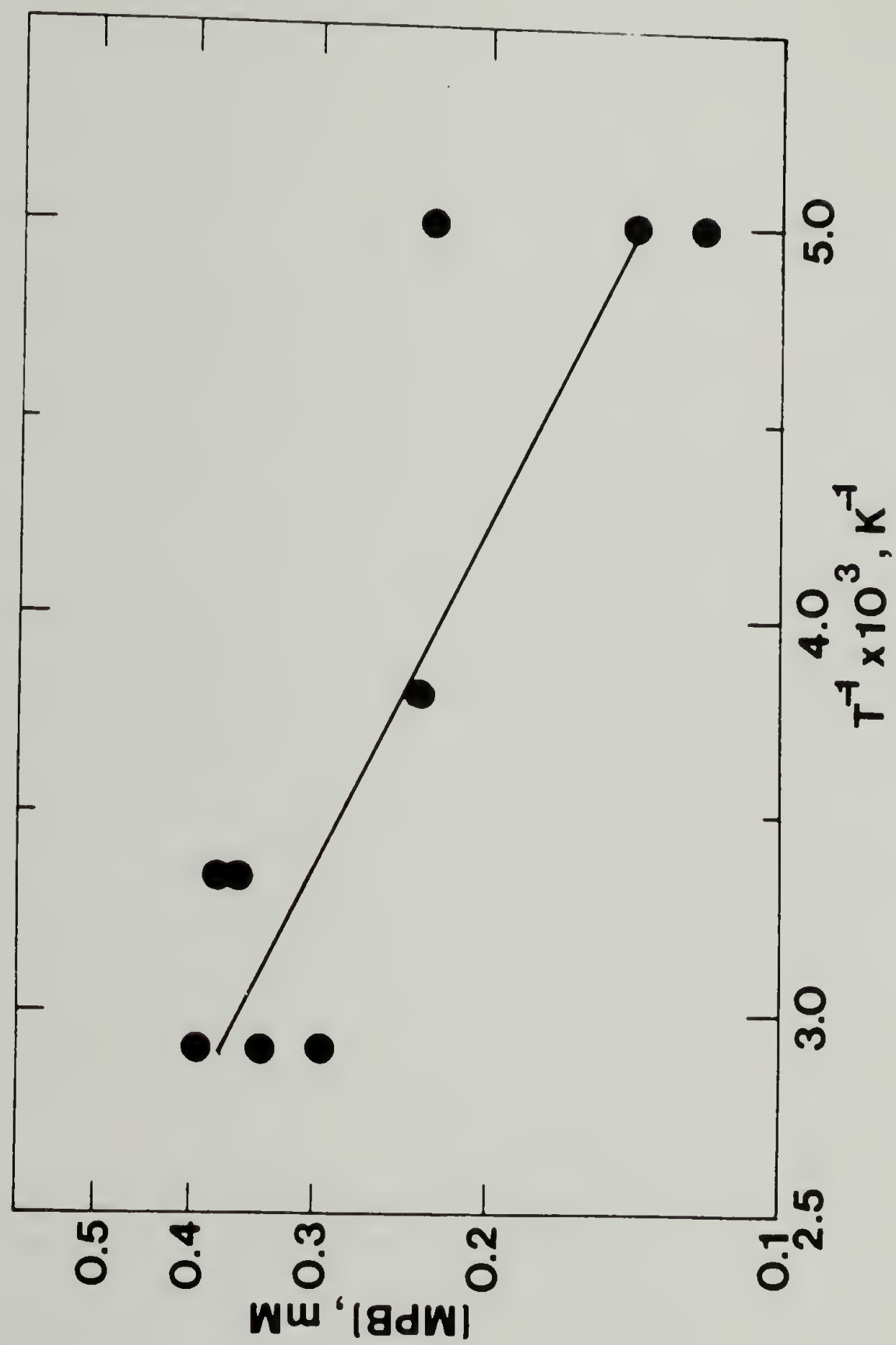


Figure 3.14 Arrhenius Plot of $[MPB]$. Polymerization Conditions as in Fig. 3.7.

active centers occurs thereafter (Eq. 3.9). Assuming bimolecular kinetics

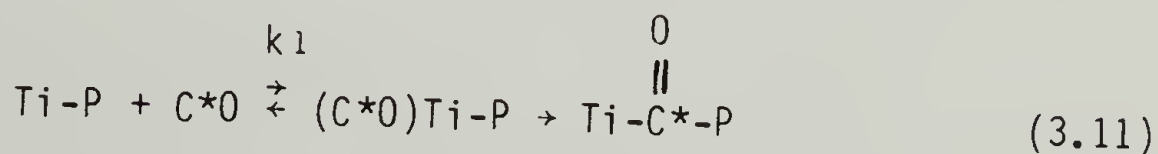
$$\frac{d[Al-P]}{dt} = K_{tr}[Ti-P][AlEt_3]^2 \quad (3.10)$$

The second power for the $AlEt_3$ concentration is consistent with the fact that the compound exists as dimers under these conditions. Figure 3.15 compares the evolution of the transfer rate over polymerization time for Al/Ti ratios of 4/1 and 10/1.

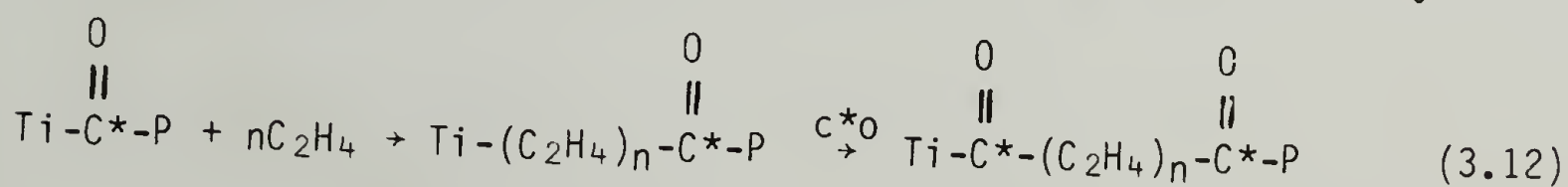
Specific Labeling Using ^{14}CO

Insertion Kinetics

As mentioned in Chapter I ^{14}CO was introduced as a "specific" quenching agent for the active centers in Ziegler-Natta catalyzed polymerization of ethylene and propylene. The initial radiolabeling was attributed to



where P is a polymer chain. Subsequent increases in specific activity was attributed to the reinsertion of monomer and copolymerization followed by insertion of additional $C^{*}O$ as illustrated for ethylene:



To inhibit copolymerization, phosphine was introduced to block the

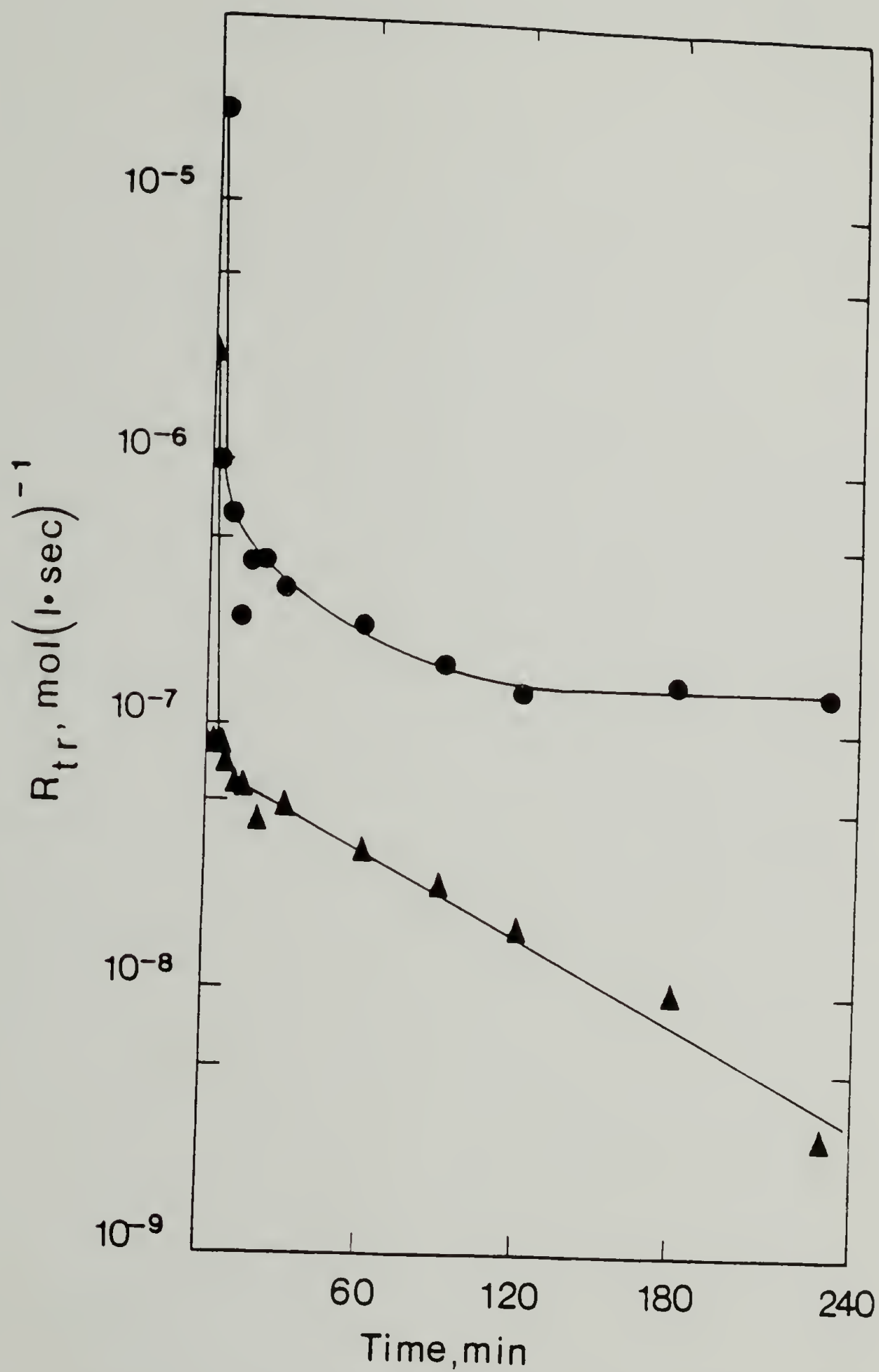
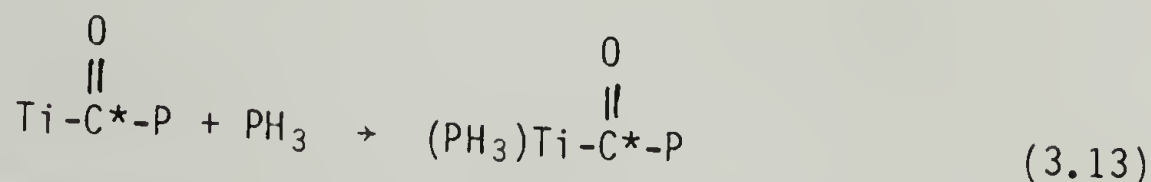
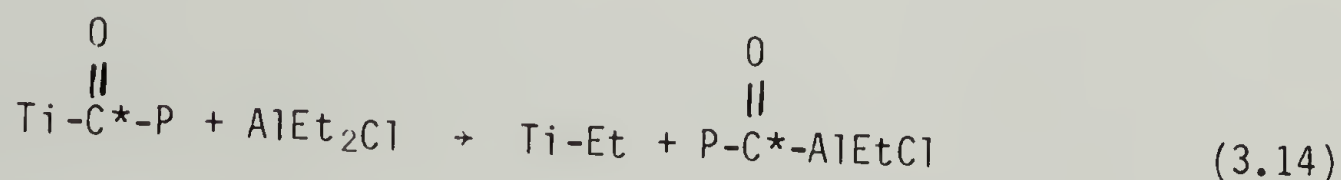


Figure 3.15 R_{tr} over Polymerization Time for (▲) Al/Ti = 4; and (●) Al/Ti = 10: $[Ti]_0 = 1$ mM, catalyst aging time = 30 min., 298 K, $P_{C_2H_2} = 760$ torr.

vacant coordination site of Ti. The phosphine was added a few minutes after the addition of C*O to prevent reaction (3.12).



A further complication was encountered when the incorporation of C*O for ethylene polymerization initiated by TiCl_2 was compared with and without AlEt_2Cl . The increase in ^{14}C specific activity with time of reaction (Eq. 3.11) is large in the presence of AlEt_2Cl , where was the small increase in its absence suggested the following exchange reaction:



Experiments were carried out to determine: (1) whether reaction (Eq. 3.12) also occurs in acetylene polymerization; (2) the rate of reaction (Eq. 3.11); and (3) the stoichiometric requirement of C*O for reaction (Eq. 3.11). After C*O was added to an acetylene polymerization a gradual incorporation was followed by a slower but steadier increase in ^{14}C specific activity in the polymer.¹⁵¹ This is apparently due to copolymerization of C*O with acetylene. If the monomer was removed before the introduction of C*O, the incorporation of C*O reached a constant value (Fig. 3.16). The polymerization conditions were $[\text{Ti}]_0 = 1 \text{ mM}$ at 298 K and a C_2H_2 pressure of 530 torr. After 2 hr. of polymerization 1.2 ml of C*O at STP was added and the reaction mixture was stirred for various lengths of time. Methanol was added at the end of the C*O reaction and the polymer was worked up for

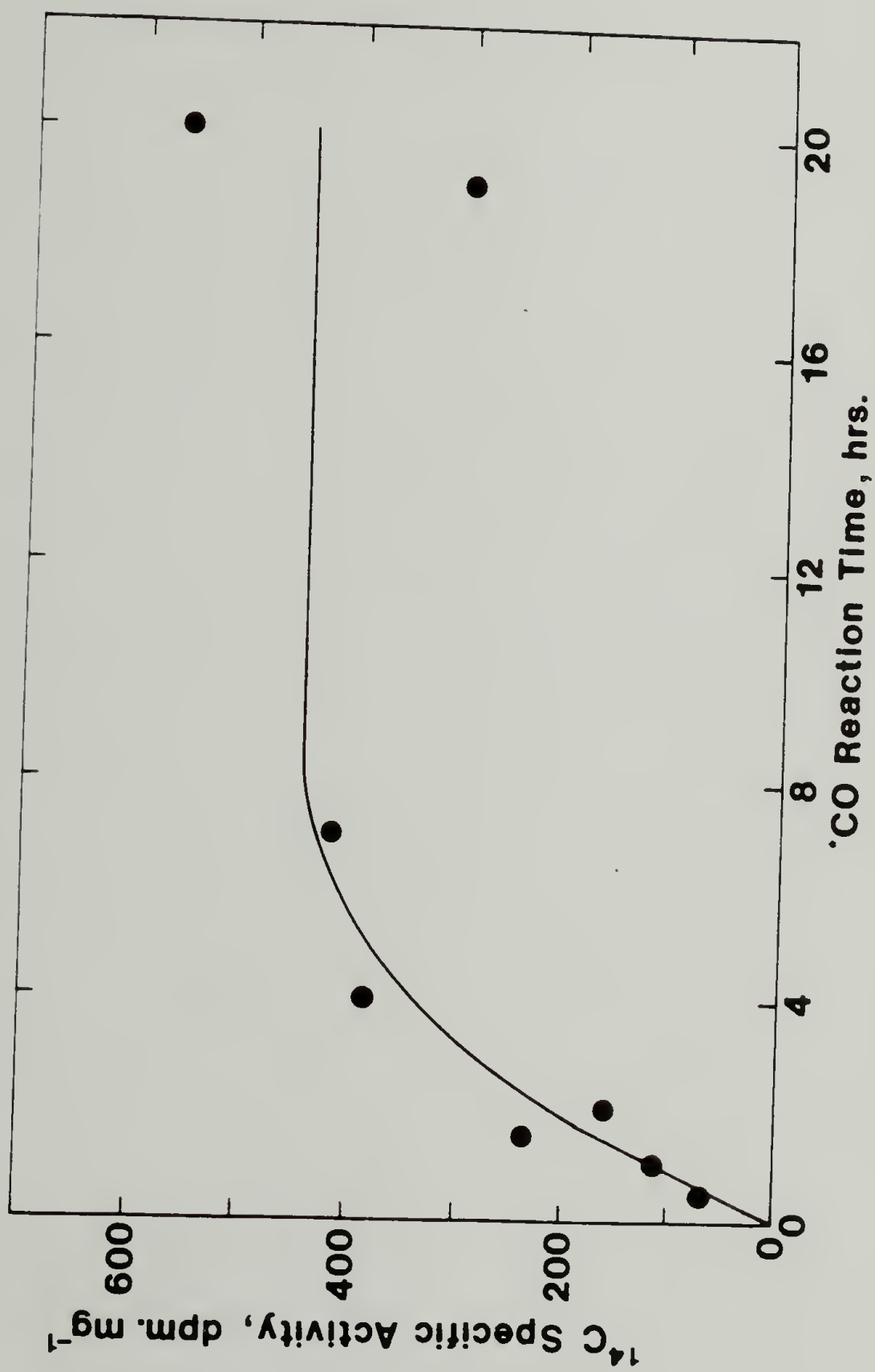
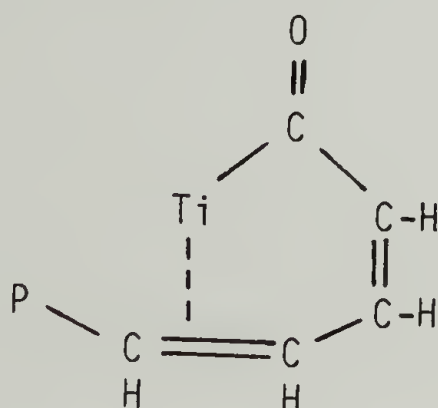


Figure 3.16 Rate of Incorporation of $C^{*}O$ in the Absence of Acetylene. Polymerization conditions: $[Ti]_0 = 1 \text{ mM}$, $Al/Ti = 4$, 298 K , $P_{C_2H_2} = 530 \text{ torr}$, $\text{time} = 2 \text{ hr}$.

radioassay. Evidently, reaction 3.11 is slow for the present system; it takes about 5 hr. to reach the maximum ^{14}C specific activity in polyacetylene.

The fact that the ^{14}C specific activity did not increase indefinitely as it did in olefin polymerizations showed that an exchange reaction analogous to Eq. (3.14) does not occur to any significant extent. This may be due in part to the stability of the acyl species:



The amount of C^*O required to react with all organotitanium bonds was determined empirically. Polymerizations with 20 ml toluene which contained 1 mM $\text{Ti}(\text{OBu})_4$, 4 mM AlEt_3 , and 1 atm acetylene were allowed to polymerize for 2 hr. Monomer was then removed by evacuation and to each various amounts of C^*O were added and allowed to react for 6 hr. The polymer was then worked up for radioassay. The results in Figure 3.17 show that maximum constant ^{14}C activity was obtained with 0.5-0.6 mL of C^*O at STP. This corresponds to 22-27 μmol of C^*O . The reaction mixtures contained 20 μmol of $\text{Ti}(\text{OBu})_4$. If every titanium was alkylated by AlEt_3 , the result would imply that C^*O reacts only with Ti-Et or Ti-P bonds but not with Ti-OBu bonds or with the organoaluminum compound. The result also confirms that no significant exchange occurs between Ti- $\text{C}^*\text{-P}$ species and aluminum alkyls.

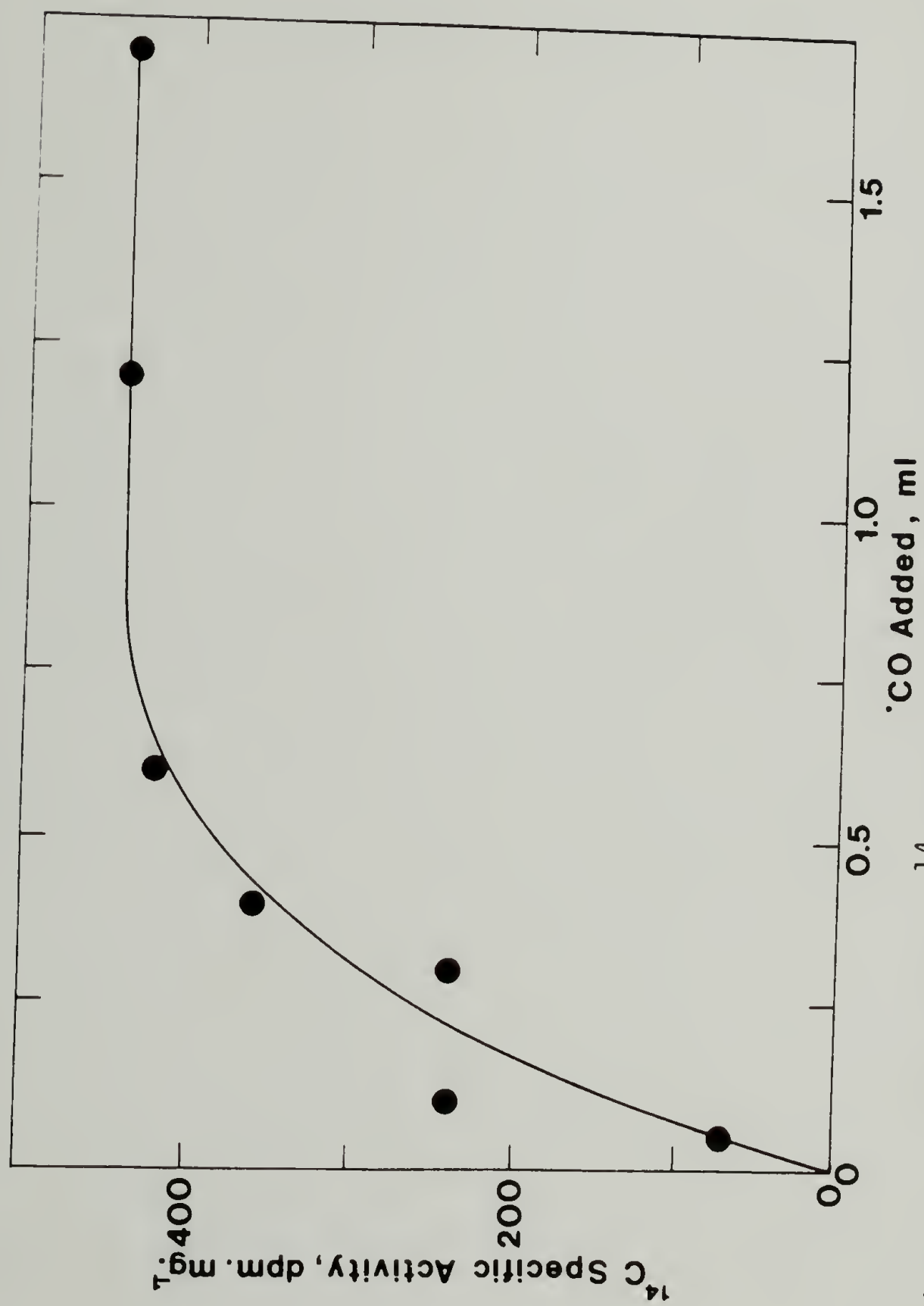


Figure 3.17 Variation of ^{14}C Specific Activity in Polyacetylene with Quantity of C^*O Added. Conditions are the same as in Fig. 3.16. C^*O Contact Time = 6 hr.

On this basis, to determine the active site concentration, $[C]$, polymerizations were stopped by cryogenic pumping for 3-15 minutes to remove unreacted monomer, 1.2 ml of ^{13}C O at STP (5.4×10^{-5} mol) was injected into the reactor and allowed to react at room temperature for five hours.

Active Center Concentration, $[C]$

Earlier in Chapter III, the polymer yield for polymerizations at 195 and 298 K $[Ti(OBu)_4]_0 = 1$ mM, Al/Ti = 4 and 10, catalyst aging time = 30 min, and $P_{C_2H_2} = 760$ torr were given. The active site concentration $[C]$, determined by ^{13}C O quenching, remained virtually constant during the first period and began to decrease only after ca. 50 min of polymerization (Figs. 3.18(a), 3.19(a), 3.20(a)). After 240 min $[C]$ decreased to one-half to one-third of the maximum initial value.

The maximum values of $[C]$ are only ca. 61 and 27 μ M at 298 and 195 K, respectively at Al/Ti = 4. This shows that only 2.7-6.1% of the $Ti(OBu)_4$ was transformed to active sites for acetylene polymerization. At an Al/Ti ratio of 10/1, $[C]_{max} = 120$ μ M at 298 K representing ca. 12% active titanium. This is, however, a rather efficient use of Ti because in many heterogeneous Ziegler-Natta polymerizations, less than 0.1% of the Ti participates in the initiation of polymerization.

The results in Figures 3.2(b) and 3.18(b) show that during the initial stage of polymerization at 298 K $[MPB] \sim 3 [C]$. In other words, on the average the active sites undergo three chain transfers. During a similar period of polymerization at 195 K the chain transfer efficiency is ca. five. At Al/Ti = 10, $[MPB] \sim 25 [C]$ during the initial

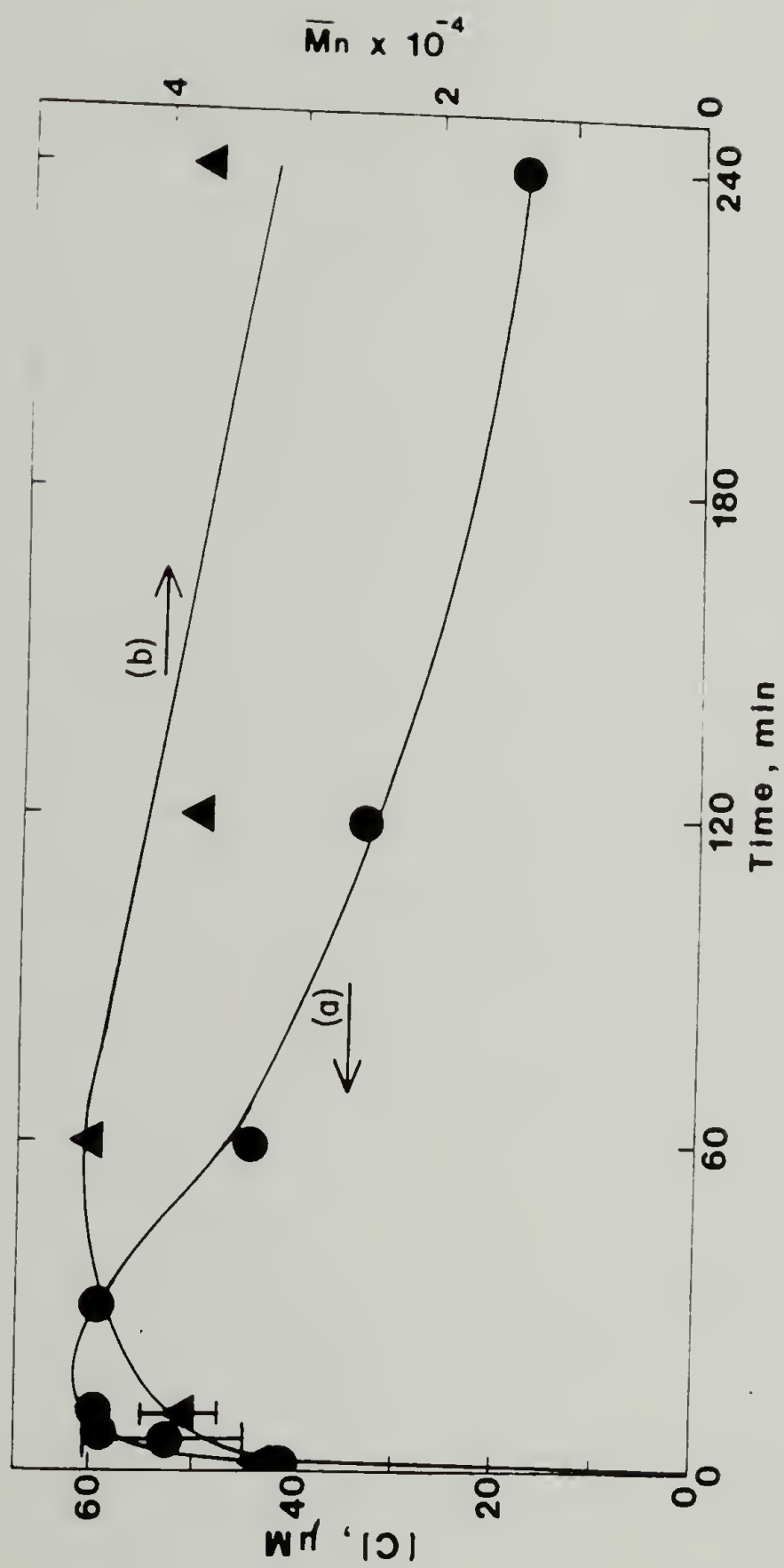


Figure 3.18 Variation of (a) $[C]$ (●) and (b) \bar{M}_n (▲) with Time of Polymerization. Conditions same as in Fig. 3.2.

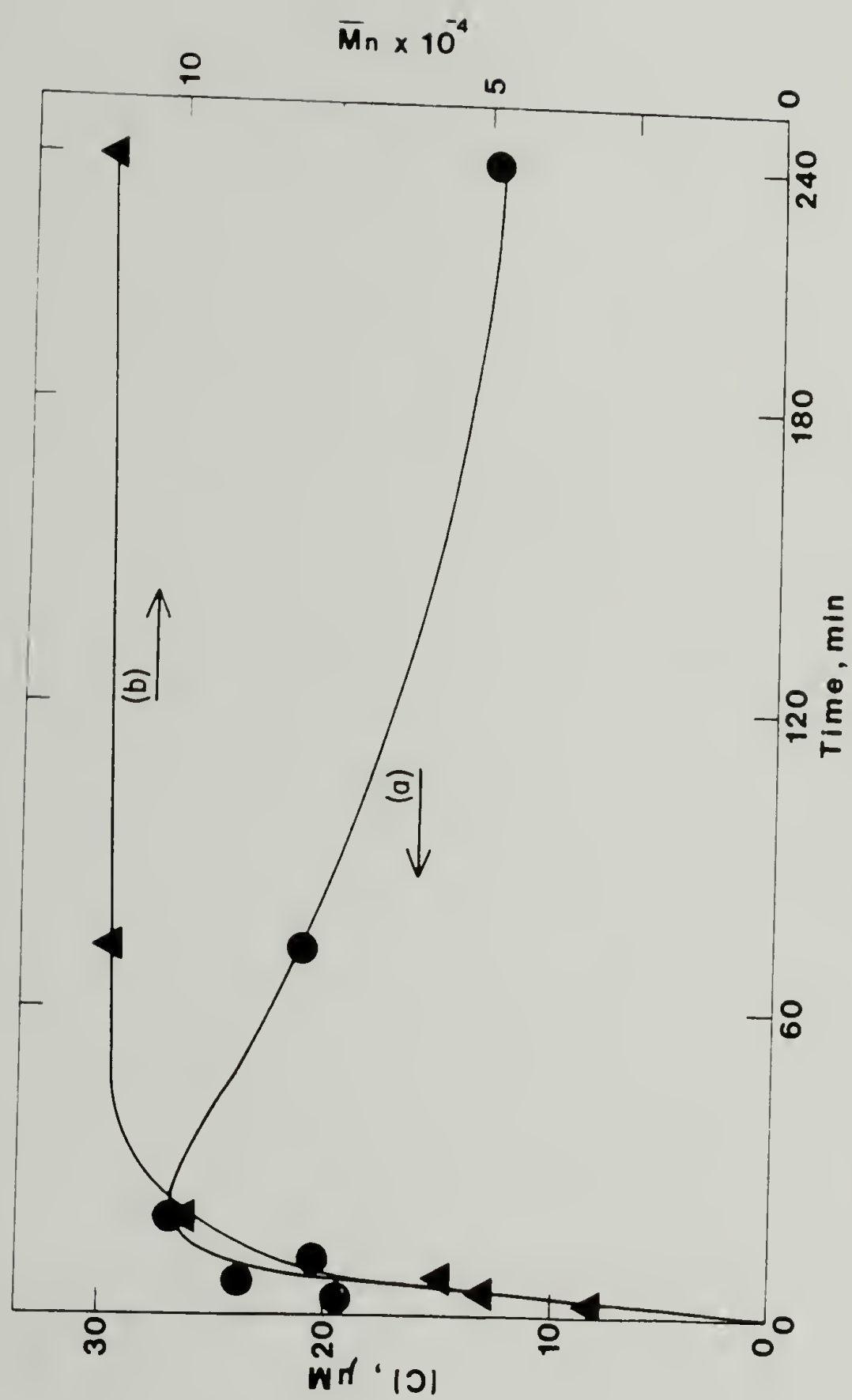


Figure 3.19 Variation of (a)(●) [C]; and (b)(▲) \bar{M}_n with Time of Polymerization. Conditions same as in Figure. 3.3.

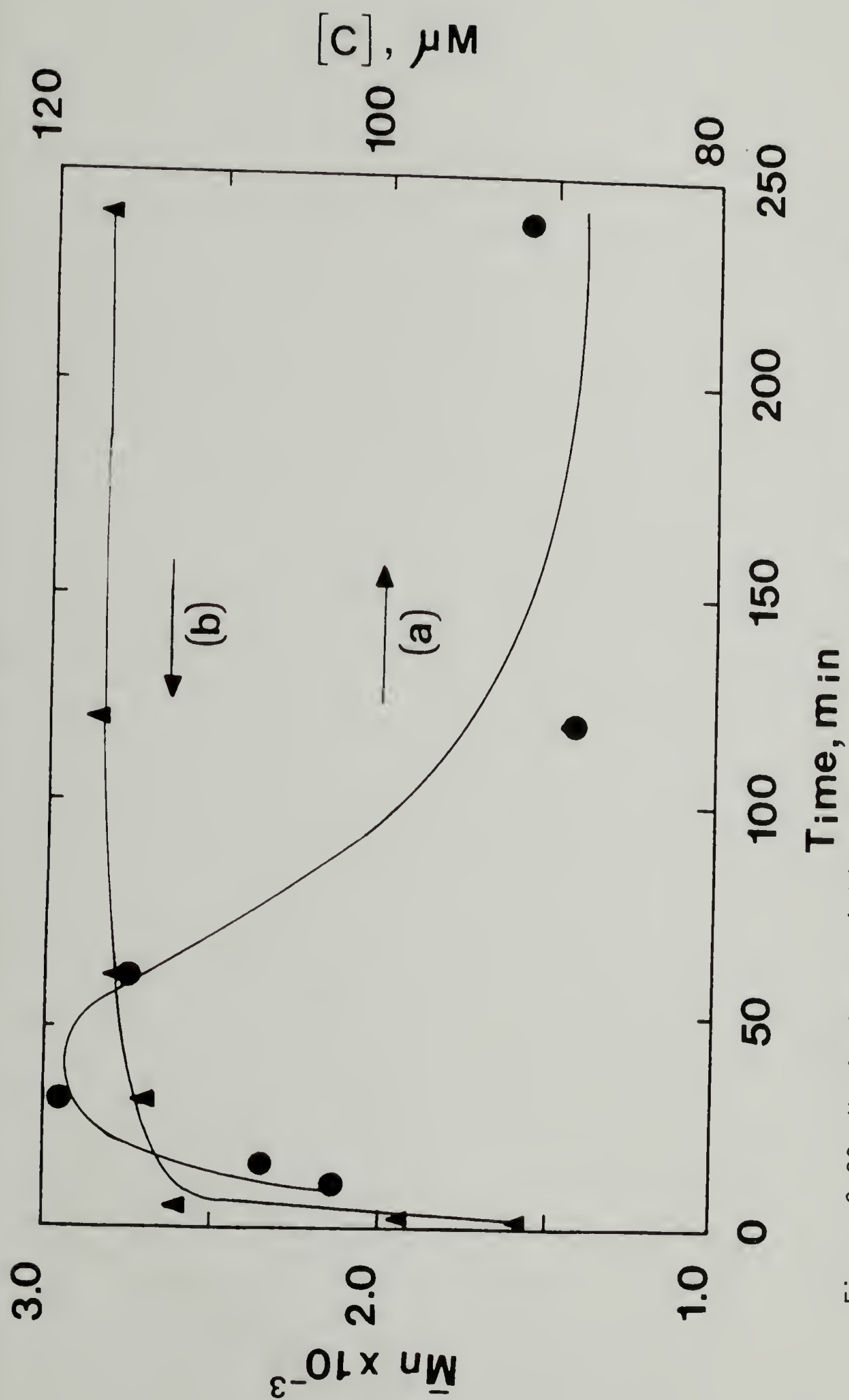


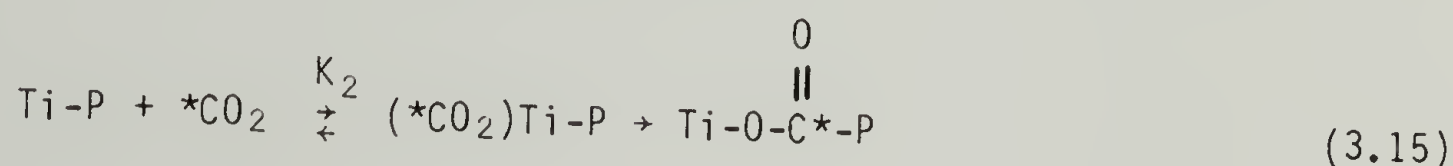
Figure 3.20 Variation of (a)(●) $[C]$; and (b)(▲) \bar{M}_n with Time of Polymerization. Conditions same as in Figure 3.4.

stage of polymerization. Therefore, for a 2.5 increase in Al/Ti ratio, a 8-fold increase in [MPB]/[C] is observed.

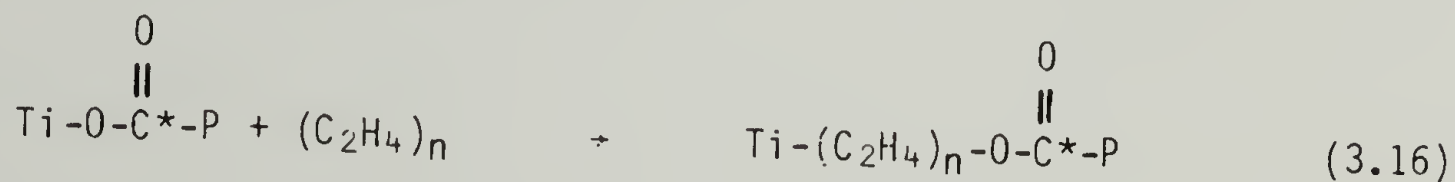
Specific Labeling Using $^{14}\text{CO}_2$

Insertion Kinetics

Zakharov and coworkers^{25,27} first mentioned the use of carbon monoxide as a specific radio label. Similarly, they also report that $^{14}\text{CO}_2$ may be used as a specific label.¹⁵² The radiolabeling reaction proceeds by insertion between the sigma titanium-carbon bond.



The advantage of using this reagent is that subsequent increases in polymer specific activity should not occur by copolymerization



However, based on retardation experiments, it appears that $K_2 < K_1$ (Eq. 3.11 and 3.15). Therefore, longer times were found to be necessary by Warzelhan³⁰ using $\text{TiCl}_4/\text{AlEt}_3$ for propylene polymerization.

The insertion kinetics for ${}^*\text{CO}_2$ in acetylene polymerization were evaluated. Figure 3.21 shows that nearly 24 hrs is needed for a constant polymer specific activity in comparison to ca. 5 hours for ${}^*\text{CO}$. Multiple labeling we believe does not taken place. An interesting point is that for the same polymerization and labeling conditions, but using reactors of different volumes, significantly differing

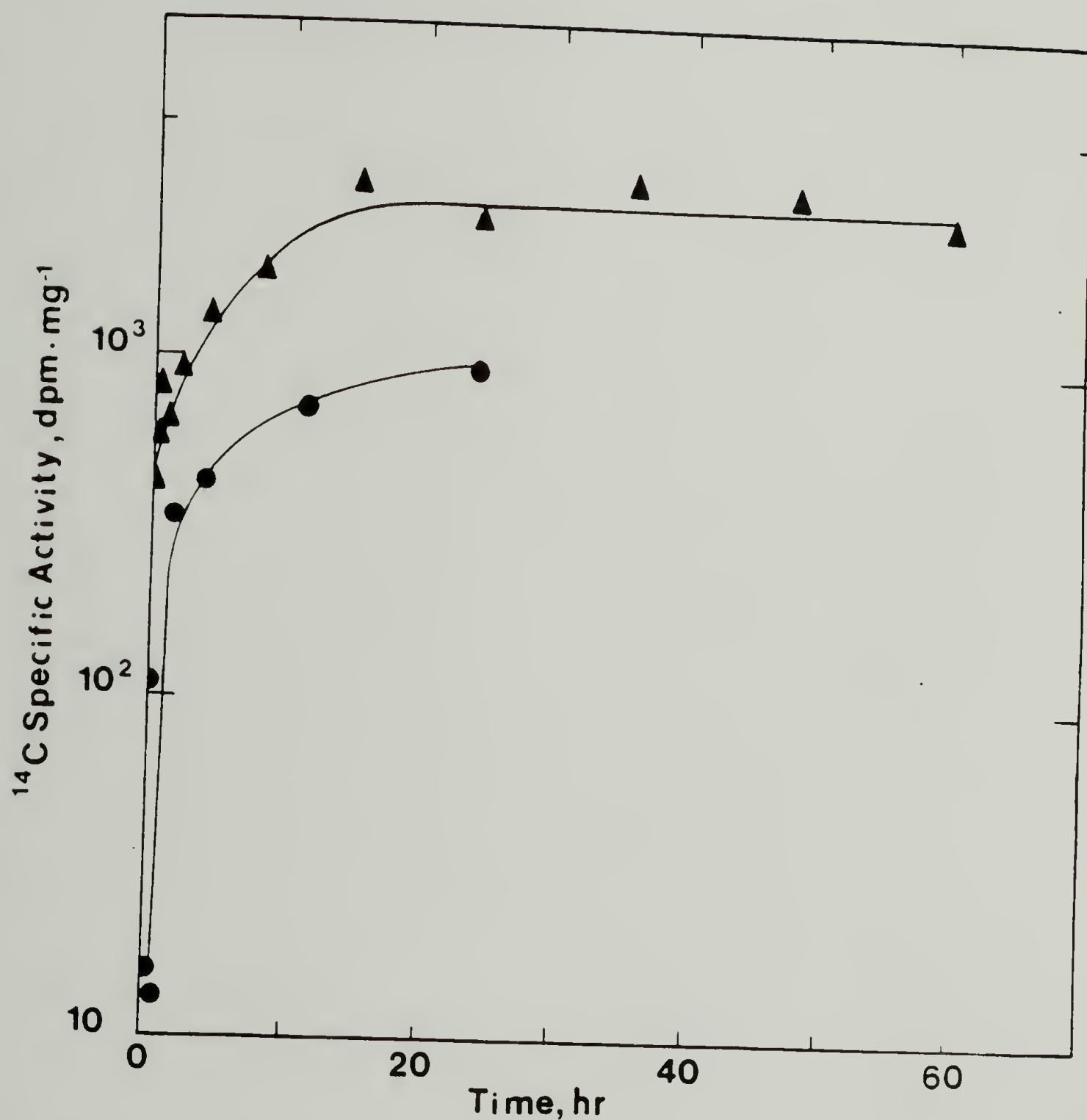


Figure 3.21 Rate of Incorporation of $C^{*}O_2$ in the Absence of Acetylene within (●) 200 ml and (▲) 40 ml Reactors. Polymerization Conditions: $[Ti]_0 = 1$ mM, $Al/Ti = 4$, 298 K, $P_{C_2H_2} = 530$ torr, time = 2 hr. Labelling Conditions: $C^{*}O_2 = 1.1 \times 10^{-4}$ mol.

polymer specific activities are observed, though the insertion kinetics are similar. This points to the equilibrium nature of the coordination reaction in Equation 3.15.

Viewing the uptake of $^*\text{CO}_2$ as a function of quenching agent (Figure 3.22), similar consequences of the equilibrium nature of Equations 3.11 and 3.15 are apparent. A constant specific activity at ca. 10^{-3} moles $^*\text{CO}_2$ is reached. This represents a 50 molar excess with regards to the titanium used for polymerization. Polymerization conditions were $[\text{Ti}]_0 = 1 \text{ mM}$, $\text{Al/Ti} = 4/1$, $P_{\text{C}_2\text{H}_2} = 530 \text{ torr}$, temperature = 298 K, polymerization time = 2 hr.

Active Center Concentration

Based on the equilibrium specific activity from Fig. 3.22, it is possible to make a direct comparison between the two labeling techniques for measuring $[\text{C}]$. Table 3.6 outlines under identical polymerization conditions the calculated active centers and catalyst efficiencies.

High and Low Molecular Weight Polyacetylenes

Based on the kinetic results as outlined above, it became apparent what experimental parameters are important for obtaining high and low molecular weight $[\text{CH}]_x$ (Table 3.7).

Close examination of these conditions suggest some degree of impracticality, especially from the view of obtaining film morphologies. For example, in the case of obtaining low \bar{M}_n polymer (LMnP), the suggested parameters would also give extremely low yields.

Figure 3.22 Variation of ^{14}C Specific Activity versus Quantity of C^*O_2 Added for (●) $[\text{Ti}]_0 = 1 \text{ mM}$, 40 ml Reactor Volume, (▲) $[\text{Ti}]_0 = 0.75 \text{ mM}$, 40 ml Reactor Volume, (■) $[\text{Ti}]_0 = 1 \text{ mM}$, 200 ml Reactor Volume. Polymerization Conditions: $\text{Al/Ti} = 4$, $P_{\text{C}_2\text{H}_2} = 530 \text{ torr}$, 298 K, Time = 2 h. Labelling Time = 24 h.

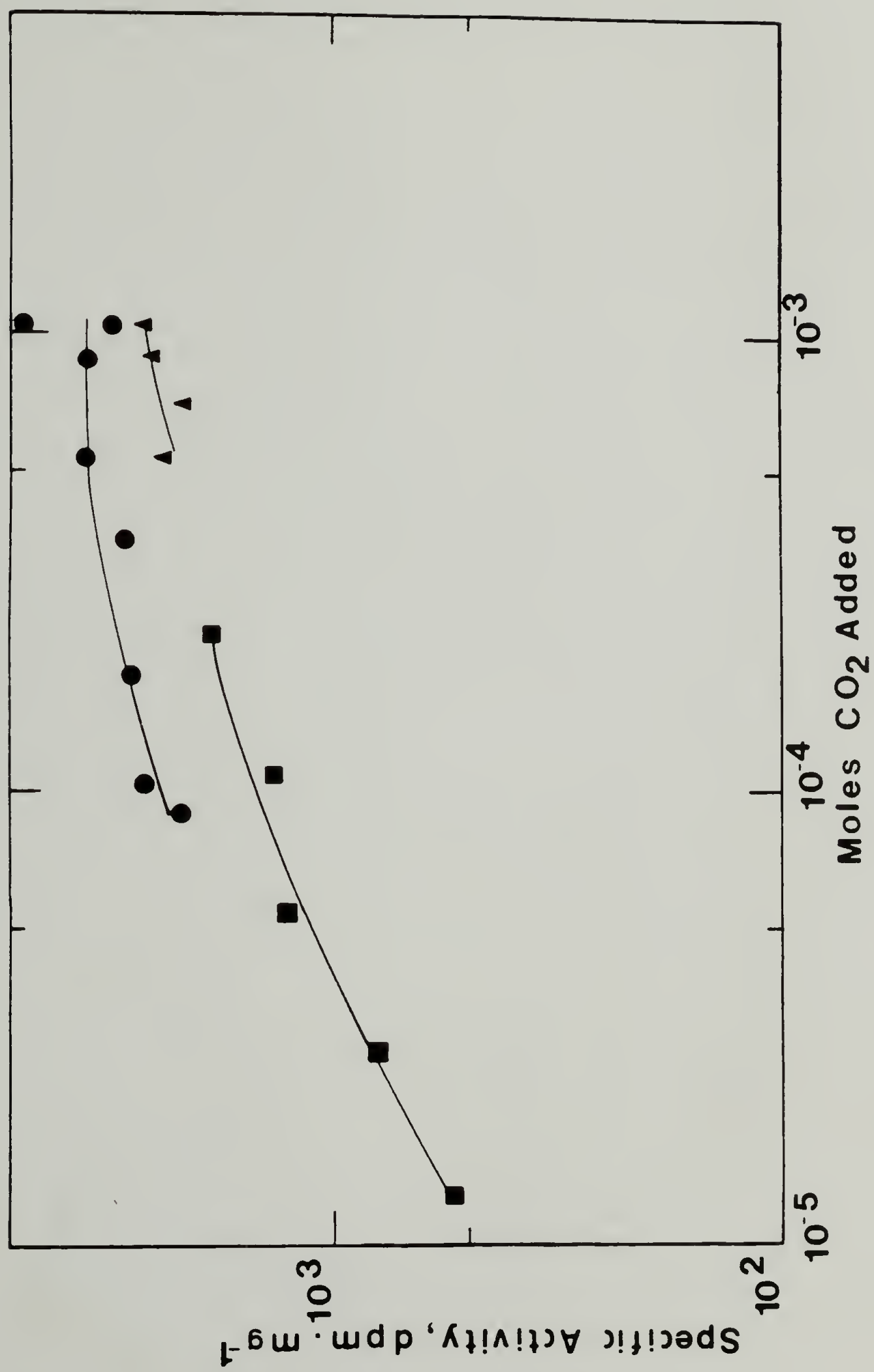


Table 3.6

Comparison of ^{14}CO and $^{14}\text{CO}_2$ Labeling.^a

	^{14}CO	$^{14}\text{CO}_2$
$[\text{C}]$	$3.3 \times 10^{-5} \text{ M}$	$3.6 \times 10^{-5} \text{ M}$
$[\text{C}]/[\text{Ti}]_0$	3.3 %	3.6 %

^a Conditions include: $[\text{Ti}]_0 = 1 \text{ mM}$, $\text{Al/Ti} = 4/1$,
 $P_{\text{C}_2\text{H}_2} = 530 \text{ torr}$, $\text{temp} = 298 \text{ K}$, $\text{time} = 2 \text{ hr.}$

Table 3.7

Ideal Polymerization Conditions for LMnP and HMnP.

	Low \bar{M}_n	High \bar{M}_n
Polymerization time	≤ 30 min.	≥ 30 min.
$[\text{Ti}]_0$	≥ 200 mM	≤ 1 mM
Al/Ti	$\geq 7/1$	4/1
$P_{\text{C}_2\text{H}_2}$	0-50 torr	≥ 760 torr
Temperature	195 K	263 K
Catalyst Aging	0 min.	30-60 min.

Consequently, in the set of conditions developed for obtaining LMnP, polymerization times of 2 hours or more are needed. In the case of obtaining high \overline{M}_n polymer (HMnP), such low catalyst concentrations would be extremely sensitive to trace impurities. Consequently, the catalyst would be deactivated. Also, while polymerization at 263 K may give the highest \overline{M}_n , it also gives ca. 70/30 cis/trans ratio in lieu of 88% cis or greater at 195 K. Polymerizations were therefore performed at 195 K and 1 mM $[\text{Ti}]_0$.

Two types of LMnP were evaluated: powders and thin films. Powders were obtained by polymerizing acetylene at 20 torr within a stirred catalyst solution at 200 mM $[\text{Ti}]_0$, Al/Ti = 7/1 at 195 K. Quenching with excess $\text{CH}_3\text{O}^3\text{H}$ gave 400-500 \overline{M}_n 's (Table 3.8). Purification of the polymer was extremely difficult. Within a glove bag, excess .10 HCl/ CH_3OH was added to deactivate the catalyst and wash it free of the polymer. However, because of the fineness of the powders, the glass fritts used for suction filtration would become clogged. Also, attempts to obtain films from powders were unsuccessful. Instead, brittle bricks of polymer would inevitably result. Consequently, only EPR measurements were possible on these materials.

Polymerization of thin films was only made possible by using the flat bottomed reactor shown in Figure 2.4. After catalyst was prepared and added to the reactor, toluene was cryogenically distilled off to near completion while the ever-increasing viscous catalyst was evenly distributed on the glass. Nearly neat catalyst at $[\text{Ti}]_0 = 740$ mM was then used for polymerization. Acetylene pressure was maintained at

Table 3.8

Molecular Weight and Yield of LMnP Powders and Films.

LMnP	Morphology	Polymer Yield/ Polymerization Time	\bar{M}_n
MS482-101	powder	167 mg/3 hr	490
MS583-77	"	115 mg/2 hr	380
MS583-91	film	~70 mg/1 hr	400
MS684-33	"	~40 mg/1.5 hr	-
MS684-85	"	~70 mg/2 hr	-

15-30 torr using a n-propyl alcohol slush bath. Labeling was accomplished as outlined in Chapter II. Resulting films were of ca. 20-60 μm in thickness, extremely brittle even at 85% cis content, and metallic black in color.

Preparing HMnP films was much more difficult to routinely obtain. Because the catalyst concentration was so low, even at 195 K the viscosity was not sufficient to apply the procedure used for standard film preparation. Secondly, because roughly 10 μmol $\text{Ti}(\text{OBu})_4$ was used for film polymerization, any trace amounts of impurities could deactivate the catalytically active complex.

Early attempts involved injecting 5.1 mM $[\text{Ti}]_0$ catalyst into a stirred solution of C_2H_2 saturated at 760 torr in toluene such that the overall $[\text{Ti}]_0 = 1.0$ mM. In all cases, low density gels resulted since after a short period, stirring could no longer be effected. Later efforts focused on the use of a flat bottomed reactor (Fig. 2.4). The most effective technique (Procedure A) involved pressurizing the apparatus to ca. 900-950 torr purified C_2H_2 and injecting 1 mM $[\text{Ti}]_0$ catalyst to give a thin, low density gel layer which collapsed upon drying into 30-100 μm films. Using a teflon disc to polymerize on instead of glass gave no greater ease in removing the film or preventing it from bursting apart upon warming to room temperature. The later point was a serious problem and was undoubtedly a result of unreacted C_2H_2 coming out of solution upon warming. Adding sufficient toluene while at 195 K to cover the film, then warming very slowly to room temperature minimized this problem.

To help in removing the thin gel layer from the reactor bottom, it was found that rinsing the reactor with 10% $\text{Al}(\text{Et})_3$ in toluene, followed by toluene alone before polymerization was very effective. By doing this, all surface siloxyl groups were reacted to give diethyl siloxyl aluminum surface groups. When catalyst was added, no chemisorption would take place.

A second procedure (Procedure B) involved the reverse addition of reactants, i.e. monomer at ca. 600-650 torr was admitted into the reactor containing a thin layer of 1 mM $[\text{Ti}]_0$ catalyst. Slowly, $\text{P}_{\text{C}_2\text{H}_2}$ would build to 760 torr. The disadvantage with this technique was that the $[\text{C}_2\text{H}_2]$ would slowly be building while polymerization was in progress.

Reproducible polymer \bar{M}_n 's were difficult to obtain. Table 3.9 lists the polymerization technique, polymer yields and molecular weights. In comparison to LMnP films, these materials were extremely flexible and easy to work with.

Discussion

As was seen in Figs. 3.2(a), 3.3(a), and 3.4(a), most of the polyacetylene was produced during the initial polymerization period. At 298 K, 60% of the polymer was obtained during the first 20 min compared to the total yield after 240 min. At 195 K, the yield after 25 min of polymerization was about 75% of that at 240 min. In other words, the rate of polymerization is initially very rapid but then decays (Fig.

Table 3.9
Molecular Weight and Yield of HMnP Gels and Films.

HMnP _a	Polymerization Procedure ^b	Yield/ Polymerization Time	\overline{M}_n
MS482-37	gel	-	62,000
MS482-77	gel	-	195,000
	"	-	206,000; 215,000
MS583-5	B	-	35,000
MS583-45	A	-	730,000; 790,000
			840,000; 920,000
HMnP-I	A	38 mg/2 hr	54,000
HMnP-III	A	33 mg/2 hr	21,400
HMnP-V	A	81 mg/2 hr	25,500; 23,000

^a references beginning with MS represent early attempts, HMP series are later attempts.

^b gel refers to polymerization technique and final morphology; A, B refers to technique used to obtain films (see text).

3.5(a) and 3.6(a)). At both temperatures, R_p decreased about 30-fold during the first 30 min of polymerization.

On the other hand, the active site concentration $[C]$, determined by C^*O quenching, remained virtually constant during the first period and began to decrease only after ca. 50 min of polymerization (Figs. 3.18(a), 3.19(a), and 3.20(a)). After 240 min $[C]$ decreased to one-half to one-third of the maximum initial value. These basic characteristics must be discussed before the detailed kinetic data can be analyzed. There are three possible causes of the observed behavior.

The first explanation is that the polymer produced forms an increasingly thick barrier to the diffusion of monomer to the active site. Schmeal and Street¹⁵³ and Singh and Merrill¹⁵⁴ proposed diffusion limitation models to account for the polydispersity of polymers obtained with catalysts of the Ziegler-Natta type. Chien considered this problem critically and defined criteria for diffusion limitation in coordination polymerization.¹⁵⁵ The findings were that, with the possible exception of highly active catalysts, most olefin polymerizations are not diffusion-limited. Recently, Chien addressed this question by performing direct experimental tests.¹⁵⁶ The new $MgCl_2$ -supported Ziegler-Natta catalyst has an activity several thousand times greater than those of the classical $TiCl_3$ catalyst and shows rapid rates of decay. They compared side-by-side polymerizations of propylene that produced insoluble stereospecific polypropylene and of decene-1 that produced soluble stereospecific poly(decene-1). The latter polymer has a melting point of only 313 K. The polymerizations

have rates within a factor of two and virtually the same decay of R_p . Consequently, diffusion limitation is highly unlikely for the present polymerization of acetylene, which is relatively slow.

A second rationalization of the results in Figures 3.2 - 3.6 is that there is only one kind of active center which undergoes rapid termination. This is not viable because $[C]$ remained unchanged when R_p decreased most rapidly.

Therefore, we are led to the third possible explanation which postulates the presence of two types of active site: an active C_1 and a much less active C_2 . Hereafter subscripts 1(2) are used to denote the values for active sites $C_1(C_2)$. There are two subcases to this postulate: (a) C_1 and C_2 are independent of each other or (b) C_1 is the precursor to C_2 . The fact that $[C]$ remained relatively constant during the period of rapid rate decline favors (b). The following shows that the kinetic analysis is consistent with this basis assumption.

First we should discuss the slow second polymerization stage which occurs between $t = 60$ min and the end of the reaction should be discussed. It is assumed that because after 30 min the steep decline in R_p levels off, all of the more active C_1 sites have decayed and only C_2 sites remain at $t > 60$ min. The rate of termination for C_2 can be obtained directly from the C^*O quenching results; the decrease in ^{14}C activity in polyacetylene may be attributed to the termination of C_2 sites. Figures 3.23 and 3.24 contain linear plots of the second-order disappearance of C_2 at 298 K and 195 K, respectively. Referring

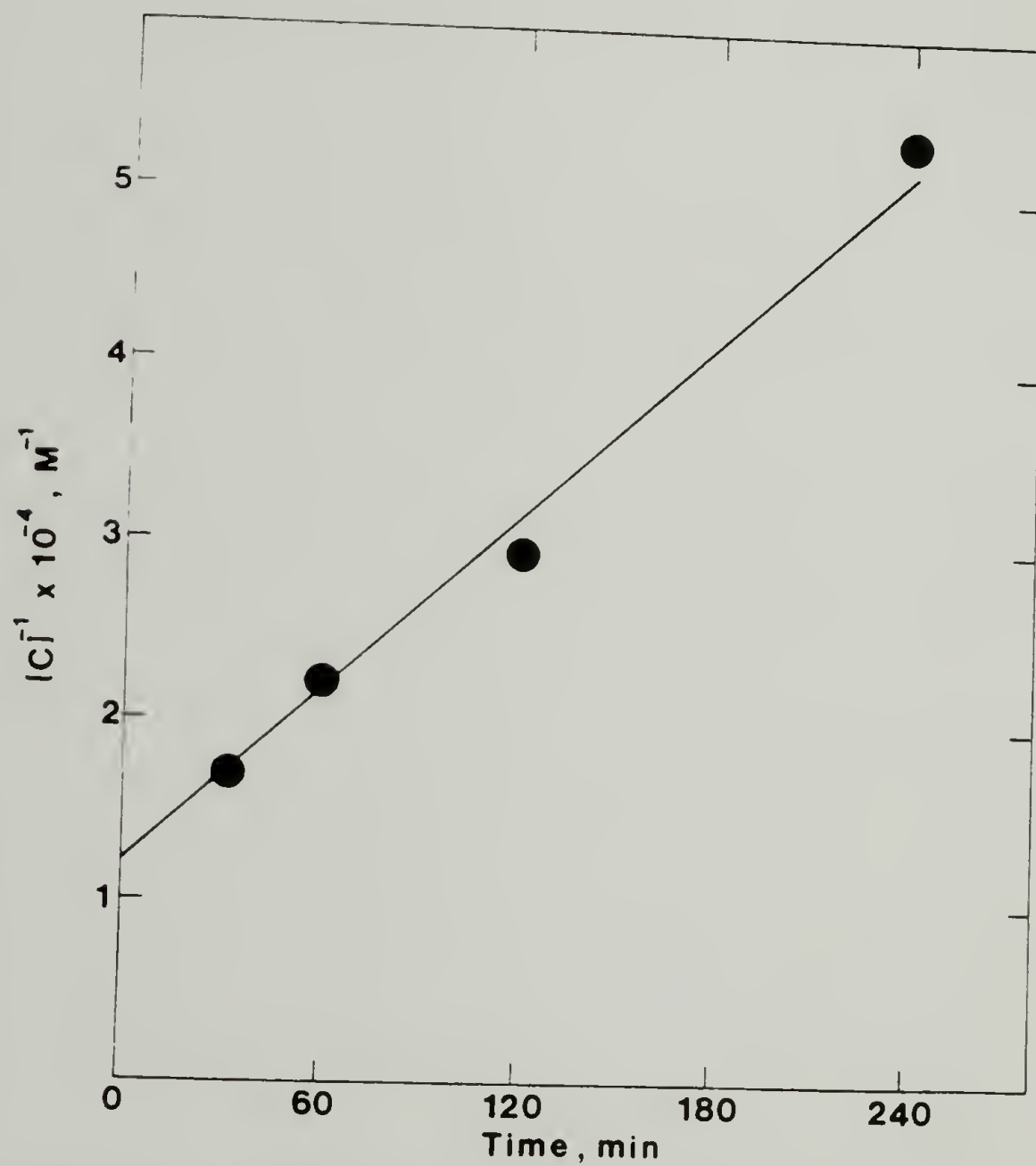


Figure 3.23 Second-Order Kinetic Plot for the Termination of Low Activity C₂ Sites at 298 K taken from Fig. 3.18(a).

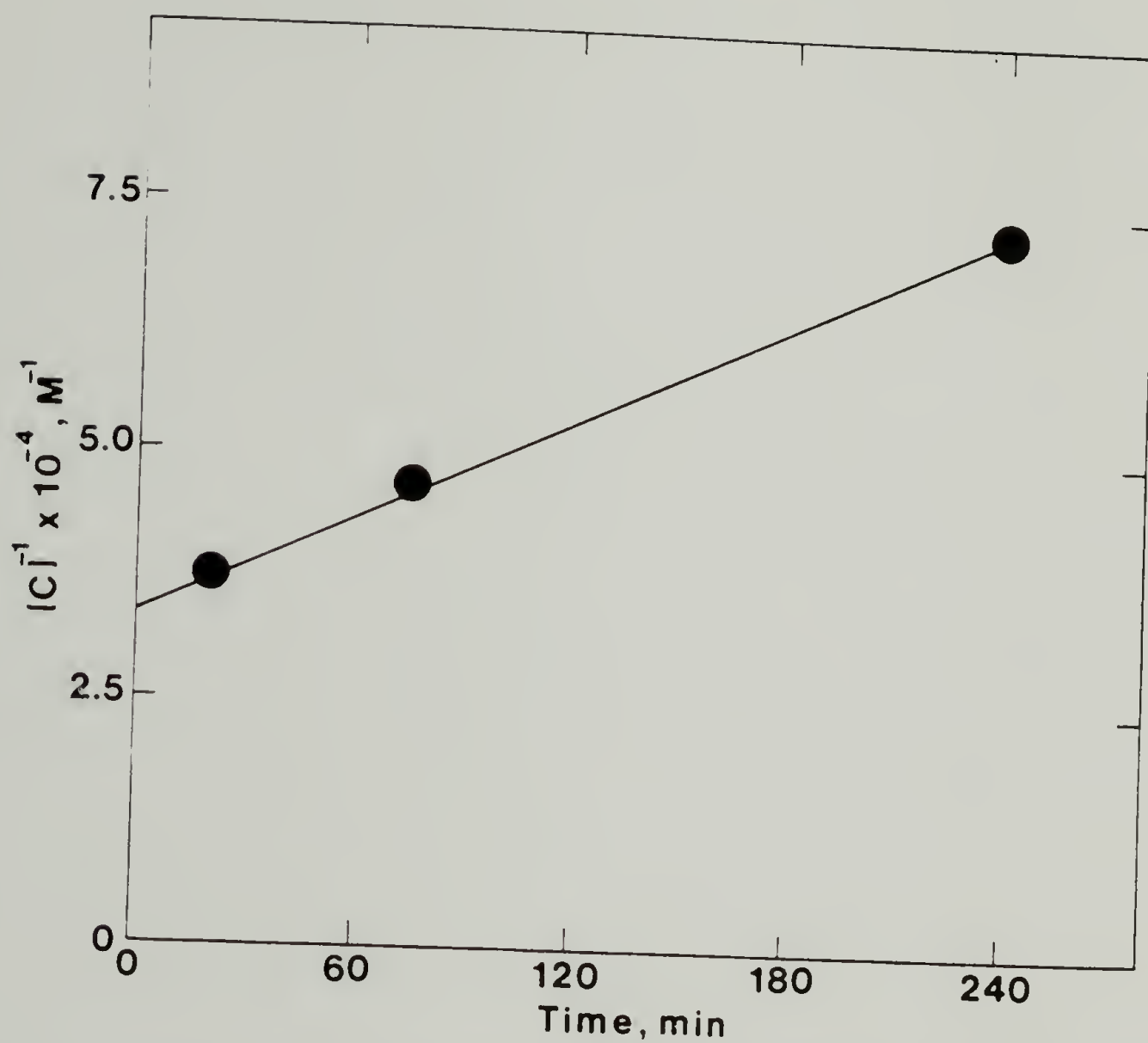


Figure 3.24 Second-Order Kinetic Plot for the Termination of Low Activity C₂ Sites at 195 K taken from Fig. 3.19(a).

back to Figures 3.5(a) and 3.6(a), we see that polymerization began immediately at a maximum rate on the injection of aged catalyst.

Furthermore, Table 3.4 shows that the catalytic activity is not lost appreciably unless aged for long period. These observations imply that the active sites are stable in the absence of monomer and suggest the involvement of monomer in the termination process. The rate of termination may be written as:

$$\frac{-d[C_2]}{dt} = k_{t_2}[C_2]^2[M] \quad (3.17)$$

From the slopes of Figures 3.23 and 3.24 and the monomer concentrations values for k_{t_2} of 0.7 and 16.8 $M^{-2}s^{-1}$ at 195 and 298 K, respectively are obtained. The activation energy for the termination of C_2 sites ΔE_{t_2} , is about 3.6 kcal mol^{-1} .

The propagation for a Ziegler-Natta polymerization is given by:

$$R_p = k_p [C][M] \quad (3.18)$$

It was calculated (Fig. 3.6b) that k_{p_2} at 195 K has a relatively constant value of 0.16 $M^{-1}s^{-1}$ between $t = 60$ and 240 min; the value is ca. 1.1 $M^{-1}s^{-1}$ between $t = 120$ and 240 min at 298 K. The activation energy for propagation is only about 2 kcal mol^{-1} .

The [MPB] increases gradually at 298 K. The rate of increase toward the end of polymerization is about $6.5 \times 10^{-9} M \cdot s^{-1}$ (Figure 3.2(b), 3.15), which suggests the transfer of polyacetylene chain from Ti to Al. The number-average molecular weight is determined by:

$$\bar{M}_n = \left(\frac{R_p}{R_t + R_{tr}} \right) 26 \quad (3.19)$$

The rate of polymerization is $8.5 \times 10^{-6} \text{ M} \cdot \text{s}^{-1}$ at $t = 150 \text{ min}$ and $3.3 \times 10^{-6} \text{ M} \cdot \text{s}^{-1}$ at $t = 240 \text{ min}$; $[C_2]$ is 31 and 19 μM at $t = 150$ and $t = 240 \text{ min}$, respectively. Using $k_{p2} = 31 \text{ M}^{-1}\text{s}^{-1}$, \bar{M}_n values of 2.5×10^4 and 1.1×10^4 at $t = 150$ and 240 min , respectively were obtained. The agreement with experimental values of \bar{M}_n (Figure 3.18(b)) is reasonable with the calculated values somewhat lower. This suggests the possibility that the chain transfer process may be reversible; that is,



The results at 195 K indicate that the process is favored at a lower temperature. Figure 3.3(b) actually showed a slow decrease in $[\text{MPB}]$ with time, whereas \bar{M}_n remained constant (Figure 3.19(b)).

To show the results to a greater advantage during the initial stage of polymerization, plots in Figures 3.25 and 3.26 were expanded to allow for all data points that could not be accommodated in Figures 3.5(a) and 3.6(a).

Estimates for k_{p1} can be obtained by assuming that the maximum initial $[C]$ corresponds to $[C_1]$. This is the consequence of our postulate that C_1 is the precursor of C_2 . With this assumption and in accordance with Eq. 3.18, the values for k_{p1} were 96 and $4.1 \text{ M}^{-1}\text{s}^{-1}$ at 298 and 195 K, respectively. An approximate value for ΔE_{p1} is 3.5

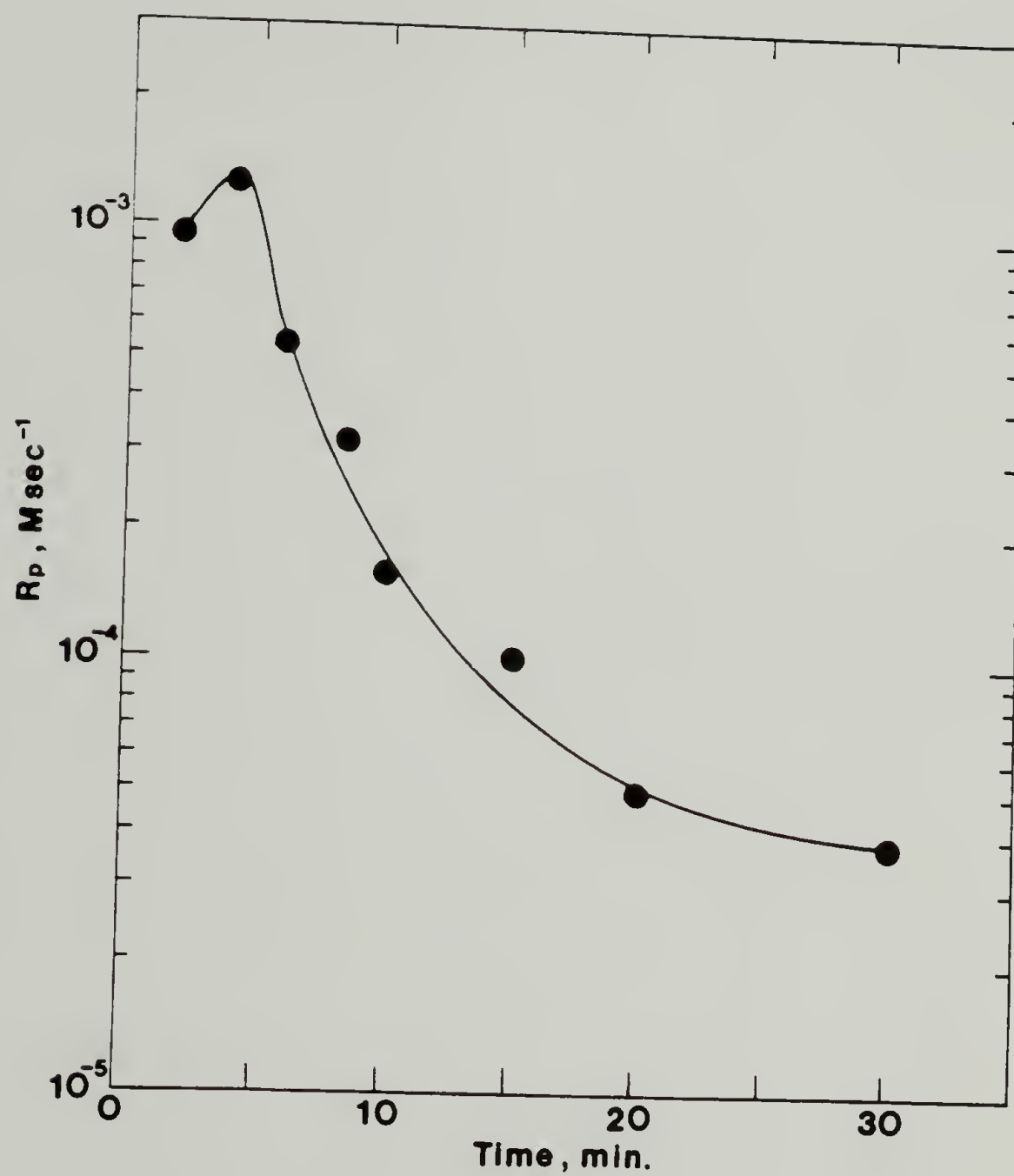


Figure 3.25 Initial Variation of R_p with Time for Fig. 3.5(a).

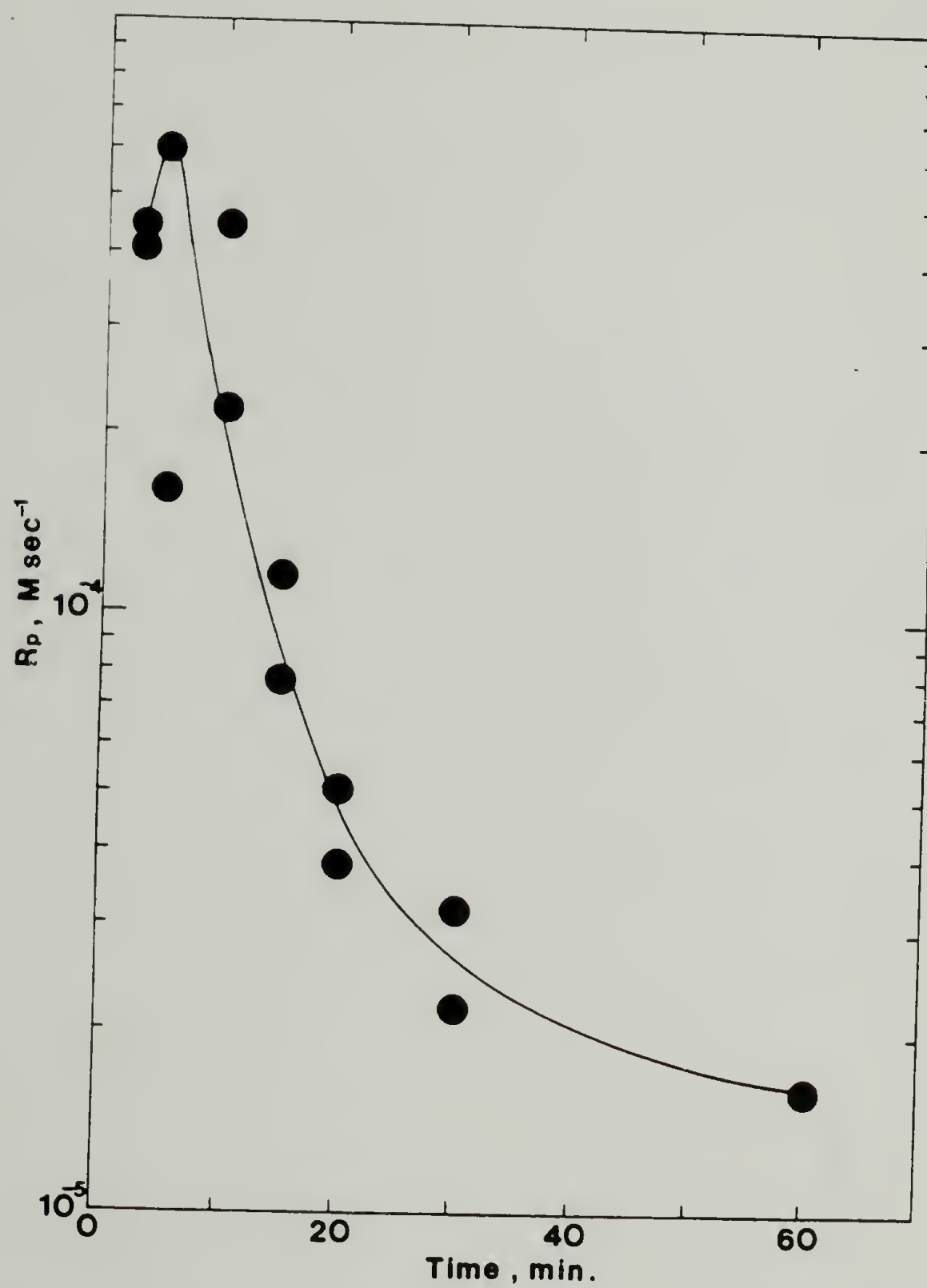


Figure 3.26 Initial Variation of R_p with Time for Fig. 3.6(a).

kcal·mol⁻¹. Therefore C₁ is about 65 times more active than C₂ at 298 K; the ratio is 8 at 195 K. The more active catalytic site has an activation energy about three times higher than for C₂ sites.

The rate of termination of C₁ can be obtained indirectly from the rate of decrease in R_p because R_p ∝ C₁ during this period. Figures 3.27 and 3.28 plot R_p⁻¹ versus time which showed that C₁ also disappeared second order kinetically. The slope is k_{p1}k_{t1}[M]² if it's assumed that monomer is involved in the termination of C₁ as it is in C₂.

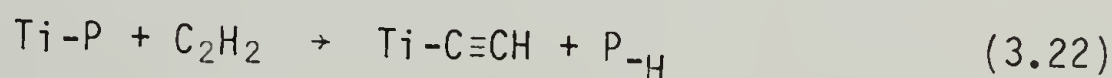
Substituting values of k_{p1} and [M], values of k_{t1} at 1.6x10⁴ M⁻²s⁻¹ and 0.96x10² M⁻²s⁻¹ at 298 and 195 K, respectively were obtained. The activation energy ΔE_{t1} is about 5.4 kcal·mol⁻¹.

The relative concentration of [C₁] at the start of polymerization and [C₂] just after most of [C₁] has decayed (k_{p2} becomes more or less constant) can be obtained from

$$\frac{[C_1]_0}{[C_2]_0} \cong \frac{(R_{p1})_0 k_{p2}}{(R_{p2})_0 k_{p1}} \quad (3.21)$$

The ratio is 1.2 at 298 K and 1.4 at 195 K. Therefore, the two active sites are comparable in numbers in support of the postulate that C₂ is derived from C₁.

Several reactions, which if they occur to a significant extent, could introduce errors to the present method of molecular weight determination. These are transfer to monomer



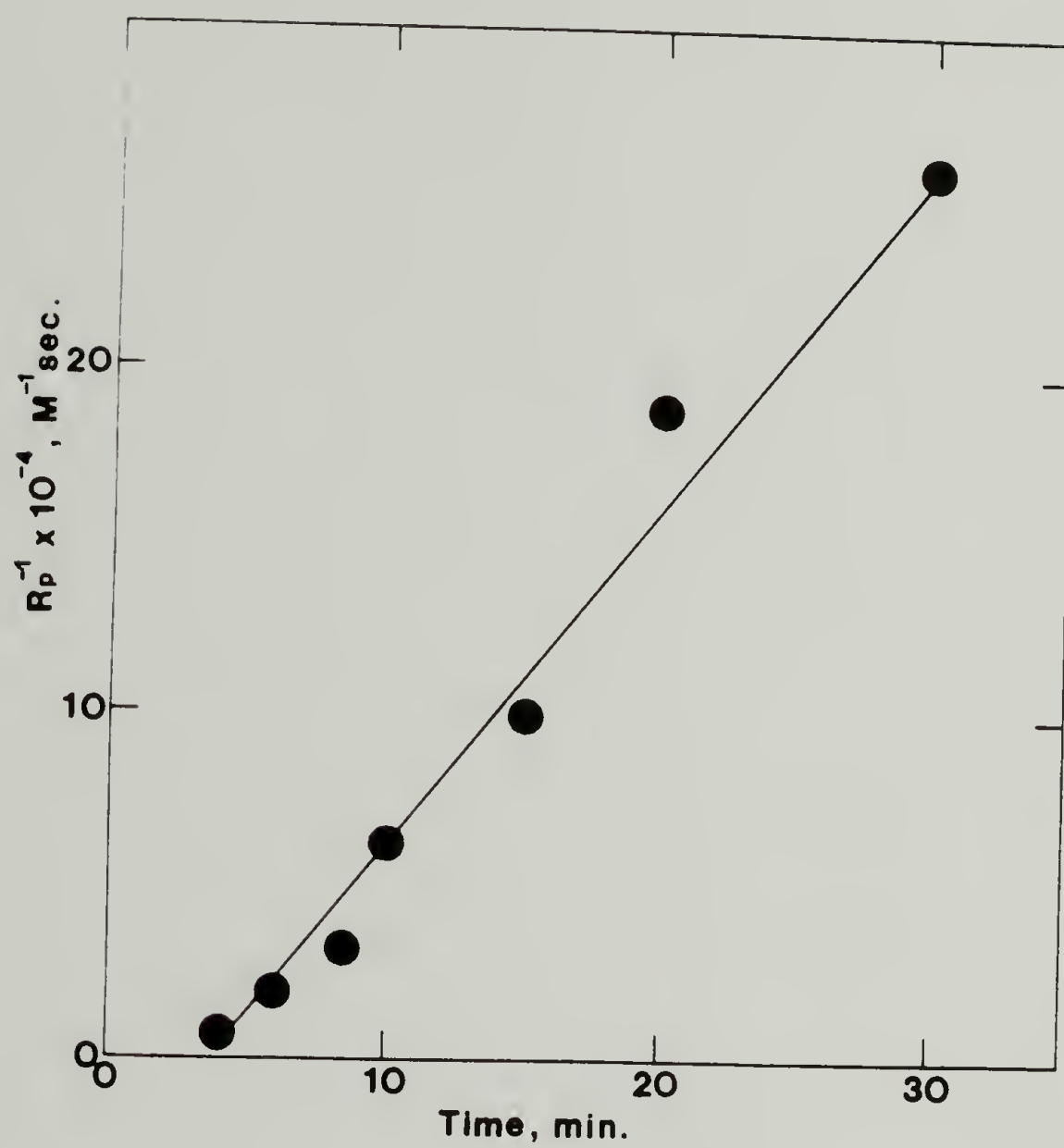


Figure 3.27 Plot of R_p^{-1} versus Time During the Initial Period for Fig. 3.5(a).

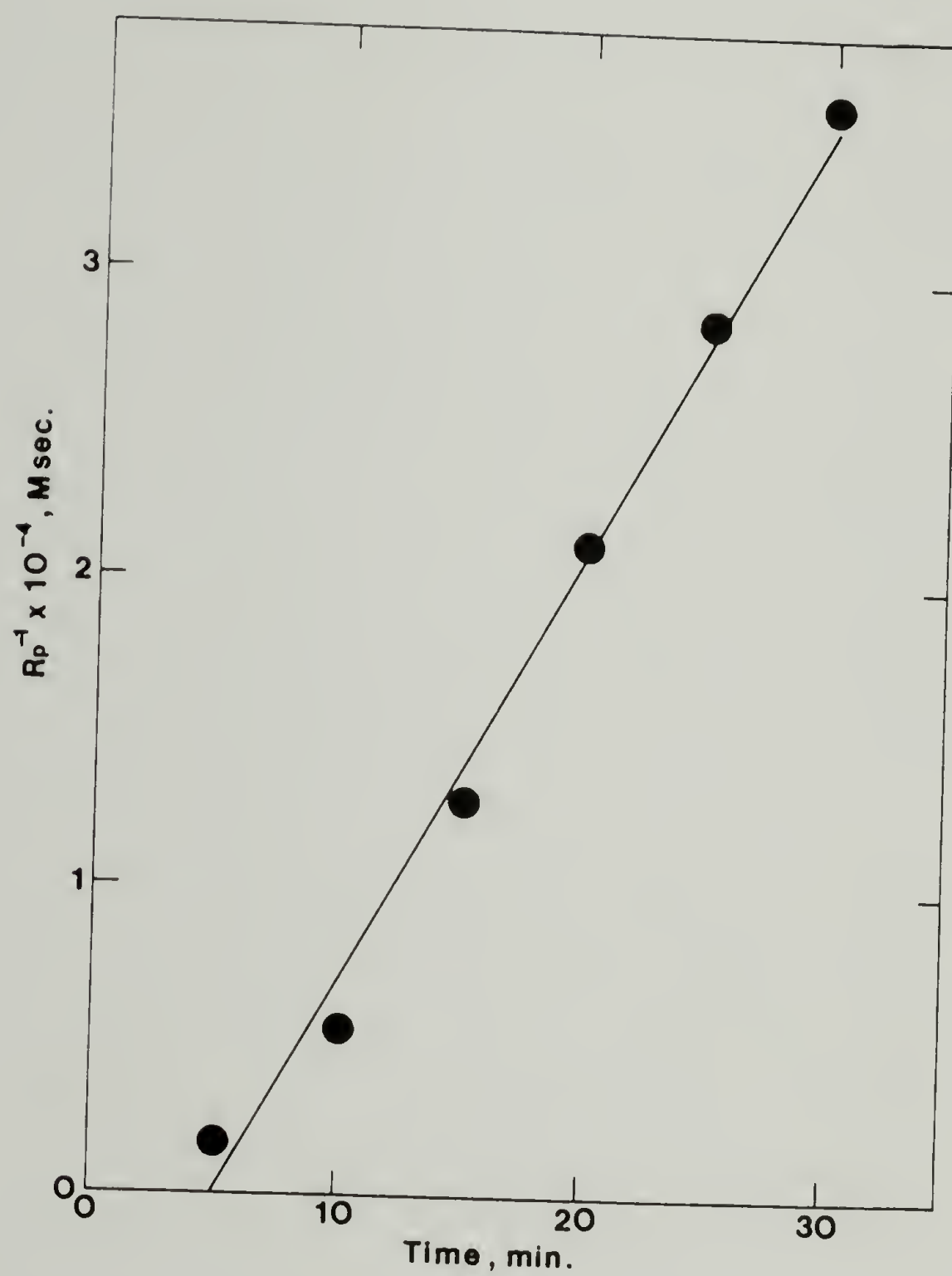
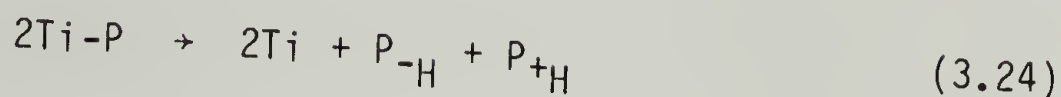


Figure 3.28 Plot of R_p^{-1} versus Time During the Initial Period for Fig. 3.6(a).

transfer by β -hydrogen elimination



reductive terminations



and other less probable reactions having similar consequences. All of these processes yield free polyacetylene molecules which will escape labeling and make the measured \bar{M}_n values higher than they actually are. Our results showed reaction 3.24 to be unimportant because it will tend to increase apparent \bar{M}_n or leave \bar{M}_n unaffected by the increase of catalyst concentration. In fact, Figure 3.10 showed a decrease of \bar{M}_n with increasing $[\text{Ti}]_0$ for the powdery polymer. With regard to transfer processes 3.22 and 3.23 they will normally be seen as \bar{M}_n independent of monomer concentration or first-order dependent on it. The present technique will have \bar{M}_n increasing with acetylene pressure whether these transfer reactions are important or not. Also under the high catalyst concentrations used here, transfer with catalyst components is favored. In ethylene polymerization transfer reactions 3.22 and 3.23 require high temperatures and pressures.

Depending on experimental conditions, three types of macro-morphologies can be prepared, each within different reaction zones. Polymer films are formed on reactor walls when a thin film of catalyst at sufficiently high concentrations is deposited. When polymerization

begins, a high density matrix of primary fibrils results. Lower density polyacetylene gels are produced using catalyst of lower concentration. At even lower catalyst concentrations, an interwoven mat of fibrils of such low density results that even the slightest agitation causes it to break up into powders. This relationship between catalyst concentration and macromorphology was first discussed by Shirakawa.⁵⁸

Yet the macromorphology obtained should be related to a three dimensional C_2H_2 pressure/Ti concentration/Ti catalytic activity dependency. The basic parameter which defines the macromorphology under quiescent conditions is the mass of interwoven fibrils within a given reaction volume. Both active site concentration and monomer concentration affect R_p given a certain catalyst activity, ie. K_p .

The role of macroscopic monomer diffusion in controlling molecular weight in acetylene polymerization was graphically pointed out. Whenever reactions gave more than a single morphology that could be separated, \bar{M}_n followed the order film > gel > powder (Fig. 3.10). Undoubtedly when a matrix of fibrils is formed that cannot be disrupted by agitation, monomer transport by thermal solvent fluctuations within the polymer matrix is the dominant transport process. A low density matrix allows convective currents, such as stirring, to aid in delivering monomer to the growth centers.

Yet macromorphology impacts molecular weight in a second way. In Fig. 3.11, it was found that the gel layer sitting within the pool of catalyst had a lower \bar{M}_n than the wall film. The catalyst on the wall is said to be effectively utilized for polymer formation. But for the gel

sitting within the catalyst, copious amounts of unreactive catalyst components are available for transfer. Again only ca 5% of the titanium appears as active sites. The denser the polymer matrix, the more these components can be excluded.

Obtaining high molecular weight $[\text{CH}]_x$ offers a great challenge to the skills of the experimentalist. Scrupulously washed and dried solvents, glassware and transferring equipment is a must. But also from the view of catalytic activity, the initial conditions when monomer and catalyst come into contact is critical. It was seen that in the absence of monomer, the $\text{Ti}(\text{OBu})_4/4\text{AlEt}_3$ catalyst is rather stable for over long periods of time. However, when in contact with monomer, our kinetic results suggest a precipitous decay in activity over the initial polymerization period. Therefore, to get high \bar{M}_n polymer, the active centers must see an instantaneously large excess of monomer. In this way, observed molecular weights were generally higher if catalyst was added to monomer, and not vice versa.

CHAPTER IV

STRUCTURAL CHARACTERIZATION

The central thrust of this chapter is to present the results of studies which were undertaken to characterize and elucidate how molecular chain length influences the configuration and conformation of polyacetylene.^{157,158} As a consequence of this work, we are now able to resolve often conflicting results reported within the literature regarding the structural aspects of polyacetylene. Through this work, we were able to lay a foundation for the analysis of magnetic and transport experiments discussed within Chapters V and VI.

Elemental Analysis

C, H, O, Ti and Al Analysis

Results from Galbraith Laboratories allowed the direct determination of all the elements listed. Carbon and hydrogen content was obtained by combustion of films in an oxygen rich atmosphere at $\geq 1000^\circ\text{C}$. Direct oxygen content was measured by very high temperature pyrolysis under an N_2 flow, with the evolved CO quantified. Low level metal analysis was by ICP (Inductive Coupled Plasma).

Table 4.1 lists the results for a number of LMnP, standard films, and HMnP. A number of very interesting conclusions may be drawn from these results. With regard to residual catalyst concentrations, acid washed polymers contain ca. 300-600 ppm Ti and 1000-2000 ppm Al. The residual Al/Ti ratio generally reflects the composition of the catalyst used for preparation.

Table 4.1

Direct Elemental Analysis Results.

Sample ^a	\bar{M}_n ^b	Isomer ^c	C	H	O ^d	Ti	Al	Total
MS583-91	400	cis	82.10	7.16	10.62	0.036	0.22	100.14
MS684-13	~500	cis	89.47	8.33	1.62	-	-	99.42
MS684-33	"	cis	89.58	8.11	2.06	-	-	99.75
MS684-85	"	cis	88.83	7.64	3.61	0.03	0.12	100.23
"	"	trans	91.12	7.99	1.01	-	-	100.11
BP(6-21)	~10,500	cis	90.68	7.53	1.45	0.23	0.22	100.11
JH-813	"	cis	89.05	8.02	2.07	0.38	0.68	100.20
"	"	trans	89.97	7.58	1.82	-	-	99.37
MS583-45	870,000	cis	90.51	8.61	-	≤0.05	0.13	99.30
" (T)	"	cis	-	-	-	0.22	0.44	-
MS583-75	14,600	cis	85.43	9.80	4.37	≤0.02	0.10	99.72
HMnP-I	54,000	cis	90.25	8.09	1.42	0.07	0.21	100.05
"	"	trans	91.56	7.69	0.68	0.058	0.10	100.09
HMnP-II	21,400	cis	83.94	7.52	5.60	0.12	1.50	98.68
HMnP-V	25,000	cis	91.28	7.71	1.17	-	-	100.16
"	"	trans	90.05	7.76	0.90	0.068	0.14	98.92
Theoretical	-	-	92.31	7.69	-	-	-	100.00

^a All samples except BP(6-21), JH-813 and MS583-45(T) were washed with dry, O₂ free 10% HCl/CH₃OH followed by methanol rinse. These samples mentioned were washed with either dried pentane or toluene.

^b \bar{M}_n reported are by CH₃O³H labeling. Approximate \bar{M}_n 's were taken from results of analogous reactions.

^c Trans samples isomerized at 453K for 15-30 min.

^d Accuracy to within ±0.2%.

Washing with inert solvents is much less effective and is reflected in ten times as much Ti and two to four times as much Al: ca. 2000-4000 ppm Ti and 2000-6000 ppm Al for pentane washed polymers.

In all samples, a significant amount of oxygen is detected; 1.5-4% is cis-[CH]_x. It has been sometimes observed that after isomerization, a thin white film is deposited on the glass wall of the sample vessel above the oil bath. This is insoluble in alcohol and water but readily soluble in 10% HCl/CH₃OH and is most likely an oxygenated titanium or aluminum residue. Infrared spectra of cis-rich polymer at times show a small absorption at 1685 cm⁻¹. Upon isomerization, this peak disappears and new, much stronger absorption shows up at 1720 cm⁻¹. Therefore, oxidation of polyacetylene is not occurring since α , α' - β , β' unsaturated aldehydes absorb at 1660-1670 cm⁻¹ and 1680-1700 cm⁻¹ respectively. In trans-[CH]_x, residual oxygen is most likely in the form of saturated aldehydes.

The empirical formula for most preparations are close to the theoretical 1:1 stoichiometry between carbon and hydrogen. For low \overline{M}_n polymer, the molar composition is:

MS684-85: cis - C_{1.0} H_{1.03} O_{0.030}

" trans - C_{1.0} H_{1.05} O_{0.008}

for standard film:

JH-813: cis - C_{1.0} H_{1.08} O_{0.017}

trans - C_{1.0} H_{1.01} O_{0.015}

and for higher \overline{M}_n films:

HMnP-I: cis - C_{1.0} H_{1.08} O_{0.012}

" trans - C_{1.0} H_{1.01} O_{0.006}

HMnP-V: cis - C_{1.0} H_{1.01} O_{0.010}

trans - C_{1.0} H_{1.01} O_{0.007}

Excessive hydrogen indicates finite level of saturated carbon impurities. Assuming these to be methylene groups, cis-[CH]_x contains on the average 1 methylene per 20 CH units and in trans-[CH]_x, ca. 1 methylene per 100 CH units. Oxygen represents a great source of impurities.

Cis-[CH]_x contains on the average 1 oxygen atom per 10-30 CH units and in trans-[CH]_x, ca. 1 per 150 CH units.

Morphology

Free standing films of polyacetylene prepared using the Shirakawa technique⁵¹ have been shown by SEM⁴³ to consist of fibrils with an average diameter of 20 nm. Direct polymerization on grids carried out by Chien and co-workers and observed by TEM show 3 nm microfibrils that aggregate into the larger, 20 nm macrofibril. The impact specimen washing and polymer \overline{M}_n has on the formation of microfibrils, chain packing within crystalline domains, and ones ability to observe these morphological features is the subject of this section.

Nascent Morphology and Effect of Contaminants

To resolve differences between Wegner et al⁶⁶⁻⁶⁸ and our work, the effect of washing with 10% HCl/methanol, methanol, or toluene on the

observed morphologies was investigated. Ziegler-Natta polymerized $[\text{CH}]_x$ specimens were prepared either by direct polymerization on EM grids or by suspension deposition on TEM grids. Catalyst concentrations of $[\text{Ti}]_0 = 1 \text{ mM}$, 5 mM , and 40 mM were used. Luttinger catalyst at $30 \text{ mM } [\text{CO}(\text{NO}_3)_2]$ and $48 \text{ mM } [\text{NaBH}_4]$ was used for direct polymerization on EM grids. Preparation at $0.35 \text{ mM } [\text{CO}(\text{NO}_3)_2]$ and $5 \text{ mM } [\text{NaBH}_4]$ yielded powders which were suspension deposited on grids.

Polyacetylene obtained at low concentration of $[\text{Ti}]_0 = 1.0 \text{ mM}$ and toluene washed consisted of fibrils, ribbons and a dark spongy mass (Fig. 4.1). No pseudo-lamellae particles were present. After the polymer was washed with methanolic-HCl, clean fibril morphology resulted (Fig. 4.2). The spongy material seems to be soluble in methanolic-HCl and the ribbons in Figure 4.1 seem to be aggregates of fibrils glued together by methanolic-HCl soluble substances such as catalyst residue or low molecular weight polymers. At a $[\text{Ti}]_0$ of 40 mM , the $[\text{CH}]_x$ after thorough toluene washing had a major portion of the specimen masked by spongy substance. There were also aggregates of shaped lamellae-like particles which form irregular, drawn fibrils. In fact, these micrographs closely resembles those published by Wegner et al.⁶⁶⁻⁶⁸ By washing with methanolic-HCl only $[\text{CH}]_x$ fibrils were observed. The number of fibrils per unit area in this sample was much greater than that of Fig. 4.2. This high $[\text{Ti}]_0$ is still lower than that commonly used in the preparation of $[\text{CH}]_x$ films which is 204 mM . Thus contribution of the catalyst residue to the dirty morphology seems to be established.

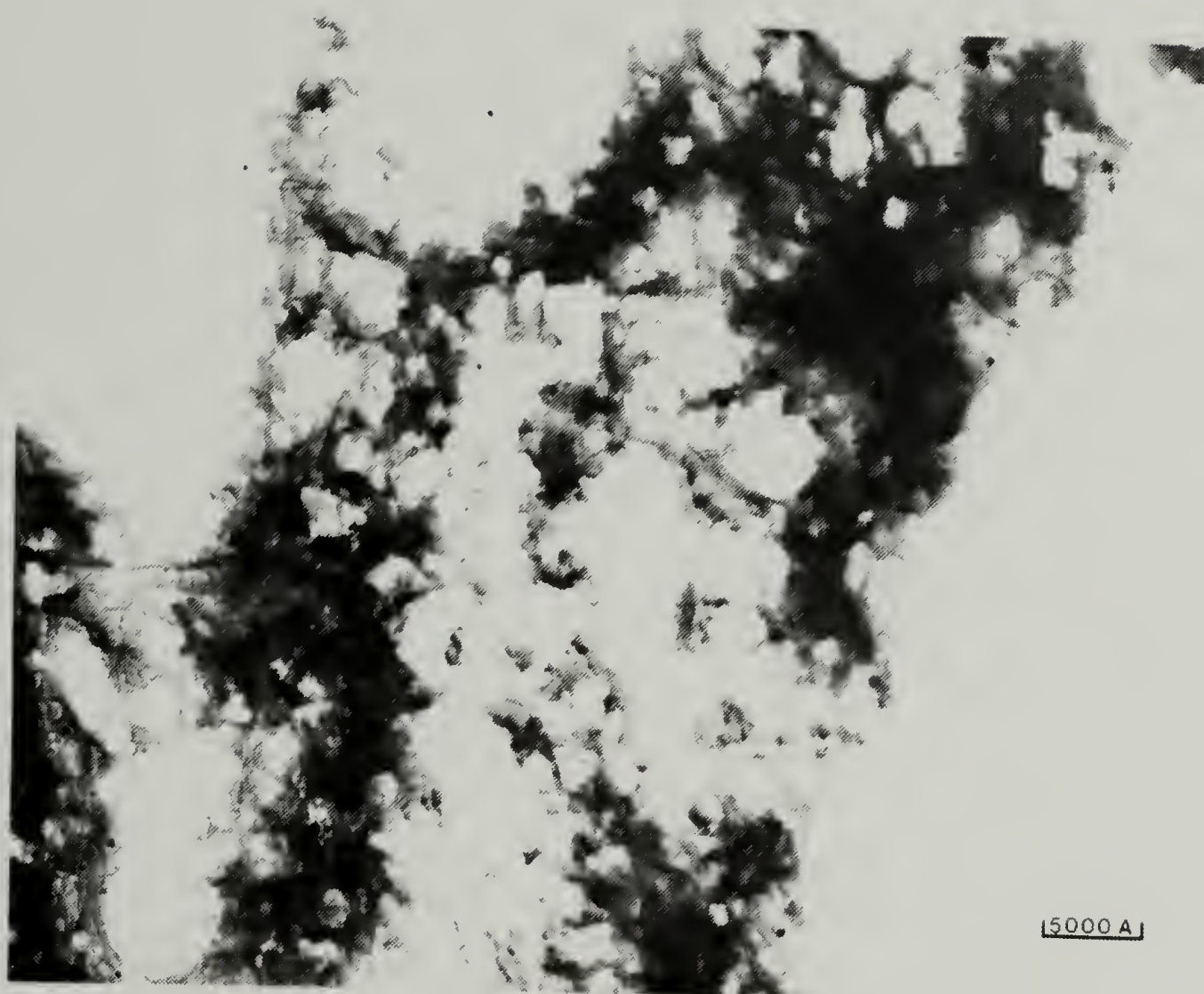


Figure 4.1 TEM of Toluene Washed $[\text{CH}]_x$ Polymerized Using $[\text{Ti}]_0 = 1 \text{ mM}$.

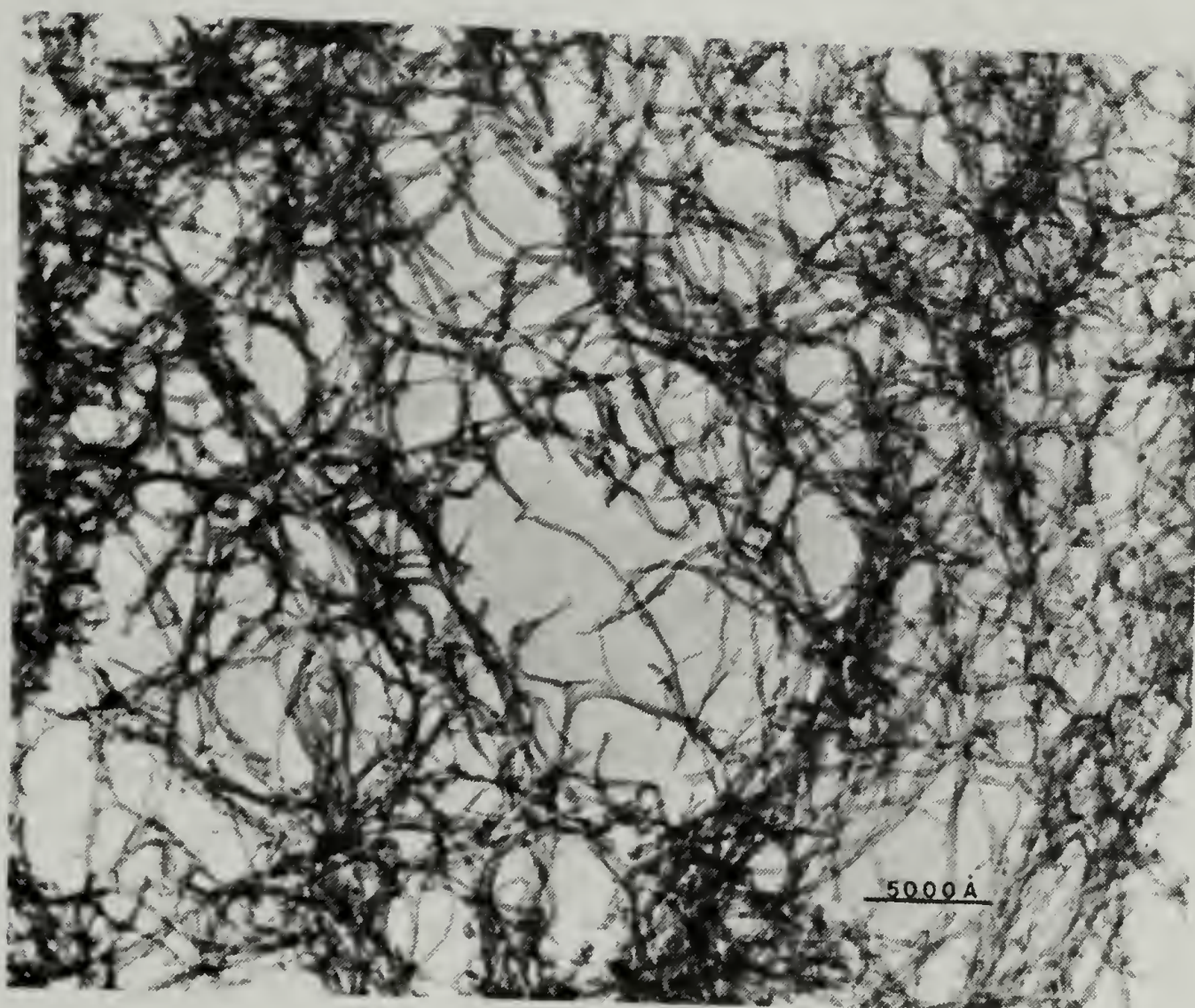


Figure 4.2 TEM of 10% HCl/ Methanol Washed $[\text{CH}]_x$ Polymerized
Using $[\text{Ti}]_0 = 1 \text{ mM}$.

Polyacetylene obtained with Luttinger catalyst [$0.35 \text{ mM Co(NO}_3)_2 / 5.3 \text{ mM NaBH}_4$], washed with ethanol showed definite fibril morphology. There were also impurity materials and the fibrils appear to have deposits of foreign materials. Using 10-fold higher catalyst concentration, EMs similar to those reported by Wegner et al⁶⁶⁻⁶⁸ were observed. If the polymer was washed with methanolic-HCl, fibrillar morphology was revealed. However, much spongy material still remained. It is apparently more difficult to remove contaminants from the polyacetylene obtained with the Luttinger catalyst than in the case of the Ziegler-Natta catalyst.

To show that the two catalyst systems produce truly identical $[\text{CH}]_x$ acetylene was polymerized directly onto EM grids using both Luttinger and Ziegler-Natta catalysts. The fibrils in the former were smooth, free of foreign substances and have diameters generally greater than in the latter. Electron diffraction patterns of selected areas with parallel bundles of fibrils in both specimens were identical to those of *cis*- $[\text{CH}]_x$ with the chain axes along the fibril axis. Furthermore, using low monomer pressure, low Ziegler-Natta catalyst concentration, and short polymerization time to obtain ultra-thin $[\text{CH}]_x$ specimens, an abundance of 3 nm diameter microfibrils were observed. These microfibrils are probably the ultimate morphological entity which aggregate to form the more commonly reported 20 nm fibrils.

Catalytic Activity and Micromorphology

Using the Ziegler-Natta catalyst, no deviation from the fibrillar morphology was observed over the molecular weight range prepared. It was, however, much more difficult to obtain thin polymer films in the case of low \overline{M}_n samples which clearly showed the fiber structure after acidic methanol washing. Also, often times an EM grid would contain polymer tightly clinging to the grid crossbars but little of any stretched in between. Presumably, washing tore free those sections due to the polymer's intrinsic brittleness.

There does appear, to be some relationship between catalytic activity and fibril diameter measured from TEM. Catalyst concentration, acetylene pressure, and temperature had no effect on fibril size. Longer catalyst aging times seem to produce smaller fibrils. Table 4.2 lists those results. At an Al/Ti ratio of 7/1 and catalyst aging of 1 hr., fibrils of ca. 100 ± 50 Å were observed. Thus, both excess aluminum and extreme catalyst aging reduce catalytic activity and consequently smaller fibrils result.

Polymerization Conditions

In Chapter II, a discussion of the interrelationship between parameters which influence the polymerization kinetics and the resulting polymer macromorphology, i.e. films, gels or powders was presented. However, a new type of polyacetylene macromorphology should be added to the list, i.e. ribbons and whiskers.

Table 4.2

Mean Fibril Diameter Versus Catalyst Aging.

Aging Time	Diameter, Å
0	700 ± 100
1 hr.	$200-300 \pm 50$
8 days	150 ± 50
50 days	100 ± 50

Meyer^{59,60} has presented results of polymerizations under controlled shear using a couette type reactor. In those reports, examples of highly aligned films were presented. It was found in this work that when acetylene is polymerized under sheared conditions, orientation of the microfibrils can give threads of highly aligned polymer. These were found to be composed of macroscopic, two-dimensional ribbons of over 1 cm long and 0.1 mm wide interwoven about a central ribbon. Each ribbon contains thousands of primary fibrils. Thus, macroscopically oriented polyacetylene, can be obtained directly during polymerization.

Under the polymerization conditions, some catalyst was adsorbed on the stirrer surface which initiated acetylene polymerization. Polymer grew from its ends as shown in Figure 4.3. As polymerization proceeded, some of the accumulated polymers separated from the stirrer. Individual macroscopic "whiskerlike" ribbons are over 1 cm long and at least 0.1 mm wide. Figure 4.4 shows the material to consist of a central ribbon with dendritic growth of secondary ribbons radiating from it. The interweaving of multiple ribbons make up the macroscopic threads. Both are highly birefringent. These radiating ribbons in some cases were smooth assemblies of densely packed fibrils (Fig. 4.5) and others were looser collections of fibrils (Fig. 4.6). In the former case, many examples were observed where the ribbons folded over themselves or were twisted though without any regular pitch. In Figure 4.6 the fibrils in one collection leave and enter other assemblies. This is particularly true at junctions of two or more ribbons.



Figure 4.3 Polymerization of Acetylene Under a Hydrodynamic Flow Field. Polymer Grown from the Ends of a Magnetic Stirbar.

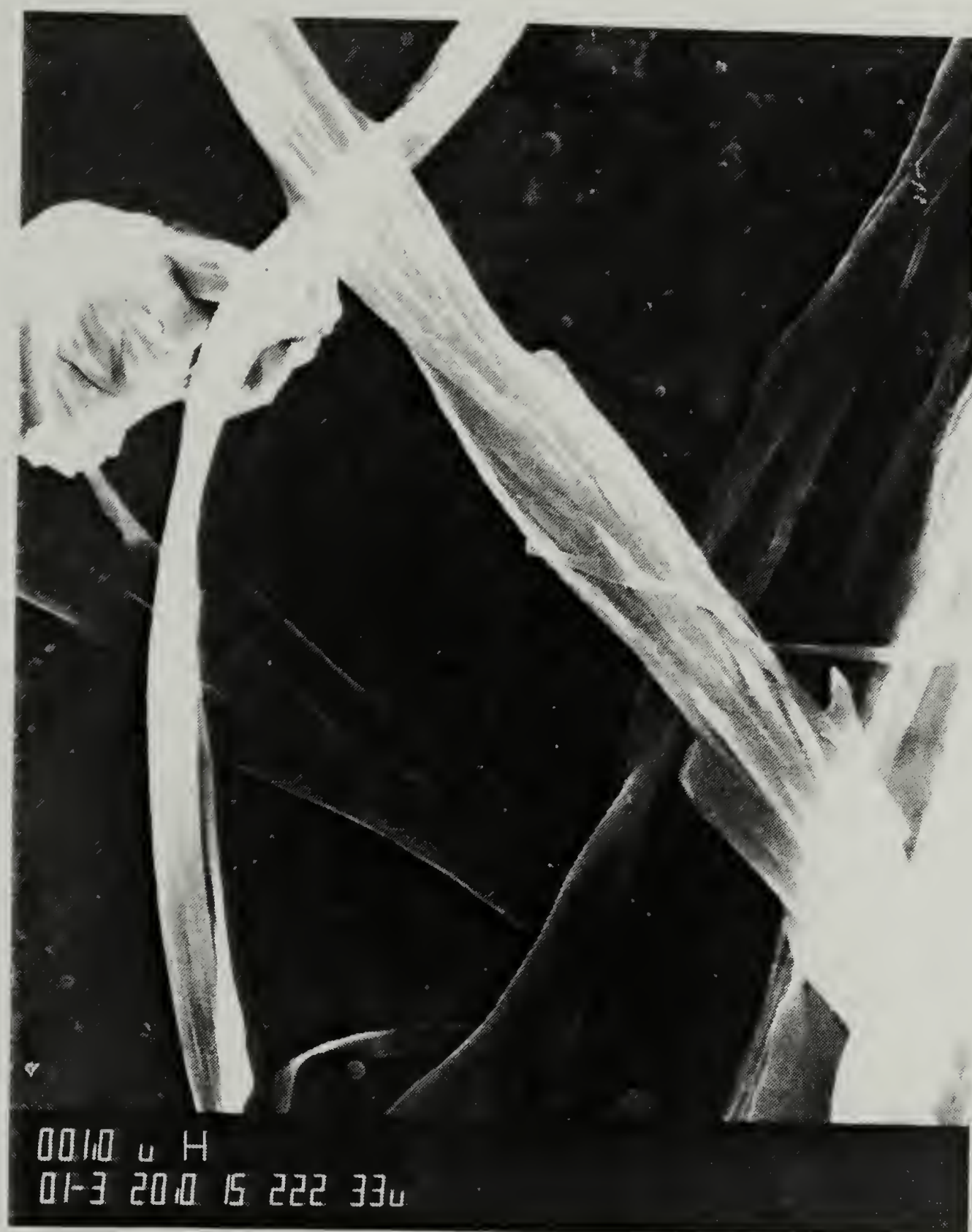


Figure 4.4 SEM of Interwoven $[\text{CH}]_x$ Ribbons Obtained from Polymerization Under a Hydrodynamic Flow Field.



Figure 4.5 TEM of Tightly Woven Two Dimensional Ribbons.

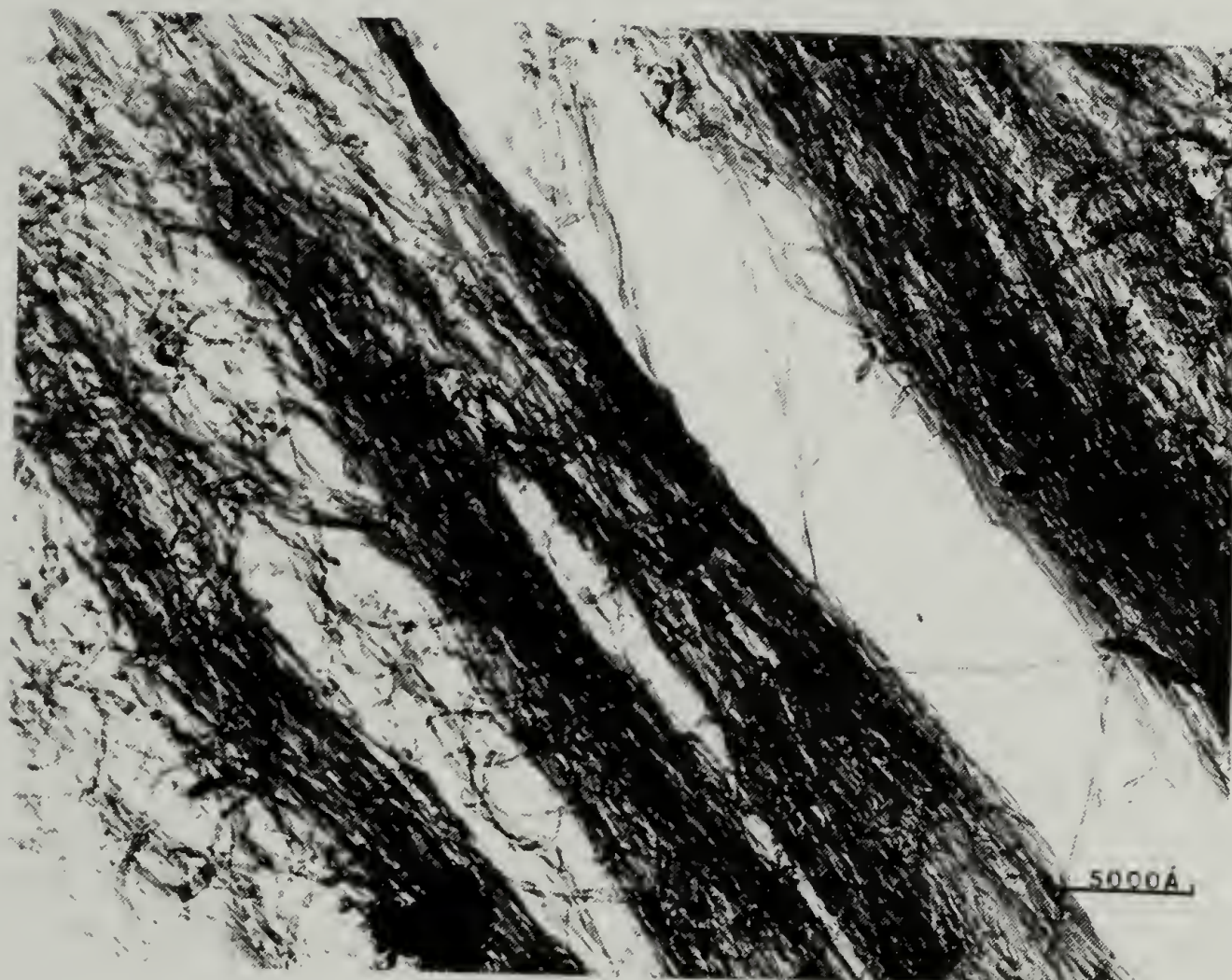


Figure 4.6 TEM of Loosely Woven Ribbon.

The ribbons are crystalline, giving electron diffraction pattern which can be indexed with the $\text{cis-}[\text{CH}]_x$ unit cell. The molecular chain axis is parallel to the long axis of the ribbon. In other words, the molecular c-axis is the fiber axis and the ribbon is comprised of nearly aligned aggregations of the fibers. Comparison with previously described electron diffraction patterns of nascent $\text{cis-}[\text{CH}]_x$ showed the former to have more diffuse and weaker arcs in the layer line suggesting the as prepared ribbon crystals possess a high degree of lateral order but not along the fiber direction.

Isomerization of the cis ribbon crystals for 3 min at 448 K gave electron diffraction patterns which were identical to that reported previously for $\text{trans-}[\text{CH}]_x$.⁶² The important finding is that the diffraction pattern had sharper layer lines than the cis pattern. Dark field images were taken with the 200 and 110 piled reflections of the cis ribbon crystals and of the trans ribbon crystals. The dark field image for the cis material was much less ordered than for the trans material. The crystalline domain sizes in the $\text{trans-}[\text{CH}]_x$ ribbons are about 70-100 nm. The data compels one to conclude that there is an annealing effect which improves the longitudinal order during thermal isomerization. This result also argues against extensive crosslinking in these polyacetylene samples as had been proposed by some workers.

Crystal Structure

Electron diffractions of LMnP were obtained for both cis and trans isomers. A side-by-side standard was used to obtain the camera

constant for the Bragg equation. All reflections could be indexed using the assignments of Shimamura and co-workers.⁶¹⁻⁶³ No new reflections were observed. Table 4.3 compares the calculated d-spacings for cis-LMnP in comparison to those determined for intermediate \overline{M}_n polymer. Much fewer equatorial reflections were observed in the LMnP, perhaps indicating a lower degree of longitudinal order.

Thermal isomerization at 453 K for twenty minutes allowed comparison of trans d-spacing against those found by Shimamura. Table 4.4 tabulates the d-spacings and their assignments.

Calculated unit cell parameters for LMnP and IMnP agree to within 1% in cis-[CH]_x and 4% in the trans isomer. Differences may be attributed to the use of a side-by-side gold standard instead of gold sputtering directly on the polymer grid. Table 4.5 compares these results.

These results are rather intriguing from the point of view that the two polymers were prepared under grossly differing polymerization conditions and kinetics. This suggests that when considering acetylene polymerization as a polymerization-simultaneous crystallization process, propagation kinetics are rate limiting.

Infrared Spectroscopy

Spectra of Pristine Polymer

Infrared spectroscopy was found to be the most convenient tool for probing subtle differences in polymer microstructure. Works by Shirakawa⁴¹ and Haberkorn⁴⁹ have assigned the IR-active vibrational modes. Comparing the cis spectra of 10,500 \overline{M}_n and 500 \overline{M}_n [CH]_x (Fig.

Table 4.3
d-Spacing and Reflection Indices for Cis-Polyacetylene.

<u>Reflection</u> (hkl)	Direction ^a	<u>d-Spacing, Å</u>	
		IMnPb	LMnP
(200)(110)	e	3.84	3.86
(210)	e	2.89	2.97
(020)(120)	e	2.33	-
(002)	m	2.19	2.21
(220)(400)	e	1.98	-
(320)(410)	e	1.70	-
(004)	m	1.10	1.10

^a e: equitorial, m: meridional.

^b Shimamura et al., 1981; $\overline{M}_n \sim 2000$.

Table 4.4

d-Spacing and Reflection Indices for Trans-Polyacetylene.

Reflection (hkl)	Direction ^a	d-Spacing, Å	
		IMnP ^b	LMnP
(110)(200)	e	3.68	3.49
(210)	e	2.75	2.64
(020)(120) (310)	e	2.12	2.02
(011)(111) (201)	off	2.08	2.00
(220)(400)	e	1.83	1.73
(002)	m	1.23	1.18
(102)(112) (202)	off	1.16	1.15

^a e: equitorial, M: meridional, off: off-meridional.^b Shimamura et al., 1981; $\overline{M}_n \sim 2000$.

Table 4.5
Unit-Cell Parameters.

Cis Polyacetylene			
	a/Å	b/Å	c/Å
LMnP	7.72	4.46	4.42
IMnPa	7.68	4.46	4.38
Trans Polyacetylene			
	a/Å	b/Å	c/Å
LMnP	6.98	4.04	2.36
IMnPa	7.32	4.24	2.46

^a Chien et al., 1982.

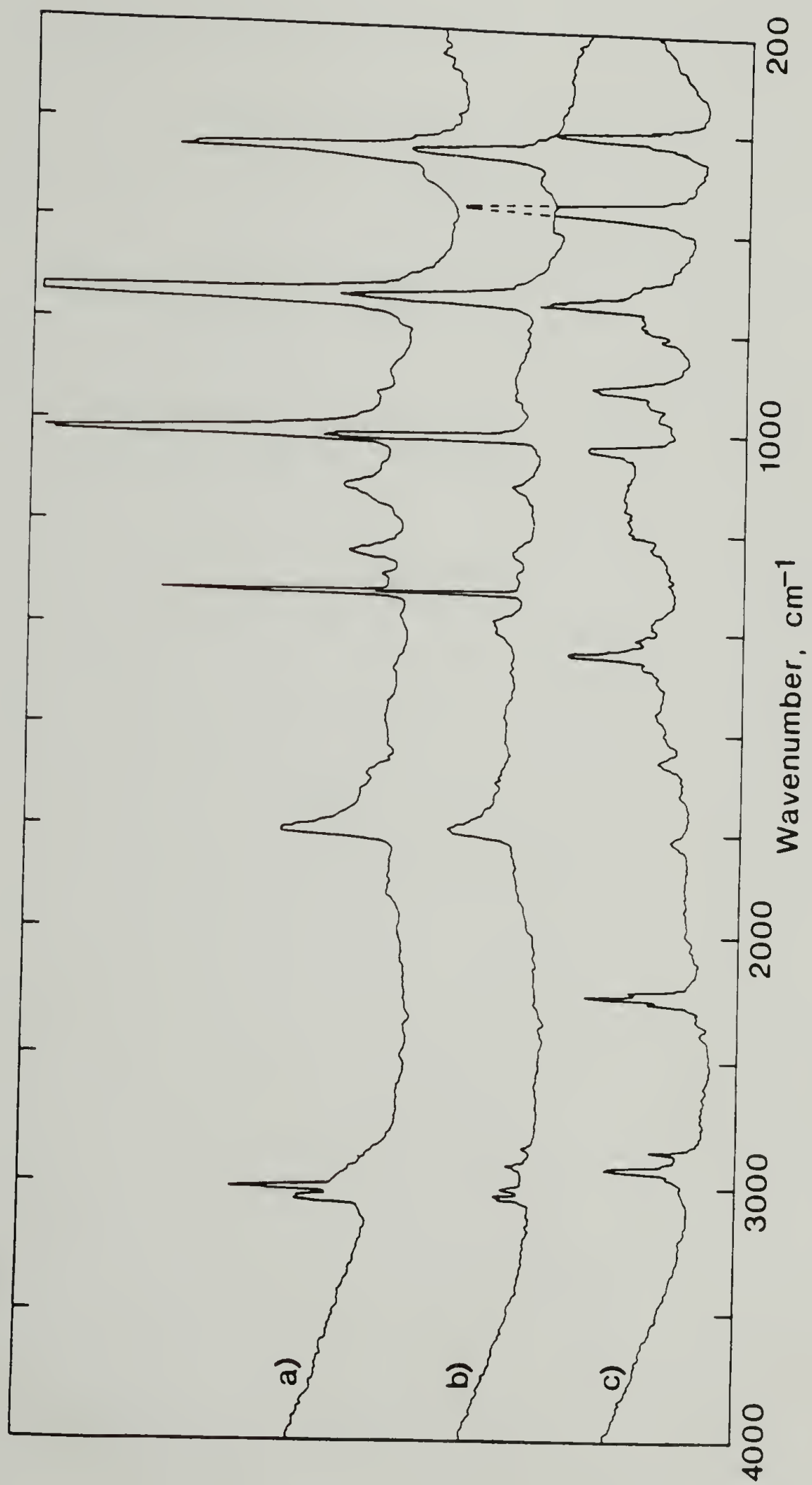
4.7(a) &(b)), one sees all the vibrational modes characteristic of an extend polyene chain. No frequency shift in the 740 cm^{-1} and 1010 cm^{-1} cis-CH out of plane and trans-CH out of plane deformations, respectively, was seen. There are two additional features characteristic of the LMnP; enhanced sp^3 -hybridized carbon stretching at $2850\text{--}2860\text{ cm}^{-1}$, and $2920\text{--}2930\text{ cm}^{-1}$ and CH_3 symmetrical bending at $1380\text{--}1420\text{ cm}^{-1}$. To help differentiate the nature of these saturated carbons, perdeuterated acetylene, (C_2D_2) was polymerized with the hydrogen containing catalyst. Figure 4.7(c) clearly reveals both saturated carbon vibrations to be unshifted, unambiguously showing these vibrations are not the consequence of interchain crosslinking (e.g. Diels-Alder reaction), or chain branching. In fact, the low frequency side of the sp^2 CD stretching at $2225\text{--}2270\text{ cm}^{-1}$ drops off sharply, also implying the polyene chain to be free of saturated defects. These sp^3 carbon centers can only be a result of either catalyst residues or ethyl endgroups on the polymer chain.

Using Eq. 1.21 and weighing the spectral intensities of the cis/trans peaks, initial cis contents were calculated for freshly prepared polymers. Results suggest a correlation between initial cis content and \bar{M}_n : $500\ \bar{M}_n$ 85%cis, $10500\ \bar{M}_n$ 88%cis, and $25000\ \bar{M}_n$ -92%cis. These results shall be discussed next.

Thermal Isomerization Kinetics and Trans Spectra

Since the peak width at half height varied as a function both of \bar{M}_n and cis/trans content, integrated peak heights were used for deter-

Figure 4.7 IR Spectra of Pristine (a) 10,500 Mn Standard Film,
(b) 500 Mn $[\text{CH}]_x$ and (c) ca. 500 Mn $[\text{CD}]_x$.



mining cis/trans ratios. Figs. 4.8 and 4.9 show the evolution of the IR spectra at 423 K isomerization temperature for both 500 \overline{M}_n and 10500 \overline{M}_n standard film polyacetylenes. From these spectra, a number of features deem discussion. In the 10500 \overline{M}_n film, even after 3 hrs, a significant cis peak remains as compared to the 500 \overline{M}_n film in which nearly no detectable cis remains after 30 min. Residual cis double bonds is consistent with recent results by Gibson et al.^{102,103} Figure 4.10 plots the cis-trans isomerization kinetics for three molecular weights at 423 K. After 30 min, the 500, 10500 and 2500 \overline{M}_n polymers contained 93%, 76% and 70% trans segments respectively. Therefore, it is possible to obtain a purer trans configuration by using low molecular weight polymer. Also from Fig. 4.9 it can be seen that at longer isomerization times, a more well defined sp^3 CH stretching at 2850-2960 cm^{-1} , CH_3 bending at 1380 cm^{-1} and CH_2 bending at 1460 cm^{-1} appear. Simultaneously broadening of the 1010 cm^{-1} peak takes place. These features can be taken to imply chain degradation and shortening of the conjugation lengths. On the other hand, at 30 min with 500 \overline{M}_n polymer, no 1010 cm^{-1} peak broadening has taken place.

Using various isomerization temperature to study 500 \overline{M}_n polymer, it became obvious that higher isomerization temperatures required shorter treatment periods and more importantly, gave higher trans content $[CH]_x$. Figure 4.11 shows the cis/trans evolution at 383 K. Even after 18 hrs only 81% trans is obtained in comparison to 93% after 30 min and 95% after 15 min at 423 K and 453 K treatments respectively. Similar results were found with 25,000 \overline{M}_n polymer. At 423 K isomeriza-

Figure 4.8 Thermal Isomerization of 500 Mn $[\text{CH}]_x$ at 423 K: (a) Pristine Cis Film, (b) $t = 5$ min., (c) $t = 15$ min., (d) $t = 30$ min.

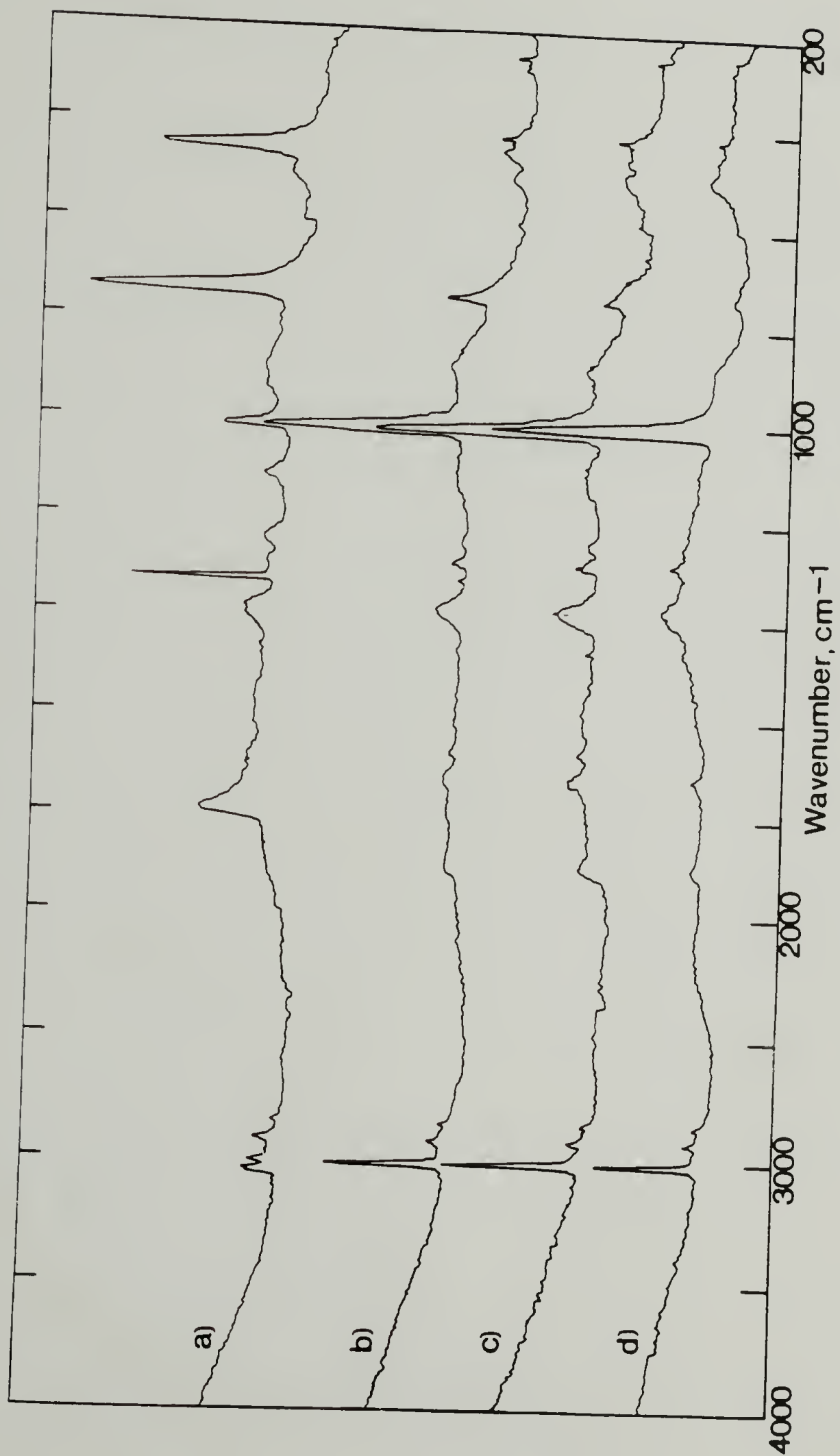
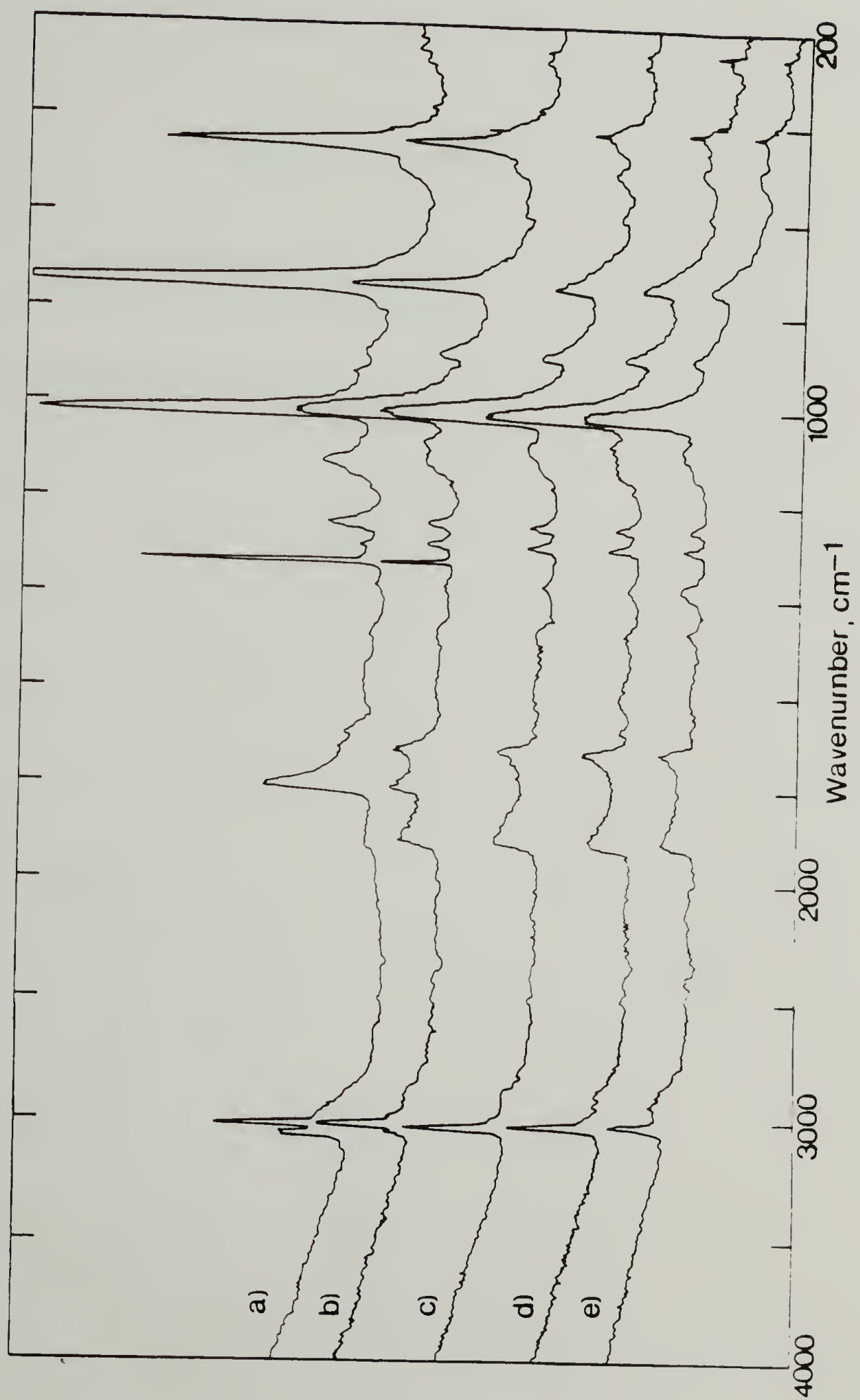


Figure 4.9 Thermal Isomerization of 10,500 Mn $[\text{CH}]_x$ at 423 K: (a) Pristine Cis Film, (b) $t = 5$ min., (c) $t = 30$ min., (d) $t = 120$ min., (e) $t = 270$ min.



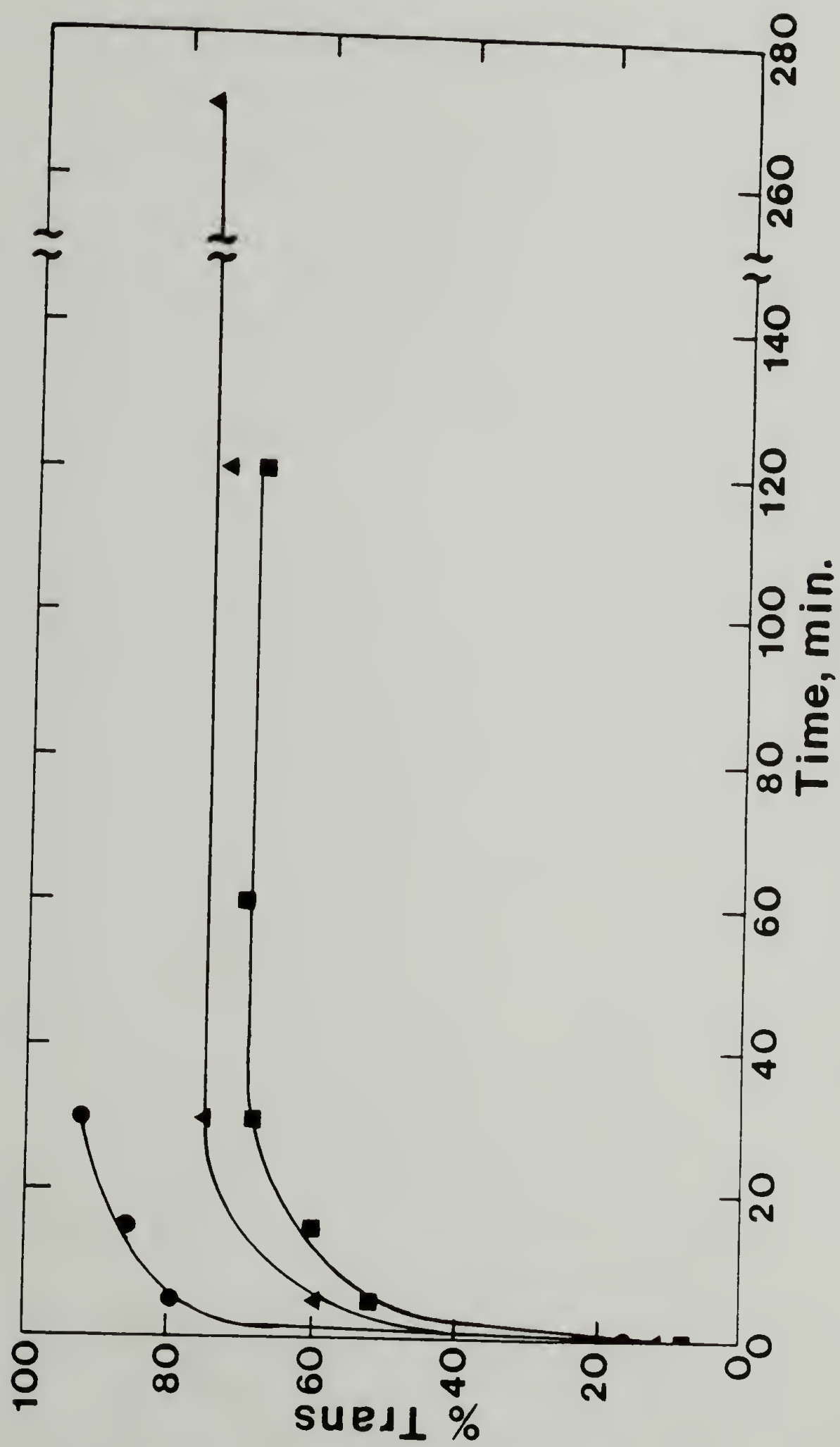
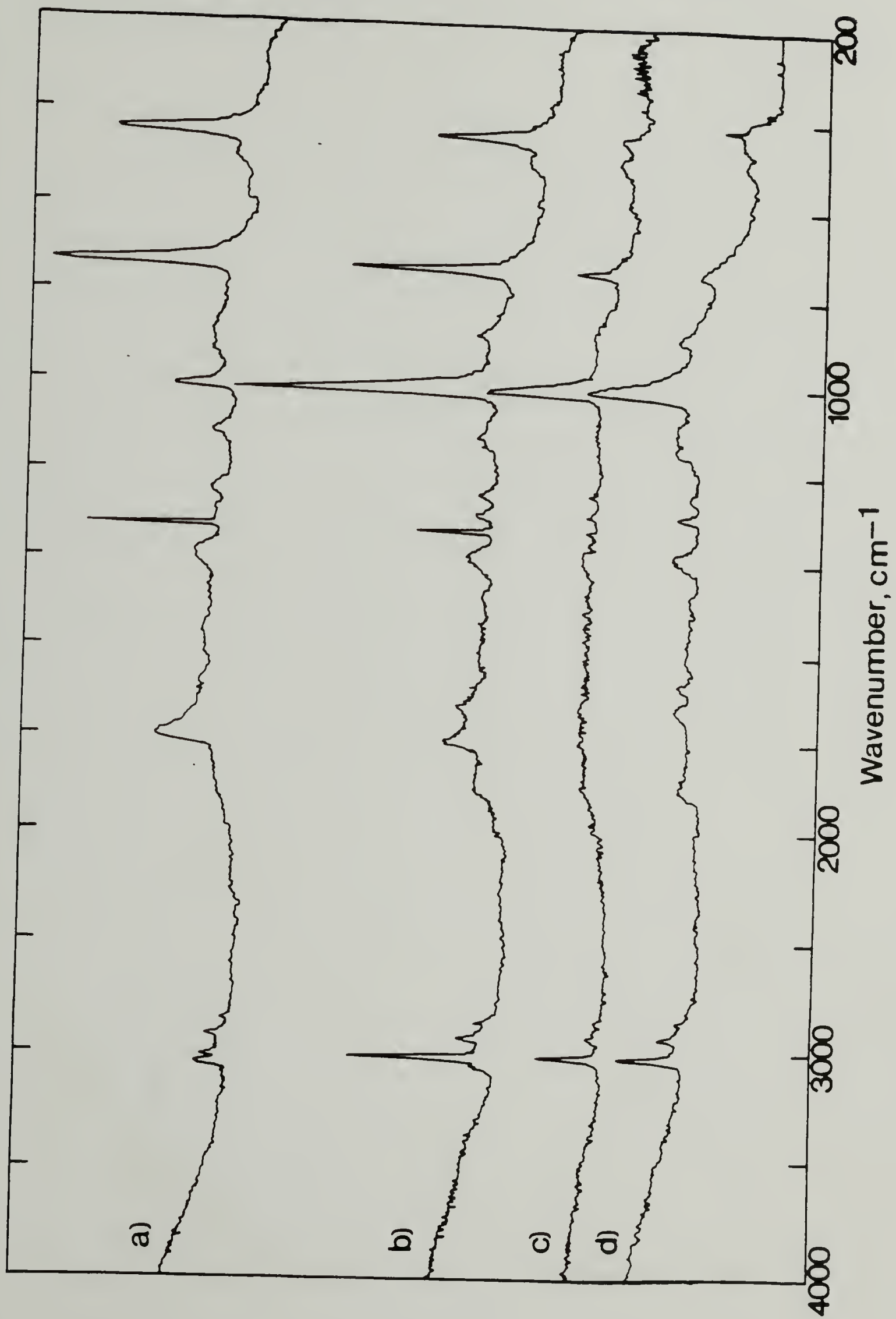


Figure 4.10 Cis-Trans Isomerization Kinetics at 423 K for (\bullet) 500 \bar{M}_n ; (\blacktriangle) 10500 \bar{M}_n ; and (\blacksquare) 25000 \bar{M}_n [CH] $_x$.

Figure 4.11 Thermal Isomerization of 500 Mn $[\text{CH}]_x$ at 383 K : (a) Pristine Cis Film, (b) $t = 30$ min., (c) $t = 120$ min., (d) $t = 18$ h.



tion, only 70% trans was obtained after 30 min. At 453 K however, 93% trans content was reached after 10 minutes.

A phenomenon not previously discussed by others is the apparent broadening of the 1010 cm^{-1} trans out of plane bending mode when either higher molecular weight polymers are isomerized or when low molecular weight samples are overisomerized. Consistently, this broadening occurs on the low frequency side of the absorption band. Figure 4.12 compares the trans spectra for the three molecular weight polymers after various isomerization times at 423 K. As can be seen, the $500\ \bar{M}_n$ polymer exhibits only a small tail below 1000 cm^{-1} and a single maxima. Higher \bar{M}_n samples show multiple maxima and an ever increasing tail below 1000 cm^{-1} . Table 4.6 compares the percentage of the trans peak that appears above 1000 cm^{-1} and the peak width at half height (PWHH) as a function of isomerization time for these samples at 423 K.

It is believed that greater effective conjugation lengths may be obtainable with low \bar{M}_n polymer. A discussion regarding this point appears in the last section of this chapter.

Perdeuterated Polyacetylene

Low \bar{M}_n $[\text{CD}]_x$ was polymerized using the techniques which yield $500\ \bar{M}_n$ $[\text{CH}]_x$. Fig. 4.13 shows the spectra of cis-rich and isomerized (423 K/30 min) trans isomers. As shown earlier, saturated sp^3 carbon content may be traced to either ethyl endgroups or catalytic residues. Most interesting is the appearance of a relatively strong stretch at 3000 cm^{-1} in the trans isomer (Fig. 4.13(b)). No sp^3 CD stretches

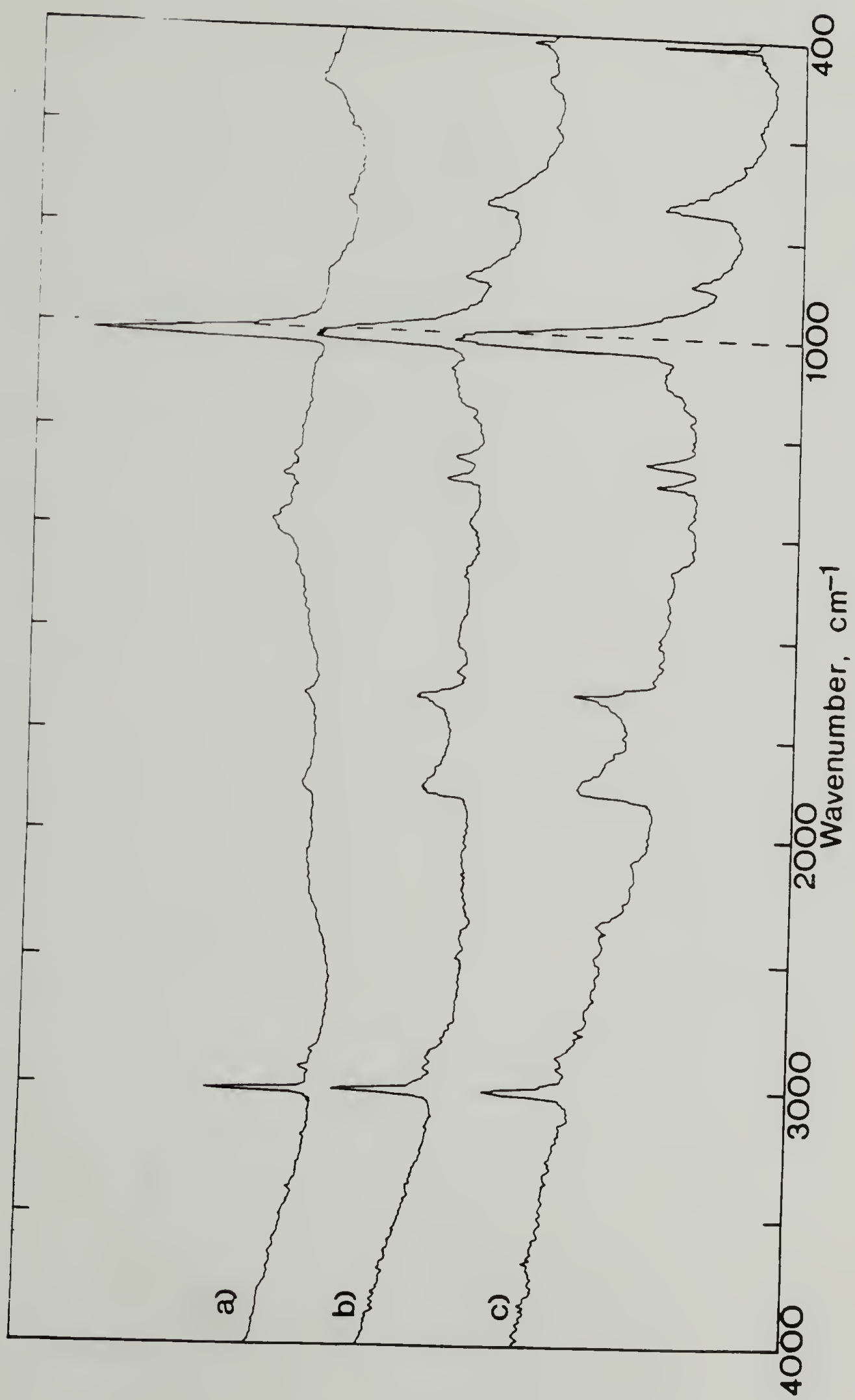


Figure 4.12 Trans Peak Position for 423 K Isomerized (a) 500 \bar{M}_n /30 min.; (b) 10500 \bar{M}_n /120 min.; (c) 25000 \bar{M}_n /120 min. $[\text{CH}]_x$.

Table 4.6
1010cm⁻¹ Peak Position and PWHH^a

\bar{M}_n	time, min	% trans	Percent Absorption ≥1000 cm ⁻¹	PWHH, cm ⁻¹
500	0	15	85	20
	5	80	77	23
	15	85	76	25
	30	93	84	20
10500	0	12	85	15
	5	59	52	45
	30	75	58	40
	120	73	59	40
	270	77	60	40
25000	0	7	76	32
	5	52	55	37
	15	60	62	40
	30	68	46	50
	60	70	44	47
	120	68	53	45

^a 423 K

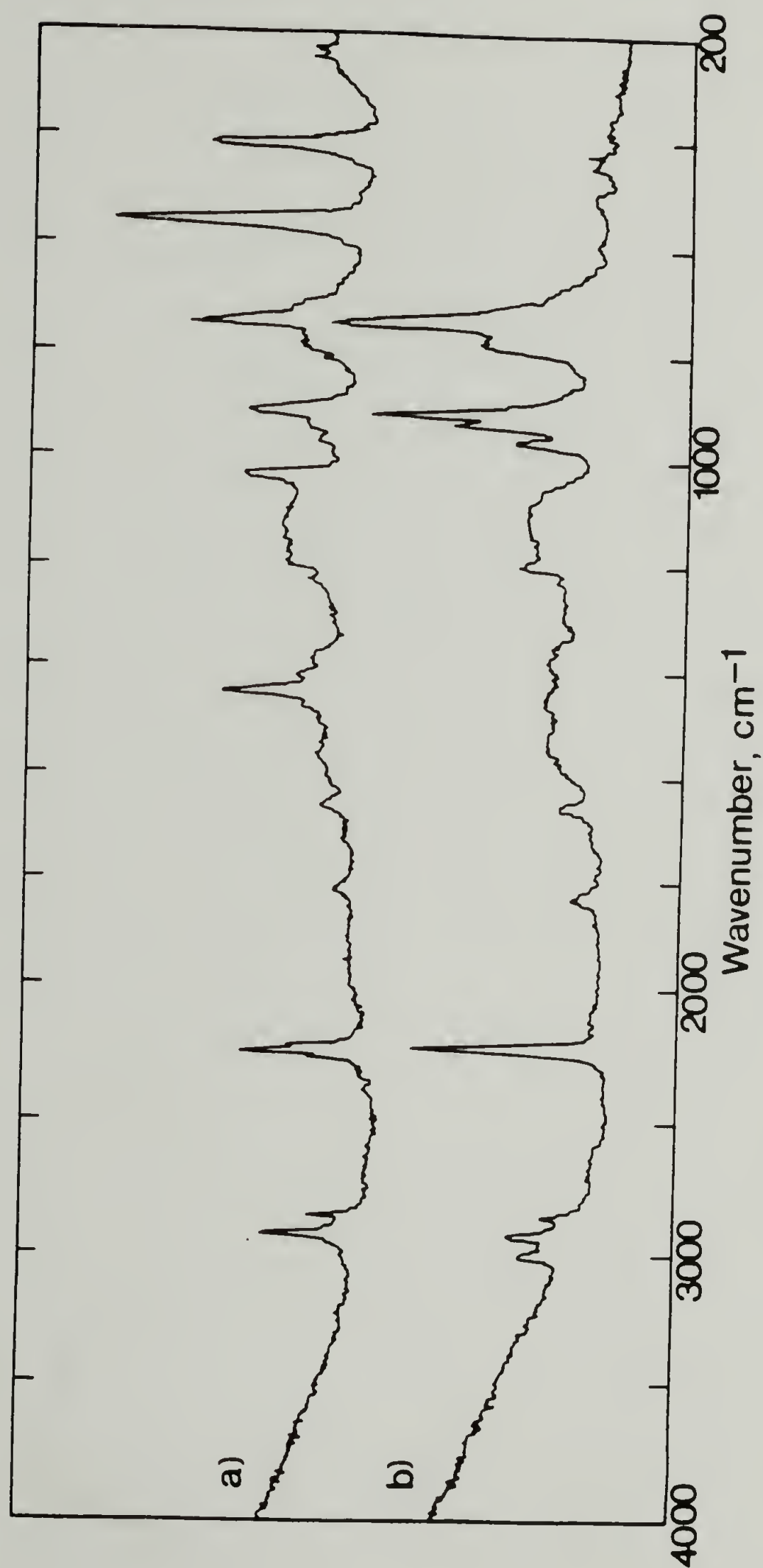
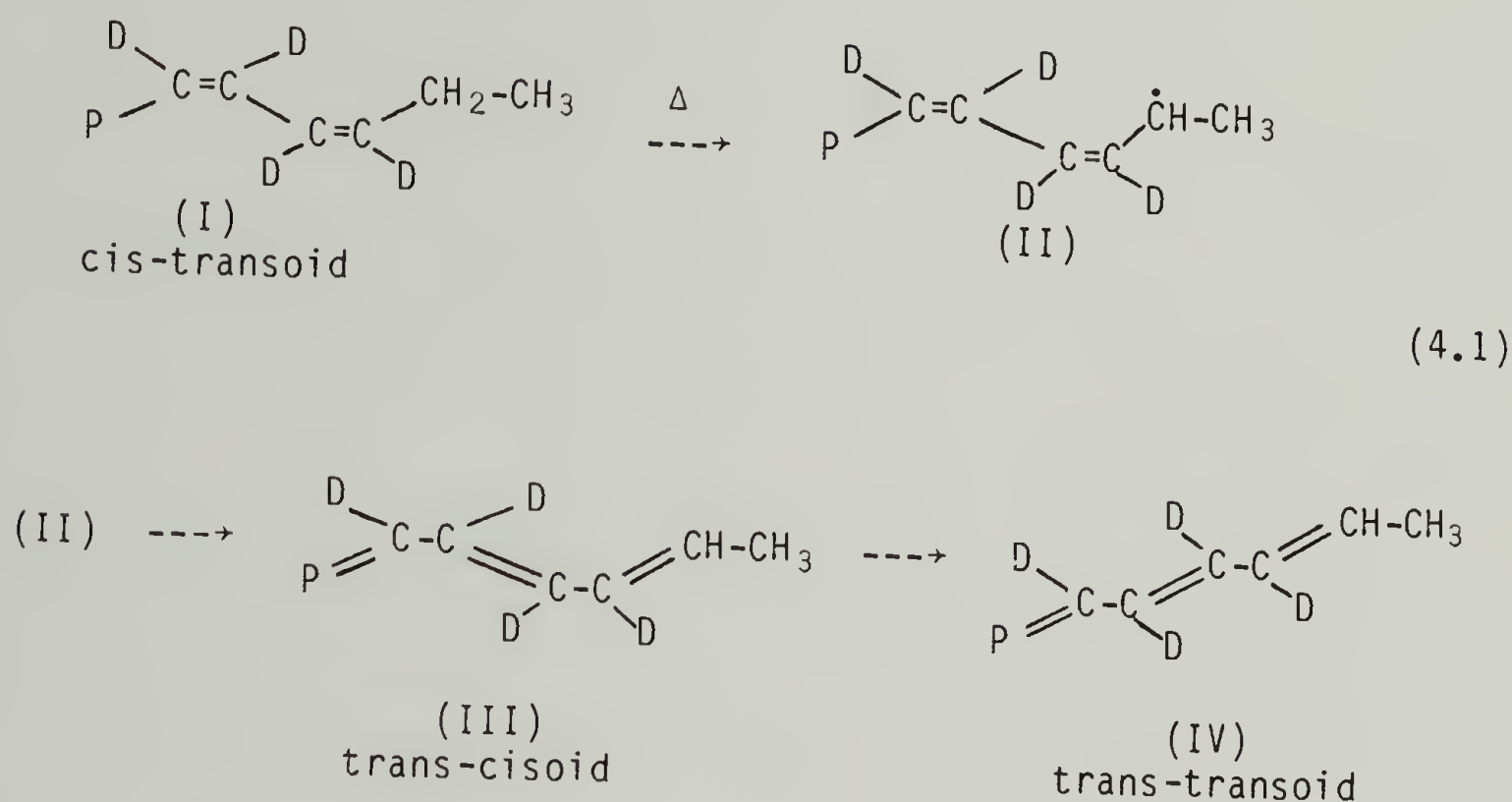


Figure 4.13 IR Spectra of (a) Pristine Cis-Rich and (b) Trans (423 K/30 min.) Low Molecular Weight Perdeuterated Polyacetylene.

appear below 2220 cm^{-1} in trans $[\text{CD}]_x$. The nature of the new vibration can be speculated to arise from the formation of P-CD=CH-CH_3 linkages as a consequence of allyl radical formations (II) during cis-trans isomerization (Eq. 4.1).



Rearrangement of (II) by electron migration to the trans-cisoid form (III) followed by facile bond rotation to (IV) is analogous to the mechanism of chemically induced isomerization proposed by Yamabe et al.⁹⁹ Normally $-\text{CH}_2=\text{CH}-$ stretching occurs at ca. 3020 cm^{-1} . Being adjacent to a deuterated carbon backbone though should result in a slight shift to lower wavenumbers. Only by polymerizing low molecular weight $[\text{CD}]_x$ and isomerizing has it been possible to observe this new sp^2 stretch.

Oxidized Polyacetylene

As mentioned earlier, cis- $[\text{CH}]_x$ may at times show a weak absorption

at ca. 1690 cm^{-1} which disappears upon isomerization, but with a concurrent appearance of a moderately intense peak at 1720 cm^{-1} . Figure 4.14(a) shows the spectra of pristine $[\text{CH}]_x$ along with a sample of polymer air oxidized (Fig. 4.14(b)) for 6 days at room temperature. Hydroxy stretching at 3500 cm^{-1} and carbonyl vibrations at 1670 cm^{-1} and 1720 cm^{-1} have developed. The 1670 cm^{-1} band may be easily assigned to either $\alpha, \alpha' - \beta, \beta'$ - unsaturated aldehydes or ketones which absorb from $1660\text{--}1680\text{ cm}^{-1}$ in model compounds. Carbonyl stretching at 1720 cm^{-1} may be attributed to either saturated aldehyde or ketonic groups.

I₂ Doped Spectra

At high levels of iodine doping, a featureless highly absorbing spectra from $200\text{--}4000\text{ cm}^{-1}$ results as a consequence of populating the midgap state. At somewhat lower levels of doping, i.e. $10^{-3.5} < Y(\text{I}_3)^- < 10^{-1.8}$, dopant induced vibrations at 950 cm^{-1} , and 1400 cm^{-1} were observed in agreement with earlier results.⁹⁰ The appearance of these bands and the onset of a featureless spectra occurred at approximately the same level of doping regardless of \overline{M}_n .

Discussion

Our results have clearly shown that using the standard Ziegler-Natta catalyst, fibrillar polyacetylene microstructures inevitably result. This is readily apparent if proper care is taken to remove catalytic artifacts. As reviewed within Chapter I, fibrillar

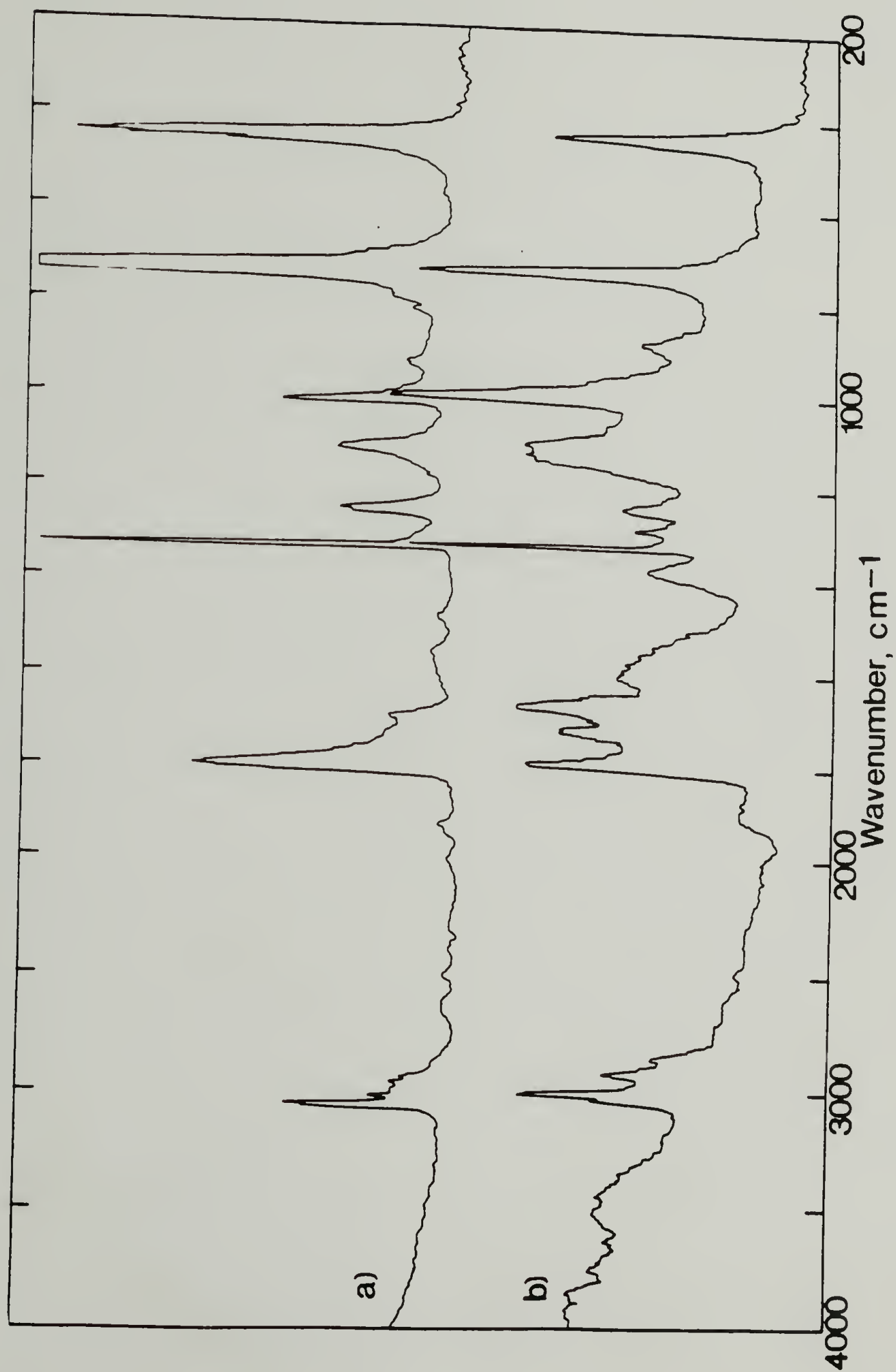


Figure 4.14 (a) Unoxidized; and (b) Air Oxidized $[\text{CH}]_x$.

microstructures in olefin polymerizations are not new. The invariance of the microstructure with varying polymerization condition which have no affect on the nature and composition of the active center is in accord with earlier works by Wunderlick³¹ and Georgiadis³³. In other words, the physical nature of the catalytic centers controls the physical structure of the polymer. By changing the catalyst composition, more or less active growth centers result, in addition to the physical nature of the sites. Even today, some investigators refer to the $\text{Ti}(\text{OBu})_4/4\text{AlEt}$ catalyst as homogeneous and others as colloidal. But most certainly, immediately after $t=0$, the system becomes heterogeneous and is controlled by heterogeneous polymerization kinetics. Fibrillar growth may then be considered as a series of polymer growth with simultaneous crystallization events, followed by adsorption onto the fibril surface either catalytically active or inactive components from solution.

In acetylene polymerization, the pseudo heterogeneous catalyst is both dispersed in the diluent and adsorbed on stirbar and glassware surfaces. The dispersed catalyst produces loose fibrils of polyacetylene. On the other hand, the polymer chains initiated by catalyst clusters adsorbed on surfaces spontaneously nucleate and crystallize to form microfibrils and further aggregate into ribbons when sheared. The rotation of the stirrer exerts a maximum velocity field on the nascent polyacetylene microfibrils growing from the stirbar tip. If the stress field experienced by the polymer is sufficient to maintain their orientation in the velocity field, the above described process of assembly

would occur. In the experiments reported, the minimum and maximum radial velocity of the stirbar ranges from 10^7 to 10^{10} Å·s⁻¹. This corresponds to a maximum shear rate of 10^2 s⁻¹ at the stirbar tips. The result of Mackley¹⁵⁹ indicates very large hydrodynamic velocity gradients along the side surface and tips of a prolate ellipsoid aligned in such a flow field. The dominant force for orientation is not the transverse velocity gradient but is rather the elongational velocity gradient which is about 10^6 s⁻¹ for a polyacetylene fibril of 20 nm diameter at a distance of 100 nm from the surface. This is of the same order as observed by Zwijnenburg and Pennings¹⁶⁰ for longitudinal crystallization of polyethylene in Poiseuille and Couette flow.

The degree of isomerization for various molecular weight polyacetylenes has offered supporting backup of our radiolabeling results. The interpretation of these results compels one to view the isomerization process as a multi-site initiating process, one of which may very well be the chain end. This would seem likely given the added free volume associated with polymer chain ends. The appearance of a new unsaturated CH stretch at 3000 cm^{-1} in $[\text{CD}]_x$ lends credence to this mechanism. Of great interest though are the results of limiting trans content in $[\text{CH}]_x$ of differing \overline{M}_n polyacetylenes. If for a given sample of $[\text{CH}]_x$ one assumes a given number of initial bond rotations to take place, then for a polymer of low molecular weight, fewer initiating sites per chain could be envisioned. Consequently, fewer residual cis-defects result.

The results from the 1010 cm^{-1} peak shape analysis at first appears to contradict radiolabeling results. One may first expect shorter conjugation lengths in low \overline{M}_n polymer. Yet the opposite seems to be true. Presumably this is due to fewer residual cis linkages in low molecular weight polymer. Resonance Raman spectroscopy studies would therefore be needed to resolve this point.

CHAPTER V

ELECTRON PARAMAGNETIC RESONANCE

In this chapter, the results of studies which investigate the nature of unpaired neutral solitons, \dot{S} , in polyacetylene are presented. Aspects under consideration include: the creation of solitons upon isomerization, their concentrations and dynamics in undoped and doped polymer, and the eventual demise of these spins at high levels of doping. Spin susceptibilities for both undoped and doped polymers are also included.

Undoped Cis-Rich Polyacetylene

Quantitative EPR

Cis-[CH]_x when handled at room temperature exhibits a weak, broad EPR signal as seen in Fig. 5.1. Often times, the signal may be so weak that catalytic debris with $g < 2.0$ become visible. Over the \bar{M}_n range prepared, no strong trend in room temperature spin concentrations were observed. Table 5.1 lists some of those results. Similar values were also obtained for 500 \bar{M}_n cis-rich [CD]_x. Inverse spin concentrations and $\log [\dot{S}]$ of 15,500 CH/spin and -4.19 respectively were determined.

Saturation and Relaxation Times

Room temperature amplitude saturation plots of two cis-LMnP's are shown in Fig. 5.2. Curve (a) is for polymer made as a film and (b) prepared as a finely divided powder. Cis-[CH]_x shows signs of partial

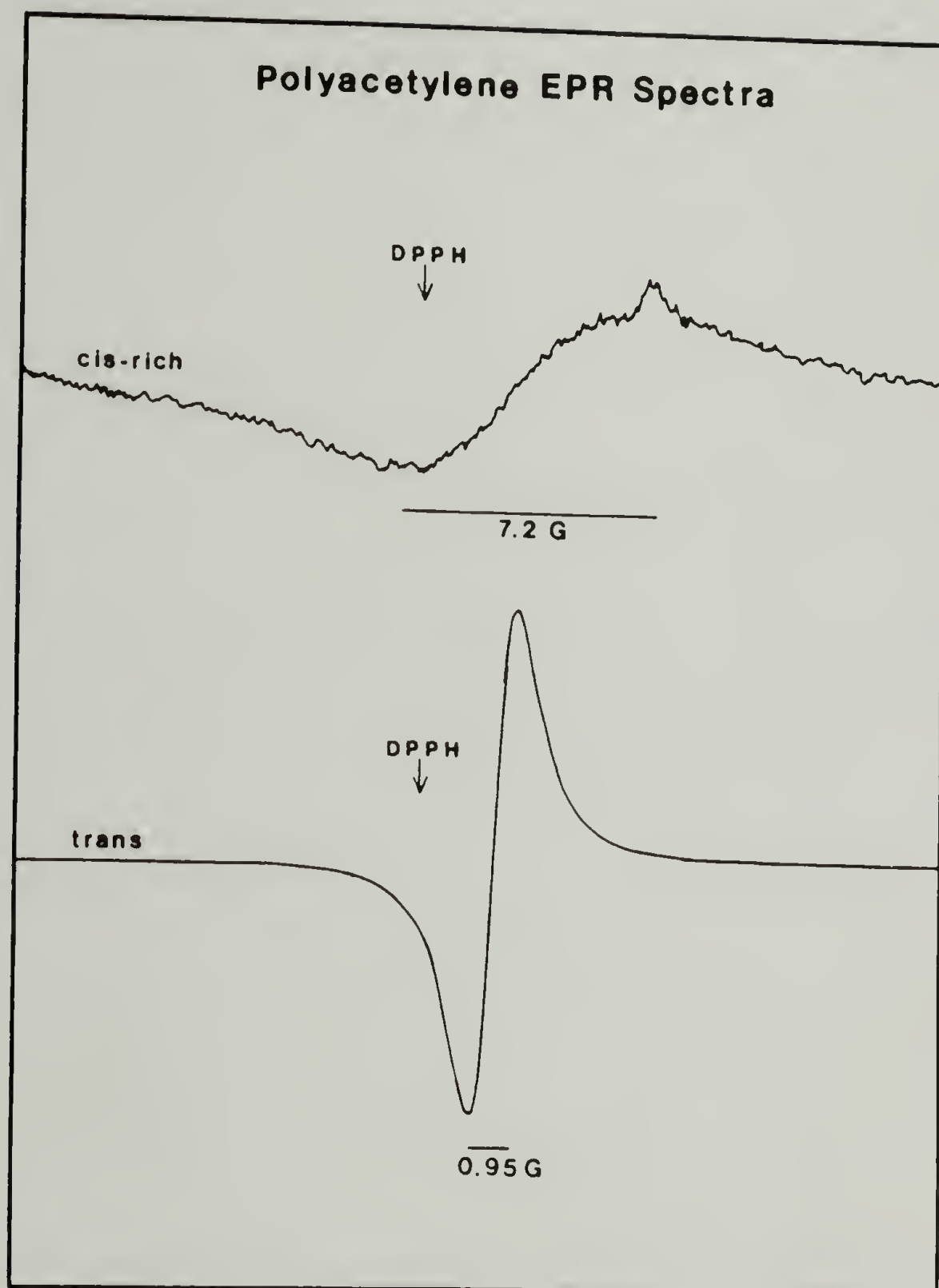


Figure 5.1 Characteristic EPR Spectrum of Cis-Rich and Thermally Isomerized Trans Polyacetylene.

Table 5.1
Cis-[CH]_x EPR Spin Concentrations.

Reference	\bar{M}_n	CH/Spin	$\log[\dot{S}]$
MS482-101a	400	11,300	-4.05
"	"	11,400	-4.06
MS583-91	500	76,000	-4.88
MS684-33	500	22,100	-4.34
"	"	12,600	-4.10
"	"	16,400	-4.21
JW ^b	10,500	25,000-50,000	-4.41 to -4.7
HMnP-V	25,000	75,300	-4.88

a Powder morphology. All others were thin films.

b Taken from Reference #110.

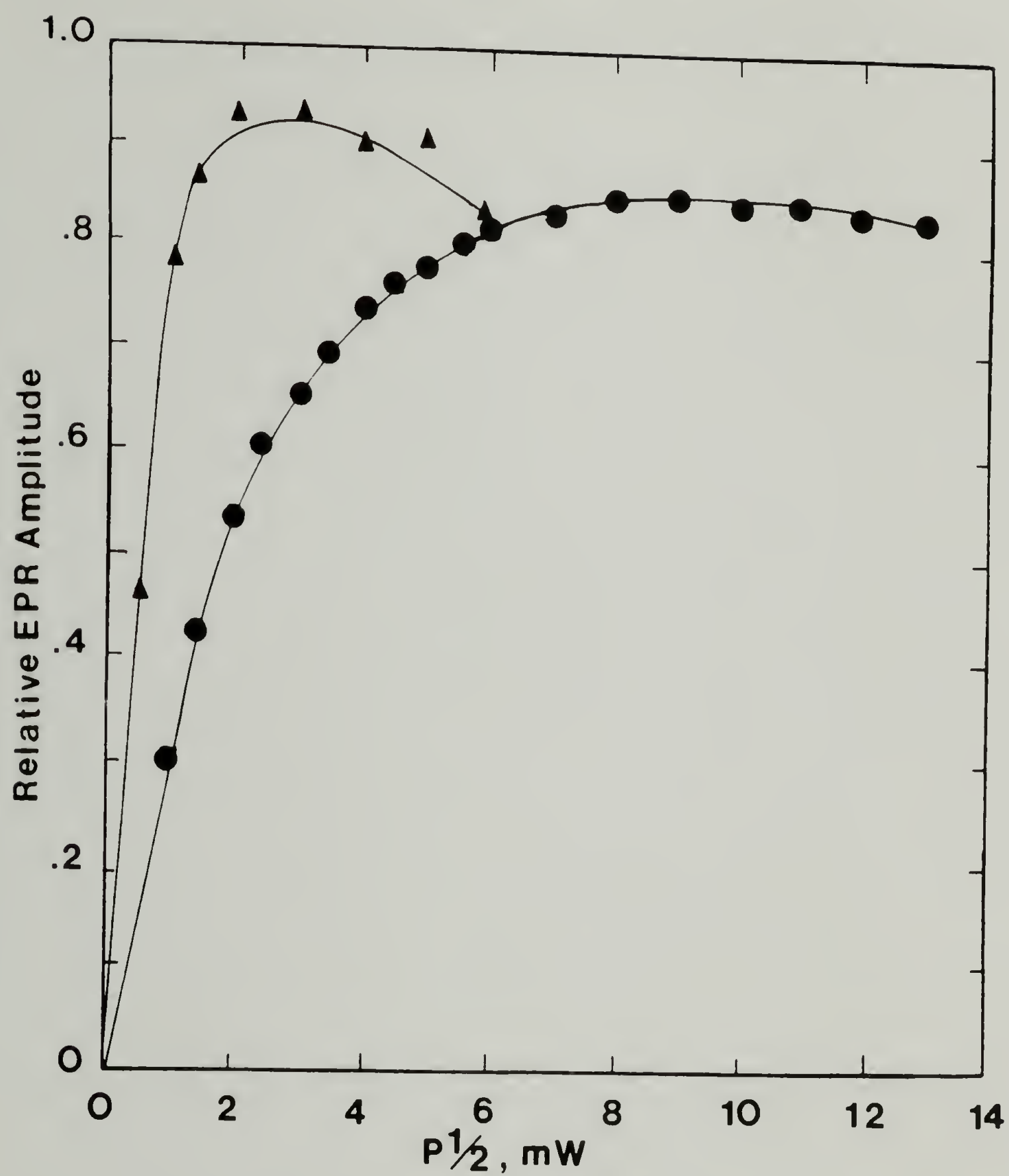


Figure 5.2 Cis-[CH]_x Signal Amplitude Saturation Plots for (▲) LMnP Film(MS684-33); and (●) LMnP Powder(MS482-101).

inhomogeneous broadening. Increases in linewidth above saturation were small, broadening by no more than 14% from 0-169 mW. ΔH_{pp}° for (a) and (b) are 5.5 G and 7.2 G respectively. Spin-lattice, T_1 , and spin-spin, T_2 , relaxation times are 180 μ sec and 12 nsec respectively for the film (a) and 18 μ sec and 9 nsec respectively for the powder (b). Earlier, Warakowski et al.¹¹⁰ reported for a number of cis 10,500 \overline{M}_n films $T_1 = 53 \pm 7$ μ sec and $T_2 = 11 \pm 1$ nsec. No signal was observed for 25,000 and 870,000 \overline{M}_n polymer. Therefore, T_1 is very sensitive to preparation and handling whereas T_2 is relatively insensitive. Relaxation mechanisms involving catalyst residues trapped within the fibrils, etc. may be responsible for the large variability in T_1 .

Cis-Trans Isomerization

Relative Spin Intensities

The evolution of neutral spins over isomerization time was measured for both 500 \overline{M}_n and 870,000 \overline{M}_n $[\text{CH}]_x$. Approximating the resonance absorption as a Lorentzian curve, signal intensities and peak-to-peak linewidths were used to calculate the relative EPR amplitude, A_0 . Figure 5.3 shows the evolution of EPR amplitude verses isomerization time for the 500 \overline{M}_n $[\text{CH}]_x$ at 383, 423, and 453 K. These results are somewhat different than those of Chien, et al.⁹⁷ for standard $[\text{CH}]_x$ films in that much shorter times were needed in their work to reach a constant EPR signal amplitude. It is uncertain whether the variation in linewidths were used in calculating the signal intensity as in the present case. The evolution of spins was reported by Chien⁹⁷ to also follow first order kinetics. Figure 5.4 shows first

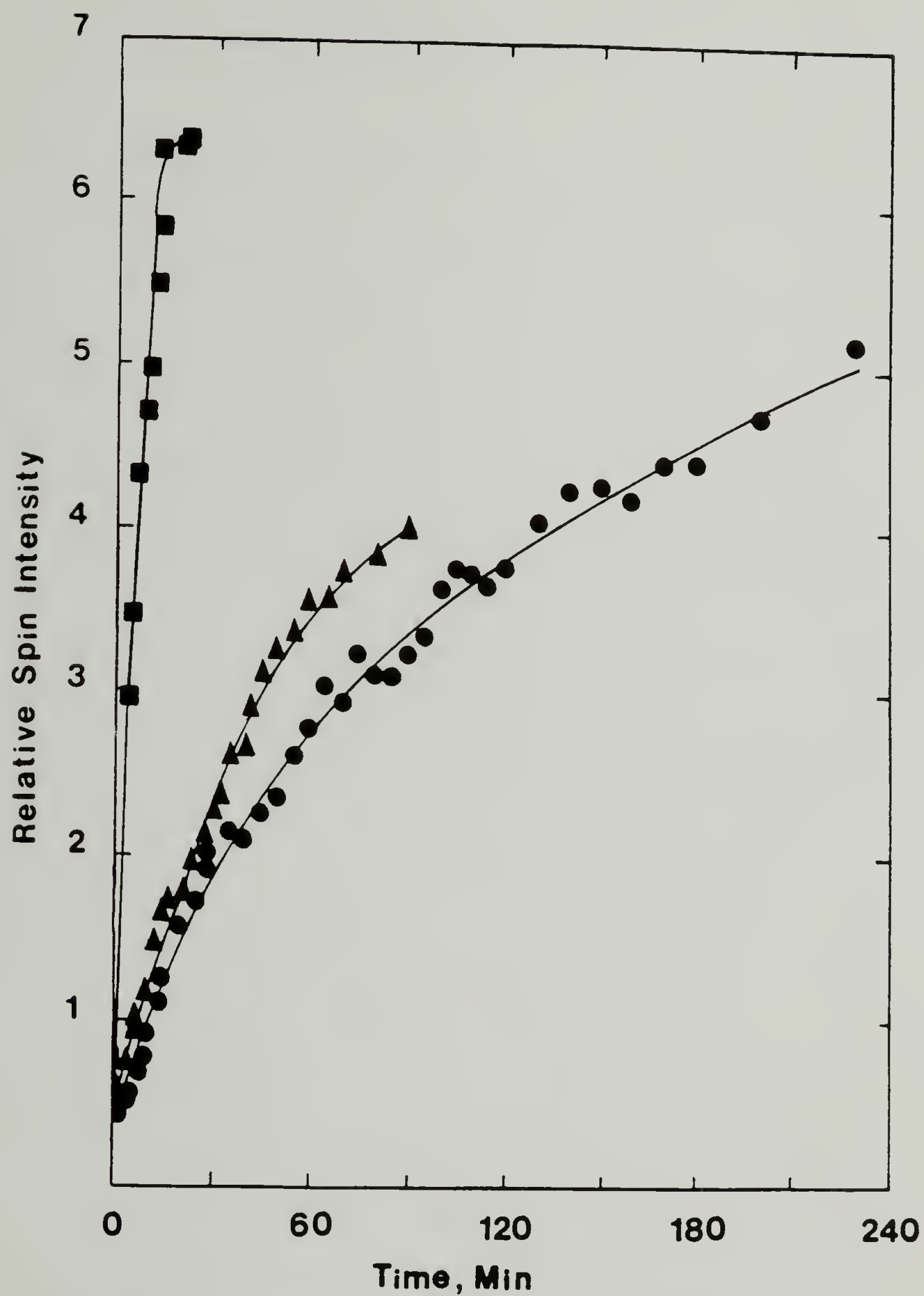


Figure 5.3 Increase in Spin Concentration $[\dot{S}]$, with Isomerization Time for 500 Mn $[\text{CH}]_x$ at (●) 383 K; (▲) 423 K; and (■) 453 K.

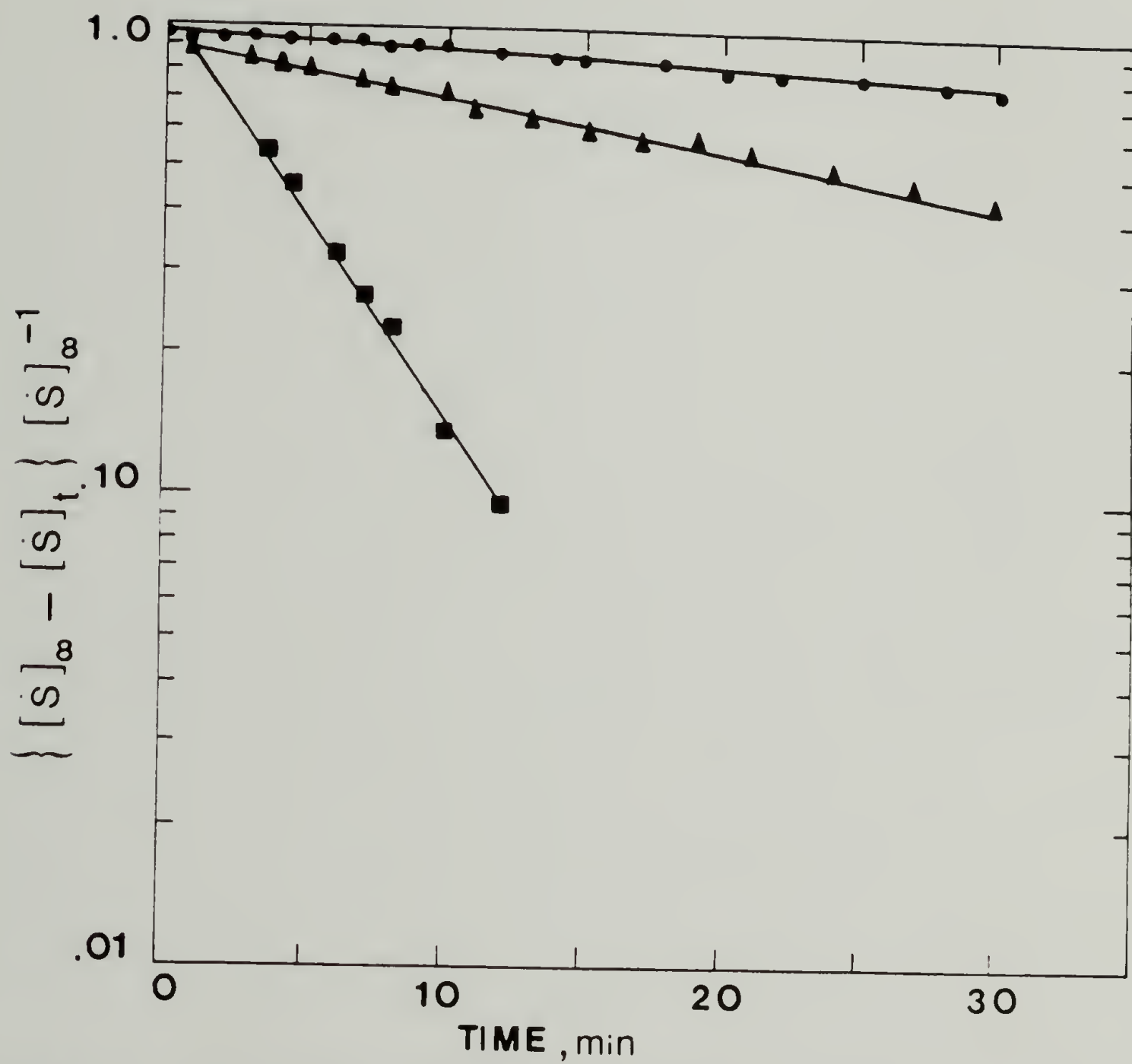


Figure 5.4 First-Order Kinetics Plot for the Formation of Unpaired Spins in 500 $\bar{\text{Mn}} [\text{CH}]_x$ at (●) 383 K; (▲) 423 K; and (■) 453 K.

order kinetics for the creation of neutral defects in 500 \overline{M}_n polymer too. Rate constants of $1.4 \times 10^{-4} \text{ sec}^{-1}$, $4.1 \times 10^{-4} \text{ sec}^{-1}$, and $4.9 \times 10^{-3} \text{ sec}^{-1}$ at 383K, 423K, and 453K respectively were found. An approximate activation energy of $\sim 17 \text{ Kcal} \cdot \text{mol}^{-1}$ is significantly higher than their estimated value of $\sim 10 \text{ Kcal} \cdot \text{mol}^{-1}$ for standard films. It is important to note that Fig. 5.4 gives a linear fit over the first 30 minutes of isomerization. At longer times, kinetically slower rates are observed. This is in agreement with the IR results of Shirakawa⁴¹ which showed an ever increasing E_A with increasing trans content. An activation energy reported by Shirakawa⁴¹ for isomerization from IR ($\sim 18 \text{ Kcal} \cdot \text{mol}^{-1}$) compares well with the presently reported $17 \text{ Kcal} \cdot \text{mol}^{-1}$. It should be remembered though that the creation of neutral defects is necessary to initiate isomerization, but not directly associated with all the processes involving structural rearrangement.

Peak-to-Peak Linewidths

When cis- $[\text{CH}]_x$ is heated, the EPR linewidth, decreases. Therefore, unpaired spins in cis and trans polymers have different linewidths. Weinberger et al.¹¹⁷ has studied this in detail and found ΔH_{pp} decreases rapidly with increasing temperature for trans- $[\text{CH}]_x$. This indicates motional narrowing mechanisms and suggests that solitons in trans- $[\text{CH}]_x$ to be mobile. Cis $[\text{CH}]_x$ linewidths are reported not to show this temperature dependency. Therefore, the evolution of the elevated temperature EPR linewidths should give an insight into the delocalization of the soliton during isomerization. Figure 5.5 shows

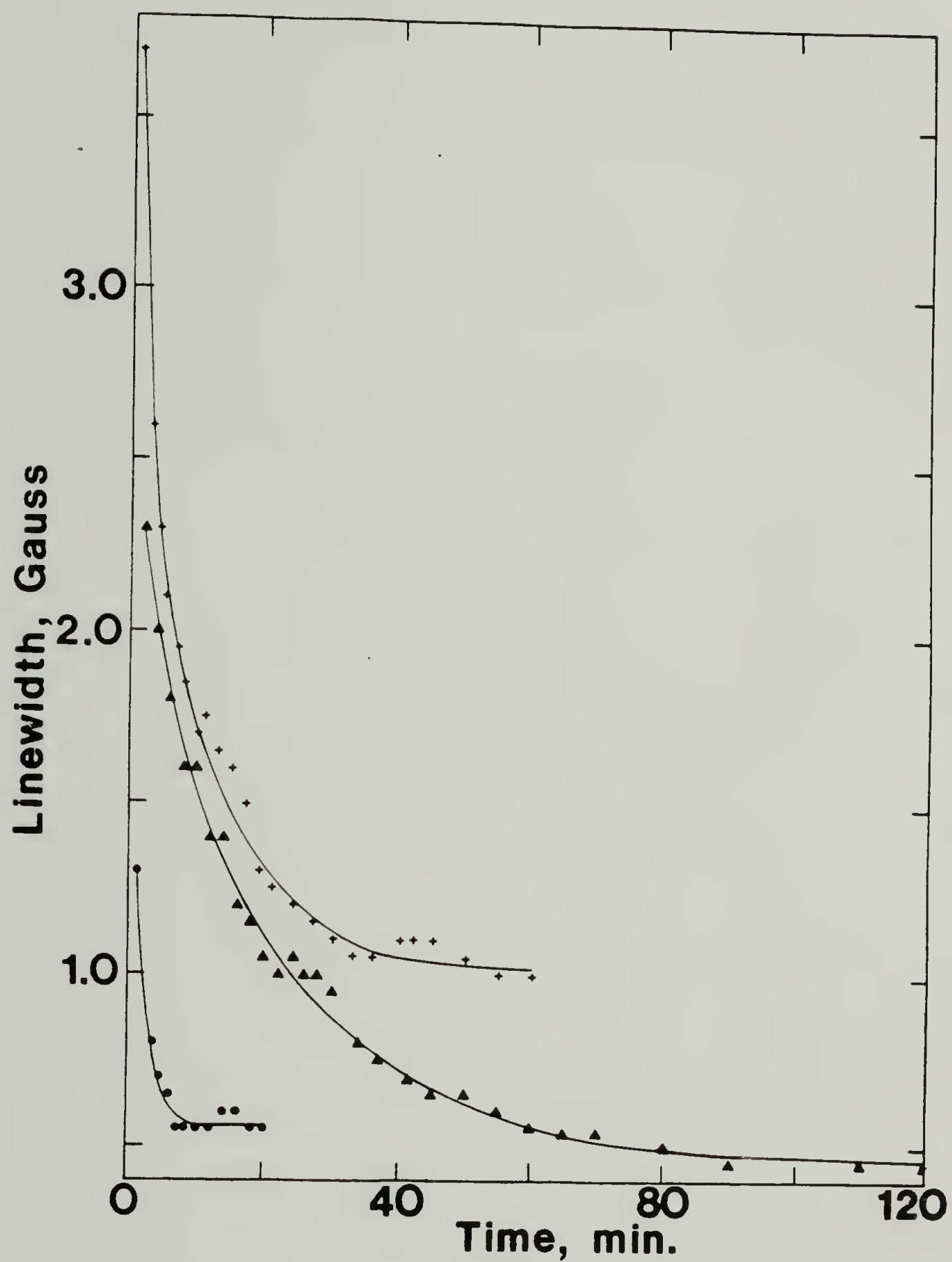


Figure 5.5 Variation of EPR Linewidth with Isomerization Time for (●) 500 \bar{M}_n / 453 K; (+) 500 \bar{M}_n / 423 K; and (▲) 870000 \bar{M}_n / 423 K.

results for 500 and 870,000 \overline{M}_n $[\text{CH}]_x$. Two important points need to be made. First, structural annealing seems to reach completion over shorter times using LMnP. Broader linewidths after isomerization for low \overline{M}_n polymer is consistent with larger T_1 values observed in the cis polymers. As expected, increasing temperature accelerates cis-trans isomerization

Undoped Trans Polyacetylene

Effect of HCl/CH₃OH Washing

It was shown in Chapter IV that washing with 10% HCl/CH₃OH removed ca. $10\times$ more organo-aluminum and titanium compounds as evidenced by elemental analysis. Cleaner morphologies were also observed. To see if such treatment, which has been claimed to slightly dope $[\text{CH}]_x$, has any ramifications on the EPR spectra, a sample of 10,500 \overline{M}_n film was isomerized and examined. Later it was soaked in deoxygenated 10% HCl/CH₃OH followed by a second EPR examination. Both samples homogeneously broadened with the signal amplitude maximizing at 16 mW in both cases. EPR linewidth broadened slightly from 0.8 to 1.0 G with treatment. T_1 and T_2 changed from 11 μsec and 77 nsec respectively before washing to 14 μsec and 66 nsec respectively after washing: all well within the range reported by Warakomski¹¹⁰ for various preparations.

Quantitative EPR

An important feature of the soliton picture is the supposedly unperturbed, highly anisotropic diffusion of spins up and down the polyene chain. Reports from various laboratories generally cite ca.

2000-3000 CH units per spin or a log spin concentration, $\log [\dot{S}]$, of -3.3 to -3.5. Based on an \bar{M}_n of 10,500 for standard film,¹⁴⁷ this averages out to ca. 0.5 spins per chain. Intuitively, this seems reasonable since on the average any one chain may have initially contained either an even or odd number of solitons. A test of these predictions is to then determine the relationship between $[\dot{S}]$ and \bar{M}_n . Table 5.2 contains the spin concentrations for trans $[\text{CH}]_x$ of various \bar{M}_n 's. No discernable variation in spin concentration was observed over an \bar{M}_n range of three orders of magnitude. This strongly implies that spin mobility, while being highly diffusive along the chain, is also three dimensional; with the transverse diffusion rates limiting the overall spin population. Even though spin diffusion anisotropies of 10^3 - 10^4 have been recorded,¹¹⁹⁻¹²⁰ as with any other macroscopic static measurement, the observed property is limited by the slowest process involved. Kivelson's theory for conduction in undoped and lightly doped $[\text{CH}]_x$ in fact even predicts a finite hopping frequency dependent on the phonon-soliton coupling and the density of impurity states. Therefore, at 2000-3000 CH units per soliton, the effective soliton domain within which soliton-antisoliton annihilation would take place is ca. $(4.3-6.5) \times 10^4 \text{ \AA}^3$, assuming a polymer density of 1. The average distance separating neutral solitons then computes to be 40-50 \AA if a spherical domain is assumed. Results from 453 K/15 min isomerized ca. 500 \bar{M}_n $[\text{CD}]_x$ also fit this model. Inverse spin concentrations from three separate isomerizations gave 1700, 1800, and 2600 CH/spin.

Gibson and co-workers¹⁰² have proposed the below relationship bet-

Table 5.2
Trans-[CH]_x EPR Spin Concentrations.

\bar{M}_n	Isomerization Conditions	CH/Spin	log [\dot{S}]
400 ^a	453 K/20 min	1600	-3.21
"	"	1700	-3.23
500	383 K/26.7 hr	2500	-3.39
"	423 K/90 min	3000	-3.48
"	453 K/12 min	2000	-3.31
"	453 K/20 min	3000	-3.48
"	483 K/5 min	2100	-3.32
5300	453 K/15 min	2900	-3.46
"	"	3100	-3.49
6200	453 K/15 min	2300	-3.36
10,500	383 K/24 hr	1800	-3.26
"	418 K/4 hr	2100	-3.32
"	441 K/2 hr	1800	-3.26
"	468 K/90 min	1600	-3.21
"	517 K/30 min	1300	-3.11
25,000	453 K/40 min	2000	-3.30
210,000	453 K/20 min	2100	-3.32
"	"	2000	-3.30
870,000	423 K/90 min	2700	-3.43
"	423 K/200 min	1900	-3.28

^a Powder sample; all others as thin films.

ween remnant cis linkages, N_c , and the number of neutral solitons created, N_s :

$$N_s = 2N_c \exp(-\delta/k_B T_a) \quad (5.1)$$

where T_a is the highest annealing temperature. The results presented in Table 5.2 and in Chapter IV do not support this picture. As was noted previously, higher ultimate trans content can be obtained in low \bar{M}_n polymer than in high \bar{M}_n polymer. Higher annealing temperatures result in higher trans contents too. The results for both 500 \bar{M}_n and 10,500 \bar{M}_n polymer suggest that $[\dot{S}]$ is independent of annealing temperature and M_n ; and consequently residual cis content.

Saturation and Relaxation Times

For the samples reported in Table 5.2, T_1 and T_2 measurements were made at room temperature. Table 5.3 lists the saturation powers, linewidths, and calculated relaxation times for polyacetylenes from 500 \bar{M}_n to 870,000 \bar{M}_n . Figures 5.6 and 5.7 plot a few representative saturation curves for these polymers. It can be seen from Fig. 5.6 that all samples homogeneously broaden with the exception of the low \bar{M}_n powder. This still exhibits remnants of the inhomogeneous broadening characteristic of cis polymer. Fig. 5.7 also shows that this sample exhibits a broad, 2.7 G, linewidth. No IR was done on this sample so residual cis content was not determined.

Saturation characteristics of low \bar{M}_n perdeuterated polyacetylene (Table 5.3) showed the characteristic linewidths narrowing due to par-

Table 5.3
Trans-[CH]_x EPR Relaxation Times.

\bar{M}_n	Isomerization Conditions	$\Delta H_{pp}, G$	P_{sat}, mW	$T_1 \times 10^6, sec$	$T_2 \times 10^9, sec$
400a*	453 K/20 min	2.75	72	8	24
		"	64	9	"
500	373 K/26.7 hr	1.5	3.0	100	44
"	423 K/90 min	2.4	12.0	40	27
"	453 K/15 min	1.2	4.0	60	55
*"	453 K/20 min	1.1	4.0	55	60
"	483 K/5 min	0.95	3.0	64	69
500 $\bar{M}_n[CD]_x$	453 K/15 min	0.5	7.0	39	130
5300	453 K/15 min	0.90	-	-	-
6200	453 K/15 min	0.6	-	-	-
10,500 ^b	383 K/24 hr	1.8	12.0	30	36
"	418 K/4 hr	0.95	6.8	28	69
"	441 K/2 hr	0.83	7.0	24	79
" *	468 K/90 min	0.80	6.0	27	82
"	417 K/30 min	1.0	7.0	29	66
25,000	453 K/40 min	0.6	4.0	30	110
210,000*	453 K/20 min	0.6	12	10	110
870,000	423 K/90 min	0.8	9.0	18	80
" *	423 K/200 min	0.7	7.0	20	94

a Powder sample; all others as thin films.

b Warakomski¹¹⁰ reports for standard films: $T_1 = (2.7 \pm 1.7) \times 10^{-5}$ sec and $T_2 = (7.8 \pm 1.0) \times 10^{-8}$ sec.

* Data plotted in Figs. 5.5 and 5.6.

Figure 5.6 EPR Signal Amplitude Saturation Curves of Trans-[CH]_x at 298 K for (●) 400 Mn Powder, (+) 500 Mn Film, (■) 10,500 Mn, (▲) 210,000 Mn, and (○) 870,000 Mn.

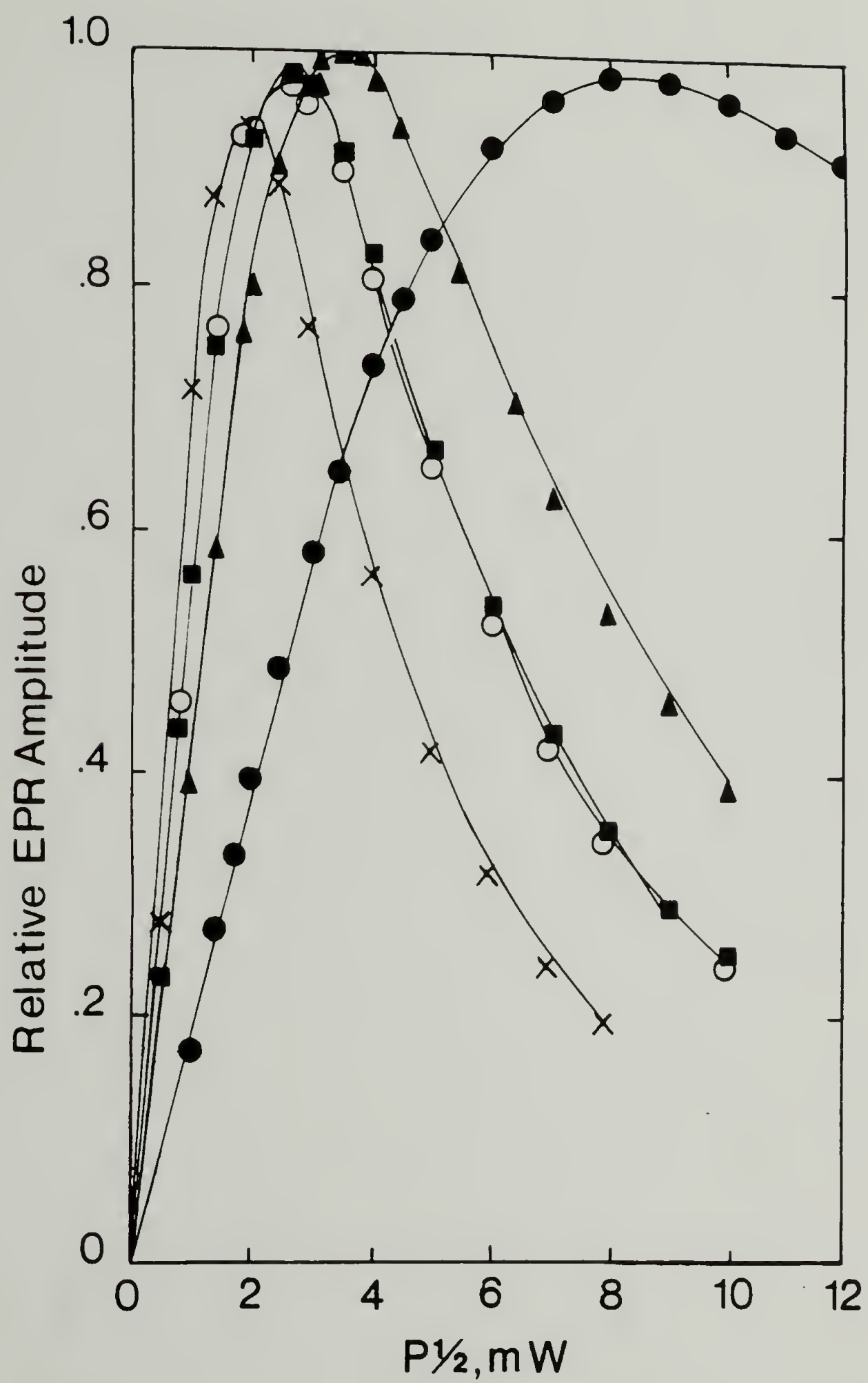
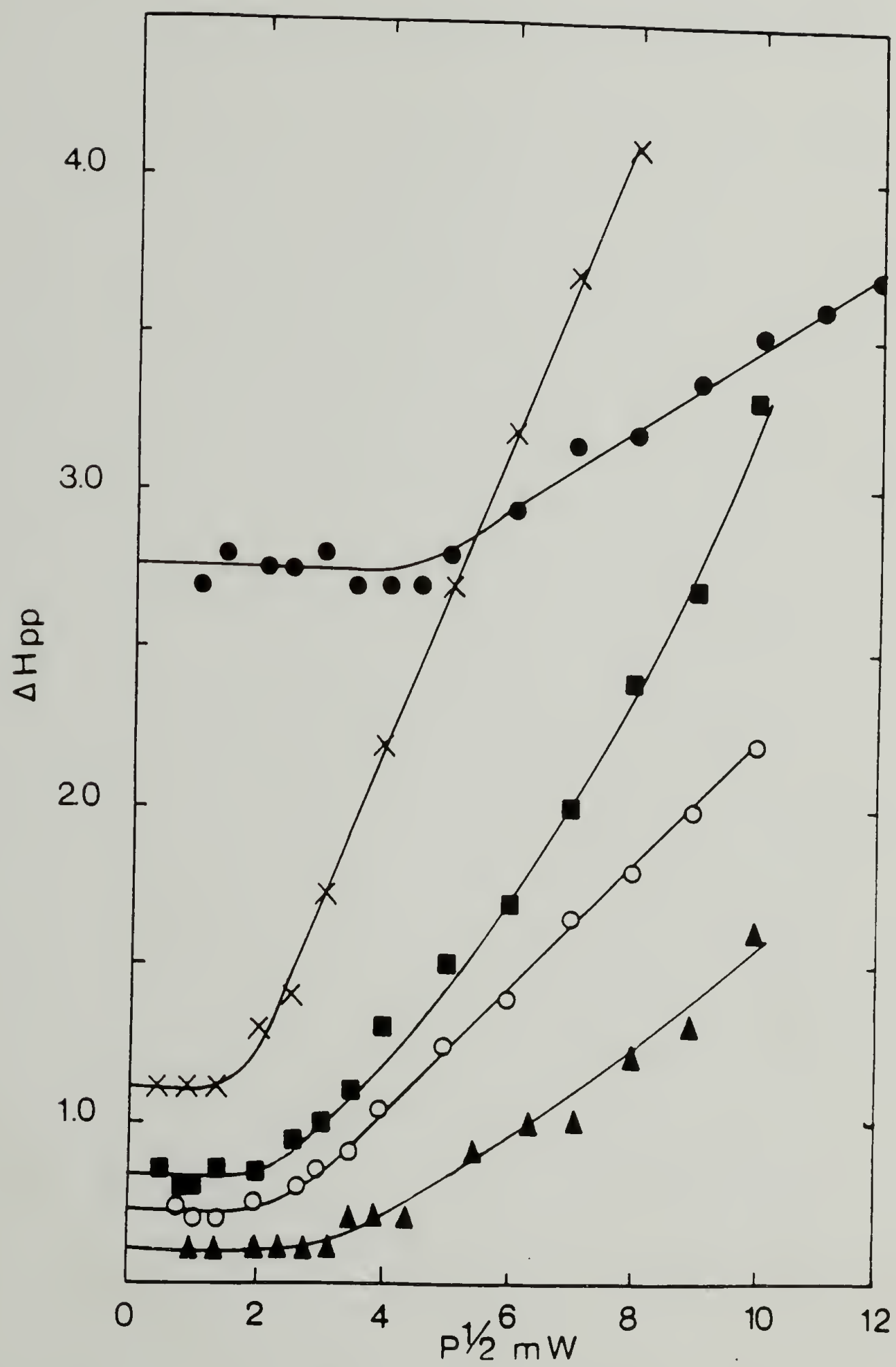


Figure 5.7 Variation of EPR Linewidth of Trans-[CH]_x at 298 K for
(●) 400 Mn Powder, (+) 500 Mn Film, (■) 10,500 Mn,
(▲) 210,000 Mn, and (○) 870,000 Mn.



tially unresolved hyperfine interactions.¹⁶¹ Slightly greater saturation powers were also found.

As seen in Fig. 5.7 and Table 5.3, consistently broader linewidths were observed in low \overline{M}_n samples. Neutral solitons in low molecular weight samples are slightly more pinned than in polymers of higher \overline{M}_n .¹¹⁷ This pinning or motional broadening could be attributed to either efficient spin-orbit coupling with impurities, i.e. residual catalyst debris or soliton diffusion limitations due to shorter chain lengths. The former does not seem to be likely for two reasons. First, in Chapter IV, it was shown that for acid washed samples, virtually no difference in remaining Ti or Al existed for all samples prepared. This is rather surprising especially since to prepare LMnP, $[\text{Ti}]_0$ of 740 mM was used as compared to 1 mM $[\text{Ti}]_0$ for HMnP. Also, Warakomski¹¹⁸ showed that T_1 is very sensitive to impurity levels as evidenced by a steady drop in T_1 during low level $^{125}\text{I}_2$ doping. In the present example, LMnP's even show a longer T_1 than for standard prepared films. These points compel one to accept that chain ends are responsible for the EPR line broadening observed.

In conclusion, it has been shown that for low molecular weight polymers, with an average 35-40 CH units per chain, the affects of chain ends as soliton barriers can be observed. Presumably at \overline{M}_n 's between 500 and 10,500, these end group affects vanish. Equally as interesting it has been shown that spin concentrations appear to be universally 1 per 2000-3000 carbon units.

I₂ Doped Cis-Low Molecular Weight Polyacetylene

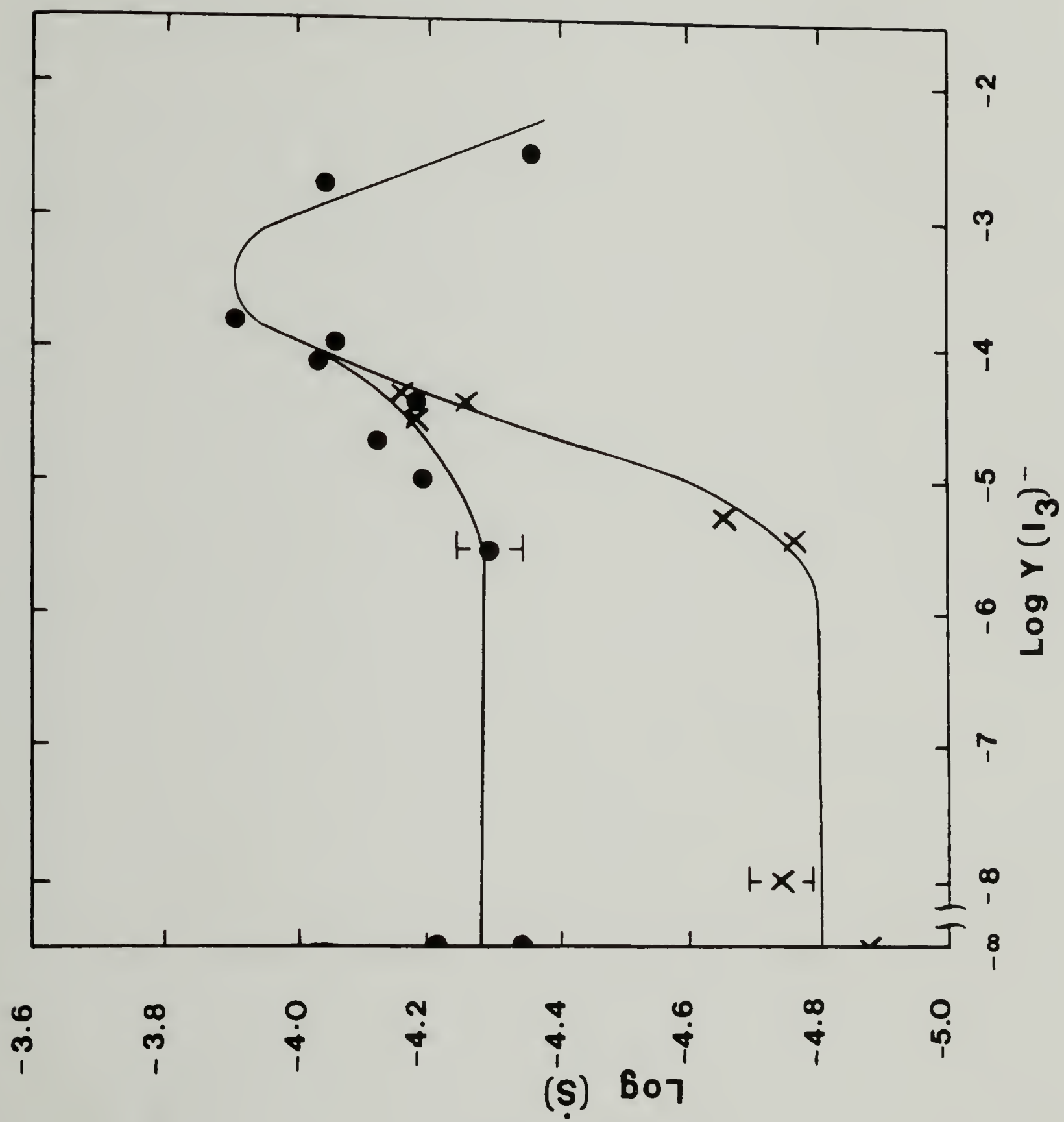
Quantitative EPR

Iodine doped cis-polyacetylene has an EPR spin concentration ca. 8-10 fold lower than trans-polyacetylene. Actual spin concentrations vary from preparation to preparation and are extremely sensitive to handling techniques. Because of this sensitivity to thermal history, controlled handling of samples is critical. Consequently, for these experiments involving ¹²⁵I₂ doping of cis LMnP, only two polymer preparations were used for generating data.

The method of slow doping outlined in Chapter II was used along with the apparatus shown in Fig. 2.8. Figure 5.8 shows the variation in \dot{S} over the dopant range for two separate samples. In both samples, at $Y(I_3)^-$ of $10^{-4.5}$ to 10^{-5} an increase in spin concentration occurs and is maximized at ca. $10^{-3.5}$ after which a drop in spin concentration is seen. Even at maximum doping, a weak yet discernable EPR signal was present, though samples of cis-LMnP could only be doped to ca. 0.3 mole % $(I_3)^-$. This compares to ca. 5.0 mole % $(I_3)^-$ as reported by Warakomski¹¹⁰ for 10,500 \bar{M}_n polymer.

It is interesting to note that the onset of increased spin concentration occurs at dopant levels which approximate the intrinsic neutral soliton concentration in the undoped polymer. These results are taken to support polaron doping in cis-[CH]_x,¹²⁴ as shown in Fig. 5.9. Su, Schrieffer, and Heeger¹¹⁴ have calculated the energy to create a soliton excitation in trans polyacetylene to be lowest, 0.45 eV, for $l=7$ (i.e., 15 atomic units). The presence of the soliton

Figure 5.8 Variation of Neutral Soliton Concentration in Cis 500 Mn $[\text{CH}]_x$ with $(\text{I}_3)^-$ Doping for (●) MS684-33 and (+) MS583-91 Polymers.



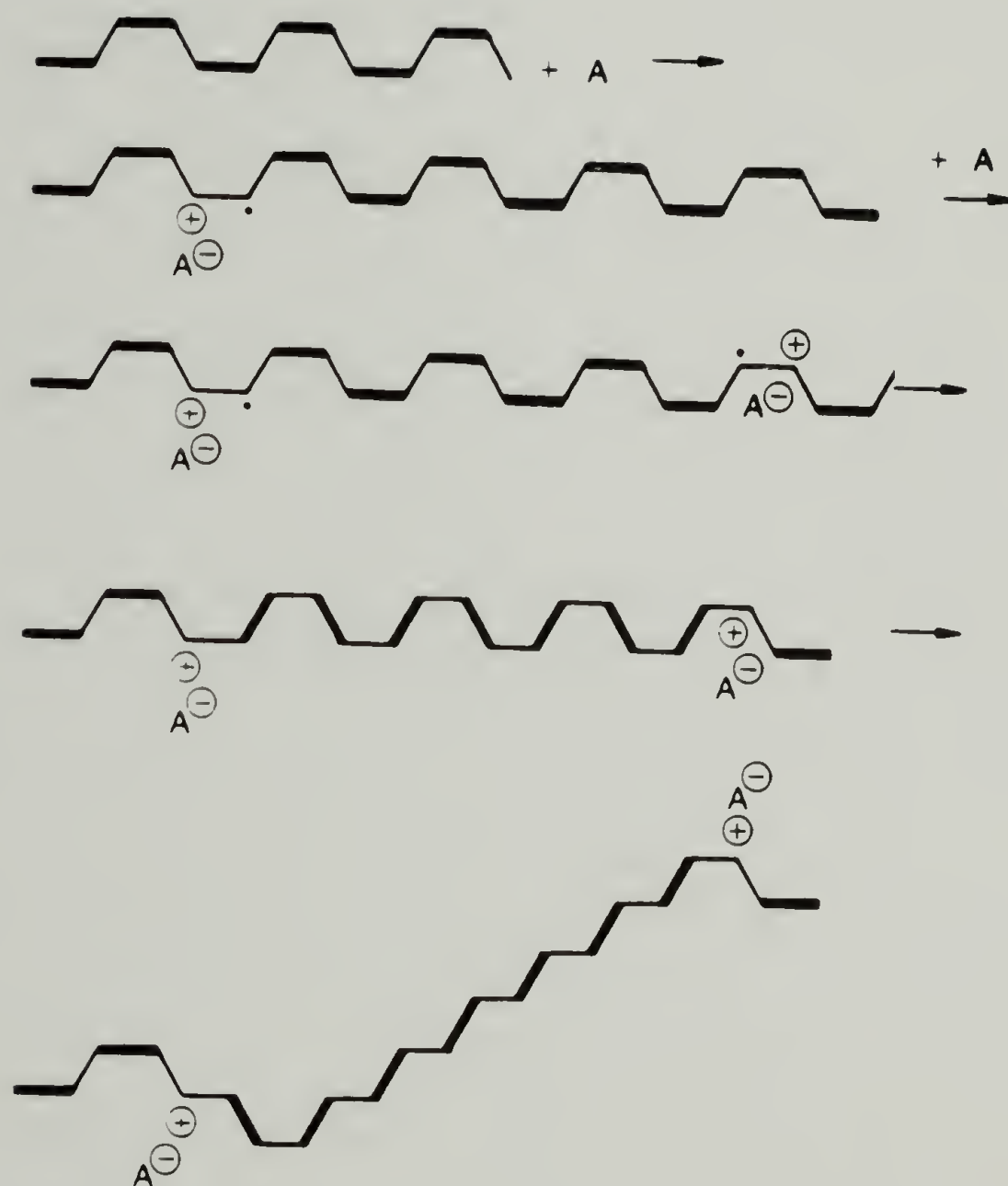


Figure 5.9 Polaron Doping in Cis-[CH]_x and Subsequent Cis-Trans Isomerization.

introduces a localized electronic state at the midgap, 0.7 eV above the valence band edge. The energy to create a positive isolated soliton defect is 0.25 eV smaller than the 0.7 eV energy required for a vertical ionization process. The energy to create the soliton does not depend on whether the soliton is neutral, negatively charged, or positively charged. Bredas on the other hand has calculated that the energy required for the formation of two defects, one charged and the other uncharged, in trans polyacetylene is smallest, 0.65 eV, when the two defects are in close proximity. The energy of these defects or polaron is minimized when the lattice distortion is distributed over 15 atomic units. With respect to the vertical ionization process, the polaron binding energy is 0.05 eV. The presence of a polaron introduces two defect levels in the gap, symmetrically placed 0.4 eV above and below the Fermi level rather than both at the Fermi level as for noninteracting defects.¹²⁵ Therefore at low levels of doping, polaron formation is expected in trans-polyacetylene. A similar argument may be used for cis-[CH]_x also.

At moderate levels of doping, the energy barrier preventing recombination, $E \sim [2 \times (0.65 \text{ eV})] - [2 \times (0.45 \text{ eV})] = 0.4 \text{ eV}$, is steadfastly reduced. At some point, chemically induced cis-trans isomerization follows, with a corresponding reduction in EPR spin concentration.

Saturation and Relaxation Times

EPR saturation curves were also generated from ¹²⁵I₂ doped cis-LMnP. Figures 5.10 and 5.11 show the evolution of spectral linewidth and saturation power over the entire dopant range. Doping of

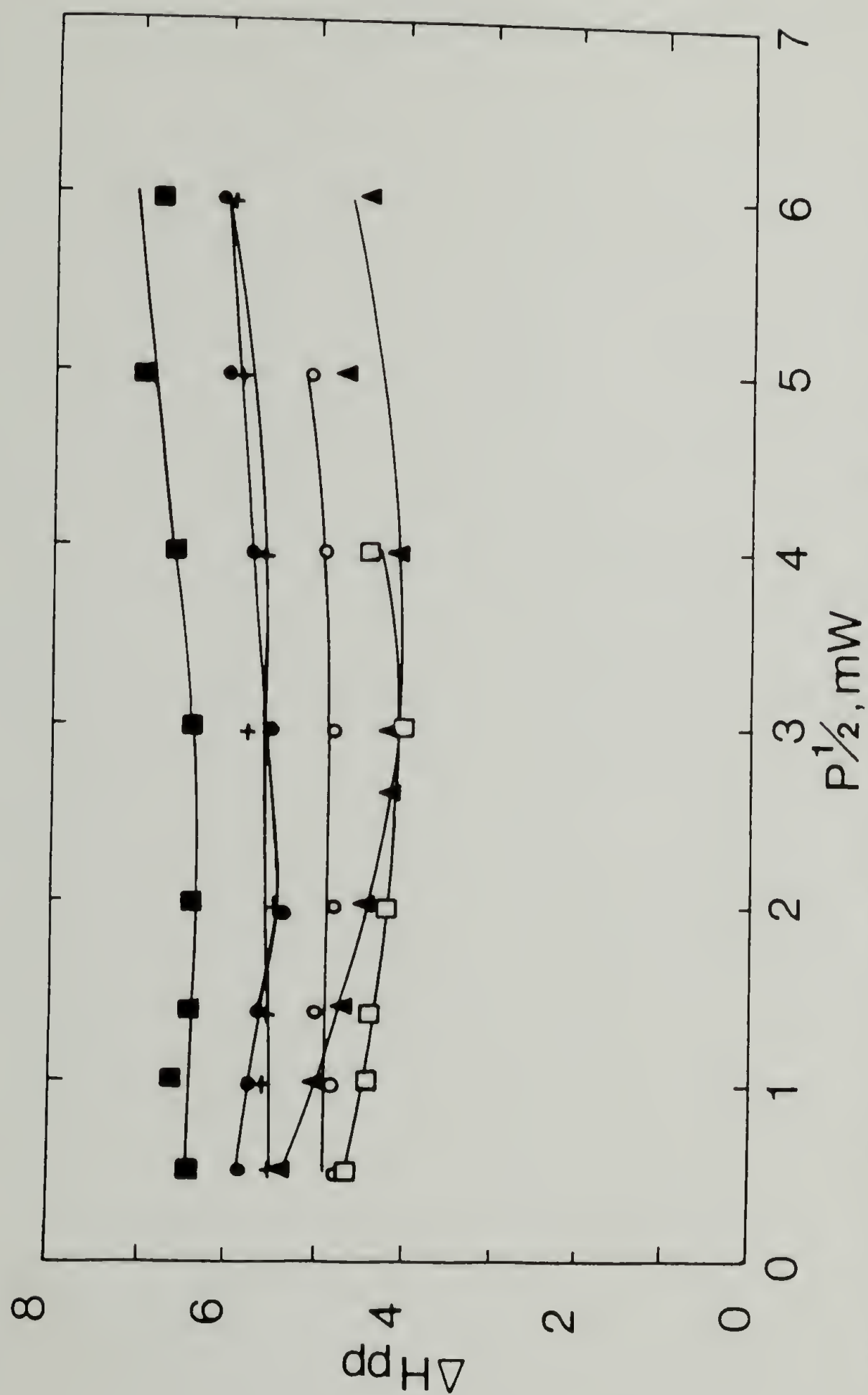
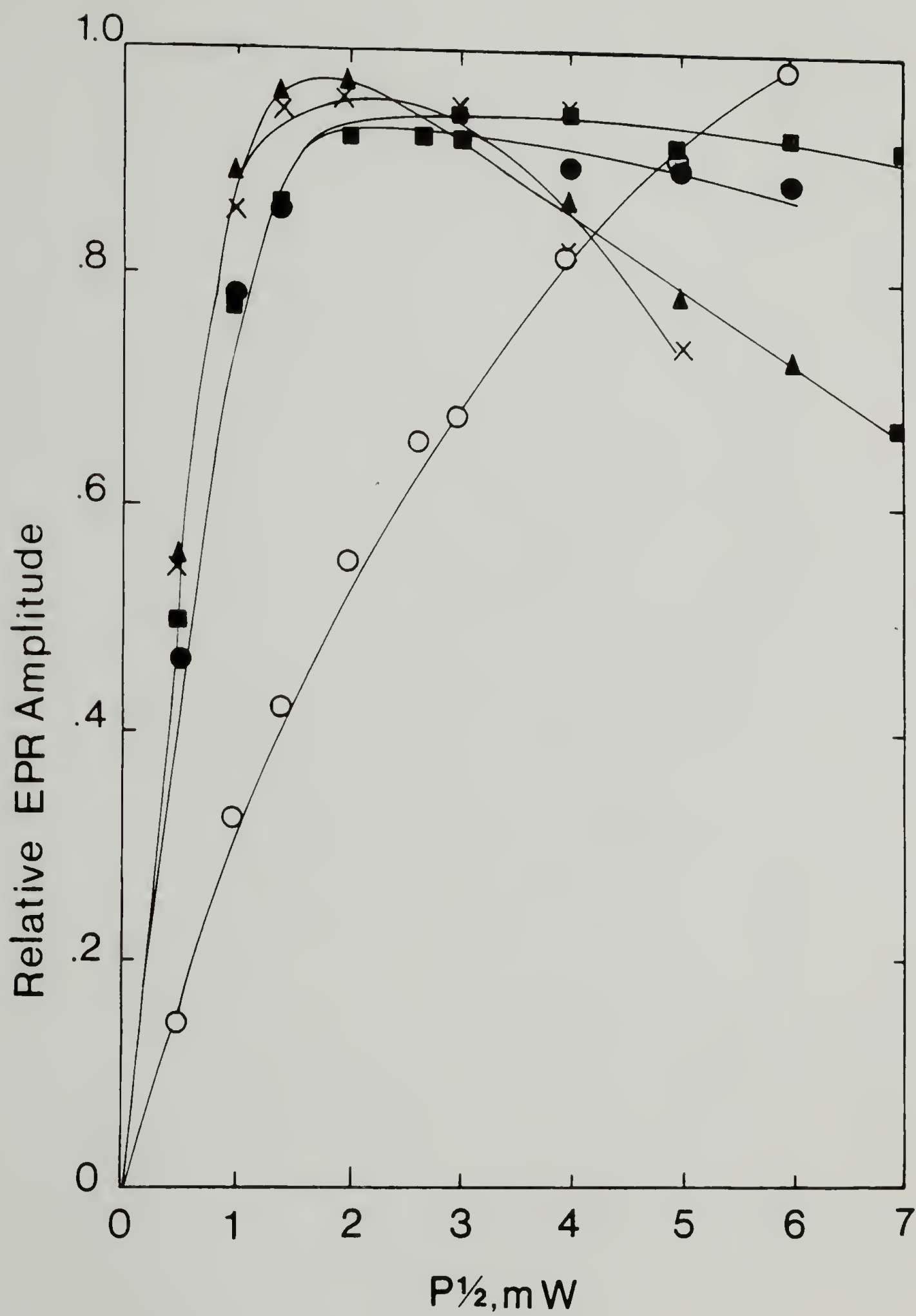


Figure 5.10 Variation of EPR Linewidth, ΔH_{pp} , of Cis-LMnP with Dopant Level. $\log Y(I_3)^- = (\bullet)$ undoped; (\blacksquare) -5.47; (\blacktriangle) -4.94; (+) -4.70; (\circ) -3.70; and (\square) -2.50.

Figure 5.11 EPR Signal Saturation Plots of Iodine Doped Cis-LMnP at $\text{Log } Y(\text{I}_3)^- = (\bullet)$ undoped, (\blacksquare) -5.47, (\blacktriangle) -4.70, $(+)$ -3.70, and (\circ) -2.76.



cis-LMnP with iodine does not significantly affect either T_1 or T_2 , up to $Y(I_3)^- = 2 \times 10^{-4}$. Below this level, $T_1 = 300\text{--}430 \mu\text{sec}$ and $T_2 = 10\text{--}14 \text{ nsec}$. Above this level of doping, the signal could not be saturated.

All EPR spectra of cis-doped LMnP were symmetrical and had a Lorentzian line shape. Since there was no narrowing of the EPR linewidth over the entire doping regime, the unpaired electrons being observed are rather localized. This could be interpreted in one of two ways. First, no long-range dopant cis-trans isomerization is taking place over the studied doping regime. This seems unlikely based on the observed ease for which thermal isomerization takes place. Secondly, and more likely, the spins being observed at moderately doped levels exist as polarons and are pinned by a 0.25 eV pinning potential.¹²⁴ Upon cis-trans isomerization, the mobile spins annihilate each other and are no longer observable.

Variable Temperature EPR

Variable temperature EPR measurements on undoped and doped cis-LMnP were made from 133 to 293 K. Figures 5.12 and 5.13 show the results for the integrated signal intensity relative to either 273 or 293 K, and the variation in linewidth respectively. Undoped cis-[CH]_x shows a detectable Curie-like spin susceptibility. There is a ca. 1.3 fold increase in spin intensity over a 160° temperature range. This is in contrast to a nearly Curie independent susceptibility reported by others for 10,500 \bar{M}_n polymer. Doped polymers below $2 \times 10^{-3} Y(I_3)^-$ exhibited slightly greater spin susceptibilities, increasing in intensity by ca. 1.5 times over 160° range. Heavily

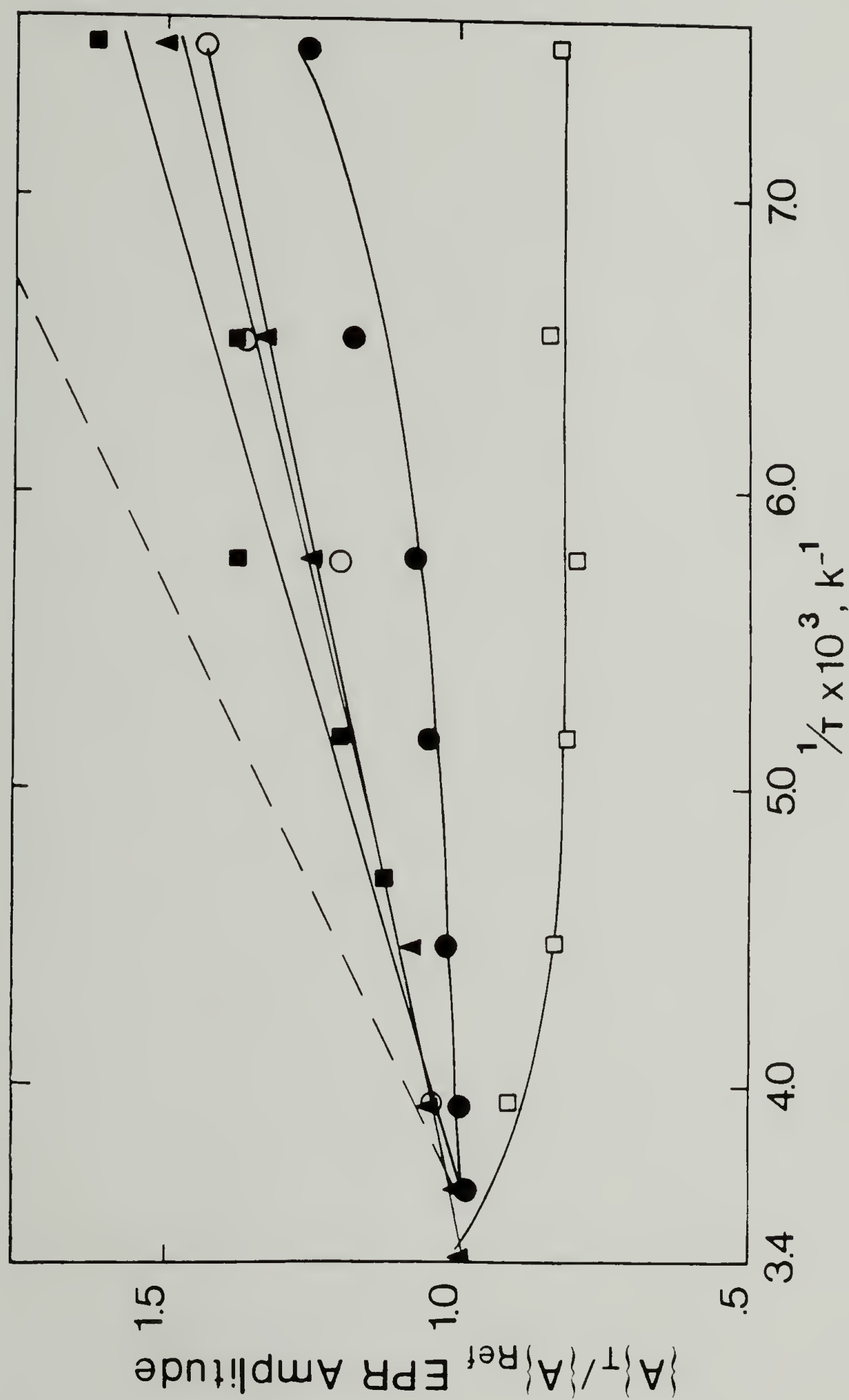
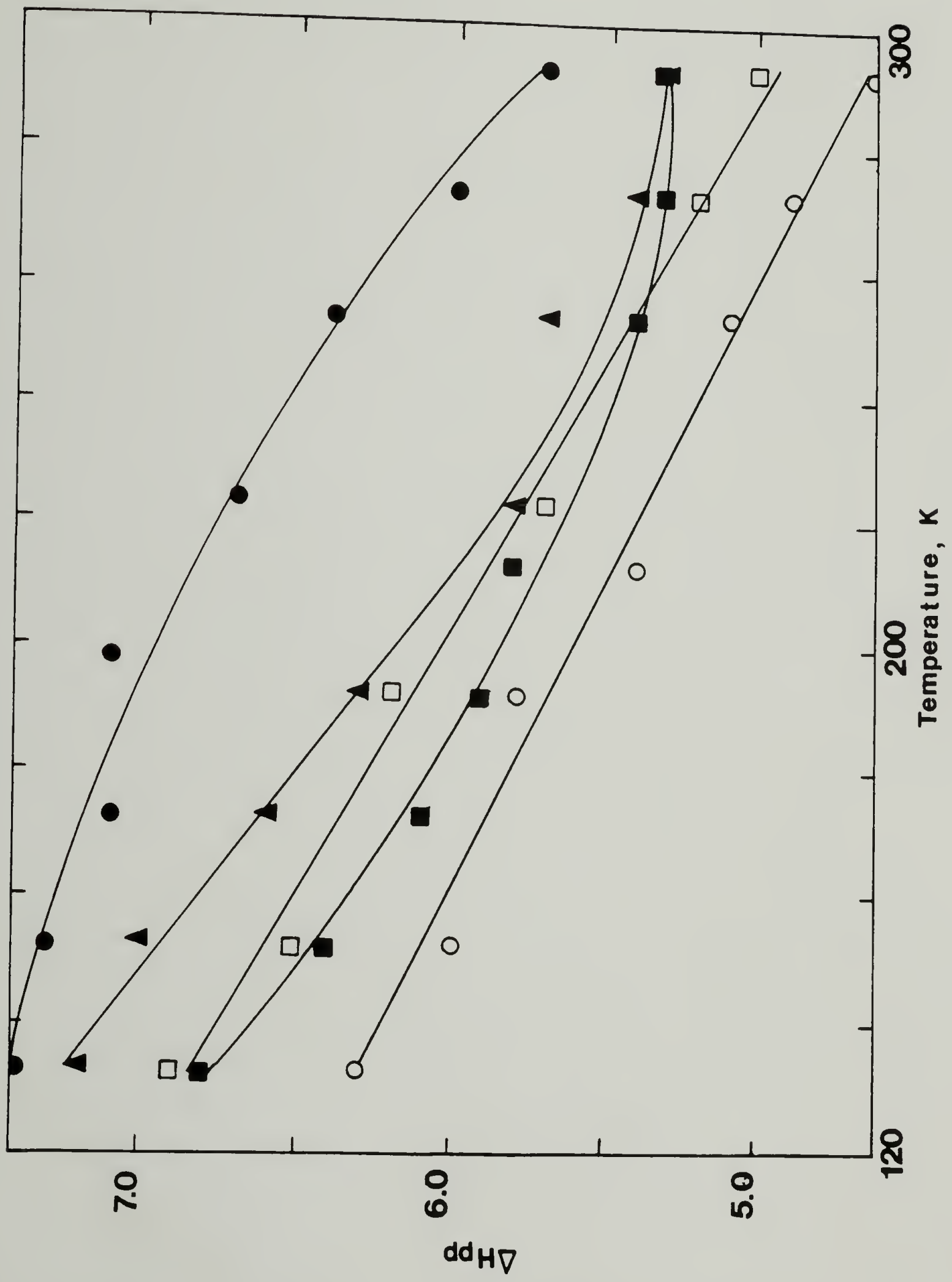


Figure 5.12 Temperature Dependence of Normalized Integrated EPR Signal Amplitude for Iodine Doped Cis LMnP at Log $Y(I_3)^- = (\bullet)$ -5.47; (\blacksquare) -4.37; (\blacktriangle) -3.70; and (\square) -2.76. Dashed Line (--) taken from Ref.#162 for Undoped Trans- $[CH]_x$.

Figure 5.13 Temperature Dependence of EPR Linewidth for Iodine Doped Cis-LMnP at $\text{Log } Y(\text{I}_3)^- = (\bullet)$ undoped, (\blacksquare) -5.47, (\blacktriangle) -4.37, and (\circ) -3.70, and (\square) -2.76.



doped polymers above the semiconductor-to-metal transition exhibited a slightly negative Curie-like dependence. The disappearance of Curie spins is consistent with the concept of homogeneous doping.

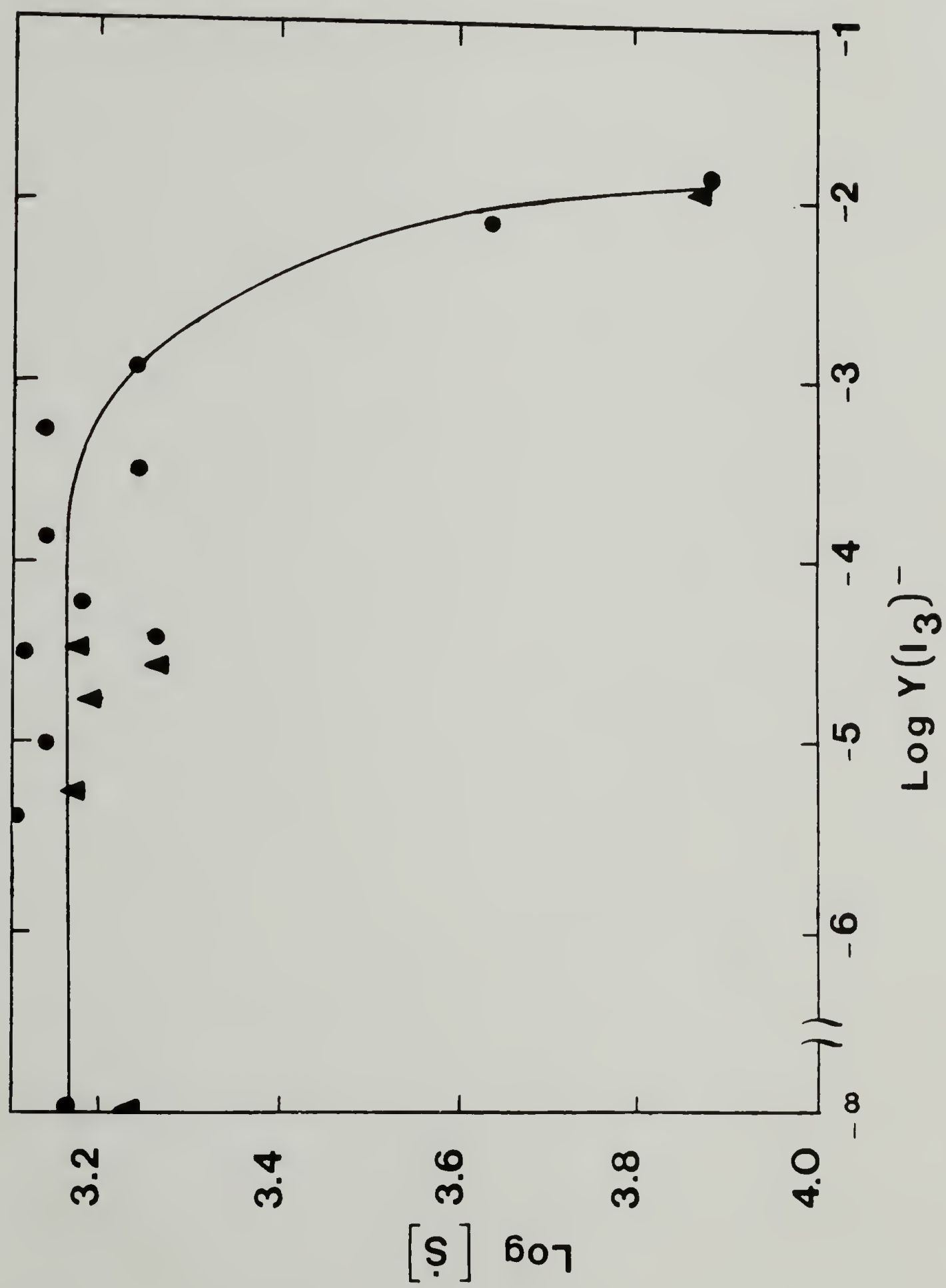
Broadening of the EPR linewidth at low temperatures was noted in all samples. Previously it had been reported that standardly prepared $\text{cis-}[\text{CH}]_x$ does not exhibit motional broadening at low temperatures. The temperature dependence observed may be a consequence of a small amount of cis/trans isomerization in LMnP samples.

I_2 Doped Trans Low Molecular Weight Polyacetylene

Quantitative EPR

Undoped trans-polyacetylene has an intrinsic spin concentration of $10^{-3.2}$ to $10^{-3.4}$ spins per CH repeat unit. The concentration was found to be insensitive to the method of polymerization and the resulting molecular weights. Using $^{125}\text{I}_2$ to dope low M_n $[\text{CH}]_x$ and $[\text{CD}]_x$ that had been isomerized at 453 K/15 minutes, quantitative EPR measurements were made against a TMO standard. Figure 5.14 shows the evolution of spins with iodine doping for these polymers. Though in this series, $[\text{CH}]_x$ samples could only be doped to $10^{-1.8}$ mole fraction I_3^- , in separate experiments involving maximum doping of trans LMnP, higher level doping could be obtained. At $Y(\text{I}_3)^- = 10^{-1.32}$ for example no EPR signal could be detected. The same is true for $[\text{CD}]_x$ at $Y = 10^{-1.39}$. Two important points can be drawn from these results. In comparison to Warakowski's¹¹⁰ work with 10,500 \overline{M}_n polymer, independent of \overline{M}_n , "soliton melting" occurs at the same point in the doping curve i.e., ca. 10^{-3} mol fraction I_3^- . Also in comparing these results with those for

Figure 5.14 Variation of Neutral Soliton Concentration with $(I_3)^-$
Doping for Trans 500 Mn (●) $[CH]_x$, and (▲) $[CD]_x$.



cis doped LMnP, spin annihilation occurs at the same point on the dopant curve.

The universality of the onset of spin annihilation clearly indicates soliton or polaron doping and transport as a three dimensional phenomenon involving strong interchain coupling. Based on the onset of spin annihilation, this "soliton melting" begins when the average distance between dopants reaches ca. 35 Å. No comment on soliton versus polaron doping can be made based on these results. Both mechanisms should result in a monotonous drop in the density of states of neutral, unpaired spin at high doping levels. This is accompanied by an ever-increasing density of charged states within the band gap.

Saturation and Relaxation Times

$^{125}\text{I}_2$ doped low \overline{M}_n $[\text{CH}]_x$ and $[\text{CD}]_x$ samples were studied for T_1 and T_2 variations over the entire dopant range. Figures 5.15 and 5.16 show the room temperature relative EPR signal amplitude plots for various dopant levels for $[\text{CH}]_x$ and $[\text{CD}]_x$ respectively. Signal intensities were normalized relative to the maximum signal amplitude at P_{sat} . Lightly doped samples retained the Lorentzian lineshape characteristic of undoped trans polymer, but with some wing broadening. At no time, even at the maximum doping level for which an EPR signal was observable ($Y \sim 10^{-1.83}$ for $[\text{CH}]_x$ and $Y \sim 10^{-1.94}$ for $[\text{CD}]_x$), were Dysonian lineshapes observed. This is taken as an indicator of homogeneous doping. Inhomogeneous doping, for example, with AsF_5 cis-polyacetylene gives asymmetric lineshapes with $A/B \sim 5$. For both polymer isotopes, saturation

Figure 5.15 EPR Signal Saturation Plots of Iodine Doped Trans LMnP
at $\text{Log } Y(\text{I}_3)^- = (\bullet)$ undoped, (\blacksquare) -4.47, (\blacktriangle) -3.46,
 $(+)$ -3.26, (\circ) -2.07.

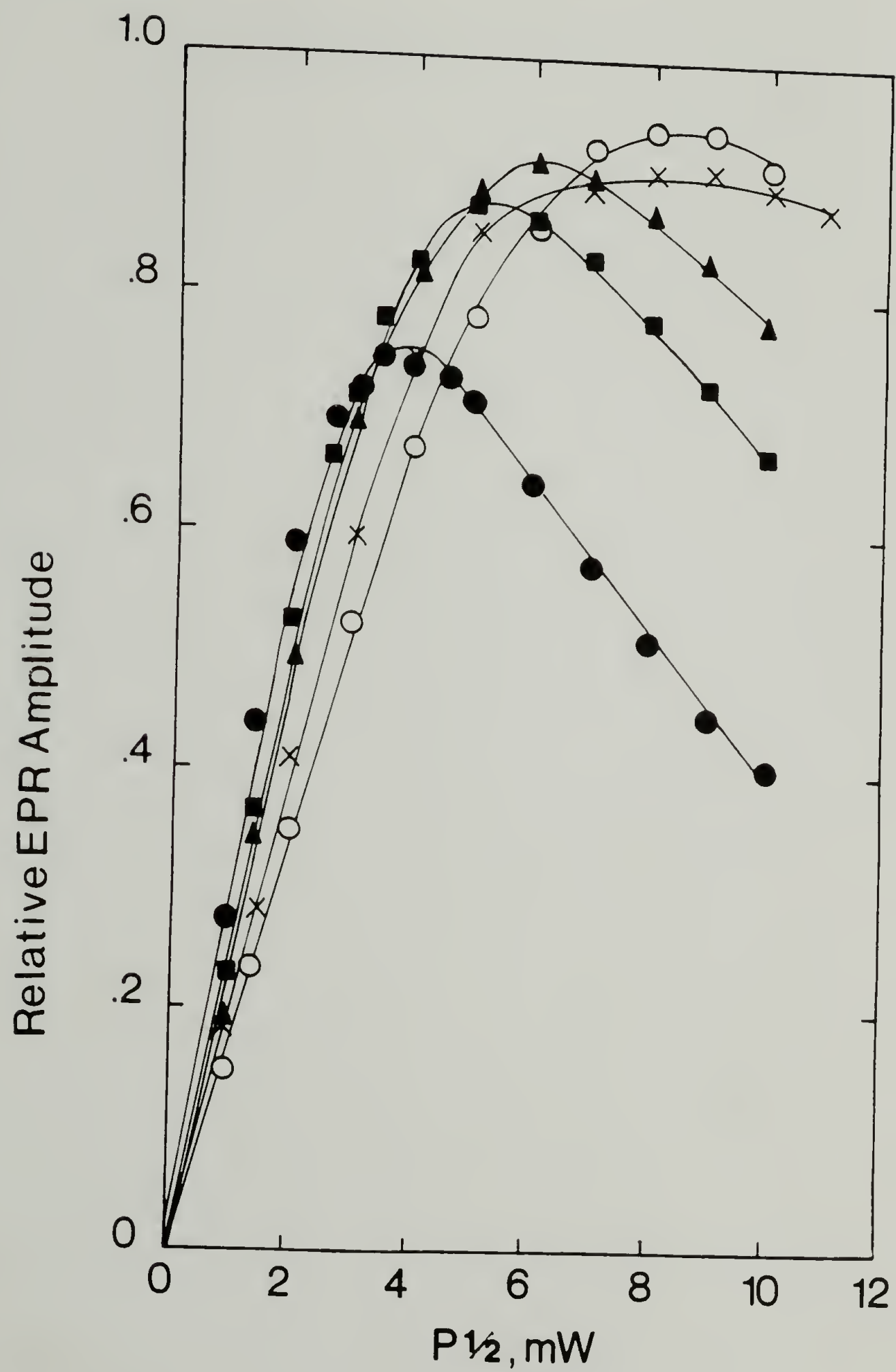
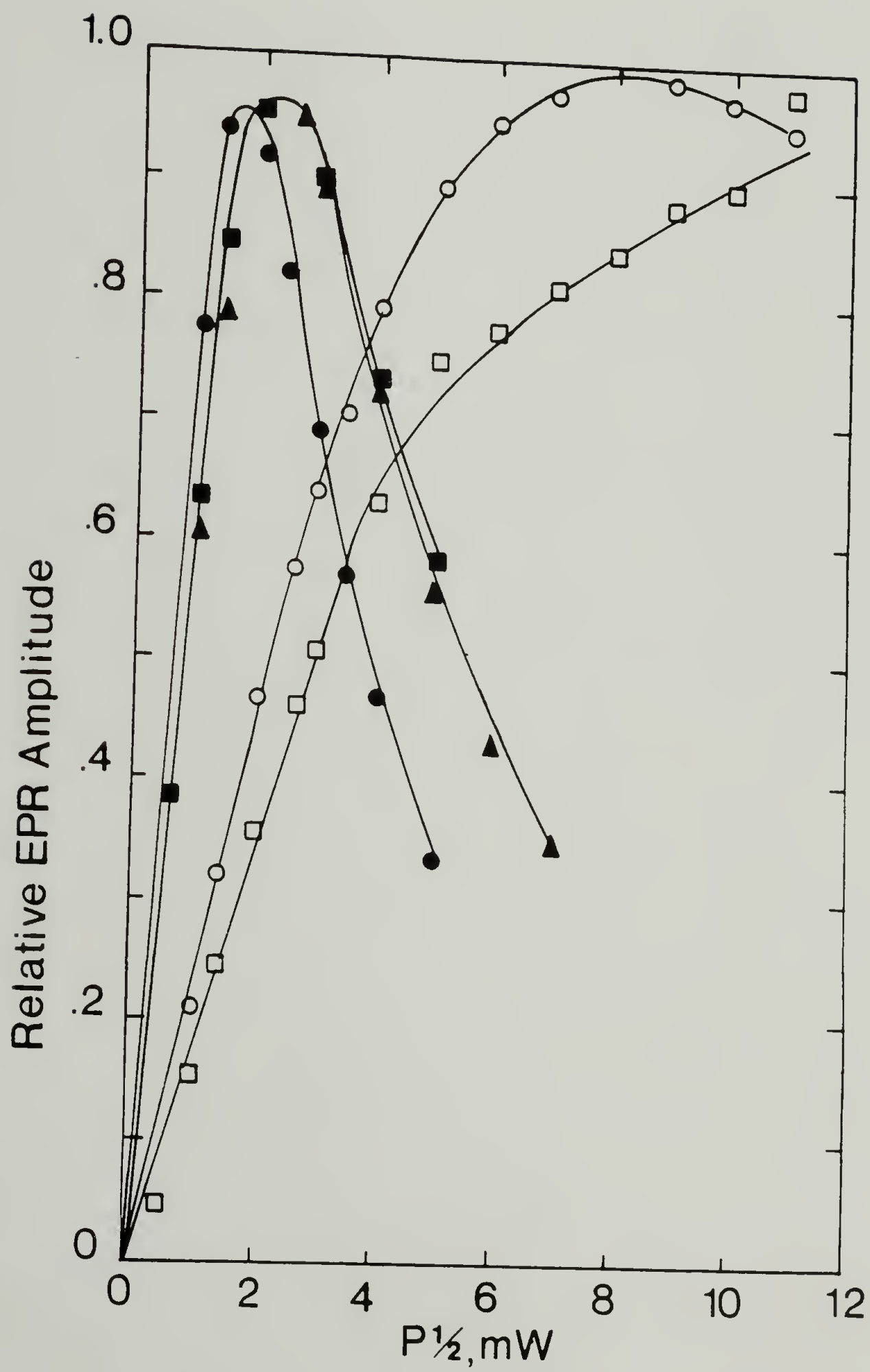


Figure 5.16 EPR Signal Saturation Plots of Iodine Doped ca. 500 Mn Trans-[CD]_x at Log $\gamma(I_3)^-$ = (●) undoped, (■) -5.26, (▲) -4.49, (○) -2.13, and (□) -1.90.



power strongly depends on the dopant concentration. In $[\text{CH}]_x$, deviations towards inhomogeneous broadening occurred above $Y \sim 10^{-3.26}$ and in $[\text{CD}]_x$, at $Y \sim 10^{-2.13}$.

The linewidth of trans low \bar{M}_n $[\text{CH}]_x$ and $[\text{CD}]_x$ doped with iodine broadened slightly with even the smallest amount of iodine from 1.1-1.2G to 1.4-1.5G in $[\text{CH}]_x$ and 0.5G to 0.6-0.65G in $[\text{CD}]_x$. Figures 5.17 and 5.18 follow the variation in linewidths over microwave power for various doping levels in $[\text{CH}]_x$ and $[\text{CD}]_x$ respectively. Figure 5.19 follows the variation in zero-power linewidth with dopant concentration in $[\text{CH}]_x$. In undoped trans low \bar{M}_n $[\text{CH}]_x$, from 0-100 mW, linewidths broaden by ca. 87%. With doping, the extend of broadening diminishes to ca. 57% at $Y = 10^{-4.47}$ and ca. 20% at $Y = 10^{-2.07}$. Maximum doped trans low \bar{M}_n $[\text{CD}]_x$ shows a similar diminished broadening: ca. 17% at $Y = 10^{-1.94}$.

From linewidth and saturation powers, spin-lattice, T_1 , and spin-spin, T_2 , relaxation times were obtained for both $[\text{CH}]_x$ and $[\text{CD}]_x$. Tables 5.4 and 5.5 tally those results.

Even low levels of iodine in $[\text{CH}]_x$ suppressed T_1 to ca. 8 μsec , which remained constant over the dopant range until a non-saturating signal was observed. In $[\text{CD}]_x$, similar results were obtained, though at high levels of doping, $Y = 10^{-2.13}$, a notable drop in T_1 was documented before an unsaturated signal developed. Figure 5.20 plots the calculated T_2 results for iodine doped $[\text{CH}]_x$. A gradual drop in T_2 was observed below $Y = 10^{-3.5}$, with a precipitous drop occurring above $Y = 10^{-3.5}$.

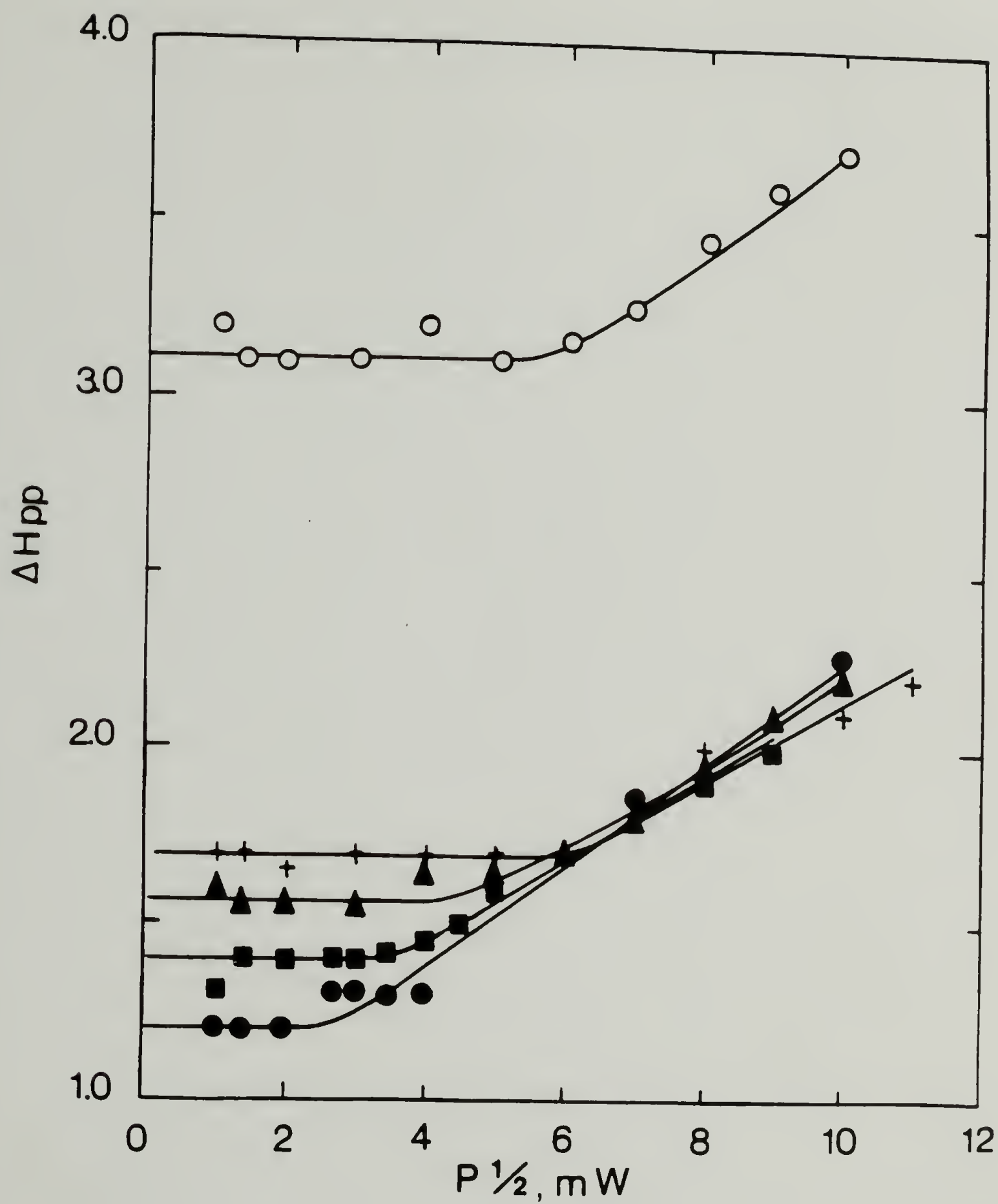


Figure 5.17 Variation of EPR Linewidth, ΔH_{pp} , with Microwave Power for 500 $\bar{\text{Mn}}$ Trans- $[\text{CD}]_x$ at $\text{Log } Y(\text{I}_3)^- = (\bullet)$ undoped; (\blacksquare) -4.47; (\blacktriangle) -3.46; $(+)$ -3.26; and (\circ) -2.07.

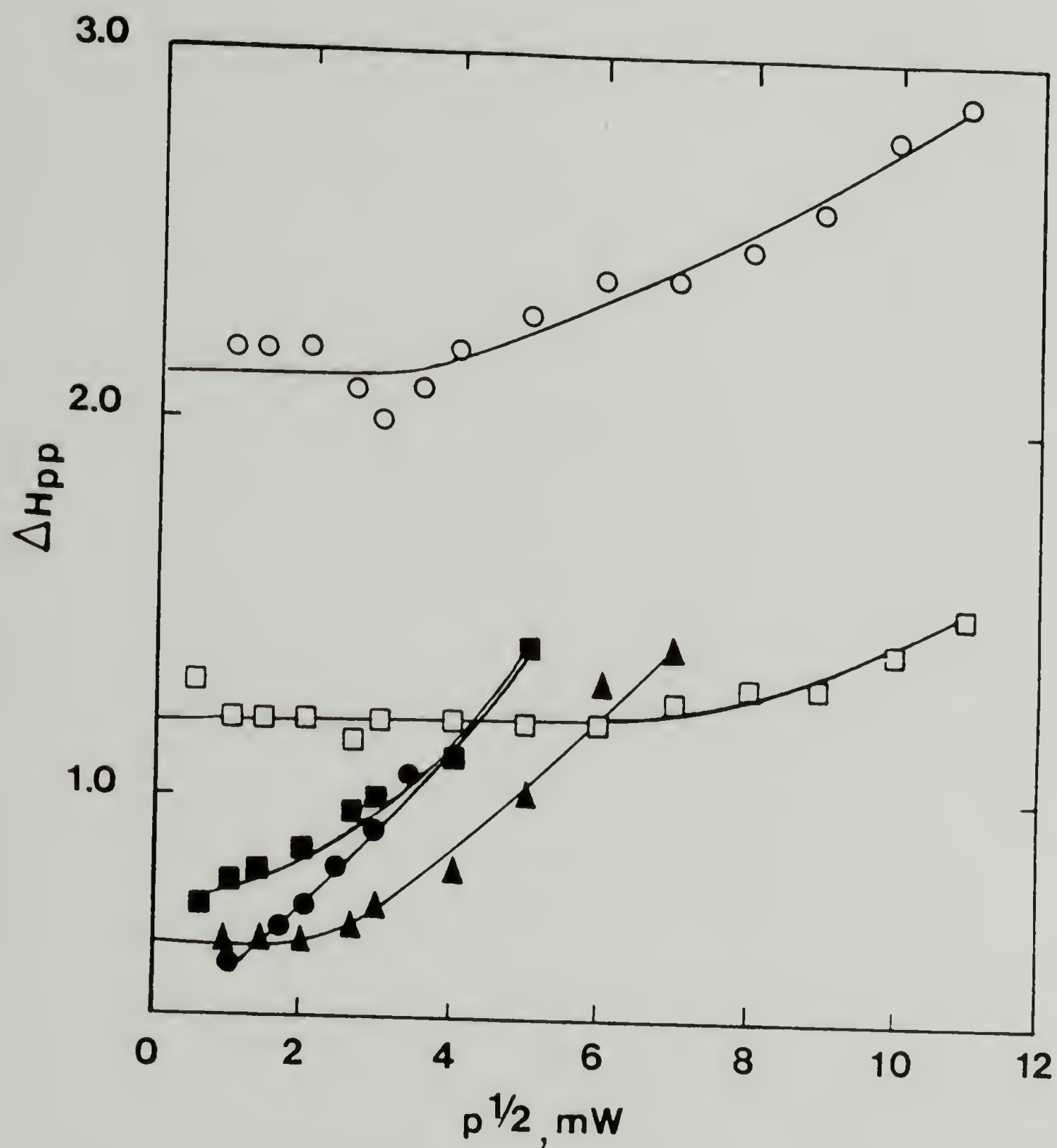


Figure 5.18 Variation of EPR Linewidth, ΔH_{pp} , with Microwave Power for ca. 500 $\bar{\text{Mn}}$ Trans- $[\text{CD}]_x$ at $\text{Log } Y(I_3)^- =$ (●) undoped; (■) -5.26; (▲) -4.49; (○) -2.13; and (□) -1.90.

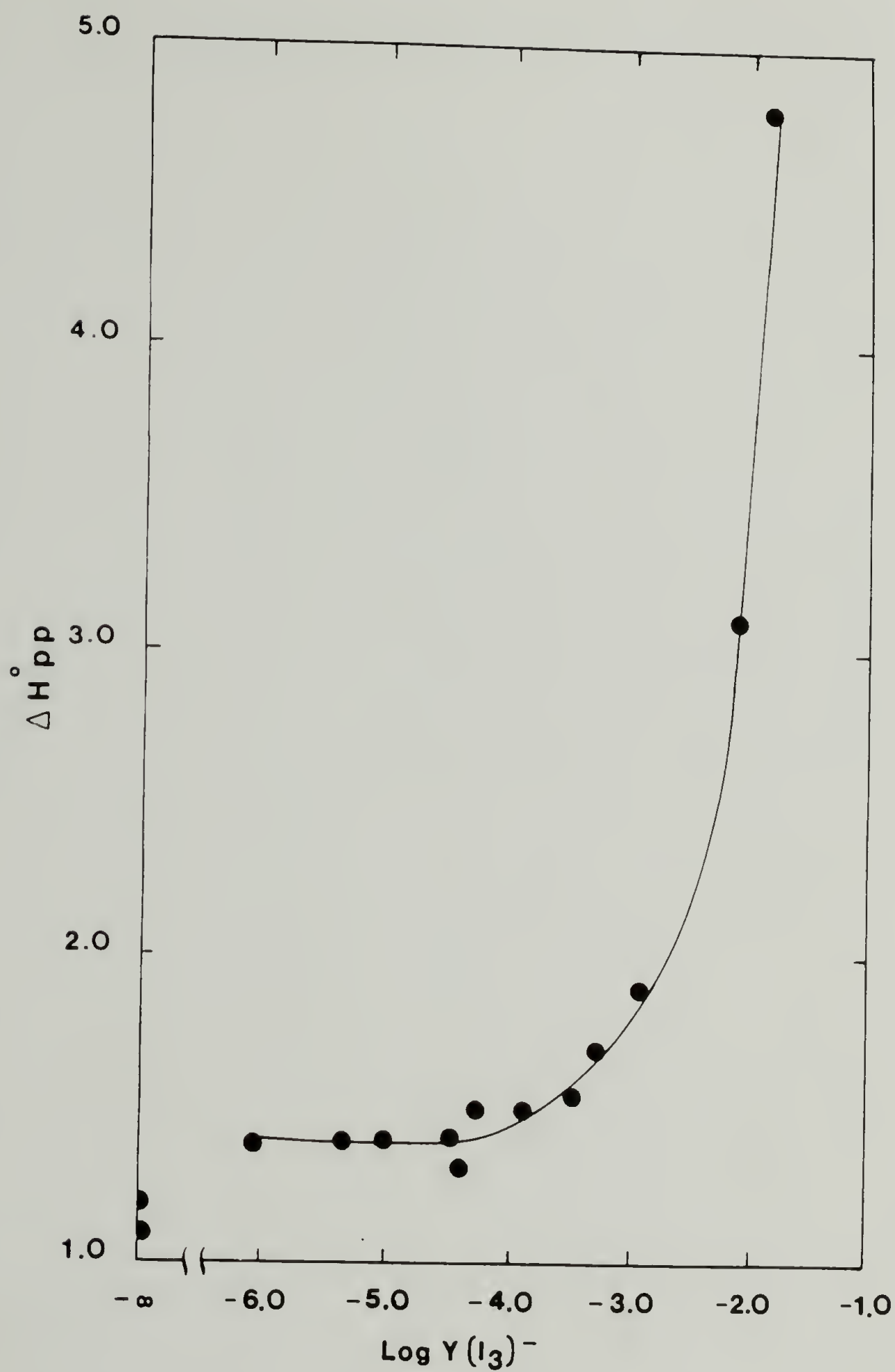


Figure 5.19 Variation of Zero-Power EPR Linewidth, ΔH_{pp} , with Iodine Concentration for 500 $\bar{\text{Mn}}$ Trans- $[\text{CH}]_x$.

Table 5.4

Iodine Doped 500 \overline{M}_n Trans-[CH]_x EPR Relaxation Times.

$\log Y(I_3)^-$	$\Delta H_{pp}, G$	P_{sat}, mW	$T_1 \times 10^6, sec$	$T_2 \times 10^9, sec$
$-\infty$	1.2	12.2	20	55
-5.34	1.4	36	8	47
-4.97	1.4	56.2	5	47
-4.47	1.4	25	11	47
-4.38	1.3	36	7	50
-4.21	1.5	36	8	44
-3.85	1.5	16	2	44
-3.46	1.55	36	9	42
-3.26	1.7	72.2	5	38
-2.89	1.9	a	-	34
-2.07	3.1	72.2	9	21
-1.83	4.8	64	6	14

a does not saturate

Table 5.5

Iodine Doped ca. 500 \overline{M}_n Trans-[CD]_x EPR

Relaxation Times.

$\log Y(I_3)^-$	$\Delta H_{pp}, G$	P_{sat}, mW	$T_1 \times 10^6, sec$	$T_2 \times 10^9, sec$
$-\infty$	0.5	2.6	39	130
-5.26	0.65	5.0	26	100
-4.49	0.60	5.0	24	110
-2.13	2.1	69	6	31
-1.94	1.2	a	-	55

a does not saturate

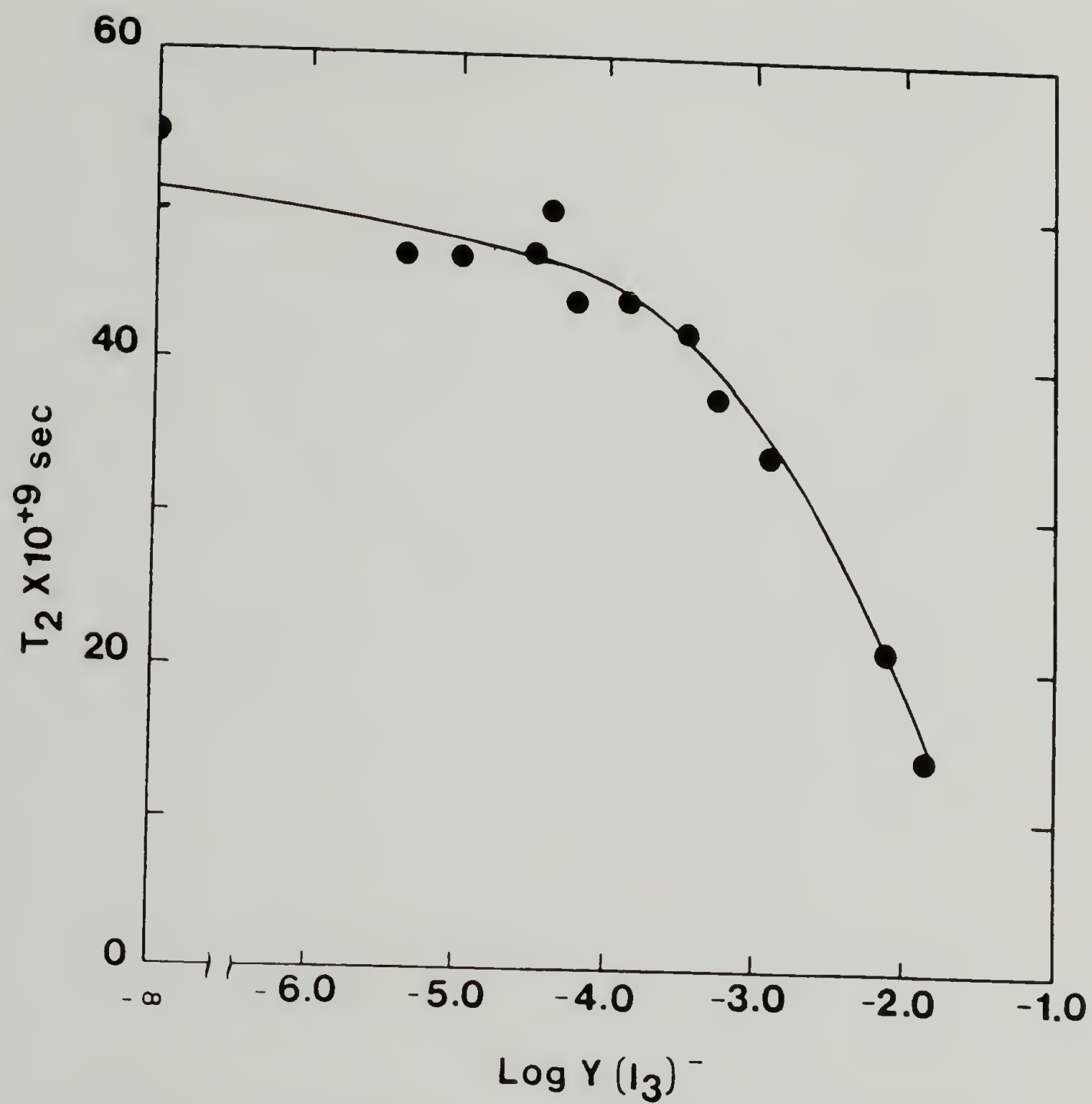


Figure 5.20 Variation of Spin-Spin Relaxation Times, T_2 , with Iodine Concentration for 500 $\bar{M}n$ Trans- $[CH]_x$.

Variable Temperature EPR

Variable temperature EPR measurements on undoped and doped trans-[CH]_x and [CD]_x were made from 133 to 293 K. Undoped trans-[CH]_x displays a Curie spin susceptibility with spin intensity growing by ca. 1.9x over a 160° temperature range (Fig. 5.21) and undoped trans [CD]_x increases by 1.8x over identical conditions (Fig. 5.23). These results are consistent with those obtained by Weinberger et al.¹⁶² for undoped trans-[CH]_x. Over the same temperature range, they report a 1.9x increase in the spin susceptibility. Upon doping low \bar{M}_n [CH]_x with iodine, very little change in Curie slope is seen up to $Y \sim 10^{-2.89}$. Below this level, no discernable trend is apparent. More heavily doped samples (Fig. 5.22), $Y \geq 10^{-2.07}$, showed a dramatic enhancement in the Curie susceptibility. These results are presented in Figure 5.24 over the dopant range. Iodine doped trans-[CD]_x did not show this behavior.

The total magnetic susceptibility may be expressed as the sum of the Core, Pauli, and Curie contributions.

$$\chi = \chi_{\text{Core}} + \chi_{\text{Pauli}} + \chi_{\text{Curie}} \quad (5.2)$$

The temperature dependent susceptibility of neutral solitons may be expressed as:

$$\chi_C(T) = n_i \mu_B^2 / k_B T \quad (5.3)$$

where n_i = number of Curie spins

μ_B = Bohr magneton

k_B = Boltzman's constant

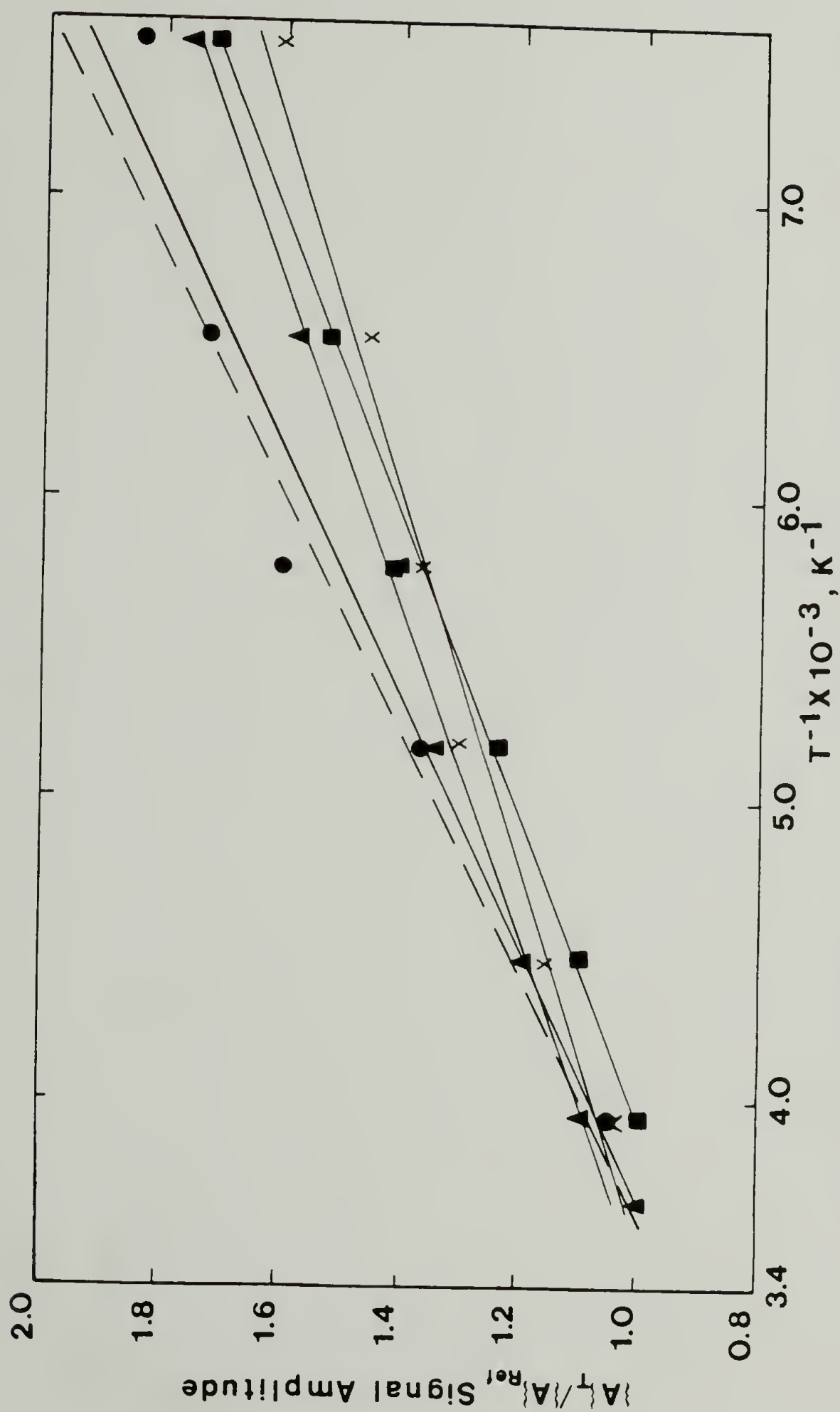
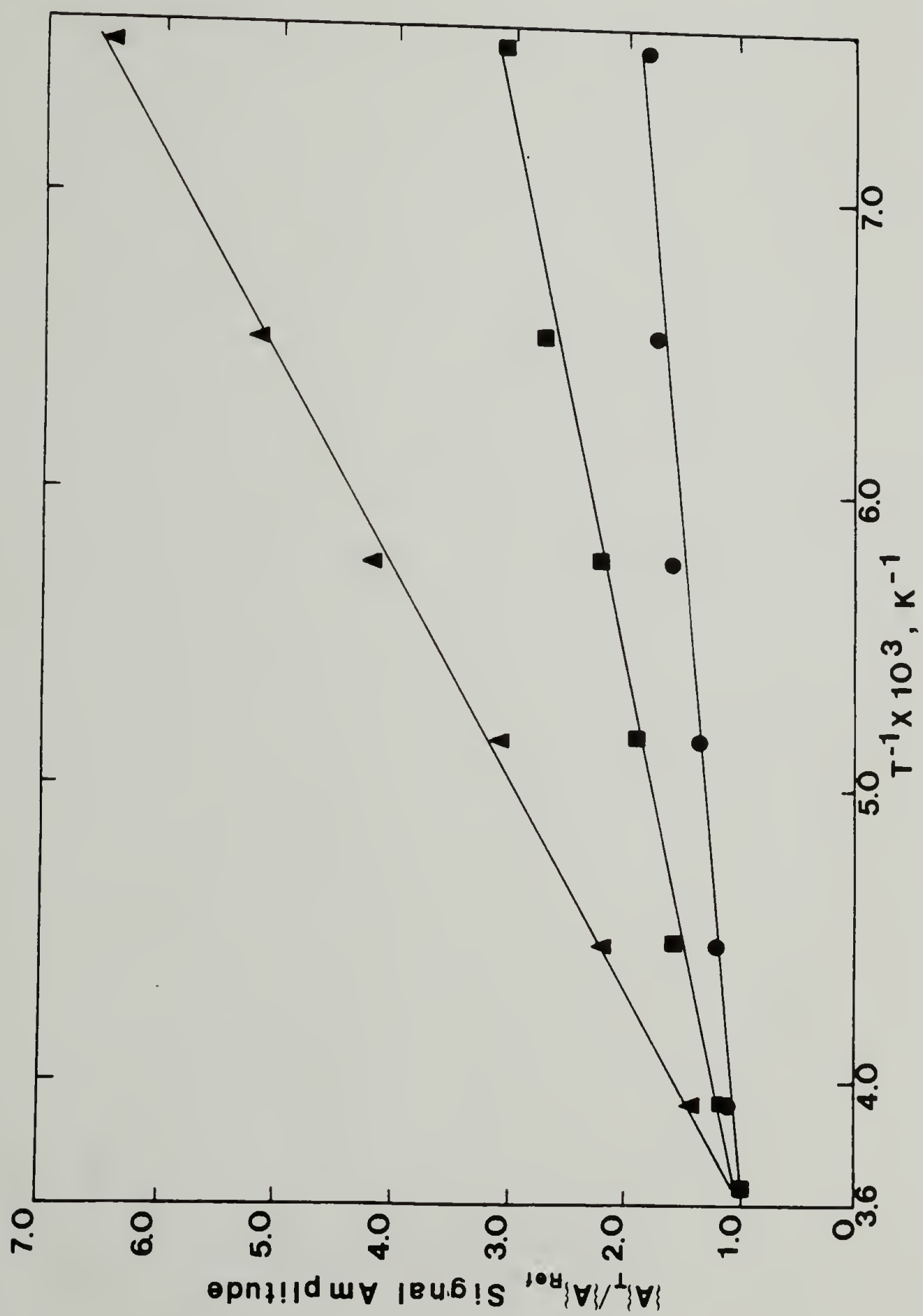


Figure 5.21 Temperature Dependence of Normalized Integrated EPR Signal Amplitude for Iodine Doped 500 \bar{M}_n Trans- $[CH]_x$ at $\log Y(I_3)^- = (\bullet) -5.34$; (\blacktriangle) -3.46 ; and (\times) -2.89 . Dashed Line taken from ref. #162 for Trans Undoped $[CH]_x$.

Figure 5.22 Same as Fig. 5.21 for $\text{Log } Y(I_3)^- = (\bullet)$ undoped, (\blacksquare) -2.07, and (\blacktriangle) -1.83.



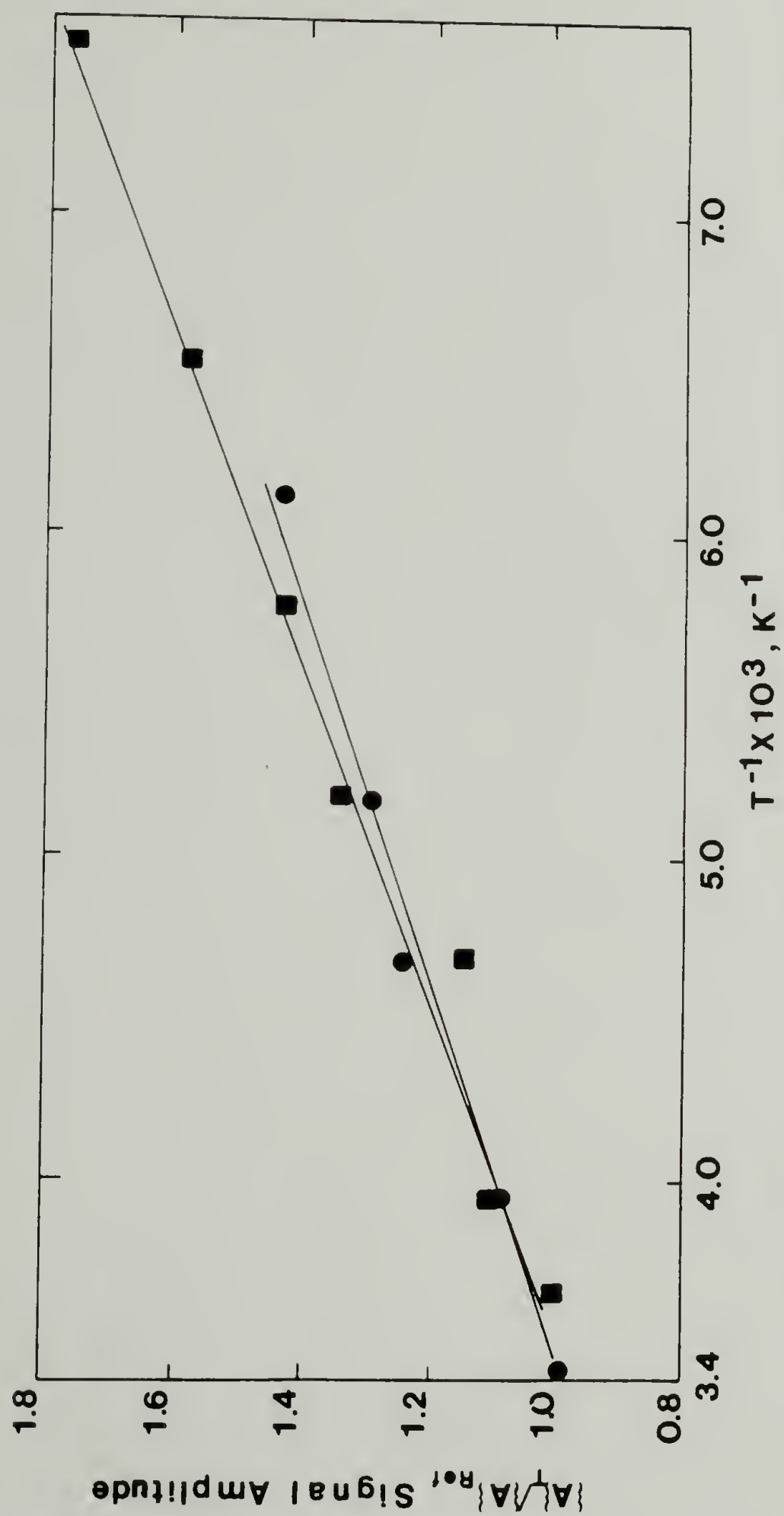


Figure 5.23 Temperature Dependence of Normalized Integrated EPR Signal Amplitude for Iodine Doped ca. 500 Mn Trans-[CD]_x at Log $\gamma(I_3)^- = (\bullet)$ undoped; and (\blacksquare) -2.10.

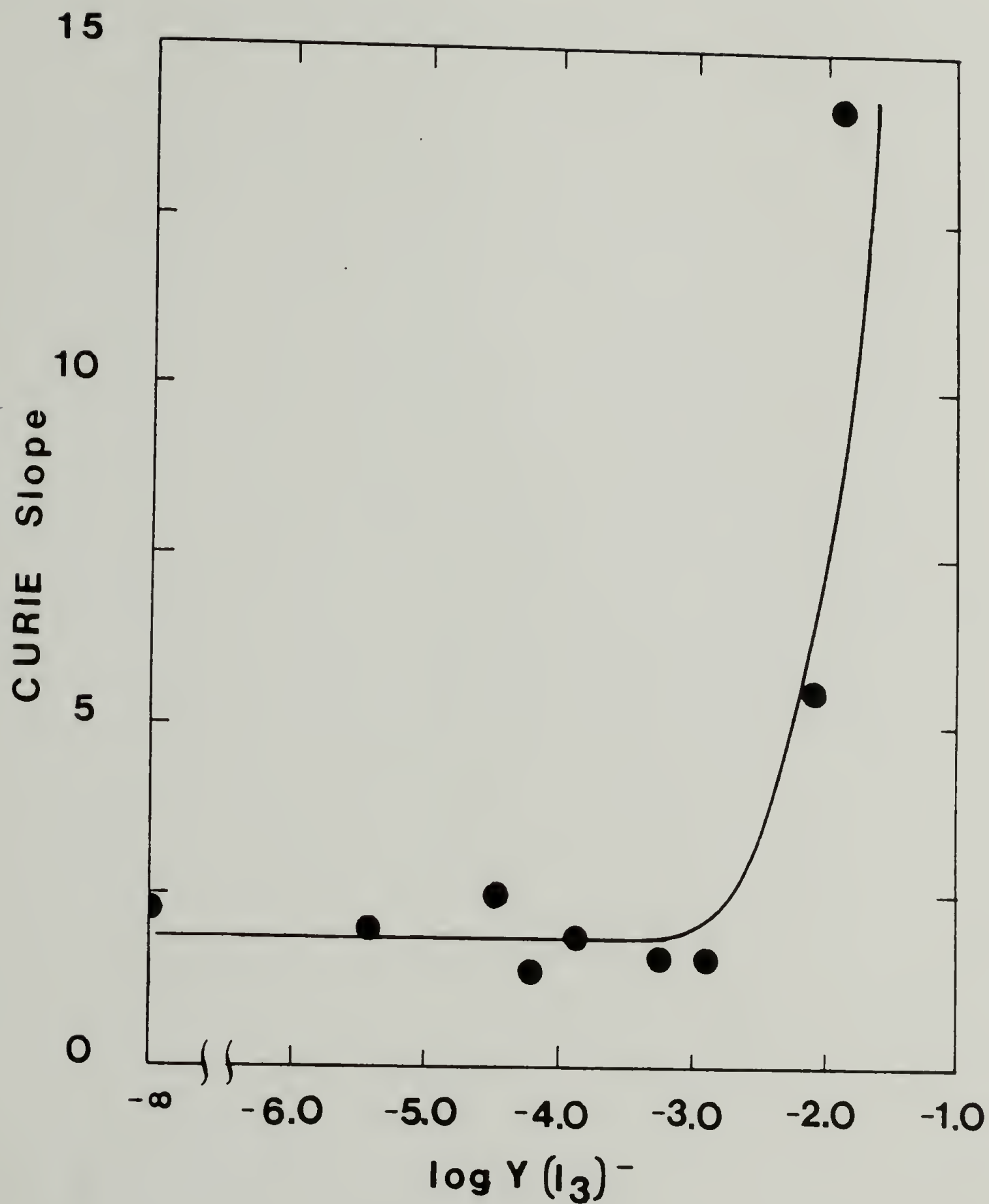


Figure 5.24 Variation of Curie Slope of 500 Mn Trans-[CH]_x over Iodine Doping.

Clearly an increased number of Curie spins will result in an enhanced susceptibility. Residual Curie spin susceptibility in heavily doped polymer is interpreted as an indication of inhomogeneous doping. In our system, films of 40-60 μm thickness did not show Dysonian line character and spin concentrations diminished at $Y \geq 10^{-3.0}$.

Figure 5.25 follows the variation in EPR signal linewidth with temperature for doped and undoped low \bar{M}_n $[\text{CH}]_x$ and $[\text{CD}]_x$. Upon doping both polymers show reduced motional narrowing upon cooling, though for heavily doped samples of $[\text{CH}]_x$ ($Y=10^{-2.07}$ and $10^{-1.83}$), unusual linewidth behavior was seen. Table 5.6 lists the percent increase in linewidth relative to undoped trans- $[\text{CH}]_x$ upon cooling from 293 to 133 K.

I_2 Doped High Molecular Weight Polyacetylene

Samples of 210,000 \bar{M}_n $[\text{CH}]_x$ were doped using $^{125}\text{I}_2$ and used for EPR investigation. Only the trans isomer was evaluated.

Quantitative EPR

Unpaired spin concentrations over the dopant range were determined against a tetra methyl piperidinoxy standard. Figure 5.26 shows the evolution of unpaired spins for both 210,000 \bar{M}_n $[\text{CH}]_x$ and, as a reference, replotted data from Warakowski¹¹⁰ for 10,500 \bar{M}_n polymer. The ordinate for the data by Warakowski has been shifted to help clarify the plot.

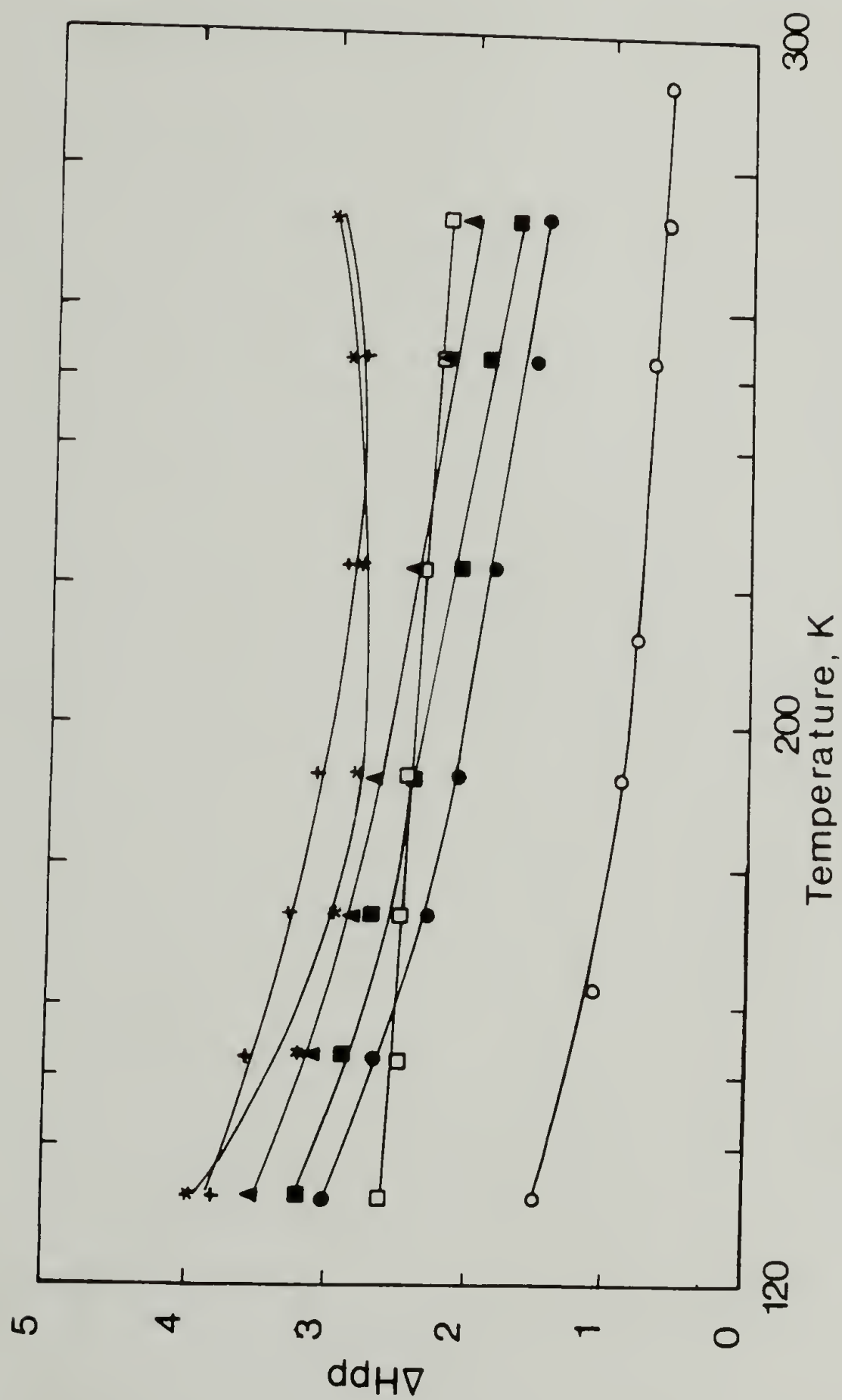


Figure 5.25 Variation of EPR Linewidth with Temperature for 500 Mn Trans-[CH]_x at Log (I₃)⁻ = (●) undoped; (■) -3.46; (▲) -2.89; (+) -2.07; and (*) -1.83. Trans-[CD]_x at Log Y(I₃)⁻ = (○) undoped; and (□) -2.10.

Table 5.6Fractional Broadening of ΔH_{pp} from 293 to 133 K.

	log γ	Percent Broadening ^a
cis $[\text{CH}]_x$	undoped	40
trans $[\text{CH}]_x$	undoped	100
"	-3.46	90
"	-2.89	75
trans $[\text{CD}]_x$	undoped	150
"	-2.10	18

^a relative to trans- $[\text{CH}]_x$.

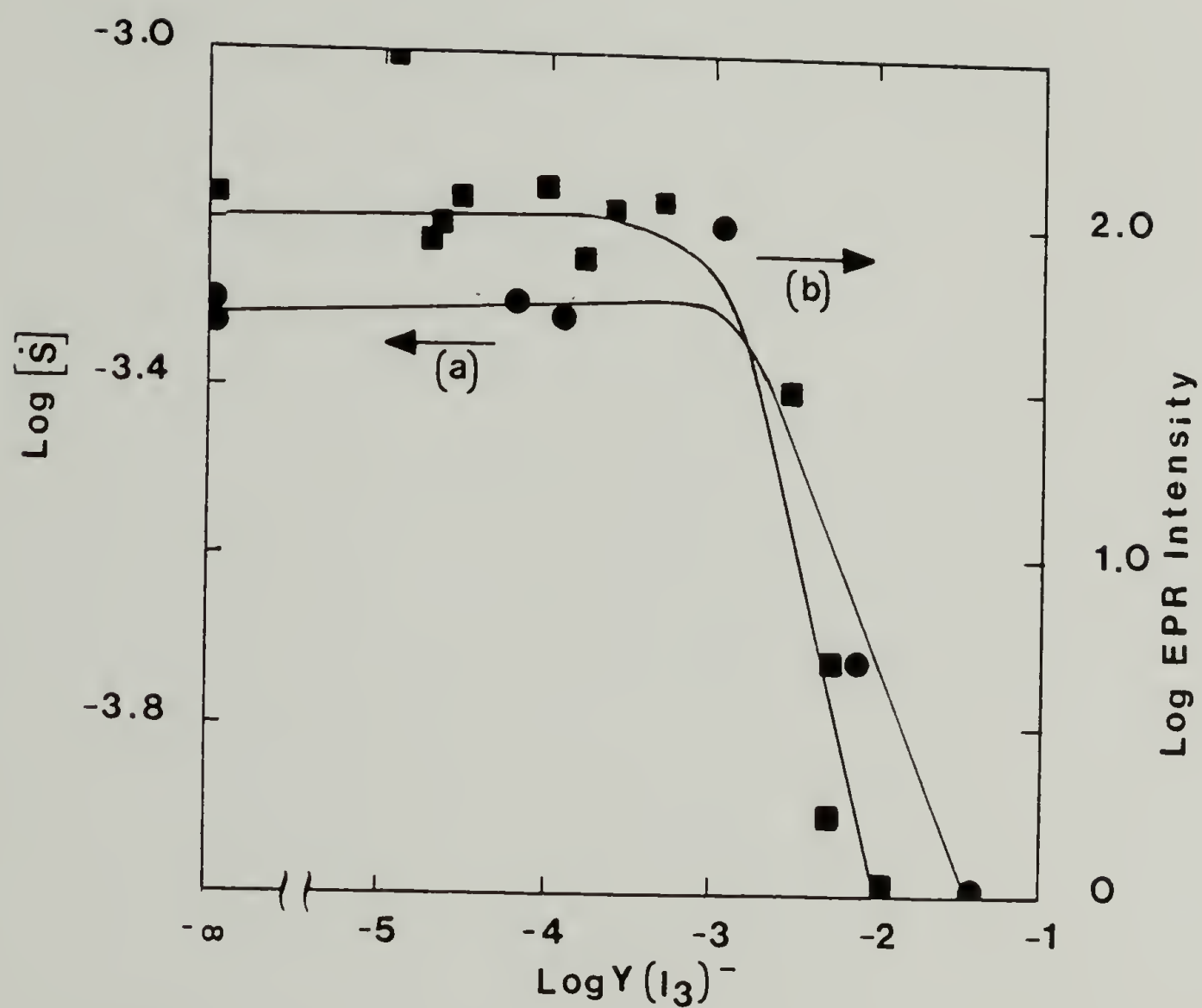


Figure 5.26 Variation of (a) Absolute Spin Concentration in Iodine Doped 210000 $\bar{\text{Mn}}$ Trans- $[\text{CH}]_x$ and (b) Relative EPR Intensity in Iodine Doped 10500 $\bar{\text{Mn}}$ $[\text{CH}]_x$. Data on 10500 $\bar{\text{Mn}}$ Films taken from ref.#110.

It was also originally plotted as EPR intensity and not absolute spin concentration. Nonetheless, the behavior between the two compositions is consistent; absolute spin concentration drops toward zero at ca. $Y=10^{-3.0}$. At $Y \geq 10^{-0.90}$, no EPR signal was observable.

These results are in agreement with EPR data on trans doped low \bar{M}_n $[\text{CH}]_x$ and $[\text{CD}]_x$. An important point which remains is whether the drop in spins is due to soliton doping, polaron-polaron annihilation or polaron-neutral soliton annihilation as iodine concentration increases.

Saturation and Relaxation Times

Saturation plots for 210,000 \bar{M}_n trans doped $[\text{CH}]_x$ are presented in Figure 5.27. At $Y \leq 10^{-2.41}$, the signal broadens homogeneously. There are deviations from Lorentzian line shape with increasing iodine doping. The signal at $Y=10^{-1.60}$, while still strong, could not be saturated since the microwave current could not be kept within limits. The sample was also warm when removed from the cavity. A mildly Dysonian lineshape with an A/B ratio of 1.32 suggests this material to be either metal-like with a continuous density of states occupying the bandgap as inhomogeneously doped. The latter is unlikely since these samples show a sharp conductivity SMT, and a monotonically diminishing unpaired spin concentration above $10^{-3} (\text{I}_3)^-$.

Table 5.7 lists the observed zero-power linewidth, saturation power and calculated relaxation times. It is interesting to note that the pre-transition doped samples show a constant T_1 that agree with the undoped polymer. T_2 times, however, shortened noticeably even with small amounts of iodine in comparison to the undoped specimen. They

Figure 5.27 EPR Signal Saturation Plots of Iodine Doped 0,000 $\bar{\text{Mn}}$ Trans-[CH]_x at Log $\gamma(\text{I}_3)^- = (\bullet)$ undoped, (\blacksquare) -3.35, and (\blacktriangle) -2.41.

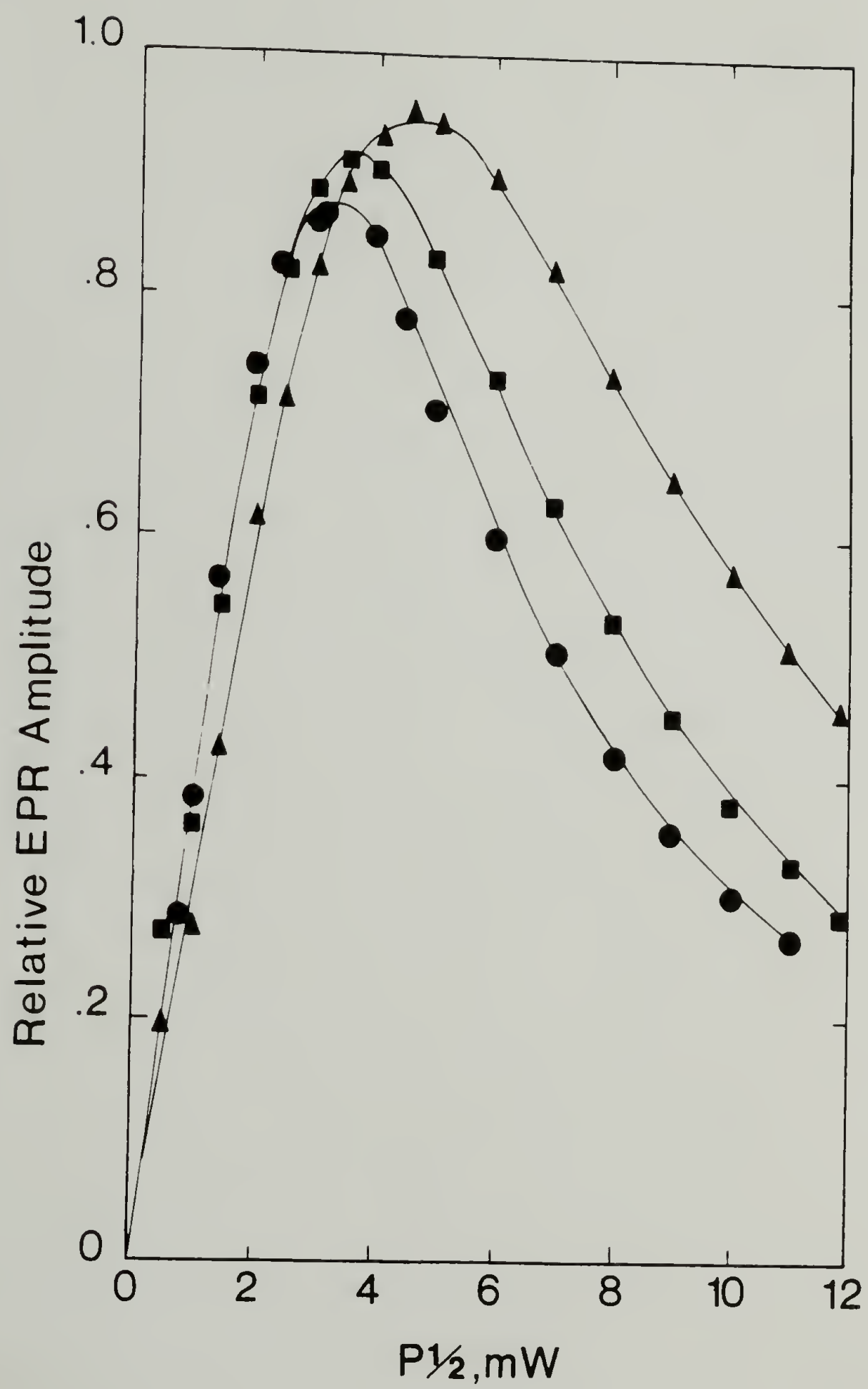


Table 5.7

I₂ Doped 210,000 \overline{M}_n [CH]_x EPR Relaxation Times.

$\log Y(I_3)^-$	$\Delta H_{pp}^\circ, G$	P_{sat}, mW	$T_1 \times 10^6, sec$	$T_2 \times 10^9, sec$
$-\infty$	0.60	10	12	110
-4.20	0.85	12	14	77
-3.87	0.90	-	-	73
-3.83	0.90	14	13	73
-2.89	0.85	20	8	77
-2.08 ^a	0.80	∞	$-\infty$	82
-1.38	-----no signal-----			

^a This sample exhibited a Dysonian lineshape with $A/B=1.32$.

then remained constant through to the transition zone.

Discussion

As was shown in this chapter, the spin populations in cis, trans and iodine doped polyacetylene first outlined by workers for 10,500 \bar{M}_n polymer also seems to be valid over the entire \bar{M}_n spectrum that is experimentally possible. The implications for this finding are far reaching and shall be discussed.

When polyacetylene is synthesized at 195 K, high molecular weight polyene chains result which are free of structural defects as evidenced by EPR. Upon warming, configurational defects in the form of neutral, spin=1/2 kinks appear. Soliton theories of Su and others¹¹³⁻¹¹⁵ predict these phase boundaries to be highly mobile along the chain direction. No interchain coupling is discussed. Experimental evidence from EPR and NMR studies support the quasi-one dimensional behavior of neutral solitons, with diffusion coefficient anisotropies of 10^3 - 10^5 reported. Yet even in the undoped state, polyacetylene is a semiconductor, i.e. macroscopic electron flow must take place. A single polymer chain cannot reach from one end of the sample to the other. Therefore a mechanism of interchain electron migration must take place. Kivelson's ISH^{131,132} model for lightly and "undoped" polyacetylene has successfully withstood the experimental scrutiny of researchers within the field. Eq. 1.22 outlines the process. Therefore the three dimensionality of soliton motion must be considered. The results of undoped trans polymers of differing molecular weights supports this concept.

Indeed one may estimate the soliton domain to be $(4.3-6.5) \times 10^4 \text{ \AA}^3$. Assuming a spherical volume element, the distance between soliton may be ca. 50 \AA .

For 500 \overline{M}_n polymer, there are on the average ~ 38 CH units per chain. Yet on the average, the soliton resides within ca. 2000 CH units. Thus one is compelled to also recognize that many polymer chains are "soliton free".

Upon p-doping, a decrease in spins has been observed for all \overline{M}_n samples, consistent with observations by Pochen et al.¹⁶³, Bernier et al.¹⁶⁴, and Warakowski.¹¹⁰ It is therefore a general observation that homogeneously doped $[\text{CH}]_x$ is free of uncharged carriers at high levels of doping. This transition occurs nearly simultaneously with the SMT measured by conductivity. This has been explained by Tokumoto et al.¹⁶⁵ for iodine doping based on two reactions: (1) conversion of neutral solitons to positive solitons, and (2) formation of charged solitons via temporal polaron formation (Fig. 1.10).

In cis- $[\text{CH}]_x$ doping must take place via polaron formation. Energetically, the radical cation pair prefer to be in close proximity rather than separated. At some density of polaron formation, cis-trans isomerization takes place with a commensurate annihilation of the soliton-antisoliton pair. Controversy abounds however as to the degree of isomerization at various doping levels. For iodine doped cis- $[\text{CH}]_x$, at $Y(\text{I}_3)^- = 0.0017$, $^1\text{H-NMR}$ results indicate 80% trans,¹⁶⁶ at $Y(\text{I}_3)^- = 0.007$ no cis was seen by IR,¹⁶⁷ and by x-ray diffraction, heavily doped polymer was completely isomerized.¹⁶⁸ On the other hand, IR indicated

that a 90% cis sample when doped to $Y(I_3)^- = 0.0031$ was still 70% cis,¹⁶⁹ and at $Y(I_3)^- = 0.005$, only 15% trans was found.¹⁷⁰ By ^{13}C -NMR, a 60% cis sample doped to $Y(I_3)^- = 0.057$ was still 40% cis,¹⁷¹ and IR indicated short cis-segments existed even at $Y(I_3)^- = 0.02$.¹⁷² From the results presented in this dissertation for 500 \overline{M}_n cis polyacetylene, chemically induced cis-trans isomerization may not be taking place until ca. 0.001 $Y(I_3)^-$. In this way the drop in spin concentrations can be explained.

CHAPTER VI

TRANSPORT PROPERTIES

When treated with oxidizing or reducing agents, the conductivity of polyacetylene increases by nearly twelve orders of magnitude. At maximum doping, the material behaves as a synthetic metal exhibiting a density of states at the Fermi level. The investigation of this phenomenon is the subject to this chapter. The central focus will be to elucidate the importance of molecular chain length on the conductive properties of polyacetylene.¹⁷³

The work presented within should be separated into two regimes: undoped and doped polymers. As discussed within Chapter I, the ISH model has successfully been able to predict the relationship between both conductivity and thermoelectric power coefficient, and trace levels of doping. It is within this context that undoped characteristics will be addressed. At doping concentrations above the semiconductor-to-metal transition, SMT, conduction via a variable range hopping among soliton-like states, VRH, appears in favor.

Undoped Cis-Rich Polyacetylene

Room Temperature Conductivities

Polyacetylene films from 500 \bar{M}_n to 870,000 \bar{M}_n were prepared at 195 K. In Chapter IV, it was shown that for low \bar{M}_n polymers, after handling at room temperature, somewhat greater trans contents were observed than for 10,500 or 25,000 \bar{M}_n polymers. This point was also reflected in the cis-rich EPR spin concentrations $[S]$ described in

Chapter V. It is within that context that the results of Table 6.1 should be examined. As can be seen, little variation in conductivities was seen, though the low \bar{M}_n materials had conductivities ca. 100 times greater than for the standard 10,500 \bar{M}_n films. This can be attributed to either an enhanced $[\dot{S}]$ concentration, or as will be discussed later in this chapter, increased charged impurity levels. In light of results from Chapter V, the later is likely.

Cis-Trans Isomerization Kinetics

A very sensitive technique for monitoring changes in the structure of polyacetylene during thermal isomerization is to measure changes in conductivity. Kivelson's ISH model for conduction in undoped trans- $[CH]_x$ directly relates the number of charged and uncharged states to the bulk conductivity (Eq. 1.22). In this way, conductivity may be used to follow the evolution from cis to trans polyacetylene.

Figures 6.1, 6.2 and 6.3 show the elevated temperature conductivities for \bar{M}_n , 10,500 \bar{M}_n , and 870,000 \bar{M}_n polyacetylenes during isomerization at temperatures from 383 K to 468 K. Fresh cis-rich samples containing from 83% to 90% cis isomer were used for all experiments. Samples were isomerized under dynamic vacuum using either a modified four probe or the isomerization chamber shown in Fig. 2.9. It should be noted that the temperatures reported here are generally much lower than those reported by Bernier et al.¹⁷⁴ Consequently, the resistivity reversal common to his results was not observed within the time frame under which these experiments were carried out.

Table 6.1
Undoped Cis-[CH]_x Conductivities.

\bar{M}_n	$\sigma_{RT}, (\Omega \cdot \text{cm})^{-1}$	$\log \sigma$
500	$(2.6 \pm 1.6) \times 10^{-9}$	-8.59 ± 0.25
ca. 500 ^a	1.8×10^{-9}	-8.74
10,500	$(2.5 \pm 1.6) \times 10^{-11}$	-10.60 ± 0.20
ca. 100,000	4.0×10^{-11}	-10.40
210,000	3.1×10^{-11}	-10.50
270,000	5.4×10^{-10}	-9.27

^a [CD]_x

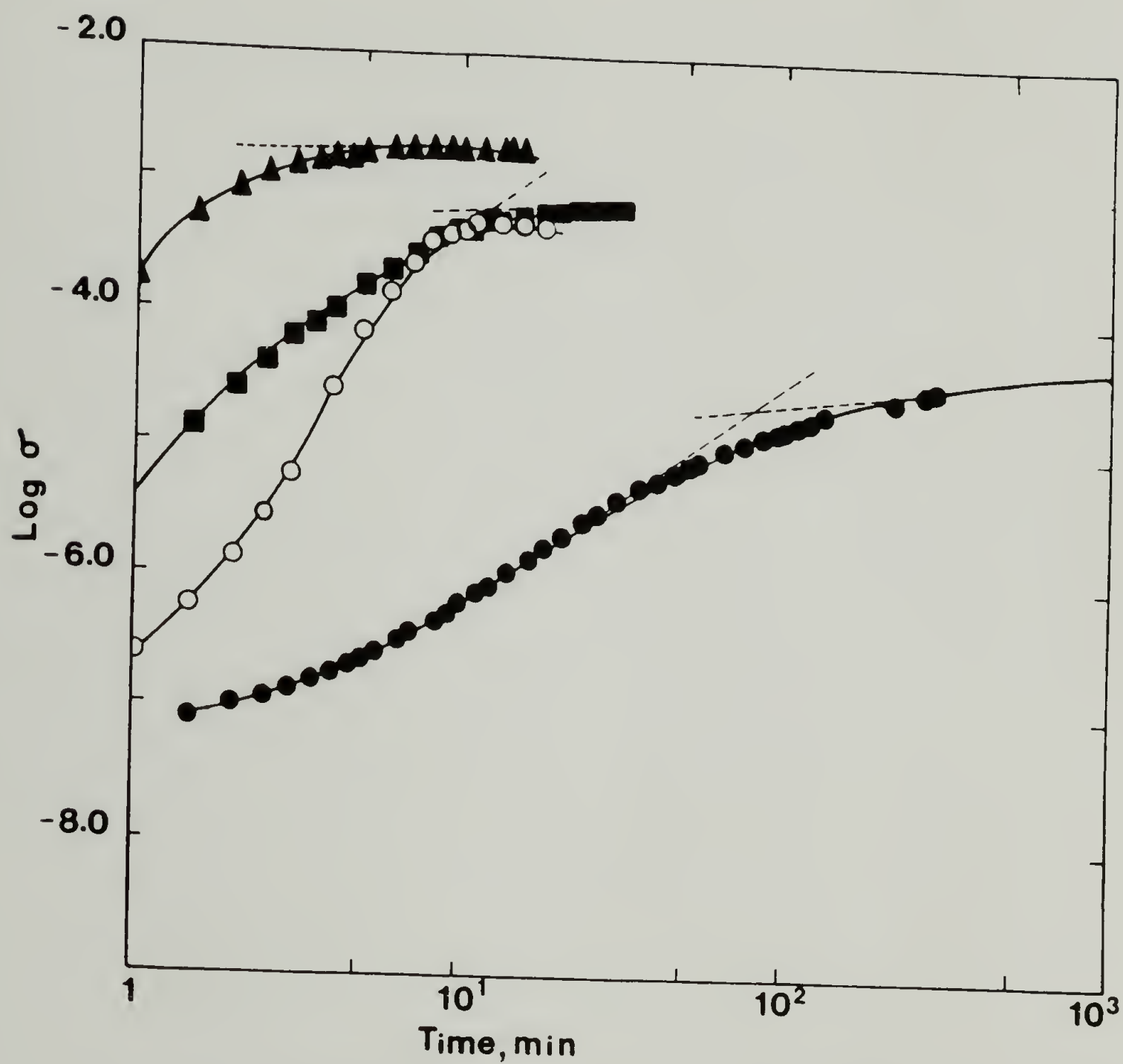
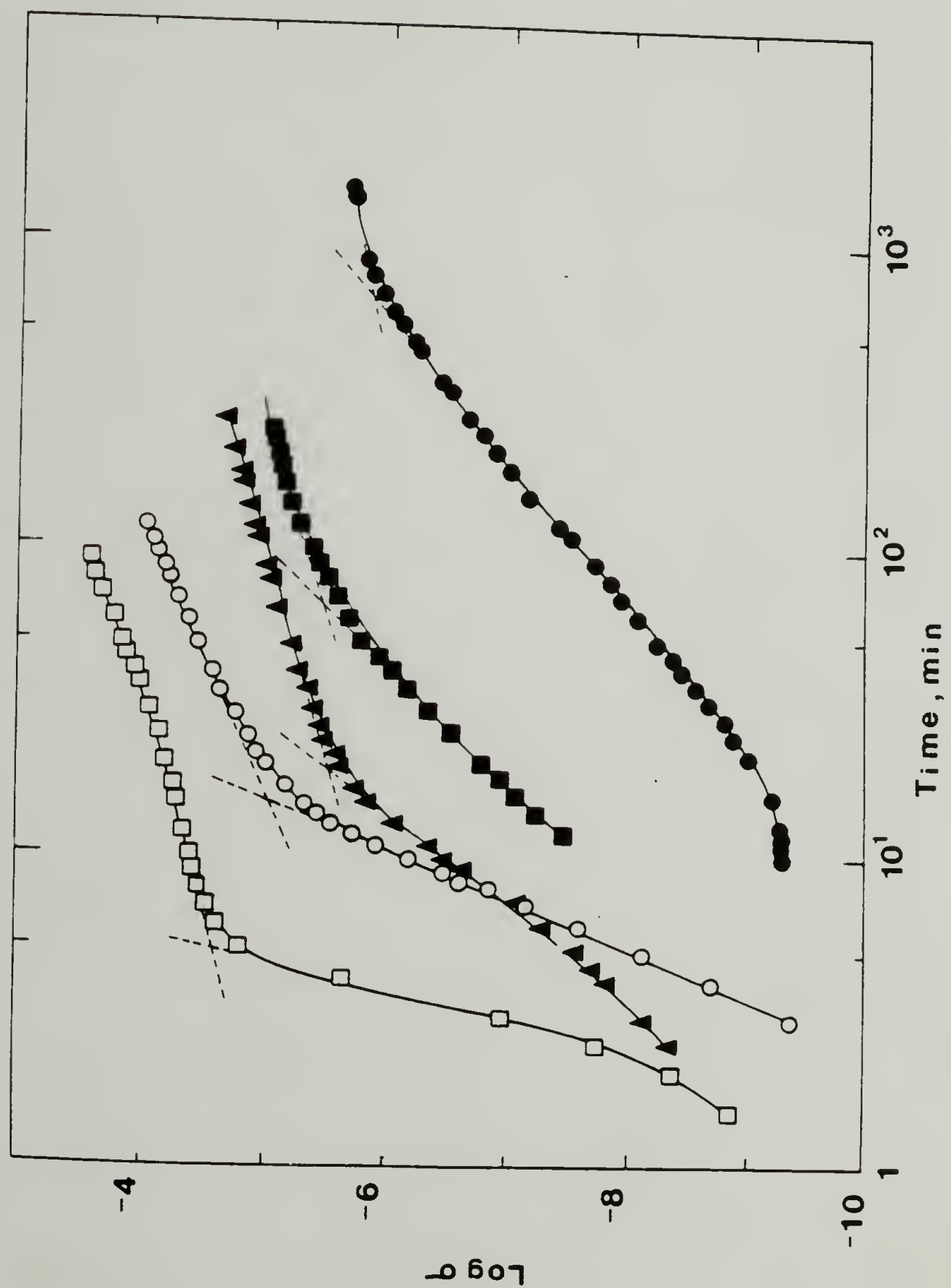


Figure 6.1 Conductivity Isomerization of: 500 $\bar{\text{Mn}} [\text{CH}]_x$ at (\bullet) 383 K; (\blacksquare) 423 K; and (\blacktriangle) 453 K. Also ca. 500 $\bar{\text{Mn}} [\text{CD}]_x$ at (\circ) 453 K.

Figure 6.2 Conductivity Isomerization of 10,500 Mn $[\text{CH}]_x$ at : (●) 383 K, (■) 418 K, (▲) 423 K, (○) 441 K, and (□) 468 K.



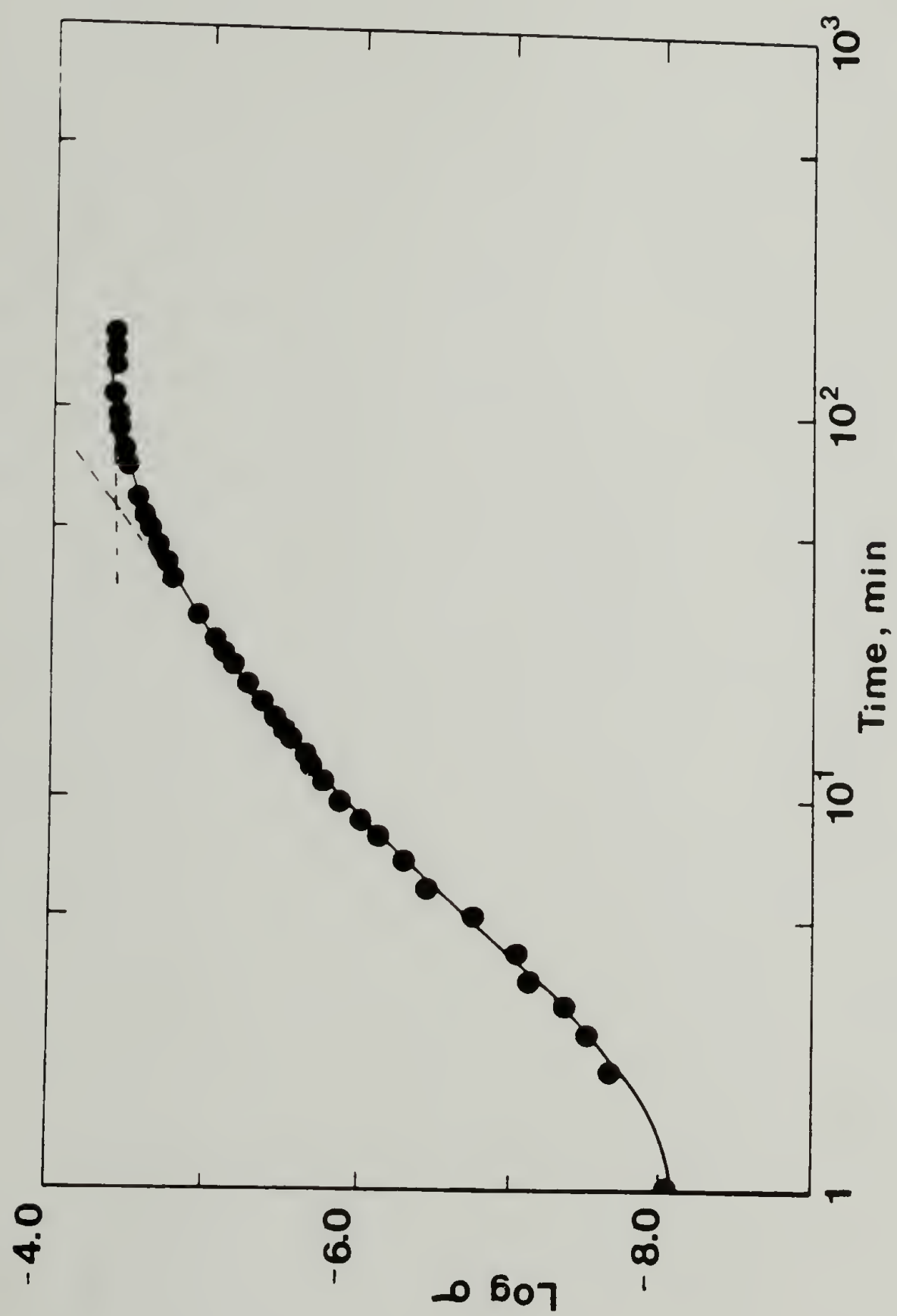
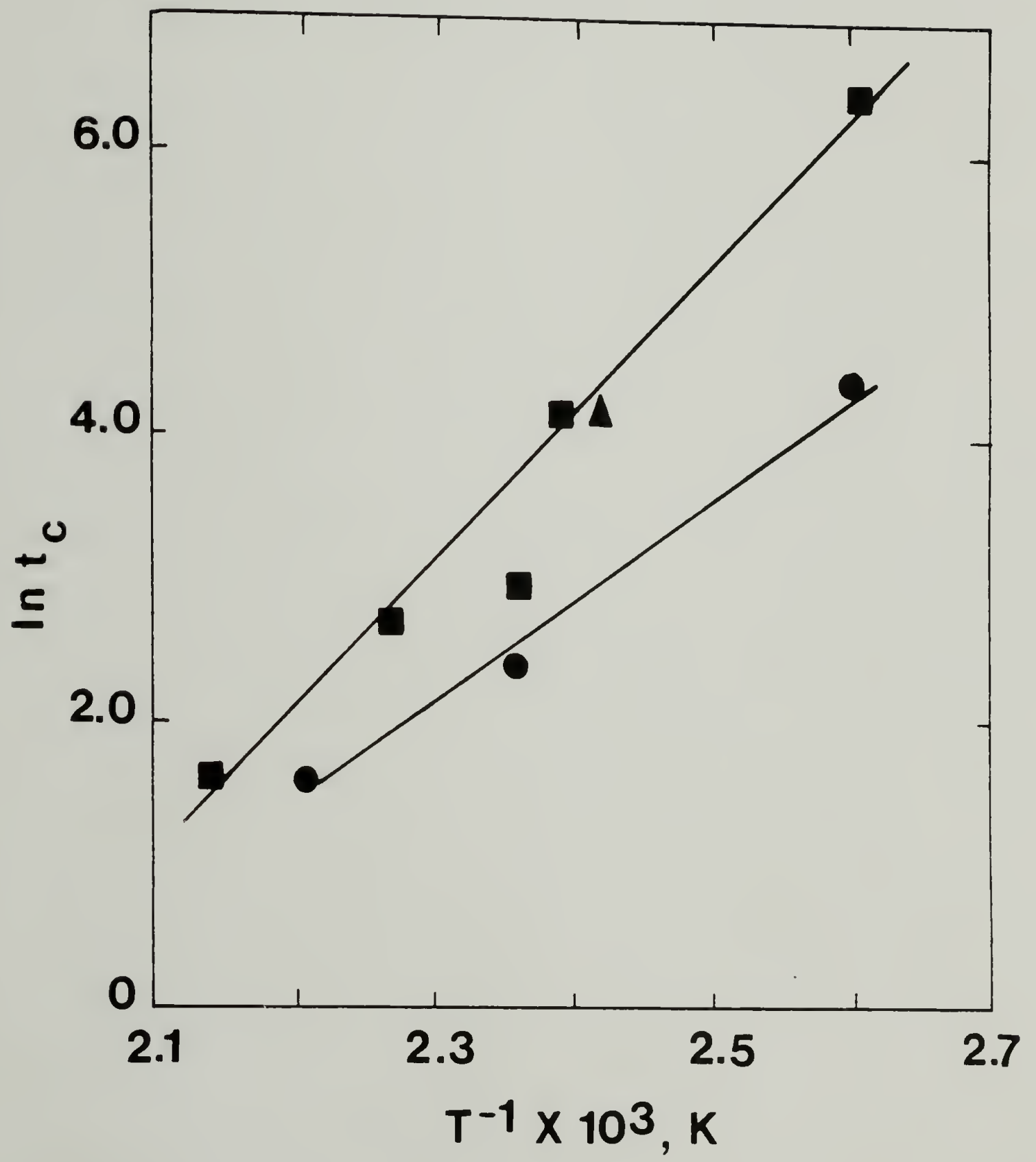


Figure 6.3 Conductivity Isomerization of 870000 \bar{M}_n [CH]_x at (●) 413 K.

In low \bar{M}_n polymer, at all temperatures above 383 K, a constant conductivity was observed after relatively short isomerization times. Therefore at 423 K it took 11 min, and at 453 K only 5 min. to reach a constant conductivity. With 10,500 \bar{M}_n polymer on the other hand, no constant conductivity values were observed even after long periods of time (Fig. 6.2). For both molecular weights at 383 K, even after 17 hrs. increases in conductivity were recorded. What seems to be occurring is a two-stage annealing process characterized by differing activation energies. The extrapolated characteristic time, t_c , at which the initial very rapid annealing process ceases and the thermodynamically more difficult second stage process commences can be obtained from the extrapolated intersection of the two characteristic processes. Figure 6.4 is the Arrhenius plot for these times for 500 \bar{M}_n , 10,000 \bar{M}_n , and 870,000 \bar{M}_n polymers. A linear relationship exists for the two lower \bar{M}_n samples, with activation energies of 14 Kcal·mol⁻¹ and 21 Kcal·mol⁻¹ for 500 \bar{M}_n and 10,500 \bar{M}_n respectively. The characteristic time for 870,000 \bar{M}_n polymer at 413 K superimposes on the curve for 10,500 \bar{M}_n polymer and perhaps may be characterized by the same E_A . It is interesting to note that the cross-over point for these two curves appears at 1 min. and 498 K. These activation energies fall on either side of the 18 Kcal·mol⁻¹ obtained by Bernier.¹⁷⁴

The concept of a two-stage structural rearrangement process is supported by recent optical spectroscopy results of Eckhardt.¹⁷⁵ In experiments involving standard polyacetylene of presumably ca. 10,500 \bar{M}_n , samples were isomerized at 383 and 443 K for various time periods. Optical absorption and reflection spectroscopy were used to study the

Figure 6.4 Arrhenius Plot of t_c for (●) 500 Mn, (■) 10,500 Mn, and (▲) 870,000 Mn.



details of the π - π^* transition. For the first time, trans spectra obtained from 443 K/30 min isomerization conditions showed detailed vibronic structure with maxima at 12000 cm^{-1} (1.49 eV) and another at 13000 cm^{-1} . As prepared cis films showed electronic transitions at 16800 cm^{-1} (2.08 eV) and at 18300 cm^{-1} (2.27 eV). Over isomerization (443 K/3 hr) lead to a decrease of the 12000 cm^{-1} band and the emergence of a broad band with a maxima around 14500 cm^{-1} . This reflection spectrum appears similar in appearance to the thin film absorption spectra found in the literature⁸⁷ which show maxima at 15200 cm^{-1} (1.88 eV) and a shoulder at 12300 cm^{-1} (1.52 eV). From this, Eckhardt hypothesises that overannealing introduces defects which shorten the conjugation length and shift the absorption band to higher energies.

This analysis is also consistent with the IR results presented in Chapter IV on thermal isomerization of $10,500\text{ } \overline{M}_n$ films. There, it was shown in $10,500\text{ } \overline{M}_n$ polymer, after a constant trans content was obtained, peak broadening on the low frequency side and a multiplet of maxima appeared for the trans 1010 cm^{-1} CH out of plane bending mode. No such phenomenon was observed in $500\text{ } \overline{M}_n$ polymer.

It is attractive to ascribe these differing activation energies to varying molecular chain lengths. Presumably structural rearrangement and neutral spin generation which accompanies cis-trans isomerization occurs more arduously with high \overline{M}_n polymer and to lower degrees of perfection. As with most polymer properties however, a critical molecular weight is soon reached after which no further differences occur. The superposition of results for $870,000\text{ } \overline{M}_n\text{ [CH]}_x$ in Figure 6.4 suggests

that this critical molecular weight occurs at or below 10,500 \bar{M}_n .

Undoped Trans Polyacetylene

Room Temperature Conductivity and Thermoelectric Power

A very large number of room temperature trans conductivity measurements, σ_{RT} , were made for samples with molecular weights ranging from 500 \bar{M}_n to 870,000 \bar{M}_n . This includes samples isomerized under various time/temperature conditions. Table 6.2 summarizes the measured undoped transport properties. All conductivity measurements were carried out on films 20-80 μ m thick, at room temperature and generally under dynamic vacuum. Thermoelectric coefficient measurements were made under dry nitrogen at room temperature and a 2-4° temperature differential.

For undoped trans- $[\text{CH}]_x$, there appears to be a trend of decreasing conductivity with increasing \bar{M}_n . For example, 500 \bar{M}_n polymer has an average $\log \sigma_{RT}$ of -5.01 ± 0.29 as compared to -6.27 ± 0.75 for 10,500 \bar{M}_n and -7.00 ± 0.88 for the higher \bar{M}_n samples. These results are supported by the zero current thermopower coefficients, S . Low \bar{M}_n polymers exhibit values of S of ca. 1100 $\mu\text{V}\cdot\text{K}^{-1}$ verses 1450 ± 150 $\mu\text{V}\cdot\text{K}$ reported by Warakomski¹¹⁰ for 10,500 \bar{M}_n polymer and 2000 $\mu\text{V}\cdot\text{K}^{-1}$ for 870,000 \bar{M}_n $[\text{CH}]_x$. No differences between $[\text{CH}]_x$ and $[\text{CD}]_x$ were observed.

The question of whether these observed conductivity variations can be traced to \bar{M}_n differences requires more attention. In acetylene polymerization, there are basically three means of controlling \bar{M}_n : (1) monomer concentration, (2) catalyst concentration and (3) catalyst acti-

Table 6.2
Undoped Trans-[CH]_x Conductivities.

\bar{M}_n	Isomerization Conditions	$\sigma \times 10^8$ ($\Omega \cdot \text{cm}$) ⁻¹	log σ	$S, \mu\text{V} \cdot \text{K}^{-1}$
500	383 K/16.7 hr	280	-5.56	1600
	423 K/30 min	1900	-4.73	1270
	423 K/20 min	860	-5.06	-
	453 K/10 min	1100	-4.95	-
	453 K/15 min	3100	-4.51	1000, 1150
	453 K/20 min	1000	-5.00	1300
	463 K/10 min	1100	-4.96	-
ca. 500 ^a	433 K/15 min	450	-5.36	-
	453 K/20 min	1200	-4.93	1020
10,500	383 K/24 hr.	4.7	-7.33	
	418 K/4 hr.	16	-6.85	
	423 K/4.5 hr.	26	-6.58	1450+150 ^b
	441 K/120 min	63	-6.22	
	468 K/90 min	400	-5.38	
	517 K/17 min	500	-5.26	
ca. 100,000	453 K/40 min	1.0	-8.00	-
	453 K/40 min	2.5	-7.60	-
210,000 ^c	453 K/20 min	3.3	-7.48	
	453 K/20 min	110	-5.95	
870,000	413 K/2.67 hr	630	-6.20	2000
	413 K/2.67 hr	190	-5.72	-

^a [CD]_x

^b Ref. 110

^c Initial value obtained within 24 hrs. of polymer preparation, second value obtained after 4 weeks storage under vacuum at 195K.

vity. The later is controlled principally by adjusting the Al/Ti ratio. Therefore, by choosing different monomer to catalyst ratios, different molecular weights are possible. In this way polymers with M_n 's greater than 10,500 were obtained. All samples in Table 6.2 with $M_n > 10,500$ were prepared at $[Ti]_0 = 1$ mM. Yet for fresh samples, undoped conductivities were roughly the same. On storage, though, an increase in σ_{RT} was observed, presumably due to adventitious low level doping by oxygen or the like. On the other hand, by enhancing the $[Ti]_0$ concentration to 200 mM for 10,500 \bar{M}_n and 740 mM for 500 \bar{M}_n polymer, a steady increase in undoped σ_{RT} resulted.

The suggestion that the enhanced conductivity of low \bar{M}_n polymer is due to charged impurities is supported by thermopower results. In general thermoelectric power may be expressed by the Heikes formula:

$$S = + \frac{k_B}{|e|} \ln\left(\frac{1-\rho}{\rho}\right) \quad (6.1)$$

Where $\rho = n \cdot N^{-1}$ is the ratio of number of holes n to the number of available sites N . This expression applies to spinless Fermi ions. Moses et al.¹⁷⁶ found that by analyzing S within the terms of ISH, Kivelson's equation may be recast into:

$$S = + \frac{k_B}{|e|} \left\{ \frac{x+2}{2} + \ln\left(\frac{y^0}{y^+}\right) \right\} \quad (6.2)$$

Their estimate of $y^+ \sim 3 \times 10^{-5}$ was based on $S \sim 850 \mu V \cdot K^{-1}$, $x=13$ and $y^0 \sim 3 \times 10^{-4}$. Using this expression and also assigning $x=13$ $k_B \cdot |e|^{-1} = 86 \mu V \cdot K^{-1}$ and $y^0 \sim 4 \times 10^{-4}$, estimates of y^+ for low, standard, and high

\bar{M}_n polymer are 2×10^{-6} , 3×10^{-8} , and 6×10^{-11} respectively.

Variable Temperature Conductivity

There are various theories of transport in amorphous semiconductors and these may be distinguished by the temperature behavior of the conductivity. Specifically for polyacetylene, it is believed that a number of mechanisms may play a role, the mechanism of which depends greatly on the impurity level. Table 6.3 lists a few of these conduction mechanisms and their temperature dependence. A number of mechanisms may predict the same temperature dependence. A study of the temperature dependence alone is therefore not always sufficient to determine the mechanism in effect. A more complete treatment of the subject may be found elsewhere.¹

The variation of conductivity with temperature below ambient conditions was studied for 500 \bar{M}_n and 25,000 \bar{M}_n polymers. $\log \sigma(T)$ plotted against T^{-1} , $\log T$, $T^{-1/4}$ and $T^{-1/2}$ for these two samples are shown in Figures 6.5, 6.6, 6.7, 6.8 respectively. For undoped trans-[CH]_x, Epstein et al.¹³³ and Moses et al.¹⁷⁶ found equally good fits for both $\log \sigma$ vs $\log T$ and $\log \sigma$ vs $T^{-1/4}$. The slope of the former was 13-14, in close agreement with a slope of 10 predicted by ISH. A thermal activation energy for bound carriers of 0.3-0.4 eV was obtained by Park et al.¹³⁰ from the Arrhenius conductivity plot, using $k_b = 8.63 \times 10^{-5}$ eV·K⁻¹. Warakomski¹¹⁰ also found this to be true for undoped trans polymer.

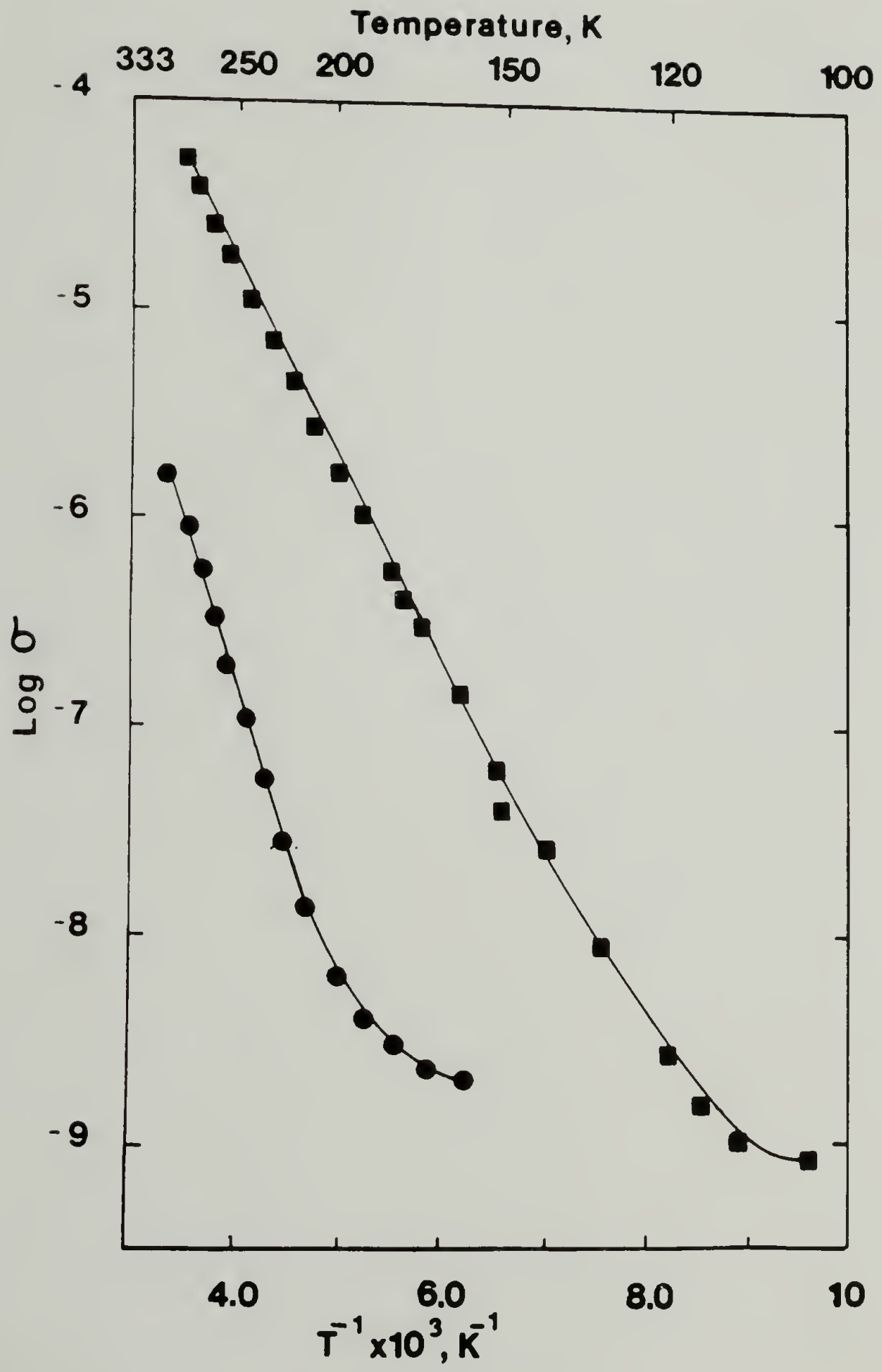
A summary of results for 500 \bar{M}_n and 25000 \bar{M}_n polymers is found in Table 6.4. For neither sample did $T^{-1/4}$ fit well. The predicted $\log T$

Table 6.3

Predicted Temperature Dependence on Conductivity for
Various Conduction Mechanisms.

Conduction Mechanism	Temperature Dependence	Reference
Thermally Activated Hopping to Extended States	$\log \sigma$ <u>vs.</u> T^{-1}	131,132
Activated Hopping in Band Tails	$\log \sigma$ <u>vs.</u> T^{-1}	179
1-D Variable Range Hopping	$\log \sigma$ <u>vs.</u> $T^{-1/2}$	177
3-D Variable Range Hopping	$\log \sigma$ <u>vs.</u> $T^{-1/4}$	178
Variable Range Hopping Among Soliton-Like States	$\log (\sigma \cdot T^{-1/4})$ <u>vs.</u> $T^{-1/4}$	135,136
Intersoliton Hopping	$\log \sigma$ <u>vs.</u> $\log T$	131,132
Fluctuation-Induced Tunneling	$\log \sigma$ <u>vs.</u> $T^{-1/2}$, $\phi < \phi_c$ $\log \sigma$ <u>vs.</u> $T^{-1/4}$, $\phi > \phi_c$	180

Figure 6.5 $\text{Log } \sigma$ versus T^{-1} for (●) 500 Mn and (■) 25,000 Mn
 $\overline{\text{Trans}}\text{-[CH]}_x$.



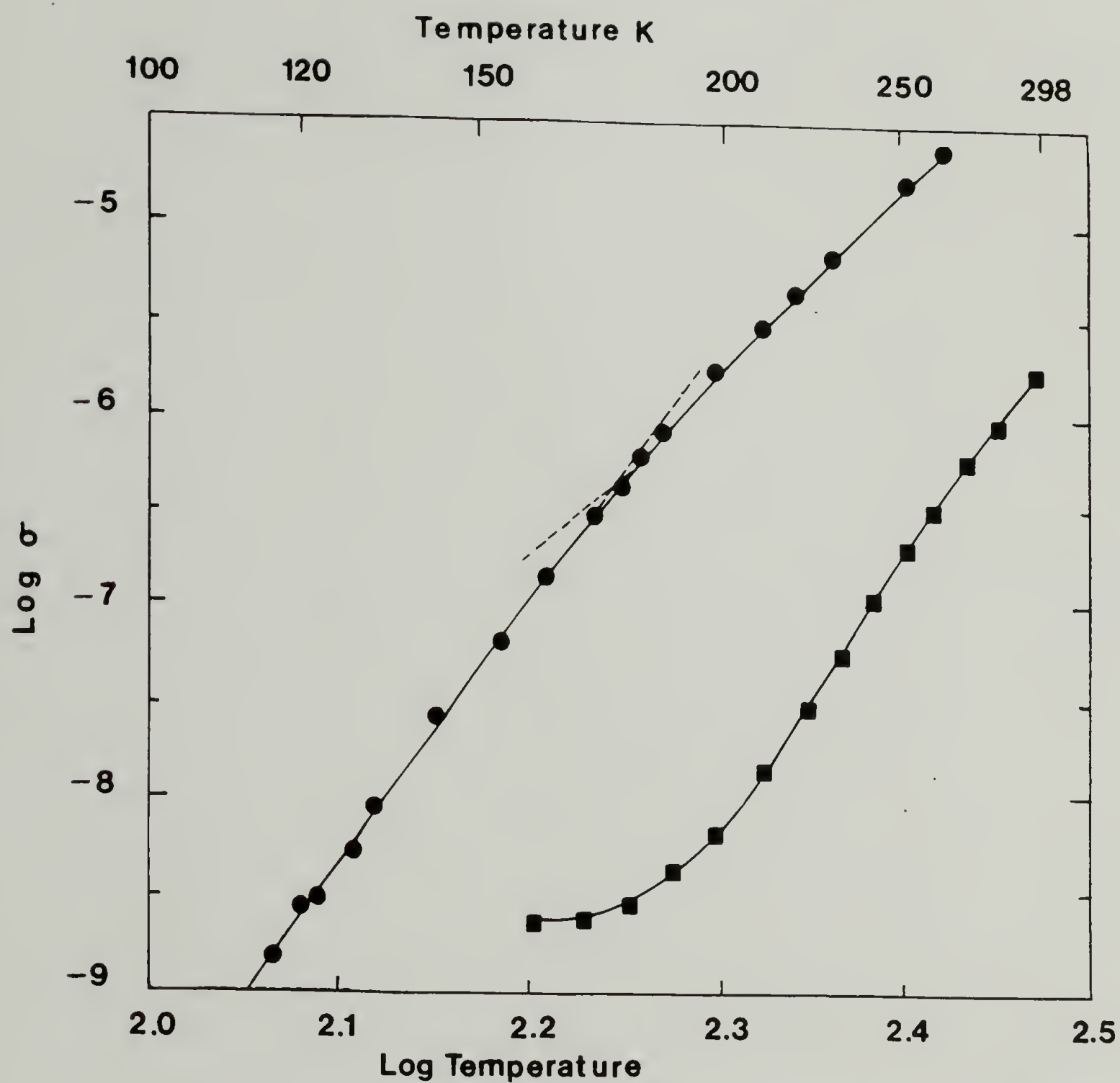


Figure 6.6 $\text{Log } \sigma$ versus Log Temperature for (\bullet) $500 \bar{M}_n$; and (\blacksquare) $25000 \bar{M}_n \text{ Trans-}[\text{CH}]_x$.

Figure 6.7 Log σ versus $T^{-1/4}$ for (●) 500 Mn and (■) 25,000 Mn Trans-[CH]_x.

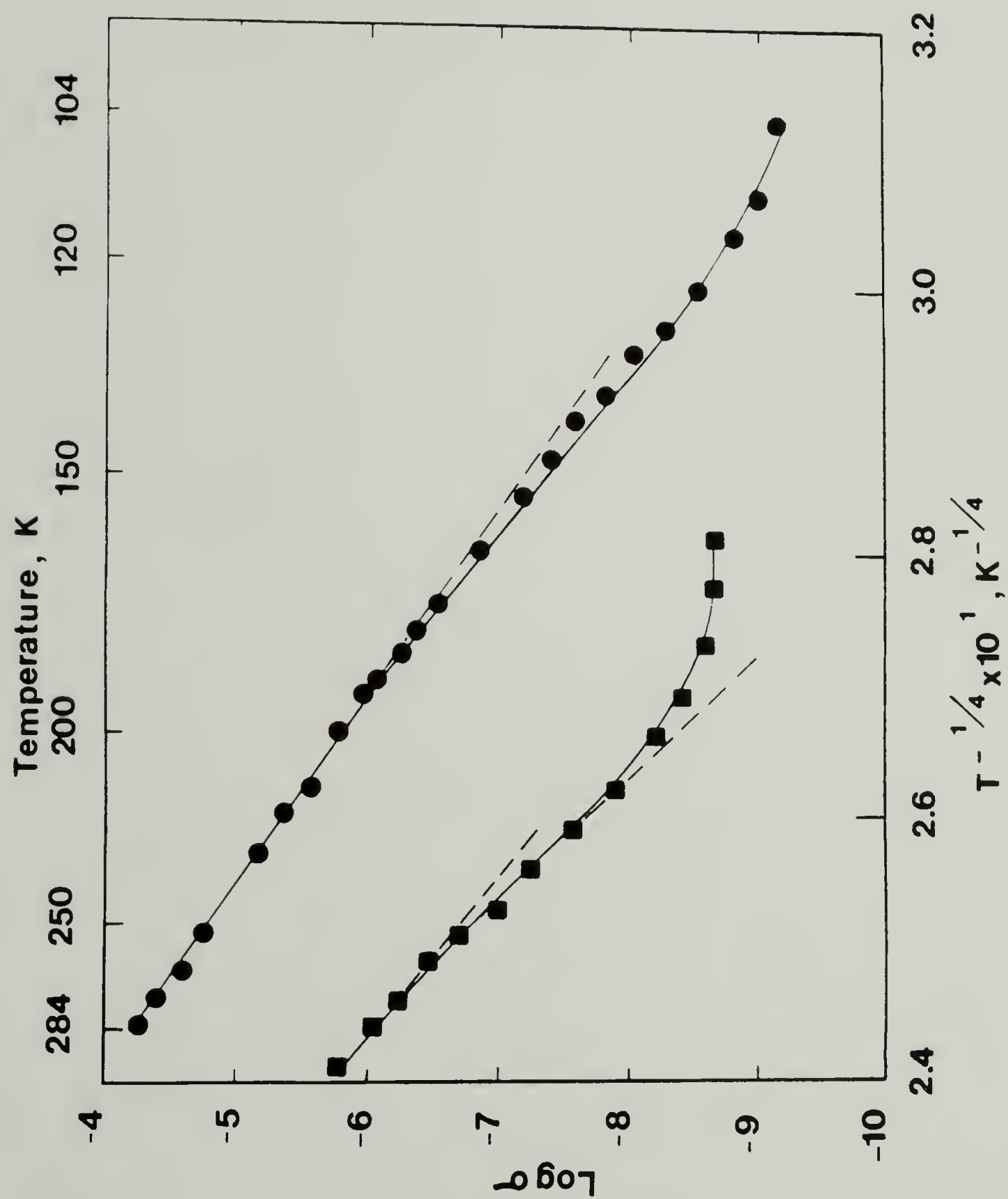


Figure 6.8 Log σ versus $T^{-1/2}$ for (●) 500 Mn and (■) 25,000 Mn Trans-[CH]_x.

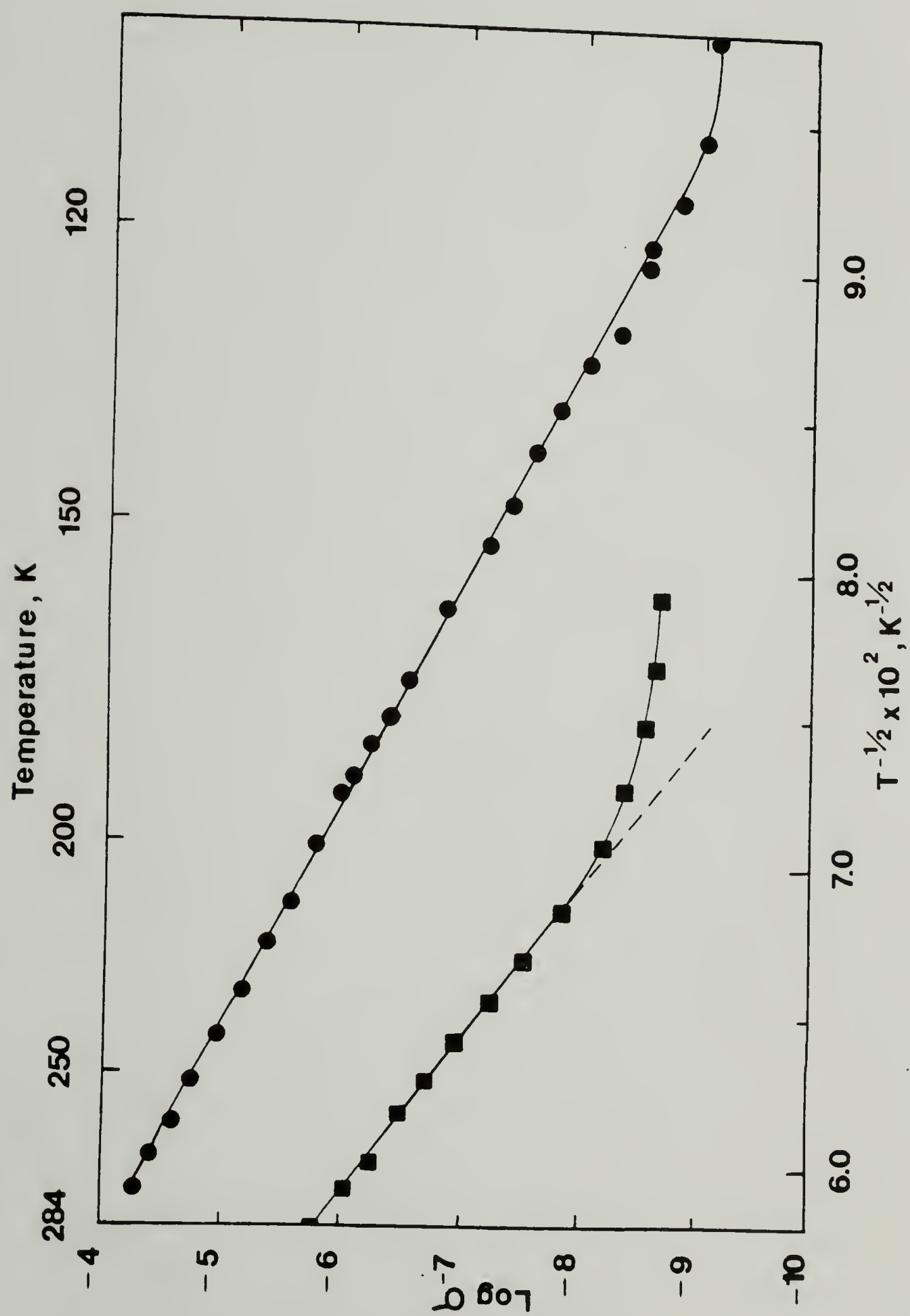


Table 6.4

Summary of Variable Temperature Conductivity Measurements.

\bar{M}_n^a	E_b^b	$\log \sigma$ vs. $\log T$ slope	Best Fitting Plot	Worst Fitting Plot
500	0.19eV	10-13	$T^{-1/2}$	$\log T, T^{-1/4}$
25,000	0.31eV	14	$\log T, T^{-1}$	$T^{-1/4}$

^a Isomerization conditions: 500 \bar{M}_n -453 K/15 min;
25000 \bar{M}_n -453 K/30 min.

behavior does not hold in 500 \overline{M}_n polymer. This polymer also showed a markedly lower binding energy in comparison to literature and the results for 25,000 \overline{M}_n polymer. Low \overline{M}_n samples routinely show higher undoped conductivities and lower thermoelectric powers and so are consistent with the lower E_b . These results also support the hypothesis of adventitious doping by catalyst components.

$^{125}\text{I}_2$ Doped Cis Low Molecular Weight Polyacetylene

Room Temperature Doped Conductivity and Thermoelectric Power Measurements

Using $^{125}\text{I}_2$, doping of cis 500 \overline{M}_n polyacetylene was carried out spanning 5.5 orders of magnitude of I_3^- . The slow doping technique as outlined in Chapter II was used. A single strip of polyacetylene was used to monitor conductivity. Doping level was measured by gamma counting. A note should be made at this time. It was found that the apparatus used and shown in Fig. 2.8 is extremely sensitive to small leaks. Consequently an equilibrium iodine distribution from one part of the chamber to the other was not always possible. Therefore a finite degree of uncertainty exists in assuming that the samples for gamma counting were doped to the same level as the sample used to measure conductivity. Consequently, for a given sample conductivity, only the fractional dopant concentration, relative to maximum doping, may be assigned.

Figure 6.9 plots the semiconductor-to-metal transition observed for cis LMnP using room temperature conductivity measurements. The mid-

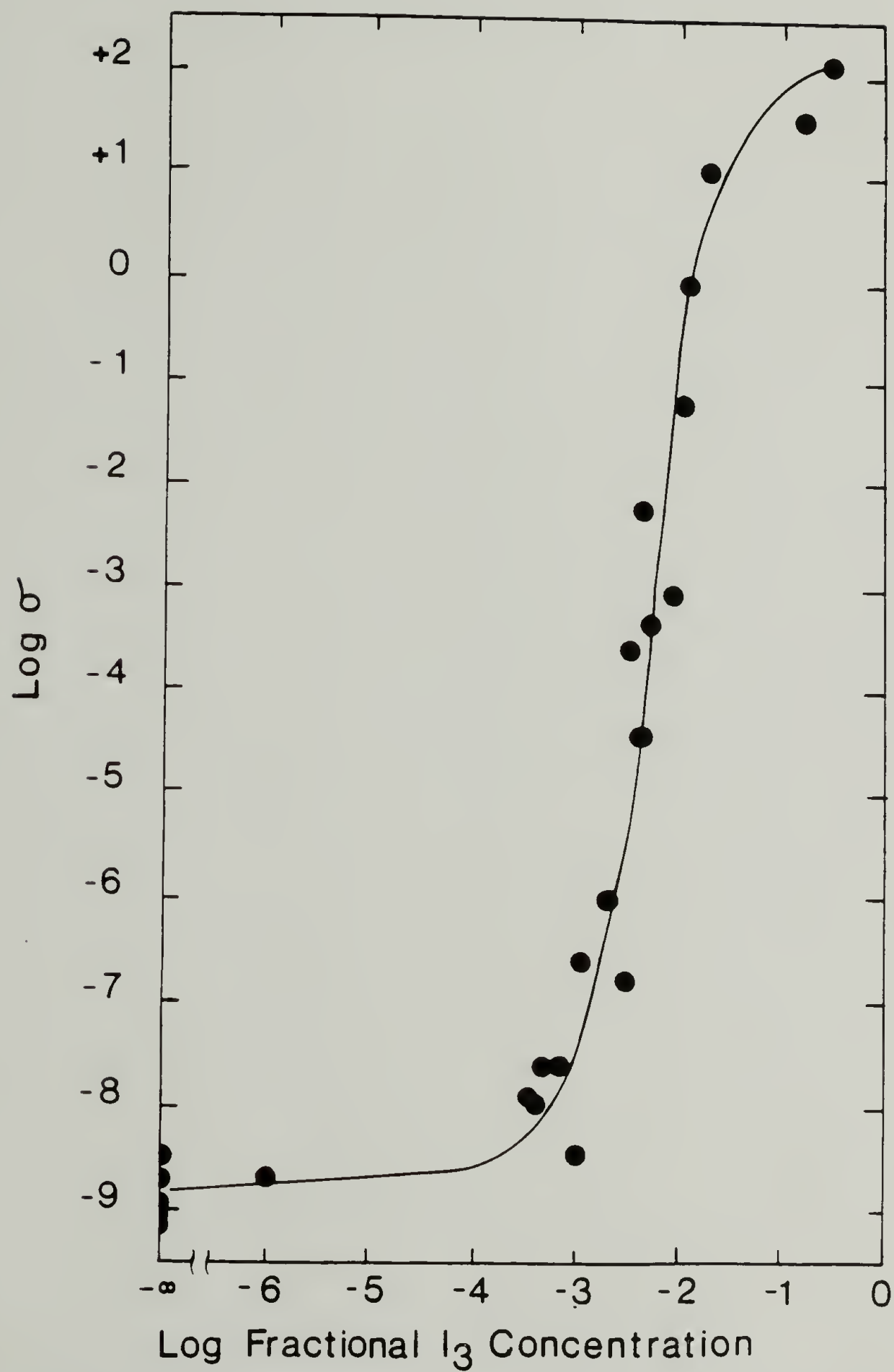


Figure 6.9 $\text{Log } \sigma$ versus $\text{Log Fractional } \text{I}_3^- \text{ Concentration}$
for $\text{Cis } 500 \bar{\text{Mn}} [\text{CH}]_x$.

point of the transition appears at ca. $10^{-2.5}$ fractional I_3^- concentration based on a maximum doping concentration of 0.3% I_3^- . Between $Y=10^{-\infty}$ and $10^{-3.5}$ fractional I_3^- concentration, the σ_{RT} remains constant and was not significantly different than for the undoped material. Above this, there is an abrupt rise in conductivity by nine orders of magnitude within one and one-half orders of magnitude increase in iodine content. Maximum doping by overnight exposure to iodine and at 0.45 mm Hg vapor pressure (room temperature conditions) gave a limiting conductivity of $130 (\Omega \cdot \text{cm})^{-1}$ at $Y(I_3)^- = 10^{-2.5}$. In a separate experiment, a maximum doped conductivity of $100 (\Omega \cdot \text{cm})^{-1}$ was obtained. Maximum doped polymer thermopower value of $+42 \mu\text{V} \cdot \text{K}^{-1}$ are in agreement with the sample being highly conductive containing a high density of positively charged carriers.

The results presented here are in general agreement with those published by Warakomski¹¹⁰ for iodine doped cis- $[\text{CH}]_x$ of $10,500 \bar{M}_n$. In that work, maximum doped conductivities of $200\text{--}400 (\Omega \cdot \text{cm})^{-1}$ and thermopowers of ca. $30 \mu\text{V} \cdot \text{K}^{-1}$ were observed. It is unfortunate that absolute iodine levels cannot be ascribed to the present results. For $10,500 \bar{M}_n$ polymer, the midpoint of the SMT occurs at ca. $10^{-3.25} I_3^-$. This compares well to the maximum in $[\dot{S}]$ observed for $500 \bar{M}_n$ polymer (Fig. 5.8) and the drop in Curie spin susceptibility.

$^{125}\text{I}_2$ Doped Trans Low Molecular Weight Polyacetylene

Room Temperature Doped Conductivity and Thermoelectric Power Measurements

Trans LMnP was also doped with $^{125}\text{I}_2$ over a concentration range

spanning four orders of magnitude. Samples were isomerized at 453 K for 20 minutes generally; the conditions found to be optimal based on IR, conductivity and EPR results. Figure 6.10 plots the observed SMT over relative iodine content. Again doping problems inherent with the cis experiments were experienced in this study. Therefore only fractional I_3^- concentrations may be ascribed. No change in conductivity was observed with low level doping. An abrupt increase in conductivity takes place at $10^{-2.5}$ fractional I_3^- content which coincides with the SMT observed for cis-[CH]_x.

Maximum doping levels for 500 \overline{M}_n polymer were in all attempts not as high as seen for 10,500 \overline{M}_n using iodine. Table 6.5 reports the results from a few experiments. It is interesting to note that also in this polymer, trans doped conductivities were generally lower than for the cis doped polymer. This phenomenon is usually observed in all conductivity studies involving polyacetylene. This, at first, would not have predicted based on the isomerization results. Low \overline{M}_n polymer was found to reach a constant conductivity at short treatment times, exhibit no spectral broadening of the trans CH out of plane bending mode at 1010 cm^{-1} , and reach a constant, narrow EPR linewidth at short isomerization times. A "purer" trans is thought possible in L \overline{M}_n P though no Resonance Raman experiments have been performed. This suggests that differences between doped cis polymer which undergoes chemically induced isomerization and doped thermally isomerized trans polymer may be related to subtle structural disorders which were not identified in this dissertation.

From the work of Warakomski,¹¹⁰ a precipitous drop in the ther-

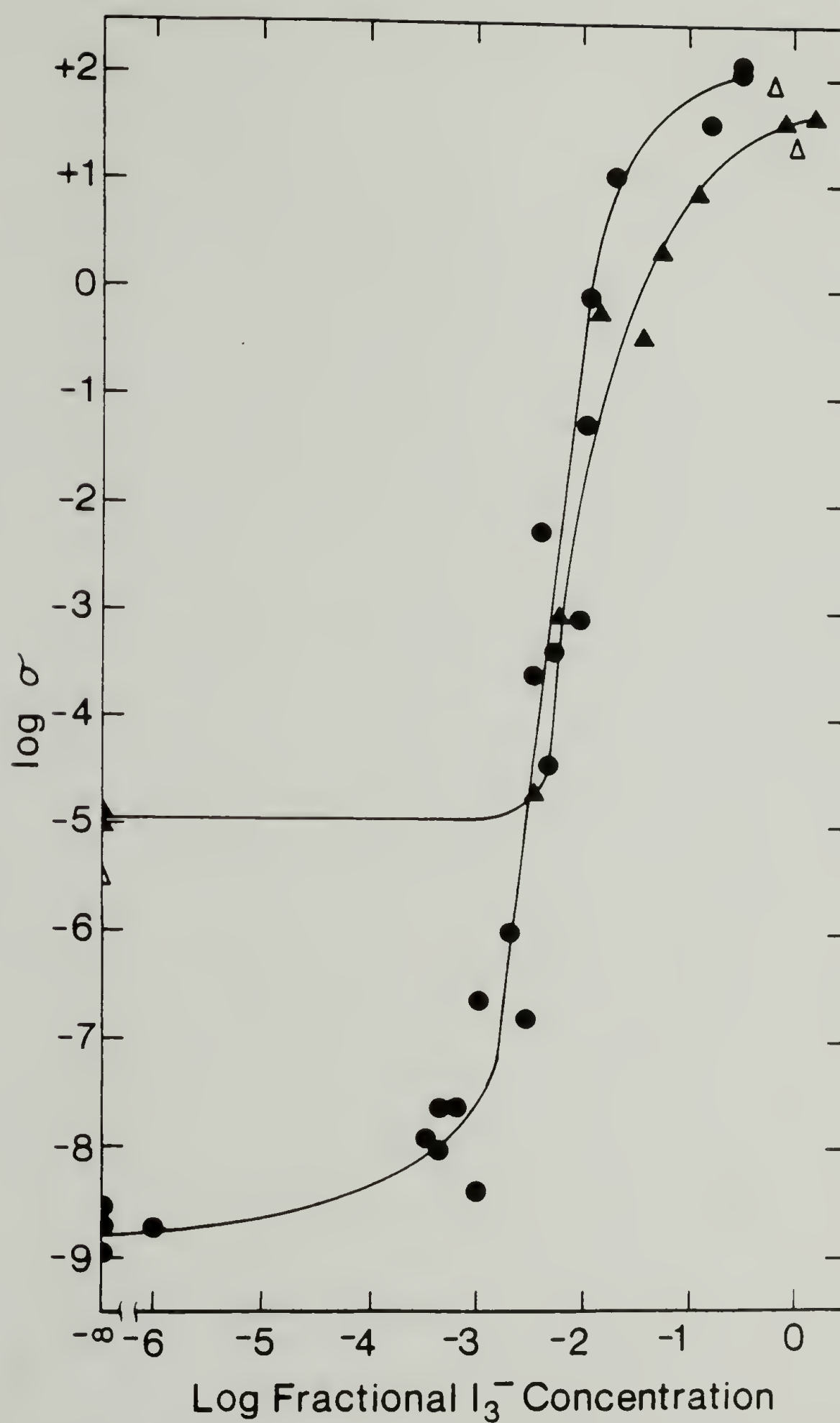


Figure 6.10 Log σ versus Log Fractional I_3^- Concentration for Trans 500 \bar{M}_n (▲) $[CH]_x$; and (Δ) $[CD]_x$. Data from Fig. 6.9 (●) superimposed.

Table 6.5

Maximum I₂ Doped Trans-500 \overline{M}_n Polyacetylene Conductivities.

Isomerization Conditions	$\log Y(I_3)^-$	$\sigma_{RT}(\Omega \cdot \text{cm})^{-1}$	$\log \sigma$	$S, \mu\text{V} \cdot \text{K}^{-1}$
423 K/20 min	-2.20	0.13	-0.87	67
453 K/20 min	-1.75	2.5	+0.40	77
453 K/15 min	-1.32	+190	+2.28	20
463 K/10 min	-1.51	10.3	+1.01	-

thermoelectric power coefficient simultaneous with an abrupt rise in conductivity was observed when 10,500 \overline{M}_n polymer was doped with iodine. Below 4.5×10^{-4} $Y(I_3)^-$, S remained relatively constant at $+1450 \mu V \cdot K^{-1}$. Between 4.5×10^{-4} and 10^{-3} $Y(I_3)^-$, S dropped to ca. $+200 \mu V \cdot K^{-1}$. A slow yet continual decrease above 10^{-3} until maximum doping of ca. $10^{-1.7}$ $Y(I_3)^-$ resulted in final S values of ca. $+50 \mu V \cdot K^{-1}$. A most important conclusion then is that the SMT as observed by σ_{RT} occurs at the same dopant level as that observed by S .

Figure 6.11 plots the SMT observed by S values for iodine doped trans 500 \overline{M}_n $[CH]_x$. A few points for undoped and maximum doped $[CD]_x$ are also included. As with 10,500 \overline{M}_n polymer, a constant S at low doping levels is observed: ca. $+1100 \mu V \cdot K^{-1}$. However, the SMT does not begin to show up until $Y \sim 10^{-3}$ I_3^- and spans about one order of magnitude in dopant concentration. Maximum doped polymer at $Y \sim 10^{-1.3}$ has an S of ca. $+50 \mu V \cdot K^{-1}$. It is important to note that this set of data was collected from the same samples that were assayed for iodine content via gamma counting. Therefore it can be said with total certainty that the SMT begins at 10^{-3} I_3^- in low molecular weight polyacetylene. These results are supported by the EPR analysis presented in Chapter V. Recall that a precipitous drop in spin concentration was observed at 10^{-3} mole percent I_3^- .

$^{125}I_2$ Doped Trans High Molecular Weight Polyacetylene

Room Temperature Doped Conductivity and Thermoelectric Power Measurements

Radioactive iodine-125 and cold iodine were used to dope samples of

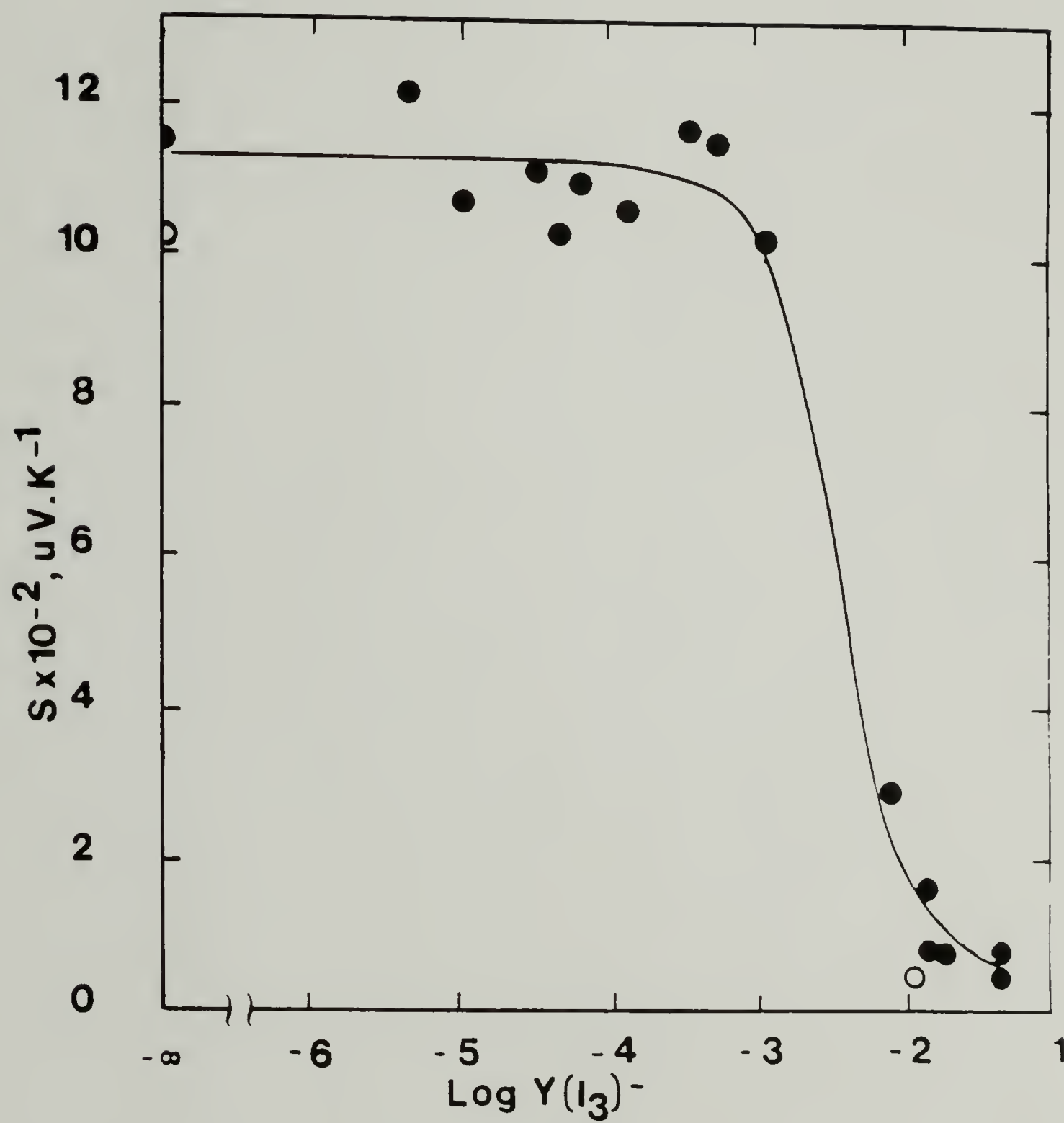


Figure 6.11 S versus $\text{Log } Y(I_3)^{-}$ for Trans 500 $\bar{\text{Mn}}$ (●) $[\text{CH}]_x$; and (○) $[\text{CD}]_x$.

210,000 \overline{M}_n trans $[\text{CH}]_x$. Samples were isomerized at 453 K for 20 min. under dynamic vacuum. Samples below 0.005 mole fraction I_3^- were doped using $^{125}\text{I}_2$ and assayed by gamma counting. Higher doping levels were quantified by measuring the sample weight uptake. For maximum doping, samples were exposed to 0.45 mm Hg iodine (room temperature vapor pressure) overnight. Excess iodine was removed the next day by cryogenic evacuation.

Figure 6.12 plots the resulting conductivity curve for these samples. Superimposed are the data points obtained by Warakomski¹¹⁰ for 10,500 \overline{M}_n polyacetylene. Both samples exhibit an abrupt rise in conductivity at ca. 10^{-3} mole fraction I_3^- . Thermoelectric power measurements at $10^{-2.1}$ and $10^{-1.4}$ $\gamma(\text{I}_3)^-$ doping level gave values of +39 and +29 $\mu\text{V}\cdot\text{K}^{-1}$ respectively; consistent with a high density of charged carriers. Maximum doped conductivities of ca. 50 $(\Omega\cdot\text{cm})^{-1}$ were obtained.

Maximum doping of trans 870,000 \overline{M}_n polymer gave results consistent with those determined for other trans polymers of differing molecular weights. Samples thermally isomerized for 20 min at 453 K and maximum doped overnight gave the following results:

$$\gamma(\text{I}_3)^- : 3 \times 10^{-2}$$

$$\sigma_{\text{RT}} : 10 (\Omega\cdot\text{cm})^{-1}$$

$$S : +75 \mu\text{V}\cdot\text{K}^{-1}$$

Discussion

Within this chapter, conductivity and thermopower results have been

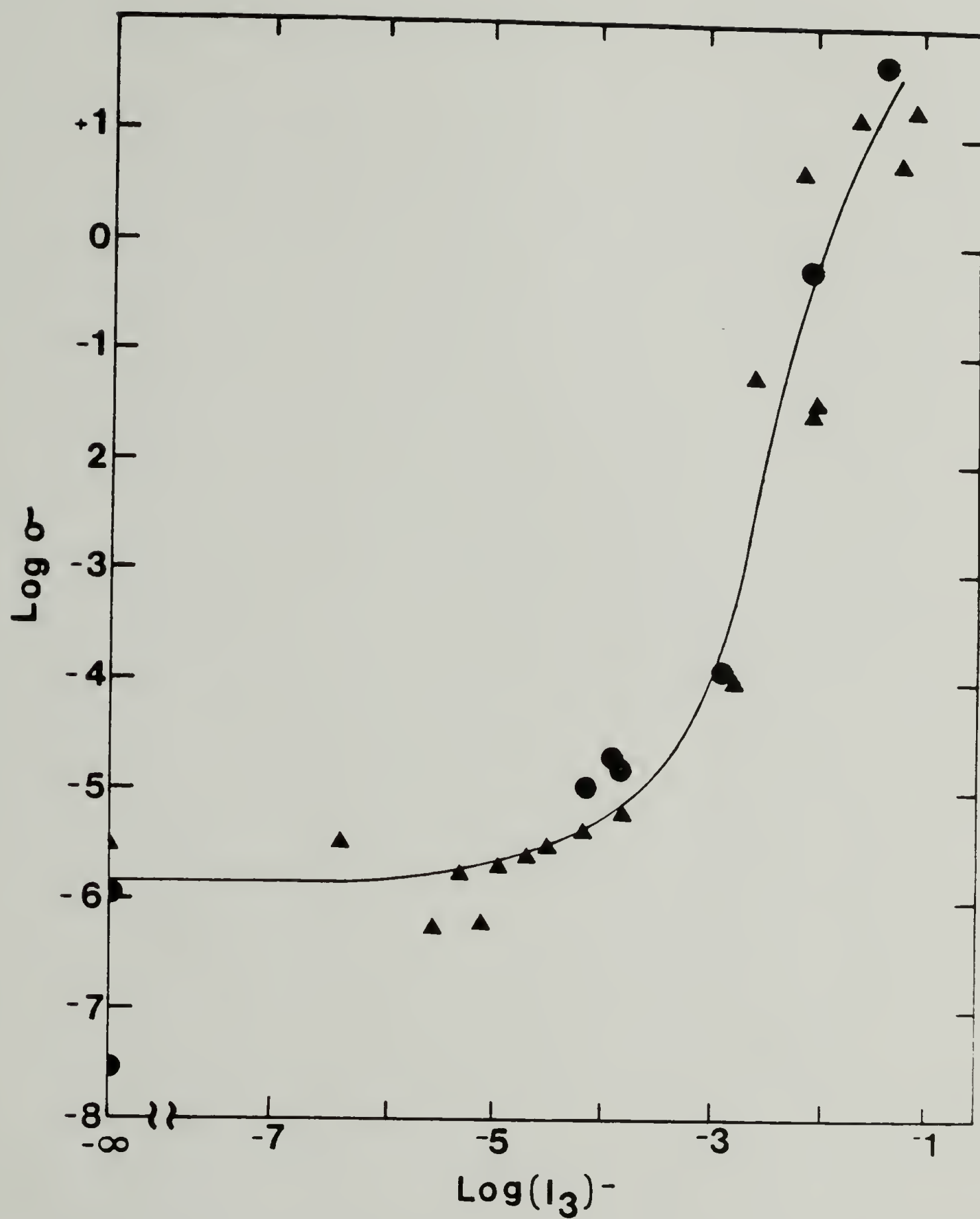


Figure 6.12 $\text{Log } \sigma$ versus $\text{Log } \gamma(I_3)^{-}$ for Trans-[CH] $_x$ (●) 21000 \bar{M}_n ; and (▲) 10500 \bar{M}_n (taken from Ref.#110).

presented for samples with molecular weights from 500 to 870,000 \overline{M}_n . For the purpose of discussion, it is useful to consider these results within the context of samples being either heavily doped, i.e. $\geq 10^{-3}$ mole fraction I_3^- or lightly and adventitiously doped with impurity levels $< 10^{-3}$ γ .

Within this framework, in discussing doped polyacetylene, it is apparent that one dimensional defects in the form of chain ends play absolutely no role in the ultimate transport properties. For both cis and trans low molecular weight polymers, conductivities comparable to those reported for iodine doped 10,500 \overline{M}_n $[CH]_x$ were obtained. Thermoelectric power coefficients and a highly absorbing IR spectra confirm the band gap to be heavily populated with positively charged carriers. No Pauli susceptibility measurements were made though Epstein et al. propose these states to be near the Fermi level. Trans 210,000 \overline{M}_n $[CH]_x$ showed similar conductivity and thermopower results. This demonstrates for the first time that interchain charge migration is the limiting factor in describing the macroscopic conductive properties. Otherwise the difference of 2000 fold in molecular chain length would be reflected in either σ_{RT} or S values. Their virtual independence upon \overline{M}_n can only mean that interchain hopping of carriers is the determining process.

The length of any $[CH]_x$ macromolecular chain is minutely compared to the gross dimension of the polymer specimen. Motion of a carrier confined to a single chain cannot be the significant factor, since there is a net flow of current through the specimen. Only by the

hopping of carriers from one chain to an adjacent one can there be a net transport. These points had been the subject of discussion and speculation by others,¹⁸¹ yet this represents the first experimental evidence in support of those conclusions.

In comparison to the experimental results on 10,500 \bar{M}_n polymer within this laboratory,¹¹⁰ there appears to be a slight trend towards lower levels of maximum doping in polymers of low \bar{M}_n . Any trend, however, is not clear-cut. If one considers polymer-dopant interactions as a one dimensional phenomenon, one would anticipate this to be so. 500 \bar{M}_n polyacetylene has number average \overline{DP} of 20, i.e. 35-40 CH units per molecule. At 6% doping, and along a single chain, one charged solitons, $\overset{+}{S}$, would be created for every 17 CH units. Therefore, at maximum 2.2 charged solitons could be created per chain. If however, iodine does not oxidize the chain near one of the ends such that a second chain oxidation could occur near the other end (two $\overset{+}{S}$ per chain) then each chain could only undergo a one-electron oxidation. In such a case, lower doping levels would be expected for low \bar{M}_n polymer.

From electrochemical doping¹⁸² polyacetylene has been shown to reach a maximum, reversible doping concentration of 6% and insensitive to fibril diameter or counter-ion. Non-reversible oxidation has been shown to reach completion at 50% mole fraction ClO_4^- .¹⁸² This corresponds directly to a perfectly alternating polyethylene-like composition. If one considers the three dimensional distribution of dopant ions at maximum reversible doping levels, a distance between charged sites of ca. 10 Å is calculated. These short distances suggest

perhaps the extent of reversible oxidation is determined by the coulombic repulsion potentials for ions of the same charge. In such a situation, no dependence on molecular chain length should enter into the picture.

The results from undoped trans polymers of differing \bar{M}_n 's offer an insight into the three dimensionality of conduction under very different circumstances. No direct measurements have ever been made of the concentration of charged impurities in undoped polyacetylene. Estimates based on Kivelson's ISH theory and based on thermopower measurements have been made. In both cases, the catalyst concentration under which the polymer has been prepared seems to adequately explain the results. Yet at these extremely low density of charged carriers, no influence of \bar{M}_n is evident. Interchain hopping processes must therefore also be the rate limiting step. These conclusions, based on conductivity measurements, are also in agreement with those from EPR experiments reported in Chapter V.

The above conclusions could not be considered valid if doping inhomogeneities were present. Certainly in the undoped regime, adventitious charged sites, if they are to be traced to catalytic components, would be homogeneously distributed throughout the fibril. At any point during the polymerization, polyacetylene chains would be exposed to impurities within the solvent before being occluded by subsequently polymerized macromolecular chains. In all systems studied, very sharp transitions in conductivity, thermopower, and spin con-

centration were observed. Such SMT's should not be seen for non-uniform samples. Indeed Chien has used these points as a criteria for uniform doping.¹²²

C H A P T E R VII

FINAL CONCLUSIONS AND FUTURE WORK

The focus of this dissertation research has been twofold. In the first phase, the emphasis was to understand the details of acetylene polymerization. To this end, experimental techniques to study olefin polymerizations were applied; specifically through the use of radioactive labels. Knowing the experimental conditions which most significantly influenced the polymerization, the emphasis of this research shifted towards controlling polymer molecular weight. With samples of grossly differing chain lengths, the structural and transport properties were examined. From this, a deeper understanding of structure-property relationships in polyacetylene as a model conducting polymer has been gained. These intrinsic relationships should be applicable to other conducting polymer compositions.

In Chapter III, the complexities of acetylene polymerization became apparent. Because of the heterogeneous nature of the polymerization, a unique dependence of molecular weight on reaction zone and macro-morphology was identified. Within any one polymerization reactor, polymer powders, gels or high density films may result. Because of catalyst exclusion and macroscopic monomer diffusion limitations, these different samples had differing molecular weights. Generally, it was seen that \bar{M}_n increased in the order powder < gel < film; though exceptions did exist.

Earlier, Shirakawa outlined a relationship between polymer macro-

morphology and catalyst concentration, $[Ti]_0$. The results of the kinetics experiments dictated an expansion of this relationship into two or three dimensions in which monomer concentration and catalyst activity represent the other two axis. What defines the macromorphology in acetylene polymerization is the density of polymer fibrils formed within a given reaction volume. Under quiescent or low shear conditions these fibrils result in an interpenetrating network. Any adjustment of polymerization conditions which enhances polymer yield favors film formation.

To adequately describe the kinetic results, a model involving the evolution of highly active centers, C_1 , into much less active C_2 sites was invoked. Bimolecular termination of active centers was defined. Initial active center concentrations represented 3-6% of the total titanium concentration. Chain transfer was found to very strongly influence the ultimate chain length.

Within Chapter IV, it was found that regardless of polymerization temperature, monomer pressure, catalyst concentration, or reaction time, primary fibrils of ca. 200 Å resulted. Variations in conditions which suppress catalytic activity tended to decrease fibril diameter and in the extreme case, fibrillar regularity. These results are consistent with works by Wunderlich,³¹ St. John Manley and coworkers,^{32,33} and Keller³⁴ involving other olefin polymerization systems. The morphology of polyolefins prepared in a simultaneous polymerization-crystallization is very much affected by the physical nature of the catalytic centers. From the work involving acetylene

polymerization using both Ziegler-Natta and Luttinger catalyst at various concentrations, the effect of catalytic contamination on polymer morphology was demonstrated. Without acidic methanol washing of Ziegler-Natta polymerized polymer, spongy, lamellae-like morphologies could be interpreted from TEM's. After washing, clear fibrillar networks became apparent and electron diffraction of these specimens gave fiber-like diffraction patterns.

Also within Chapter IV, some real differences distinguishing low molecular weight polyacetylene from high molecular weight polymer became apparent. From IR results, thermally isomerized LMnP was found to contain greater ultimate trans content. This was based on the observation that higher \overline{M}_n polymers exhibited more intense residual 740 cm^{-1} out of plane CH bending mode characteristic of the cis isomer. Therefore, more "pure" trans isomer was obtainable in $500\ \overline{M}_n\ [\text{CH}]_x$. Another point which became apparent from the IR experiments involved long-time annealing affects. In $10,500\ \overline{M}_n$ and higher polymers, after a relatively constant trans content was obtained, spectral broadening of the trans 1010 cm^{-1} CH out of plane bending mode on the low frequency side was observed. A multiplet of maxima simultaneously appeared. These results were interpreted as being due to structural disorganization involving intermolecular crosslinking or other chain degradation processes. A build up of shorter trans conjugation lengths then results.

From the IR spectra of perdeuterated low molecular weight polymer, no evidence of sp^3 hybridized C-D stretching was found for optimally

isomerized polymer (453 K/20 min). In addition, these samples showed sharp trans out of plane bending absorptions. Therefore, if polymer decomposition does take place upon thermal annealing, it does not commence to any significant degree until the thermodynamically more favored bond rotation processes go to completion, as is the case with low \overline{M}_n polymer, or until the activation energy for further isomerization becomes comparable to that for polymer degradation. These conclusions are supported by works presented in Chapter VI, by Shirakawa and co-workers,⁴⁴ and Bernier et al.¹⁷⁴ From IR data, Shirakawa identified an activation energy of $17 \text{ Kcal}\cdot\text{mol}^{-1}$ for cis-trans isomerization at high cis contents, increasing up to $38 \text{ Kcal}\cdot\text{mol}^{-1}$ at 80% trans. Our work based on the increase in conductivity upon isomerization identified an initial activation energy from 14 to $21 \text{ Kcal}\cdot\text{mol}^{-1}$ depending on polymer \overline{M}_n . For the same experiment, Bernier identified an activation energy $18 \text{ Kcal}\cdot\text{mol}^{-1}$. Based on EPR line width broadening, he also showed that degradation processes to have an activation energy of $\sim 30 \text{ Kcal}\cdot\text{mol}^{-1}$.

Within Chapters V and VI, EPR, σ_{RT} and S measurements were reported for all molecular weights which showed upon doping a sharp transition to occur. These features are taken to imply uniform polymer doping. The fact that one dimensional limitations in the form of chain ends do not play a significant role in dictating the observed transport properties is extremely important. In the case of heavily doped polymers, these results are not surprising. The variable range hopping among soliton-like states mechanism by Epstein et al.¹³⁶ does not con-

sider restrictions imposed by molecular chain lengths. However, in the undoped transport model proposed by Kivelson, the predicted undoped σ_{dc} is inversely related to the N : the number of carbon atoms per chain. No such relationship appears in this work.

The question of how molecular chain length influences the transport properties of conducting "polymers" was addressed by Kossmehl¹⁸³ for oligomeric thiophenediyl vinylenes and poly(thiophenediyl vinylene). In a homologous series of model compounds ranging from one to six repeat units, the band gap energy reached a constant value at $n=6$. This was also true for measured conductivities. Transport properties for the polymeric material exhibited the same property values as the $n=6$ oligomer.

A more recent theoretical approach to elucidating the importance of molecular weight was given by Bredas et al.¹⁸⁴ Using the valence effective Hamiltonian (VEH) technique, the ionization potentials, optical transition energies, and electron affinities of oligomeric and polymeric acetylene compounds were computed. For $[CH]_x$ a 0.4 V oxidation potential vs. standard calomal electrode (SCE) and reduction potential of -1.1 V were calculated. Both are in good agreement with experimentally observed values. The properties predicted by VEH theory are linearly dependent on the inverse of the chain length. According to this work, 500 \overline{M}_n polymer with a number average $\overline{DP} \sim 20$ should exhibit to within 20% the bandgap energy seen in infinitely high molecular weight polymer.

More recent experimental results by Yaniger et al.¹⁸⁵ probe the

importance of conjugation length to transport properties of both undoped and doped $[\text{CH}]_x$. Polyacetylene was first n-doped with sodium naphthalide, and later compensated using deuterated alcohols, ROD. After redoping the deuterated polymer with AsF_5 , they identified a power law dependence of σ_{RT} on l , the average conjugation length: that is, $\sigma_{\text{RT}} \sim l^{3.2}$. In a similar work by Soga et al.,¹⁸⁶ a 3.5 power dependency was determined for iodine doped polymers.

These results clearly reveal a strong dependency of transport properties on conjugation lengths. However, at 17% mole deuterium addition reported, one sp^3 hybridized defect for every six-CH units would result if the original n-doping is homogeneous. In that context, these results are clearly in line with the similar results of Kassmehl.¹⁸³ The point remains, however, that for the range of molecular weights which may be prepared using the Ziegler-Natta catalyst, no relationship between molecular weight and transport properties exist. Therefore, from a conductivity viewpoint, compositions with only short conjugation lengths or conductive segments need be prepared. However, if one is interested in obtaining a conducting polymer which exhibits the mechanical and physical properties usually associated with polymeric materials high molecular weight compositions are needed.

The results of this dissertation leave open a number of points worthy of future work. Based on conductivity and EPR neutral soliton concentration results, it was inferred that low molecular weight polymer contained an intrinsically greater number of charged carriers. Thermopower measurements support this hypothesis. However, no direct

measure of $[\dot{S}]^+$ has been made. Recent results by Baker⁷⁸ described the visible absorption spectra at 0.7 eV as he compensated pristine and trans $[CH]_x$ with ammonia. A dramatic decrease in absorption from 8×10^{-2} to 2×10^{-3} was observed. Using radioactive labels, such as N^3H_3 or ^{14}C -acetic anhydride, the uptake of nucleophile could be quantified using liquid scintillation counting and correlated to the absorption spectrum. In this way, direct determination of positively charged solitons would be possible and their intrinsic concentration correlated to preparative conditions. An extension of this work would be to correlate the degree of doping using $^{125}I_2$ to the number of oxidation steps which occurred by compensating the doped polymer with a labeled nucleophile.

Within Chapter IV, infrared results showed for trans low \bar{M}_n polymer a very narrow singlet absorption at 1010 cm^{-1} characteristic of trans out of plane bending. In contrast, 10,500 \bar{M}_n and above polymers showed low frequency broadening and a multiplet of maxima. It would, therefore, be of extreme interest to perform Resonance Raman experiments on these polymers to confirm a true variation in conjugation distribution length exists between high and low molecular weight trans polymers. The phenomenon of spectral shift towards higher frequencies as the lasing excitation energy increases has been attributed to either "hot luminescence"⁸⁵ or a distribution of effective conjugation lengths.^{80,82} Recently, Resonance Raman experiments on partially deuterated polyacetylene support the later explanation.¹⁸⁷

REFERENCES

1. J. C. W. Chien, Polyacetylene: Chemistry, Physics and Material Science, Academic Press, NY, 1984.
2. G. Odian, Principles of Polymerization, John Wiley & Sons, New York, 1981.
3. J. Soto, M. L. Steigerwald, R. H. Grubbs, J. Am. Chem. Soc., 104, 4479 (1982).
4. C. F. Feldman, E. Perry, J. Polym. Sci., 46, 217 (1960).
5. A. Schindler, J. Polym. Sci., B3, 147 (1965).
6. P. Cossee, J. Catal., 3, 80 (1964).
7. E. J. Arlman, J. Catal., 3, 89 (1964); E. J. Arlman, P. Cossee, 3, 99 (1964).
8. M. L. H. Green, Pure Appl. Chem., 50, 27 (1978).
9. T. C. Clarke, C. S. Yannoni, T. J. Katz, J. Am. Chem. Soc., 105, 7787 (1983).
10. A. Zambelli, M. G. Giongo, G. Natta, Makromol. Chem., 112, 183 (1968).
11. A. A. Berlin, M. I. Cherkashin, Vysokomol. Soedin, A13, 2298 (1978).
12. C. Simionescu, S. V. Dumitrescu, I. Negulescu, V. Percec, M. Grigoras, I. Diacomì, M. Leanca, L. Goras, Vysokomol. Soedin., A16, 790 (1974).
13. J. Boor, Jr., Ziegler-Natta Catalysts and Polymerizations, Academic Press, NY, 1979.

14. J. C. W. Chien, ed., Coordination Polymerization, Academic Press, N.Y. 1975.
15. G. Natta, I. Pasquon, Adv. Catal., 11, 1 (1959).
16. T. Keii, Kinetics of Ziegler-Natta Polymerization, Chapman and Hall, 1972.
17. F. Eirich, H. Mark, J. Colloid Sci., 11, 748 (1956).
18. L. Reich, A. Schlindler, Polymerization by Organometallic Compounds, Wiley Interscience, N.Y., 1966.
19. D. Burfield, I. McKenzie, P. Tait, Polymer, 13, 302 (1972).
20. I. McKenzie, P. Tait, D. Burfield, Polymer, 13, 307 (1972).
21. D. Burfield, P. Tait, Polymer, 13, 315 (1972).
22. D. Burfield, P. Tait, I. McKenzie, Polymer, 13, 321 (1972).
23. J. C. W. Chien, J. Am. Chem. Soc., 81, 86 (1959).
24. J. C. W. Chien, J. Polym. Sci., Part A-1, 1, 425 (1963).
25. V. A. Zakharov, G. D. Bukatov, N. B. Chumaerskii, Yu. I. Yermakov, React. Kin. Cat. Lett., 2, 247 (1974).
26. V. A. Zakharov, P. A. Zhedan, E. E. Vermel, S. G. Artamonora, Kinet. Katal. 16, 1184 (1975).
27. N. B. Chumaevskii, V. A. Zakharov, G. D. Bukatov, G. I. Kuznetzova, Yu. I. Yermakov, Makromol. Chem., 177, 747 (1976).
28. J. Mejzlik, M. Lesna, Makromol. Chem., 178, 261 (1977).
29. G. D. Bukator, V. A. Zakharov, Yu. I. Yermakov, Makromol. Chem., 179, 2097 (1978).
30. V. Warzelhan, T. F. Burger, D. J. Stein, Makromol. Chem., 183, 489 (1982).

31. B. Wunderlich, *Angew. Chem. Int. Ed.*, 7(12), 912 (1968).
32. P. Blais, R. St.John Manley, *J. Polym. Sci., Part A-1*, 6, 291 (1968).
33. T. Georgiadis, R. St.John Manley, *Kolloid-Z.u. Z. Poly.*, 250, 557 (1972).
34. A. Keller, F. M. Willmouth, *Makromol. Chem.*, 121, 42 (1969).
35. H. D. Chanzy, B. Fisa, R. H. Marchessault, *Crit. Rev. Macromol. Sci.*, 1(3), 315 (1973).
36. L. A. M. Rodriguez, J. A. Gabant, *J. Polym. Sci.*, C4, 125 (1964).
37. J. Y. Guttman, J. E. Guillet, *Macromolecules*, 1(5), 461 (1968).
38. C. W. Hock, *J. Polym. Sci., Part A-1*, 4, 3055 (1966).
39. P. Mackie, M. N. Berger, B. M. Grieverson, D. Lawson, *J. Polym. Sci.*, B5, 493 (1967).
40. G. Natta, G. Mazzanti, P. Corradini, *Atti. Acad. Nazl. Lincei, Rend Classes. Sci. Fis. Mat., Nat.*, 25, 3 (1958).
41. H. Shirakawa, S. Ikeda, *Polym. J.*, 2, 231 (1971).
42. H. Shirakawa, T. Ito, S. Ikeda, *Polym. J.*, 4, 460 (1973).
43. T. Ito, H. Shirakawa, S. Ikeda, *J. Polym. Sci., Polym. Chem. Ed.*, 12, 11 (1974).
44. T. Ito, H. Shirakawa, S. Ikeda, *J. Polym. Sci., Polym. Chem. Ed.*, 13, 11 (1975).
45. Y. Tabata, B. Saito, H. Shibano, H. Sobue, K. Oshima, *Makromol. Chem.*, 76, 89 (1964).
46. E. Tsuchida, C. Shid, I. Shinohara, S. Kambara, *J. Polym. Sci.*, A2, 3347 (1964).

47. W. Deits, P. Cukor, M. Rubner, H. Jopson, J. Elect. Mat., 10(4), 683 (1981).
48. M. Hatano, S. Kambara, S. Okamoto, J. Polym. Sci., 51, 26 (1961).
49. H. Haberkorn, H. Naarmann, K. Fenzien, J. Schlag, P. Simak, Synth. Met., 5, 51 (1982).
50. L. B. Luttinger, J. Org. Chem., 27, 1591 (1962).
51. M. Varonkov, V. Pukhnarevich, S. Suchchinskaya, V. Z. Annenkova, V. M. Annekova, N. Andreeva, J. Polym. Sci., Polym. Chem. Ed., 18, 53 (1980).
52. M. Aldissi, C. Linaya, J. Sledgz, F. Schue, L. Giral, J. M. Farbre, M. Rolland, Polymer, 23, 243 (1982).
53. J. H. Edwards, W. J. Feast, Polymer, 21, 595 (1980).
54. M. Takeda, K. Iimura, Y. Nozawa, M. Hisatome, N. Koide, J. Polym. Sci., C23, 741 (1968).
55. H. Hirai, K. Hiraki, I. Noguchi, S. Makishima, J. Polym. Sci., Part A-1, 8, 147 (1970).
56. J. C. W. Chien, F. E. Karasz, G. E. Wnek, A. G. MacDiarmid, A. J. Heeger, J. Polym. Sci., Polym. Chem. Ed., 18, 45 (1980).
57. M. Aldissi, F. Schue, L. Giral, M. Rolland, Polymer, 23, 246 (1982).
58. H. Shirakawa, S. Ikeda, Synth. Met., 1, 175 (1979).
59. W. H. Meyer, Synth. Met., 4, 81 (1981).
60. W. H. Meyer, Mol. Cry. Liq. Cryst., 77, 137 (1981).
61. K. Shimamura, F. E. Karasz, J. A. Hirsch, J. C. W. Chien, Makromol. Chem., Rapid. Commun., 2, 473 (1981).

62. J. C. W. Chien, F. E. Karasz, K. Shimamura, J. Polym. Sci., Polym. Lettr. Ed., 20, 97 (1982).
63. J. C. W. Chien, F. E. Karasz, K. Shimamura, Macromolecules, 15, 1012 (1982).
64. G. E. Wnek, Ph. D. Dissertation, University of Massachusetts, Amherst, MA, 1980.
65. P. Ingram, A. Schindler, Makromol. Chem., 111, 267 (1968).
66. V. Enkelmann, W. Muller, G. Wegner, Synth. Met., 1, 185 (1979/80).
67. G. Lieser, G. Wegner, W. Muller, V. Enkelmann, Makromol. Chem. Rapid Commun., 1, 621 (1980).
68. G. Lieser, G. Wegner, W. Muller, V. Enkelmann, Makromol. Chem., Rapid Commun., 1, 627 (1980).
69. G. Lieser, M. Monkenbusch, V. Enkelmann, G. Wegner, Mol. Cryst. Liq. Cryst., 77, 169 (1981).
70. D. White, D. C. Bott, R. H. Weatherhead, Polymer, 24, 805 (1983).
71. R. H. Baughman, S. L. Hsu, G. P. Pez, A. J. Signorelli, J. Chem. Phys., 68, 5405 (1978).
72. R. H. Baughman, N. S. Murthy, G. G. Miller, J. Chem. Phys., 79 (1), 515 (1983).
73. K. Soga, S. Kawakami, H. Shirkawa, S. Ikeda, Makromol. Chem. Rapid Commun., 1, 523 (1980).
74. V. Enkelmann, G. Lieser, M. Monkenbusch, W. Muller, G. Wegner, Mol. Cryst. Liq. Cryst., 77, 111 (1981).
75. C. R. Fincher, M. Ozaki, A. J. Heeger, A. G. MacDiarmid, Phys. Rev. B., 19, 4140 (1979).

76. C. R. Fincher, D. L. Peebles, A. J. Heeger, M. A. Druy, Y. Matsumura, A. G. MacDiarmid, H. Shirakawa, S. Ikeda, *Solid St. Commun.*, 27, 489 (1978).
77. N. Suzuki, M. Ozaki, S. Etemad, A. J. Heeger, A. G. MacDiarmid, *Phys. Rev. Lett.*, 45, 1209 (1980).
78. G. L. Baker, *Polym. Prepr., ACS Proc.*, 25(2), 225 (1984).
79. I. Harada, M. Tasuni, H. Shirakawa, S. Ikeda, *Chem. Letts.*, 1411 (1978).
80. H. Kuzmany, *Phys. Stat. Sol. (b)*, 97, 5121 (1980).
81. S. Lefrant, L. Lichtmann, H. Temkin, D. B. Fitch, P. C. Miller, G. E. Whitewell, J. M. Burlitch, *Solid State Commun.*, 29, 191 (1979).
82. H. Kuzmany, *Chem. Scr.*, 17, 155 (1981).
83. D. B. Fitch, *Mol. Cryst. Liq. Cryst.*, 83, 95 (1982).
84. Y. Furukawa, T. Arakawa, H. Takeuchi, I. Harada, H. Shirakawa, *J. Chem. Phys.*, 81 (7), 2907 (1984).
85. E. J. Mele, *Solid St. Commun.*, 44 (6), 827 (1982).
86. E. J. Mele, M. J. Rice, *Solid St. Commun.*, 34, 339 (1980).
87. M. Tanaka, A. Watanabe, J. Tanaka, *Bull. Chem. Soc., Jpn.*, 53, 645 (1980).
88. E. J. Mele, M. J. Rice, *Phys. Rev. Lett.*, 45, 926 (1980).
89. S. Etemad, A. Pron, A. J. Heeger, A. G. MacDiarmid, E. J. Mele, M. J. Rice, *Phys. Rev. B*, 23, 5137 (1981).
90. J. F. Rabott, T. C. Clarke, G. B. Street, *J. Chem. Phys.*, 71(11), 4614 (1979).

91. T. C. Clarke, M. T. Krounbi, V. Y. Lee, G. B. Street, J. Chem. Soc. Chem. Commun., 384 (1981).
92. P. Bernier, F. Schue, J. Sledz, M. Rolland, L. Giral, Chem. Sci. 17, 151 (1981).
93. M. Mehring, H. Weber, W. Muller, G. Wegner, Solid St. Commun., 45 (12), 1079 (1983).
94. T. Terao, S. Maeda, T. Yamabe, K. Akagi, H. Shirakawa, Chem. Phys. Lettr., 103(5), 347 (1984).
95. C. S. Yannoni, T. C. Clarke, Phys. Rev. Lettr., 51(13), 1191 (1983).
96. A. Karpfen, R. Holler, Solid St. Commun., 37, 179 (1981).
97. J. C. W. Chien, F. E. Karasz, G. E. Wnek, Nature (London), 285, 390 (1980).
98. L. Lauchlan, S. Etemad, T. C. Chung, A. J. Heeger, A. G. MacDiarmid, Phys. Rev. B, 24, 3701 (1981).
99. T. Yamabe, K. Akagi, H. Shirakawa, K. Ohzeki, K. Fukui, Chem. Scr., 17, 157 (1981).
100. T. Yamabe, K. Akagi, K. Ohzeki, K. Fukui, H. Shirakawa, J. Phys. Chem. Sol., 43, 577 (1982).
101. X. Jing, Y. Wu, X. Gong, H. Yu, W. Zhang, F. Wang, Makromol. Chem. Rapid Commun., 5, 311 (1984).
102. H. W. Gibson, R. J. Weagley, R. A. Mosher, S. Kaplan, W. M. Priest, Jr., A. J. Epstein, Mol. Cryst. Liq. Cryst., in press.
103. H. W. Gibson, J. M. Pochan, S. Kaplan, J. Am. Chem. Soc., 103, 4619 (1981).

104. H. W. Gibson, R. J. Weagley, W. M. Priest, R. Mosher, S. Kaplan, J. Phys.(Paris) - C3, 44(6), 123 (1983).
105. M. Rolland, P. Bernier, S. Lefrant, M. Aldissi, Polymer 21, 1111 (1980).
106. P. Bernier, C. Linaya, M. Rolland, M. Aldissi, J. Phys.(Paris) Lett., 42, 295 (1981).
107. P. Robin, J. P. Pouget, R. Comes, H. W. Gibson, A. J. Epstein, Phys. Rev. B, 27(6), 3938 (1983).
108. C. Riekel, Makromol. Chem., Rapid Commun., 4, 479 (1983).
109. J. C. W. Chien, L. C. Dickinson, unpublished results.
110. J. M. Warakowski, Ph. D. Dissertation, University of Massachusetts, Amherst, MA, 1984.
111. Mol. Cryst. Liq. Cryst., 77 (1981); 83 (1982).
112. J. Phys.(Paris) - Colloq. C3, 44(6), (1983).
113. W. P. Su, J. R. Schrieffer, A. J. Heeger, Phys. Rev. Lett., 42 (25), 1698 (1979).
114. W. P. Su, J. R. Schrieffer, A. J. Heeger, Phys. Rev. B, 22(4), 2099 (1980).
115. W. P. Su, Solid St. Commun., 35, 899 (1980).
116. I. B. Goldberg, H. R. Crowe, P. R. Newman, A. J. Heeger, A. G. MacDiarmid, J. Chem. Phys., 70, 1132 (1979).
117. B. R. Weinberger, E. Ehrenfreund, A. Pron, A. J. Heeger, A. G. MacDiarmid, J. Chem. Phys., 72, 4749 (1980).
118. J. C. W. Chien, G. E. Wnek, F. E. Karasz, J. M. Warakowski, L. C. Dickinson, A. J. Heeger, A. G. MacDiarmid, Macromolecules, 15, 614 (1982).

119. M. Nechtschein, F. Devreux, R. L. Green, T. C. Clarke, G. B. Street, *Phys. Rev. Lett.*, 44, 356 (1980).
120. M. Nechtschein, F. Devreux, F. Genoud, M. Guglielmi, K. Holczer, *Phys. Rev. B*, 27, 61 (1983).
121. N. S. Shiren, Y. Tomkiewicz, T. G. Kazyaka, A. R. Taranko, H. Thomann, L. Dalton, T. C. Clarke, *Solid St. Commun.*, 44, 1157 (1982).
122. J. C. W. Chien, J. M. Warakowski, F. E. Karasz, W. L. Chia, C. P. Lillya, *Phys. Rev. B.*, 28 (12), 6937 (1983).
123. D. Davidov, S. Roth, W. Neumann, H. Sixl, *Z. Phys. B-Condens. Mat.*, 51, 145 (1983).
124. J. Brédas, R. R. Chance, R. Silbey, *Phys. Rev. B*, 26(10), 5843 (1982).
125. D. S. Boudreaux, R. R. Chance, J. L. Brédas, R. Silbey, *Phys. Rev. B*, 28(12), 6927 (1983).
126. J. R. Reynolds, Ph. D. Dissertation, University of Massachusetts, Amherst, MA, 1985.
127. S. L. Hsu, A. J. Signorelli, G. P. Pez, R. H. Baughman, *J. Chem. Phys.*, 69, 106 (1978).
128. T. Matsuyama, H. Sakai, H. Yamaoda, Y. Maeda, H. Shirakawa, *Solid St. Commun.*, 40, 563 (1981).
129. C. K. Chaing, Y. W. Park, A. J. Heeger, H. Shirakawa, E. J. Louis, A. G. MacDiarmid, *J. Chem. Phys.*, 69, 5098 (1978).
130. Y. W. Park, A. J. Heeger, M. A. Druy, A. G. MacDiarmid, *J. Chem. Phys.*, 73, 946 (1980).

131. S. Kivelson, Phys. Rev. Lett., 46(20), 1344 (1981).
132. S. Kivelson, Phys. Rev. B, 25(6), 3798 (1982).
133. A. J. Epstein, H. Rommelmann, M. Abkowitz, H. W. Gibson, Phys. Rev. Lett., 47, 1549 (1981).
134. D. Moses, A. Feldblum, A. Denenstein, T. C. Chung, A. J. Heeger, A. G. MacDiarmid, Mol. Cryst. Liq. Cryst., 83, 87 (1982).
135. A. J. Epstein, H. W. Gibson, P. M. Chaikin, W. G. Clark, G. Gruner, Phys. Rev. Lett., 45, 1730 (1980), and Chem. Scr., 17, 135 (1981).
136. A. J. Epstein, H. Rommelmann, R. Bigelow, H. W. Gibson, D. M. Hoffman, D. B. Tanner, Phys. Rev. Lett., 50(23), 1866 (1983).
137. A. J. Epstein, R. W. Bigelow, A. Feldblum, H. W. Gibson, D. M. Hoffman, D. B. Tanner, Synth. Met., 9, 155 (1984).
138. R. R. Chance, J. L. Bredas, R. Silbey, Phys. Rev. B, 29(8), 4491 (1984).
139. J. L. Brédas, B. Themans, J. M. Andre, R. R. Chance, R. Silbey, Synth. Met., 9, 265 (1984).
140. D. R. Perrin, W. L. F. Armarego, Purification of Laboratory Chemicals, 2nd ed., Pergamon Press, Oxford, 1980, pp. 476, 557.
141. Environmental Health and Safety Division, Radiation Safety Manual, University of Massachusetts, Amherst, MA, 1977.
142. R. A. Vaires, B. H. Parks, Radioisotopic Laboratory Techniques, John Wiley & Sons, New York, 1973, Chapter 5.
143. I. Ito, H. Shirakawa, S. Ikeda, J. Polym. Sci., Polym. Chem. Ed., 13, 1943 (1975).

144. E-9 EPR Spectrometer System Technical Manual, Publication #87-125-003, Varian Analytical Instruments Division, Palo Alto, CA 94303.
145. H. M. Swartz, J. R. Bolton, D. C. Borg, Biological Applications of Electron Spin Resonance, Wiley-Interscience, NY, 1972.
146. J. C. W. Chien, J. D. Capistran, F. E. Karasz, L. C. Dickinson, M. A. Schen, J. Polym. Sci., Polym. Lett. Ed., 21, 93 (1983).
147. J. C. W. Chien, F. E. Karasz, M. A. Schen, J. A. Hirsch, Macromolecules, 16, 1694 (1983).
148. M. A. Schen, F. E. Karasz, J. C. W. Chien, J. Polym. Sci., Polym. Chem. Ed., 21, 2787 (1983).
149. M. A. Schen, J. C. W. Chien, F. E. Karasz, J. Phys.(Paris)-C3, 44(6), 163 (1983).
150. D. R. Bufield, C. M. Savarian, Macromolecules, 12, 243 (1979).
151. G. E. Wnek, J. Capistran, J. C. W. Chien, L. C. Dickinson, R. Gable, R. Gooding, K. Gourley, F. E. Karasz, C. P. Lillya, K. D. Yao, Conductive Polymers, R. P. Seymour, Ed., Plenum, NY, 1981, pp. 183-208.
152. V. A. Zakharov, G. D. Bukatov, N. B. Chumaevskii, Yu. I. Yermakov, React. Kinet. Catal. Lett., 1, 247 (1974).
153. W. R. Schmeal, J. R. Street, AIChE J., 17, 1188 (1971).
154. D. Singh, R. P. Merrill, Macromolecules, 4, 599 (1971).
155. J. C. W. Chien, J. Polym. Sci. Polym. Chem Ed., 17, 2555 (1979).
156. J. C. Wu, Ph. D. Dissertation, University of Massachusetts, Amherst, MA, 1982.

157. J. C. W. Chien, Y. Yamashita, J. A. Hirsch, J. L. Fan, M. A. Schen, F. E. Karasz, *Nature*, 299, 608 (1982).
158. J. C. W. Chien, F. E. Karasz, M. A. Schen, Y. Yamashita, *Makromol. Chem., Rapid Commun.*, 4, 5 (1983).
159. M. R. Mackley, *Colloid Polym. Sci.*, 213, 373 (1975).
160. A. Zwijnenburg, A. J. Pennings, *Colloid Polym. Sci.*, 254, 868 (1976).
161. A. Snow, P. Brant, D. Weber, N. L. Yang, *J. Polym. Sci., Polym. Lett. Ed.*, 17, 263 (1979).
162. B. R. Weinberger, J. Kaufer, A. J. Heeger, A. Pron, A. G. MacDiarmid, *Phys. Rev. B.*, 20 (1), 223 (1979).
163. J. M. Pochan, H. W. Gibson, *Polym. Commun.*, 24, 322 (1983).
164. P. Bernier, M. Rolland, M. Galtier, A. Montaner, M. Regis, M. Candille, C. Benoit, M. Aldissi, C. Linaya, F. Schue, J. Sledz, J. M. Fabre, L. Giral, *J. Phys.(Paris) Lett.*, 40, 297 (1979).
165. M. Takumoto, N. Kinoshita, S. Kuroda, T. Ishiguro, H. Shirakawa, H. Nemoto, *J. Phys.(Paris)-Colloq. C3*, 44, 299 (1983).
166. L. Mihaly, S. Pekker, A. Janossy, *Synth. Metal.*, 1, 349 (1979/80).
167. C. Benoit, O. Bernard, M. Palpacuer, M. Rolland, M. J. M. Abadie, *J. Phys.(Paris)*, 44, 1307 (1983).
168. P. Robin, J. P. Pouget, R. Comes, H. W. Gibson, A. J. Epstein, *J. Phys(Paris)-Colloq. C3*, 44, 87 (1983).
169. D. M. Hoffman, H. W. Gibson, A. J. Epstein, D. B. Tanner, *Phys. Rev. B.*, 27, 1454 (1983).

170. K. Tanaka, K. Yoshiyawa, K. Ohzeki, T. Yamabe, *Solid St. Commun.*, 45, 391 (1983).
171. I. Heinmaa, M. Alla, A. Vainrub, E. Lippmaa, M. L. Khidekel, A. I. Kotov, G. I. Kozub, *J. Phys(Paris)-Colloq. C3*, 44, 357 (1983).
172. M. Palpacuer, O. Bernard, C. Deloupy, M. Rolland, J. J. M. Abadie, *Polymer*, 23, 1847 (1982).
173. M. A. Schen, F. E. Karasz, J. C. W. Chien, *Makromol. Chem., Rapid Commun.*, 5, 217 (1984).
174. P. Bernier, S. Lefrant, M. Rolland, M. Aldissi, M. Galtier, A. Montaner, C. Linaya, F. Schue, *J. Elect. Mat.*, 12(2), 289 (1983).
175. H. Eckhardt, *J. Chem. Phys.*, 79(4), 2085 (1983).
176. D. Moses, J. Chen, A. Denenstein, M. Kavch, T. C. Chung, A. J. Heeger, A. G. MacDiarmid, *Solid St. Commun.*, 40, 1007 (1981).
177. D. J. Thouless, *Phys. Rev. Lett.*, 39, 1167 (1977).
178. P. W. Anderson, E. Abrahams, T. V. Ramakrishnan, *Phys. Rev. Lett.*, 43, 718 (1979).
179. E. A. Davis, N. F. Mott, *Philos. Mag.*, 22, 903 (1970).
180. P. Nagels, R. Callerts, M. Denayer, R. DeConinck, *J. Non-Cryst. Sol.*, 4, 295 (1970).
181. G. Wegner, *Angew. Chem. Int. Ed. Engl.*, 20, 361 (1981).
182. J. C. W. Chien, J. B. Schlenoff, *Nature(London)*, 311, (5984), 362 (1984).
183. G. Kossmehl, *Ber. Bunsenges. Phys. Chem.*, 83, 417 (1979).
184. J. L. Bredas, R. Silbey, D. S. Boudreaux, R. R. Chance, *J. Am. Chem. Soc.*, 105 (22), 6555 (1983).

185. S. I. Yaniger, M. J. Kletter, A. G. MacDiarmid, Polym. Prepr. Proc. ACS, 25(2), 264 (1984).
186. K. Soga, M. Nakamaru, J. Chem. Soc., Chem. Commun., 1495 (1983).
187. S. I. Yaniger, private communication.
188. B. R. Weinberger, J. Kaufer, A. J. Heeger, A. Pron, A. G. MacDiarmid, Phys. Rev. B, 20(1), 223 (1979).

